Sigma-Hole Non-Covalent Interactions in Anion Host-Guest Chemistry and the Mechanical Bond

Jane Y. Liew

St. Peter's College

A thesis submitted for the degree of Doctor of Philosophy

in Inorganic Chemistry

Michaelmas Term, 2020

This thesis is dedicated to my parents

Prof. Richard Liew and Dr. Tan Liang See.

Sigma-Hole Non-Covalent Interactions in Anion Host-Guest Chemistry and the Mechanical Bond

Jane Y. Liew, St. Peter's College, University of Oxford

Abstract of thesis submitted for the degree of Doctor of Philosophy, Michaelmas Term 2020

This thesis describes the use of σ-hole interactions in acyclic, macrocyclic and mechanically interlocked receptors for anion recognition and sensing.

Chapter 1 provides an overview of the field of supramolecular host-guest chemistry with particular focus on host systems bearing σ-hole donor motifs for anion guest binding, followed by a discussion of mechanically interlocked host molecules for anion recognition and sensing.

Chapter 2 describes the synthesis of air and water stable acyclic tellurium and selenium-based chalcogen bonding receptors followed by an investigation of their thermodynamic anion binding properties in organic and mixed aqueous/organic solvent media. The integration of halogen bonding and chalcogen bonding motifs into mechanical interlocked molecular structural frameworks is also explored.

Chapter 3 details combining σ-hole donors and the BINOL motif to form chiral host receptors. The synthesis of a chiral halogen bonding [2]rotaxane structure is described as well as chiral acyclic and macrocyclic receptors possessing four integrated halogen bond-donors which are shown to be capable of binding chiral carboxylate anions. The enantioselective properties of these receptors were determined by monitoring the fluorescence changes of the respective receptor's integrated BINOL or pyrene fluorophore upon chiral anion guest binding.

Chapter 4 introduces the use of halonium cation species in supramolecular chemistry. Primarily, this chapter investigates the stability of iodonium species in pyridyl-based pseudorotaxane assemblies and mechanically bonded [2]rotaxanes using NMR spectroscopy.

Chapter 5 summarises the conclusions of this thesis.

Chapter 6 describes the experimental procedures carried out in this work detailing characterisation of novel compounds presented in chapters 2-4. Additional information pertaining to crystallographic data and computational work are provided in the Appendices.

Acknowledgements

First and foremost, I would like to thank my supervisor Prof. Paul Beer for the opportunity of a lifetime to carrying out my PhD in the Beer group at the University of Oxford. His support, patience and kindness throughout my research in Oxford has spurred me on in the most trying times. I would also like to thank my supervisors Dr. Evan Moore, Assoc Prof. Shih-Chun Lo and Prof. Mark Riley from UQ for encouraging me to apply to Oxford. Their expertise and patience have provided me with endless opportunities.

The Beer group has changed vastly throughout the years and you lot have definitely left a lasting impact in my time spent in the lab. In particular, I must give thanks to my lab mentor Dr. Jason Lim for showing me the ropes around the lab and sharing your vast knowledge in chemistry. I have shared many moments; highs and lows, banters and frustrations with the different personalities in the lab, all of which I deemed necessary on this PhD journey. I would like to give big thanks to the OG team who have welcomed me into the Beer group with open arms, in particular, 'big' Tim Barendt, Valentine Bunchuay, Hena Bagha, Harry Klein, Andrew Docker, Rob Hein, George Li and the occasional Arseni Borissov, for all your help not just in chemistry, but also for your friendships. To the new crew: you guys have changed the dynamics of the Beer group bringing your positive vibes into the lab. Big hugs to Krzystof Bąk, Jess Pancholi, TJ Mitchell, Richard Tse, Laura-Olivia duo, ZongYao Zhang for brightening my days. Another Thank you to those whom have been so 'lucky' to have been picked to proof-read this thesis. To my running/gym buddy Tanya Rogova, thanks for dragging me out of the lab for bolts of endorphins and breakfasts, we all needed that pause from the lab once a week.

Reflecting on the past 4 years in Oxford, this small city has given me a unique opportunity to meet so many wonderful people in and out of college, from all walks of life, all over the world. And at least two-handfuls of lovelies that I know I will have their friendship for a long time. My college has provided me with lots of free cheese and wine, but more importantly, it has acted as a portal to some very good friends that I have made. Firstly, my housemates Oli, Oly, Olivia and Dom, we have come thus far and have all come out of the other side relatively unscathed, that in itself is an achievement. Thank you for being so much fun and tolerable; *vice versa*. I would also like to thank Fran for always reminding me that there is more to life than just chemistry and the lab, Nat for showing me your perspective of nature. And not the very least, Allie and Rachael whom I have shared many drinks, laughter and exactly one karaoke with.

I cannot forget the friends I left behind in Australia all of whom injected me with a little bit of that aussie spirit. To Isaac, Gina, Bowie, Eunice, Josh and Divya, thank you for the amazing Aussie

experience and friendship you have shared with me! The end of 2020 marks the 17th anniversary of my friendship to Yumin, Sher and Angela, you girls have always been there for me and our togetherness has only strengthened through time.

My parents have supported me financially throughout my 20s allowing me to plunge heedlessly into my selfish pursuit of dreams and ambitions with no repercussions. And for that, I cannot repay enough, thank you papa and mama for your love and support. The strong and resilient characters who raised me, not just my Dad but my Mum, aunties Rosalind and Irene and my grandmother, you have all shaped and moulded my personality and sense of ambition in more ways than you think you have. To my brothers John and Jovin, thank you for always being jovial, there's definitely less fighting over toys or beating each other up and more fun and interesting conversations over food and drinks like civilised (almost)-adults!

Lastly, I would like to give special thanks to my primary school teacher Miss Clarinda Choh and her husband for encouraging me to make the leap to Oxford.

To my future self, you've done pretty well this past decade. You have gotten comfortable in your skin, you know that you should surround yourself only with good people. Hopefully that would still be true whenever you read this. And don't be afraid.

Jane Liew

October 2020

“A journey will have pain and failure. It is not only the steps forward that we must accept. It is the stumbles. The trials. The knowledge that we will fail. That we will hurt those around us. But if we stop, if we accept the person we are when we fail, the journey ends. That failure becomes our destination.”

- Brandon Sanderson, Oathbringer

Publication

Thermodynamics of Anion Binding by Chalcogen Bonding Receptors.

Jason Y. C. Lim, Jane Y. Liew and Paul D. Beer, *Chem. Eur. J.*, **2018**, 24, 14560-14566

Oral Presentation

Thermodynamics of Anion Binding by Chalcogen Bonding Receptors. ***ISXB-3 and the IUPAC Workshop on Group 14-16 Interactions***, June 2018, South Carolina, USA.

Poster Presentation

Thermodynamics of Anion Binding by Chalcogen Bonding Receptors. ***14th International Symposium on Macrocyclic and Supramolecular Chemistry***, June 2019, Lecce, Italy.

List of Abbreviations

δ	chemical shift
λ	wavelength
µ	micro
Δ	change in (a physical quantity)
Å	Ångstrom
a.u.	arbitrary units
AMT	active metal template
BINOL	1,1'-Bi-2-naphthol
br.	broad
cat.	catalytic
ChB	chalcogen bonding
CuAAC	copper(I)-catalysed azide-alkyne cycloaddition
DABCO	1,4-diazabicyclo[2.2. 2]octane
DBU	1,8-diazabicycloundec-7-ene
DIPEA	N,N-diisopropylethylamine
DMAP	4-Dimethylaminopyridine
DMF	N,N-dimethylformamide
DMSO	dimethyl sulfoxide
DNA	deoxyribonucleic acid
e.g.	*exempli gratia*
EDTA	ethylenediaminetetraacetate
eqv.	equivalents
ESI	electrospray ionisation (mass spectrometry)
ESP	Electrostatic potential
g	gram
G	Gibbs free energy
Grubbs' I/ II	Grubbs' first/ second generation catalyst
H	Enthalpy
HB	hydrogen bonding
HMBC	Heteronuclear Multiple Bond Correlation
Hz	Hertz
IDH	isocitrate dehydrogenase
i.e.	id est
J	coupling constant
K	Kelvin (Temperature SI Unit)
K_a	association constant
K_d	dissociation constant
L	litre
M	molar (moles per litre)
m/z	mass to charge ratio
Me	methyl
MIM	mechanically-interlocked molecule
MOM	methoxymethyl acetal (protecting group)
MS	mass spectrometry
Ms	mesyl

NMR	nuclear magnetic resonance
PEG	Polyethylene glycol
PET	Photo-induced electronic transfer
ppm	parts per million
(*R*)-Pro	(*R*)-Proline
(*R*)-Leu	(*R*)-Leucine
(*R*)-Trp	(*R*)-Tryptophan
(*R*)-Tar	(*R*)-Tartrate
(*R*)-Glu	(*R*)-Glutamate
R.T.	room temperature
RCM	ring-closing metathesis
Rf	retention factor
ROESY	rotating-frame nuclear Overhauser effect correlation spectroscopy
S	entropy
(*S*)-Pro	(*S*)-Proline
(*S*)-Leu	(*S*)-Leucine
(*S*)-Trp	(*S*)-Tryptophan
(*S*)-Tar	(*S*)-Tartrate
(*S*)-Glu	(*S*)-Glutamate
TBA	tetrabutylammonium
TBTA	tris[(1-benzyl-1,2,3-triazol-4-yl)methyl]amine
TEG	Tetraethylene glycol
TFA	trifluoroacetic acid
THF	tetrahydrofuran
TLC	thin layer chromatography
TMS	trimethylsilyl (protecting group)
Ts	tosyl
UV	ultra-violet
v/v	volume/ volume percent
vis.	visible
VT	variable temperature
XB	halogen bonding

Contents

1 | Introduction

1.1. Fundamentals of Anion Supramolecular Chemistry

1.1.1. The Field of Supramolecular Chemistry

The Nobel Prize has been awarded twice in the field of supramolecular chemistry since its origin in the late 1960s. Pedersen, Lehn and Cram were awarded the Nobel Prize in 1987 for their work in the "development and use of molecules with structure-specific interactions of high selectivity". Specifically, they took advantage of non-covalent interactions such as electrostatic ion-dipole interactions, van der Waals forces, π-interactions and hydrophobic effects to design novel host molecules for the recognition of cationic guest species.

Pedersen serendipitously discovered the first crown ether, dibenzo[18]crown-6, a neutral synthetic receptor with an affinity for alkali metal cations.[1] Importantly, he determined a complementary crown ether cavity – alkali metal cation diameter size match, where for example, dibenzo[18]crown-6 formed the strongest complex with the potassium cation. (Figure 1i). Lehn went on to build on Pedersen's work on crown ethers to synthesise three-dimensional analogues, the cryptands which exhibit even higher affinity for alkali metal cations.[2] Having a cavity of complementary size, the [2.2.2]cryptand was observed to bind potassium cation selectively (Figure 1ii).

Cram subsequently introduced the concept of preorganisation where the more preorganised and desolvated a host is, the more strongly the host system will bind its guest.[3] To illustrate, he specifically designed a conformationally rigid macrocycle known as a spherand consisting of octahedrally arranged aryl methoxy oxygen donors whose cavity bound the lithium cation with exceptional strength. (Figure 1iii). Cram's work expanded to a wide variety of supramolecular structures with emphasis on preorganised cavities, all of which contributed to the stimulated growth of supramolecular host-guest chemistry from which evolved the self-assembly field of supramolecular chemistry.

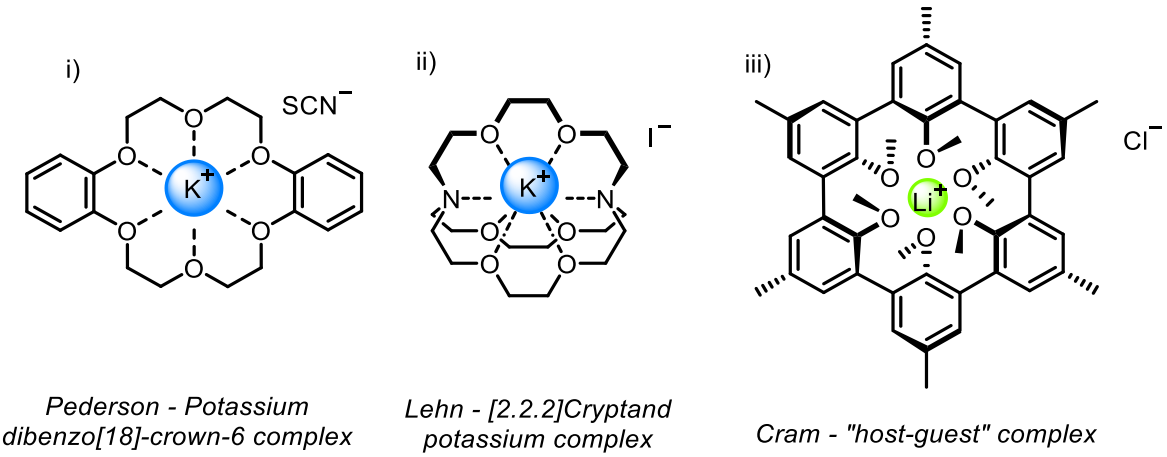

Figure 1. i) Pedersen´s dibenzo[18]crown-6 K^+ complex, ii) Lehn´s 2.2.2 cryptand K^+ complex, iii) Cram's preorganised octahedral arrangement of methoxy oxygen donors within the spherand Li^+ complex.

Advancement of the field continued to surpass expectations with the 2016 Nobel Prize in Chemistry being awarded to Sauvage, Stoddart and Feringa "for the design and synthesis of molecular machines". Sauvage and Dietrich-Buchecker published the first high-yielding, practical synthesis of a catenane using Cu(I) in a novel template approach.[4] Inspired by coordination chemistry, bidentate binding of Cu(I) by phenanthroline ligands in an orthogonal, tetrahedral stereochemical coordinating fashion provided preorganisation of catenane precursors. Subsequently, double ring closing with tetraethylene glycol ditosylate, Cs_2CO_3 in DMF under high dilution conditions resulted in the formation of Cu-bound [2]catenane in 27 % isolated yield (Figure 2i). The use of transition metals as templates for the formation of mechanically interlocked molecules was the first of its kind and

has since inspired others in their synthesis of these supermolecules. Stoddart and co-workers took advantage of aromatic donor-acceptor interactions as a template method to thread an electron-deficient viologen macrocycle onto an electron-rich hydroquinone containing axle precursor (Figure 2ii). The resulting interpenetrated assembled structure, termed a pseudorotaxane, was then capped at both ends to form a [2]rotaxane. Furthermore, the authors were able to induce shuttling motion of the viologen macrocycle by manipulation of its chemical, redox and photophysical properties.[5]

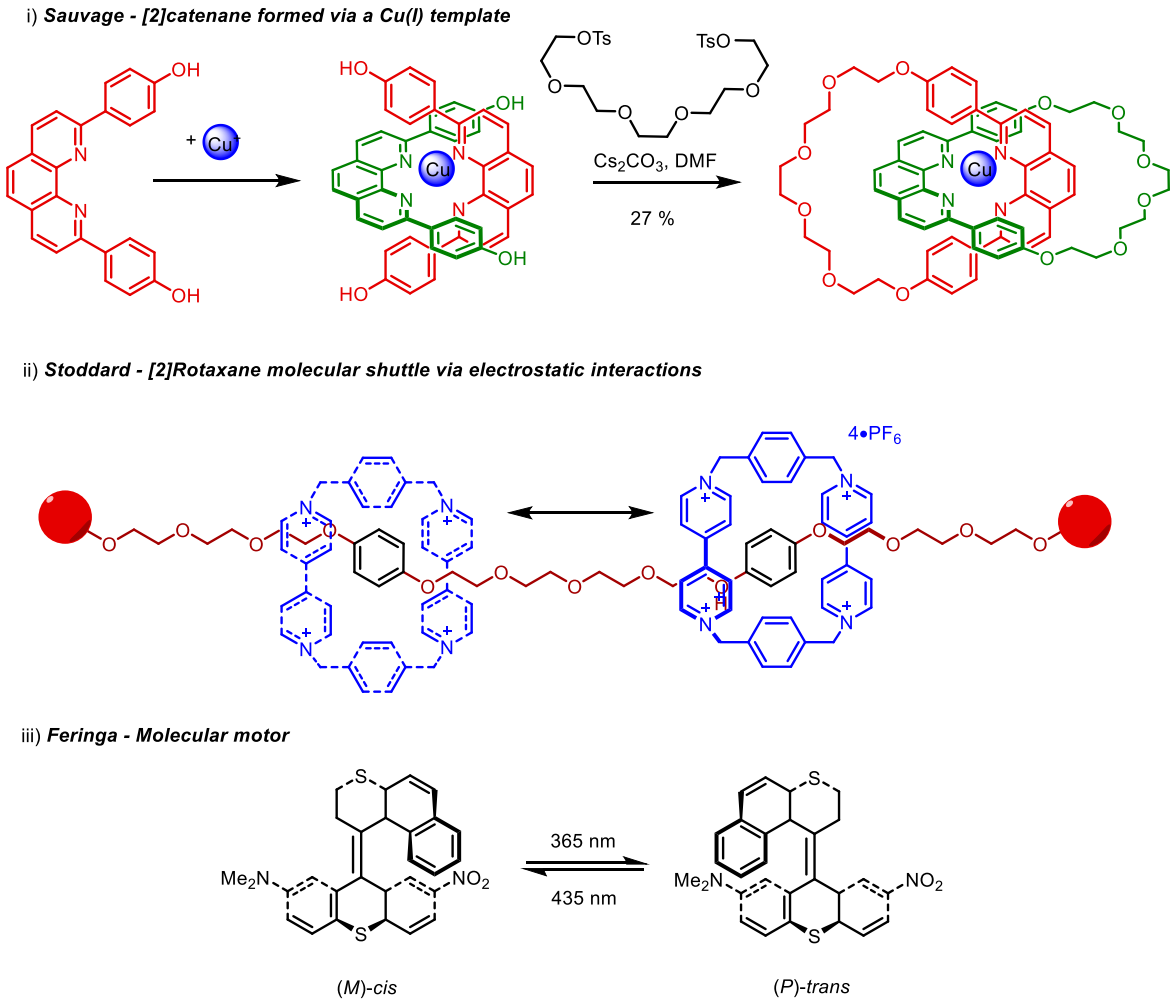

Figure 2i) Sauvage´s solid state structure of a [2]catenane with Cu-bound by two phenanthrolines, ii) Stoddart´s donor-acceptor molecular shuttle and iii) Feringa's unidirectional light-driven molecular motor.

Feringa synthesised the first unidirectional molecular motor based on the photoinduced isomerisation of a carbon-carbon double bond (Figure 2iii).[6] Due to the advantage of moving molecules via a "non-

invasive" fashion, this chemistry was able to be applied to a broad range of applications including photopharmacology[7,8] and nanocars[6,9]. The use of such molecular machines has been expanded to a wide range of applications, where a molecular elevator[10] made use of electrostatic interactions via acid/base reactions to stimulate the movement of a tris(macrocycle) along tripodal arms, light-induced conformational change of a foldamer for selective chloride recognition[11], redox-mediated intramolecular ion translocation[12] as well as anion-induced molecular shuttling[13].

The project theme of this thesis primarily focuses on molecular receptors for anion recognition. In the following sections, this introductory chapter discusses the importance and challenges of anion coordination chemistry, a brief review of the types of synthetic receptors binding anions through various non-covalent interactions and how mechanically interlocked molecules can be exploited for anion recognition and sensing applications alongside other examples.

1.1.2. Importance & Challenges of Anion Coordination Chemistry

Anions play fundamental important roles in living organisms, where highly selective biotic anion receptors have evolved to bind anions selectively. Phosphate species, essential for life are found in the backbone of nucleic acids (DNA/RNA), crucial in storing genetic information, and in ATP and ADP, which are vital in metabolic pathways and energy transfer in cells.[14] Due to the apparent limited bioavailability of phosphorus, biomechanisms developed to have high-affinity and high-specificity for phosphate over a plethora of competing anions. An example is the binding of phosphate by the phosphate binding protein (PBP; K_d = 0.31 × 10^6 M at pH 8.5)[15] which occurs at relatively low concentrations to meet the metabolic demands of cell bacteria.[16] The binding site of PBPs (*E. Coli*, *Mycobacterium tuberculosis*) comprise of 8 amino acid residues forming 12 hydrogen bonds with the phosphate anion, where the key residue (aspartate) was found to have a short contact forming a low barrier hydrogen bond (Figure 3i). This was suggested to be responsible for the high

selectivity of phosphate over geometrically similar anions such as arsenate (~3 orders of magnitude) or sulphate (~5 orders of magnitude).[17]

Chloride-ion channels (CIC) are transmembrane proteins regulating ion concentration in cells, genetic mutations of which gives rise to incurable diseases such as cystic fibrosis, renal salt loss and hyperekplexia.[18] In a study on the mechanism of chloride binding in CIC proteins (Salmonella enterica Serovar Typhimurium, *E. coli*), analysis of the crystal structure reveals a hydrogen-bonding anion binding site complemented by an electrostatically favourable arrangement of helices for chloride binding (Figure 3ii).[19]

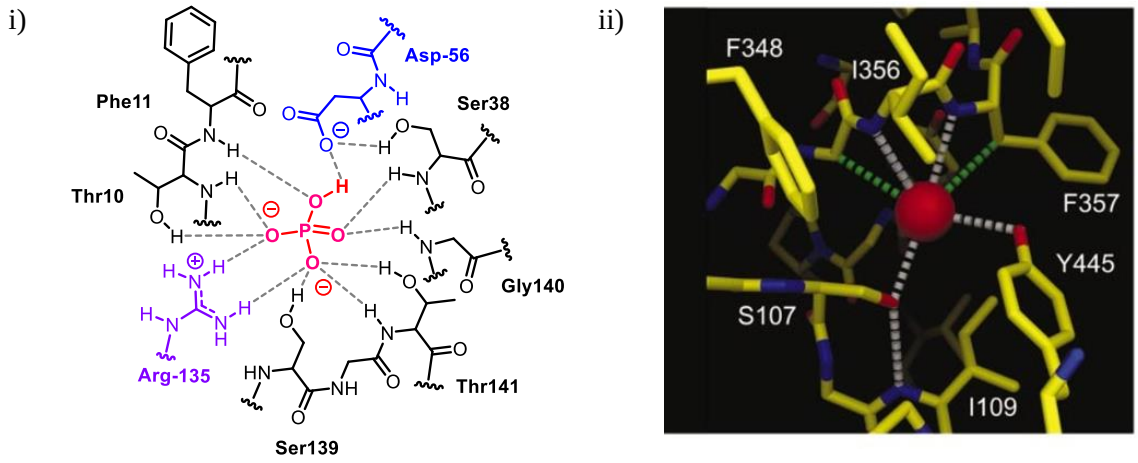

Figure 3. i) Phosphate-binding protein with 12 hydrogen bonds involved [17] ii) Binding site of chloride-ion Channel (CIC) with hydrogen bonds (white dashed) and hydrophobic (green dashed) contacts of amino acid side chains to chloride anion(red ball).

The agricultural overuse of nitrogen- and phosphorous-based fertilisers results in contaminated soil and ground water entering freshwater lakes leading to eutrophication and the disruption of aquatic life cycles. Nitrate in particular causes a stimulation of soil microbes which convert nitrogen to nitrous oxide (N_2O), a long-lived greenhouse gas and stratosphere-depleting substance.

The ubiquitous presence of anions in diverse environments results in their selective recognition being a major challenge. The examples presented in this section highlight the crucial role anions play in biology, physiology and the environment. Nature has perfected the mechanism of selective anion

recognition and from this, inspiration is drawn in the design and synthesis of abiotic anion receptors. Research methodologies have been established to recognise and sense target anions of relevant importance by means of understanding the intrinsic properties of anions (see next section) and rational receptor design (Section 1.2) taking advantage of non-covalent interactions (Section 1.3).

Intrinsic Properties of Anions

The intrinsic properties of anions take into consideration the following: i) ion size and geometry, ii) charge density, iii) polarizability, iv) pH sensitivity and v) enthalpy of hydration.[18,20–23] Anions are larger in ionic radius compared to cations, and therefore, have smaller Coulombic interactions due to their lower charge density. They also vary in geometry ranging from simple spherical anions like halides to tetrahedral anions like sulfate or phosphate to complex anionic structures like chiral amino acids or DNA structures (Figure 4).

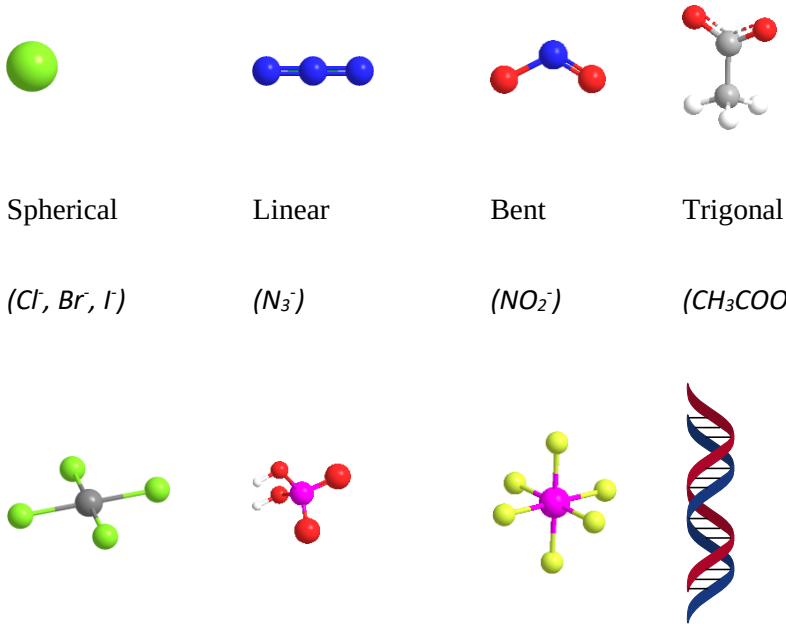

Figure 4. Molecular models showcasing different anion geometries.

Furthermore, anions are pH sensitive; they can become protonated at relatively moderate pH values. They also possess higher hydration energies compared to the smaller isoelectric cations. This is reflected in the Hofmeister series (Figure 5).

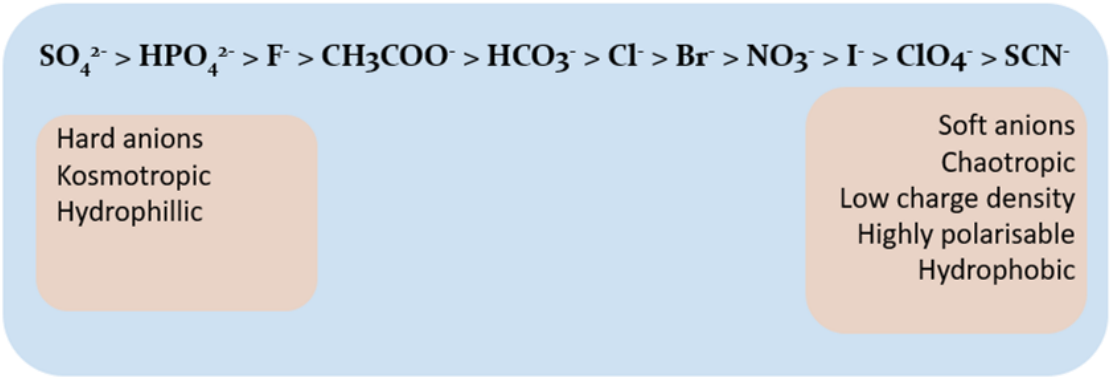

Figure 5. The Hofmeister series from hard anions (left) to soft anions (right).[18]

The Hofmeister series was established through the study of salts and their effect on the solubility of proteins. The most stabilising anions were found to be strongly hydrated anions while those that destabilised the protein the most were found to be hydrophobic in nature. Since then, the Hofmeister series has been used to pertain to the classification of anion solvation. As anion binding studies take place in solution, the nature of host and guest solvation is particularly important in determining binding strength and selectivity. Compared to cations of similar charge and size, anions have inherently higher free energies of solvation. For example, ions with similar ionic radius F^- and Na^+ possess standard free energies of hydration ($\Delta G_{hyd}°$) that are significantly different; $\Delta G_{hyd}°$ (F^-) = -465 kJ mol^{-1} and $\Delta G_{hyd}°$ (Na^-) = -365 kJ mol^{-1}.[24] Consequently, anion receptors have a larger enthalpic term to overcome upon binding an anion, where weakly associating aprotic solvents (chloroform or acetone) allow for relatively easier binding of anions while competitive protic solvents (water or methanol) can form hydrogen bonding interactions forming highly solvated host and anion guest species.

When it comes to the ability to selectively bind anions with high affinity, chemists look towards nature, which has devised highly efficient and selective building blocks for recognition. The question is then, can synthetic receptors be designed to mimic nature's host-guest recognition capability? In

an attempt to do this, chemists have explored a vast range of host designs for anion recognition, including acyclic, macrocyclic and mechanically interlocked structures such as rotaxanes and catenanes. As a result, anion supramolecular chemistry has found applications in a wide variety of areas. From nuclear waste management where efficient, selective recovery of radioactive material like pertechnate (TcO_4^-) is performed,[25] to synthetic receptors for medical purposes like drug delivery or therapy[26]. In all cases, selective anion binding is achieved by careful consideration of host design, including preorganisation, host-guest complementarity and the appropriate choice of non-covalent interactions.[22] The latter can, for example, include electrostatics, hydrogen bonding and σ-hole donor interactions like halogen bonding (XB) and chalcogen bonding (ChB), which will be discussed further in Section 1.2.

1.2. Fundamental Aspects and Considerations for Anion Host Design

1.2.1. Complementarity

The abundance of anions with different shapes and sizes requires the design of highly specific hosts in order to achieve selective binding. Complementarity of host cavity to guest *shape* and *size* has been explained by two concepts: i) the 'lock and key' concept based on enzyme-substrate relationships and later ii) the induced fit model where the enzyme undergoes a conformational change to improve its binding of substrates.[27]

1.2.2. Principle of Preorganisation

The concept of preorganisation, first introduced by Cram states that "the more highly hosts and guests are organized for binding and low solvation prior to their complexation, the more stable will be their complexes".[28] One such example is the macrocyclic effect whereby a macrocyclic host, providing high structural integrity and a shielded environment (i.e. from solvent), will form a more stable complex with its guest. With the evolution of the field, it has been observed that preorganisation of a receptor results in thermodynamically stronger host-guest association, where

cavity shape complementary and low solvation increases from acyclic < macrocyclic (see spherand example Figure 1iii) < mechanically interlocked molecules (MIMs).

1.3. Non-covalent Interactions in Anion Supramolecular Chemistry

As mentioned in Section 1.1, non-covalent interactions are a fundamental aspect of supramolecular chemistry. These non-covalent interactions differ in interaction strength with the strongest interaction approaching the strength of a covalent bond (Table 1). This section will briefly discuss those non-covalent interactions that are commonly exploited in anion host design, specifically, electrostatic interactions, hydrogen bonding, σ-hole interactions and anion-π interactions.

Table 1. Non-covalent interaction strength in kJ mol^{-1} compared to covalent bonds[29]

Type of Interaction	***Strength (kJ/mol)***
Covalent Bond	*150-450*
Ion-Ion	*100-300*
Ion-Dipole	*50-200*
Dipole-Dipole	*5-50*
Hydrogen Bond	*5-120*
π-π Interaction	*0-50*
van der Waals	*< 5*

Electrostatic interactions are the attractive or repulsive forces between charged species. This can be described by Coulombs' Law where the force (F) is equal to the product of each charge (q_i), divided by the square distance between their centres (r) and multiplied by Coulombs' constant k.

$$F = k\frac{q_1 q_2}{r^2}$$

As a consequence of this relationship, ion-ion, ion-dipole and dipole-dipole interactions have various degrees of interaction energy dependent on the distance between the species (Table 1).

Hydrogen bonding (HB) describes the attractive force between a hydrogen atom covalently bonded to an electronegative atom such as N, O or F, creating an induced dipole moment along the covalent bond which then allows interaction with a Lewis Base such as an anion. This interaction is usually linear (180°); where the closer the angle of interaction is to 180°, the stronger the HB interaction and the closer the contact is.[30] HB interaction strength can range between 5 – 120 kJ/mol (Table 1).

σ-Hole interactions involving Halogen Bonding (XB): σ-holes were first observed in halogenated methanes $(CH_3)_3CX$, where X = halogen) where analysis of the molecular electrostatic potential (MEP) revealed that the electrostatic potential (ESP) around the halogen atom is anisotropic with regions of positive and negative values. In 2013, the International Union of Pure and Applied Chemistry (IUPAC) presented a recommended definition of the halogen bond,[31] which "occurs when there is evidence of a net attractive interaction between an electrophilic region associated with a halogen atom in a molecular entity and a nucleophilic region in another, or the same, molecular entity".

i)

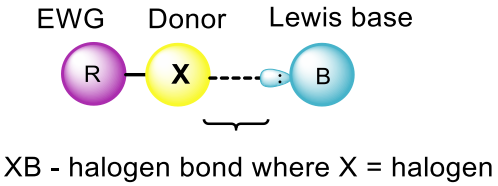

ii)

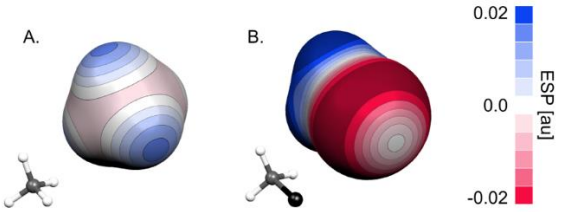

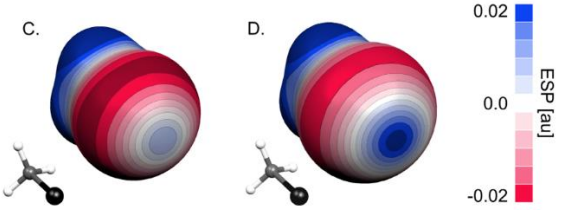

iii)

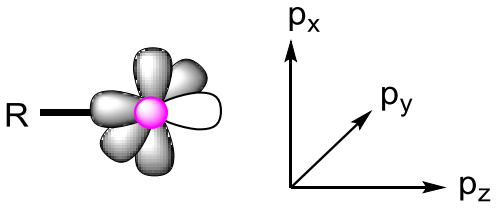

Figure 6. i) Representation of a halogen bond where the electron withdrawing group covalently bound to a donor atom induces an electropositive region which interacts with a Lewis base (A) ii) Electrostatic potential (ESP) in Hartrees projected on a surface of 0.001 au[32] of methane (A), chloromethane (B), bromomethane (C) and iodomethane (D).[33] iii) Halogen bond donor orbitals filled (dark lobes) and a region of electropositive area (empty lobe) suitable for interaction with a Lewis Base.

The halogen bond (XB) is the non-covalent interaction between an electron deficient halogen atom (X), which is covalently linked to an electron withdrawing group R, and a Lewis base (B) (Figure 6i).[21,34] The σ-hole is situated at the halogen atom pole and is more electropositive than the rest of the ESP of the halogen atom. Halogen bond strength increases from chlorine to bromine to iodine, as iodine is the largest, most polarisable and electropositive of the halogens (Figure 6ii).[21,33–36] XB interaction strength has been measured to be between 10-200 kJ/mol, comparable to HB.[21] Atomic orbital analysis of this interaction found low significance in hybridisation of halogens, thus electrons were found to be localised around the p_x, p_y and inner half of p_z orbitals, leaving the outer p_z orbital to be electron deficient (Figure 6iii).[33]

σ-hole interactions involving chalcogen bonding (ChB), pnictogen bonding (PnB), tetrel bonding (TB): In recent years, σ-hole interactions other than XB have started to gain research traction. The

rapid increase in interest led to the IUPAC workshop (Interactions Involving Group 14 - 16 Elements as Electrophilic Sites: A World Parallel to Halogen Bond, 2017, South Carolina, USA) where the scientific community discussed the definition, use of terms and emerging research in chalcogen bonding (ChB) (Group 16), pnictogen bonding (PnB) (Group 15) and tetrel bonding (TB) (Group 14). Although these names were coined recently, literature examples were found to have dated back more than 30 years ago.[37]

The chalcogen bond (ChB), like XB, involves the attractive interaction between a chalcogen (S, Se or Te) and a Lewis base (R-Ch---A) mediated by σ-holes on the chalcogen donor atom when bonded to an electron withdrawing group R. The Lewis acidity of heavier atoms in each periodic group increases as the size, polarizability and electropositivity increases with atom size. However, due to its polyvalent character, the electron distribution of these chalcogenide molecules leads to the formation of multiple σ-holes on the molecular electrostatic potential (ESP) (Figure 7). In particular, ESPs have been a popular visualisation tool for σ-hole energy values where perfluoro-covalently bonded halogen, chalcogen, pnictogen and tetrel group molecules were investigated *in silico* to calculate the strength of their σ-holes (Figure 7i).[38] Where iodine monofluoride possesses a single concentrated area of electropositivity, TeF_2 exhibits a more diffused electropositive area. Due to the geometry of SbF_3, the whole top of Sb is electropositive with a more intense belt around it while tetrel SnF_4 has pronounced pockets of σ-holes around its sides. In the molecular ESP calculated for iodopentafluorobenzene and benzotellurodiazole, the nature of donor atom (polarizability, electropositivity due to atom size) are similar, however the expression of σ-holes differ significantly (Figure 7ii).

i)

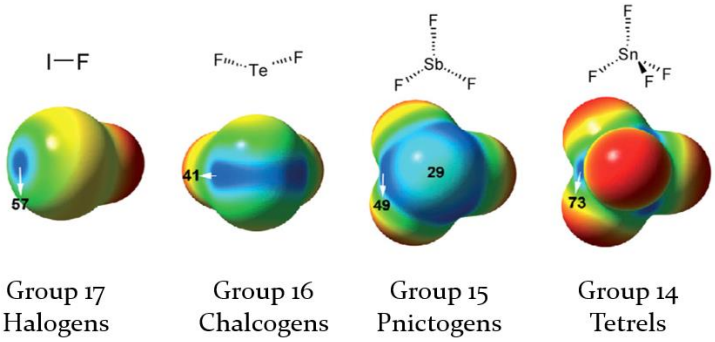

ii)

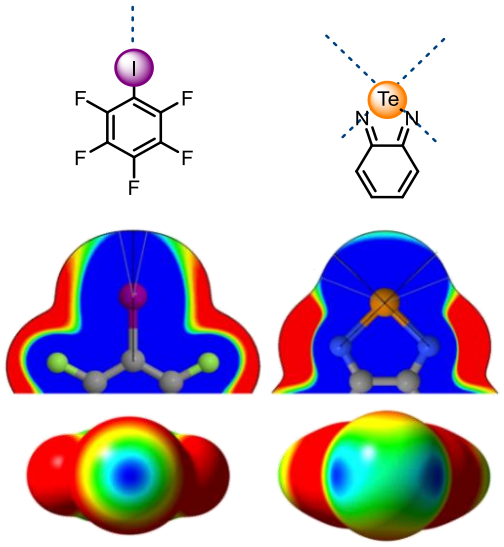

Figure 7. i) Molecular electrostatic potential calculated at the MP2/aug-cc-pVTZ level of theory with MEP energy values indicated in kcal/mol.[38] ii) ESP of C_6F_5I and benzotellurodiazole projected to an electron density of 0.001 electrons/bohr^3. Colour scale: 0.0 kcal/mol (red) to $V_{s,max}$ value at 0.001 electrons/bohr^3 (blue). Black lines show extension of covalent C-I or N-Te bonds while grey lines show σ-hole positions.[39]

Anion-π interactions involve the attractive interaction between an anion with an electron deficient (π -acidic) aromatic surface, stemming from electrostatic interactions and ion-induced polarisation.[40,41] Among the different π-interactions, the ones involving anions are less studied due to weaker binding. (Section 1.1.2) π-interactions are usually described with the use of quadrupole moment (Q_{zz}) which defines the charge distribution above and below the central plane of the aromatic system. π -basic arenes have negative Q_{zz} which is repulsive to anions, while π -acidic arenes have

positive Q_{zz} which can form attractive interactions with anions (Figure 8).[42,43] π- π interactions have been found to have strengths up to 50 kJ/mol. (Table 1)

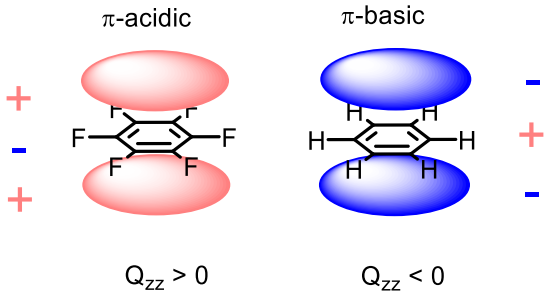

Figure 8. Representation of quadrupole moment (Q_{zz}) above and below plane of arenes where electronegative arenes (eg. hexafluorobenzene) have positive quadrupole moments and arenes such as benzene have negative quadrupole moments.

1.4. Synthetic Receptors for Anion Recognition

One of the key factors in anion host design is the choice of binding motif. Inspired by Nature, early reports of synthetic anion receptors exploited positively charged NH-based motifs such as polyammonium and guanidinium. Following which, the development of neutral NH-based receptors involving amide, urea, pyrrole and carbazoles started to gain popularity. CH-based receptors were less popular and not as widely investigated until crystallographic evidence of CH···Cl^- hydrogen bonding interactions were reported by Taylor and Kennard.[44] This was further highlighted in Desiraju and Steiner's book "The weak hydrogen bond" alongside examples of hydrogen bonding interactions involving haloalkanes.[45] Since then, reported examples of CH-based hosts for anion recognition have become widespread and it remains a popular motif. (HB, Section 1.4.1) Receptors bearing σ-holes for anion recognition have gained recent popularity,[46] stemming in particular from solid state crystal engineering halogen bonding (XB) materials[21] (Section 1.3).

This section discusses in detail cationic and neutral anion binding receptors that function *via* hydrogen bonding (HB), halogen bonding (XB) and chalcogen bonding (ChB) motifs. Positively charged receptors have traditionally been used to function in protic polar organic and aqueous media while neutral receptors operate largely in non-polar aprotic solvents. The ability to design receptors

that can function in a variety of solvents has led to their modification with reported groups for use as sensors. (Section 1.5)

1.4.1. Hydrogen Bonding Anion Receptors

Hydrogen bonding donor motifs are the most widely utilised in anion receptors. Their versatility and ease of incorporation facilitates the opportunity to design suitable anion host receptors taking advantage of the high directionality of HB interactions. Examples of motifs covered in this section include cationic and neutral NH- and CH-donors.

1.4.2. NH-based Anion Receptors

Positively Charged Anion Receptors

The first synthetic anion receptor reported in 1968 by Park and Simmons describes a macrobicyclic ammonium cryptand which, in acidic aqueous TFA solution was demonstrated to bind Cl^- via ^1H NMR studies (Figure 9i).[55] Subsequently, Lehn and co-workers developed a hexacationic polyammonium cryptand containing a cavity of complementary size and shape for the linear shaped N_3^- binding (Figure 9ii).[47] Protonation of the 6 NH motifs requires acidic conditions (pH < 3) limiting its use and that of related polyammonium hosts to certain pH windows. Having a pK_a of 13.5, the guanidinium-motif remains protonated over a wide range of pH and its preorganised Y-shaped HB donor capability is suitable for oxoanion binding.[48] A rigid chiral guanidinium based receptor was utilised for the recognition of aromatic anions, binding *p*-nitrobenzoate with an association constant of 1609 M^{-1} in $CDCl_3$ (Figure 9iii).[49]

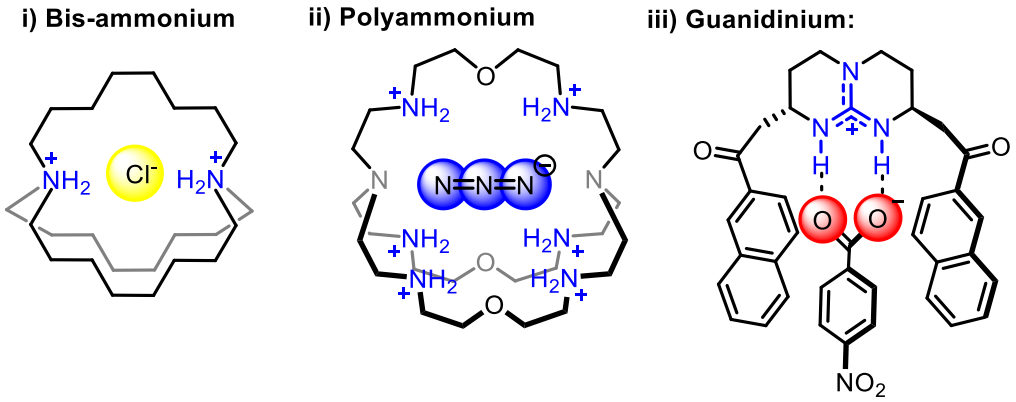

Figure 9. Charge-assisted NH-based anion receptors. Polyammonium receptors featuring i) Park and Simmons first macrobicyclic bis-ammonium cryptand[50] and ii) Lehn's hexaprotonated cryptand with an affinity for N_3^-.[47] iii) Guanidinium receptor with Y-shaped anion binding motif suitable for oxoanions.[49]

Neutral Anion Receptors

Amide bonds are commonly found in Nature making up peptide backbones in proteins such as the phosphate binding protein (PBP detailed in Figure 3i). Inspired by convergent HB interactions found in proteins, the first amide receptor was reported in 1986 by Pascal and co-workers.[51] They synthesised a neutral cage-like structure with three amide functionalities capable of forming hydrogen bond interaction with inorganic anions such as F^- in DMSO solution. During the ensuing years, numerous amide-based receptor systems have been reported. Kubik and co-workers described a "*molecular oyster*" which comprises of alternating *L*-proline and 6-aminopicolinic acid subunits forming a hexacyclic synthetic peptide (Figure 10i).[52] This biomimetic receptor forms 1:1 host-guest 'sandwich' complexes with SO_4^{2-} and I^- in highly competitive 1:2 H_2O/CH_3OH solvent systems where association constants were found to be 3.5×10^5 and 8900 M^{-1} respectively.

The highly acidic squaramide group has been put to use in acyclic and macrocyclic anion receptor design. Jolliffe and co-workers synthesised a series of macrocyclic squaramide-containing receptors which were found to exhibit remarkable affinity towards sulfate in DMSO/H_2O solvent mixtures (Figure 11).[53] They argued that the combination of cavity size complementary and preorganisation of the tetra-functionalised squaramide macrocycle was responsible for sulfate selectivity over other tetrahedral divalent anions such as selenate, phosphate and chromate. Replacing the benzene spacers

with 2,6-pyridine motifs further improved sulfate binding strength and degree of selectivity.[54] Sulfonyl squaramides[55] and sulfonylamides[56] have also been exploited for their high N-H acidity.

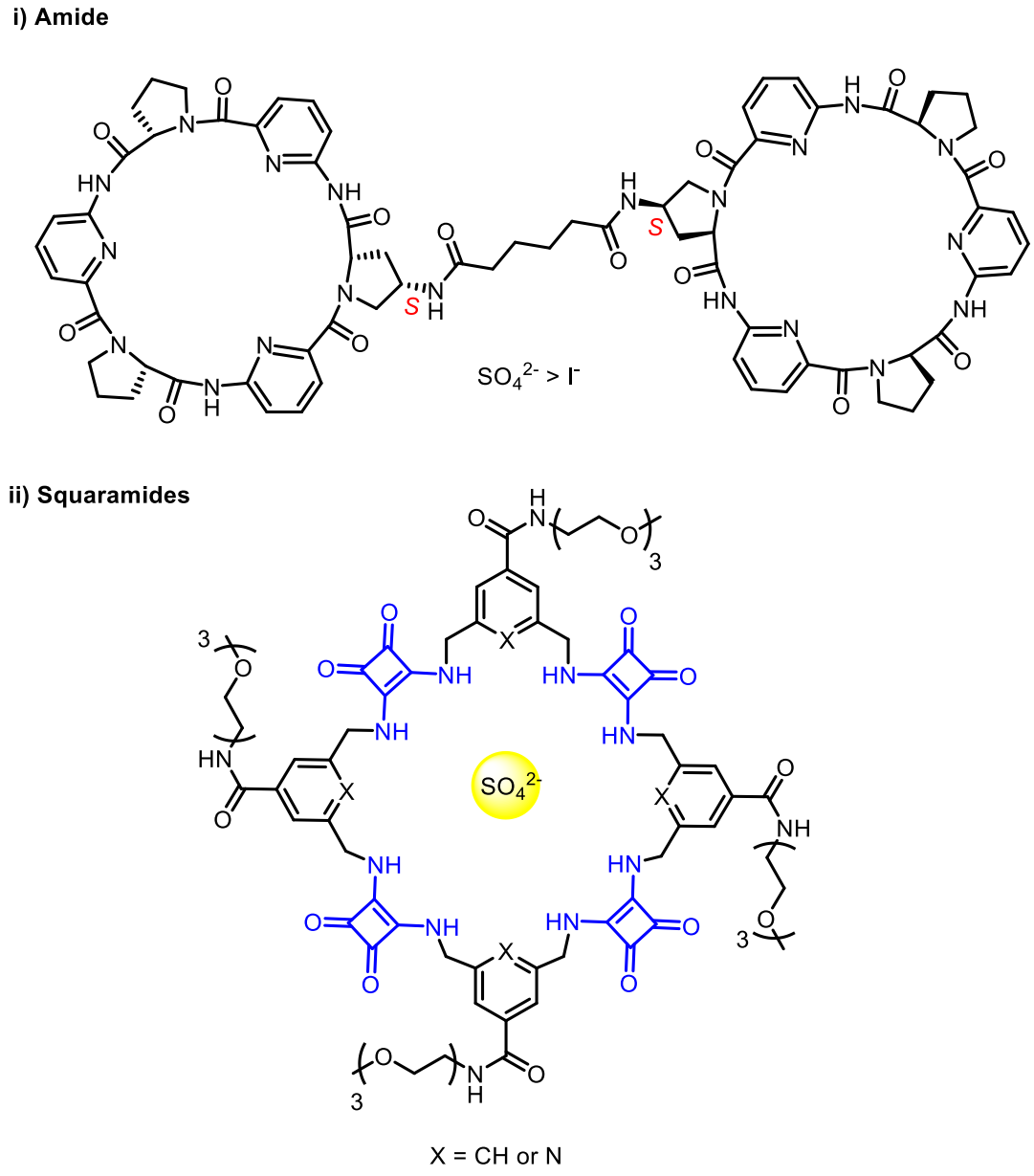

Figure 10. Hydrogen bond motifs arising from i) squaramides and ii) amides and sulfonylamide examples.

A popular HB-donor that has been extensively incorporated into anion receptors is the urea motif (Figure 11). It is synthetically accessible and the acidity of the N-H protons can be enhanced by changing the C=X substituent from O to S or Se. Exploiting the Y-shaped N-H donors, urea containing receptors have been widely employed for the recognition of anions with complementary geometry, for example carboxylates. Gunnlaugsson and co-workers reported a bis-urea-based

receptor with two urea binding sites designed to target dicarboxylate binding (Figure 11i).[57] By monitoring fluorescence changes of the anthracene spacer group, it was found that the urea anion receptor binds malonate (logβ = 2.66) and glutarate (logβ = 3.77) in DMSO. In another example, Reinhoudt and co-workers synthesised a macrocycle comprised of 4 urea units capable of binding $H_2PO_4^-$ within its cavity (Figure 11ii).[58] The macrocycle exhibits a 100-fold selectivity towards $H_2PO_4^-$ over Cl^- with an association constant of 4×10^3 M^{-1} in DMSO-d_6. Thiourea receptors functionalised with anthracene-glucopyranosyl groups were found to be capable of the chiral enantiomeric recognition of amino acids in acetonitrile (Figure 11iii).[59] Fluorescence titration studies revealed enantioselectivity of the thiourea receptor for L-Boc-alanine with an association constant of 23 900 M^{-1} and enantioselectivity of K_L/K_D = 10.4. Expanding on previously published tripodal urea and thiourea receptors as transmembrane anion transporters,[60] Gale and co-workers synthesised a tripodal selenourea receptorwhich exhibited Cl^- selectivity in acetonitrile with an association constant of 4.9×10^5 M^{-1} from UV-Vis titrations (Figure 11iv).[61]

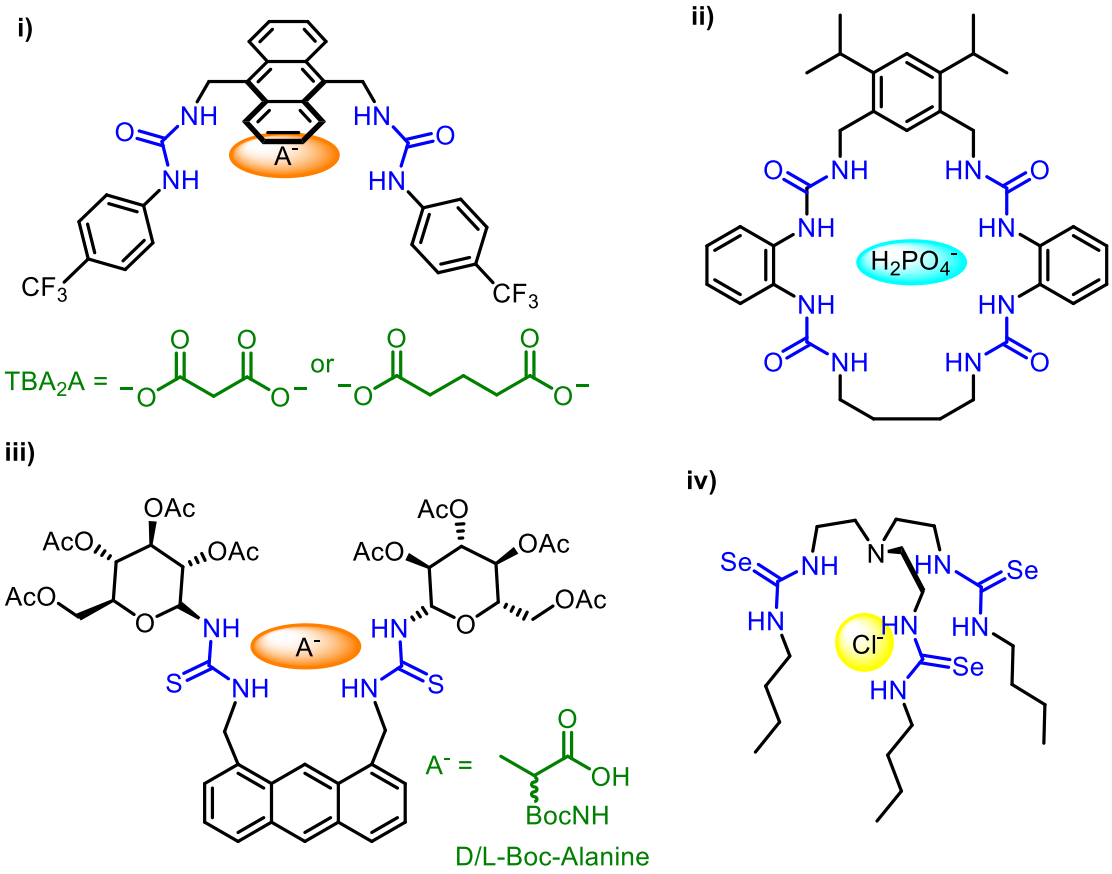

Figure 11. Neutral HB anion receptors bearing motifs.

Pyrrole is another robust NH-based HB-donor popularised by the pioneering work of Sessler and co-workers with the high-yielding one-step synthesis of calix[4]pyrrole[62]. In its simplest form shown in Figure 12i, the macrocycle was found have an affinity for F^- in DCM. Solid state evidence revealed the adoption of a cone conformation with the F^- guest sitting just above the plane of the macrocycle stabilised by 4 pyrrole NH···F^- hydrogen bond interactions.[63] Three indocarbazole motifs covalently linked together in a foldamer type structure was found to be highly selective for binding SO_4^{2-} with HB contributions from 6 NH and 2 OH groups in the binding site. The anion-induced structural conformational change also led to a red-shift in the foldamer's emission wavelength, from which an association constant of 6.4×10^5 M^{-1} (10% v/v CH_3OH/CH_3CN) was determined (Figure 12ii).[64]

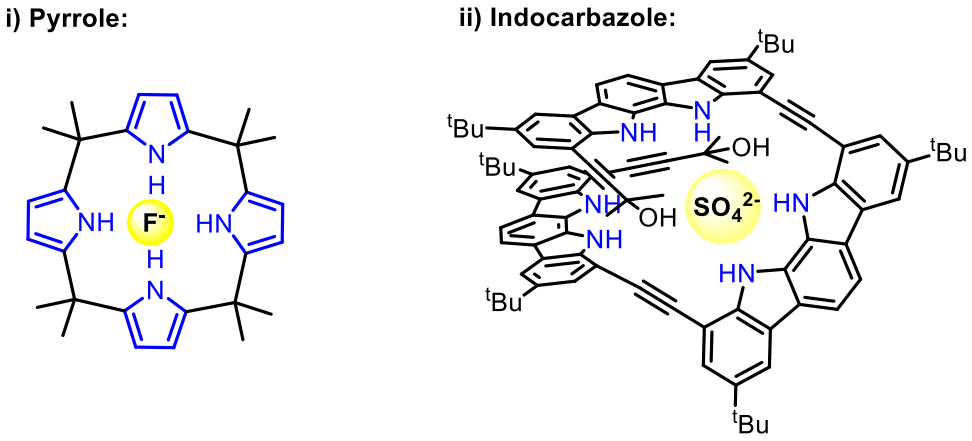

Figure 12. Hydrogen bond motifs arising from i) pyrrole-based receptor as a Cl^- receptor and ii) Indocarbazole with an affinity for SO_4^{2-} in highly competitive organic solvent mixture.[64]

1.4.3. CH-based Anion Receptors

Neutral Anion Receptors

Hydrogen bonding CH···anion interactions are generally weaker than their NH- or OH- analogues because of the greater electronegativity of the N and O atoms[65]. One of the early examples was from the work of Farnham, Dixon and co-workers where a fluorinated macrocyclic ether bound F^- interacting with CH_2 hydrogens (Figure 13i).[66] More recently, Sessler and co-workers took advantage of an aromatic $CH\cdots X^-$ interaction from a phenyl ring incorporated into a strapped calix[4]pyrrole receptor to efficiently bind Cl^- within its cavity (Figure 13ii).[67] Stronger Cl^- binding was observed in the strapped receptor (2.2×10^6 M^{-1}) compared to free calix[4]pyrrole (2.2×10^5 M^{-1}) in acetonitrile.

With the emergence of 'click' chemistry, there has been a surge of popularity in triazole-based motifs in anion receptor design due to their ease of incorporation. In an example provided by Flood and co-workers, a triazole-based macrocycle (Figure 13iii - left) displayed significant hydrogen bond interactions forming a 1:1 host-guest complex with HF_2^-, as evidenced through ^1H NMR studies as well as UV-vis titrations in CH_2Cl_2.[68] Building upon this work, Flood and co-workers recently reported a triazole cryptand with an exceptional affinity to Cl^- (10^8 M^{-1}) in polar DMSO (Figure 13iii

- right).[69] Solid state structural evidence revealed Cl^- stabilised by 6 short CH··· Cl^- hydrogen bonds from triazoles and 3 contacts from phenylenes.

As CH···anion interactions are known to be weak, neutral receptors with CH-motifs that can bind anions in water are uncommon. One such example is the bambusuril macrocycle described by Sindelar and co-workers[70]. The water soluble bambus[6]uril receptor (Figure 13iv), consisting of six repeating units of glycouril with methylene bridges, binds weakly hydrated anions such as BF_4^-, PF_6^- and ClO_4^- with association constant values of up to $5.5 \times 10^7\ M^{-1}$ for the latter anion (D_2O, 20 mM K_2DPO_4, pD 7.1). They concluded that the host-guest complex is stabilised by multiple weak CH···A^- hydrogen bond interactions from the methylene units that form an equatorial position in the macrocycle.

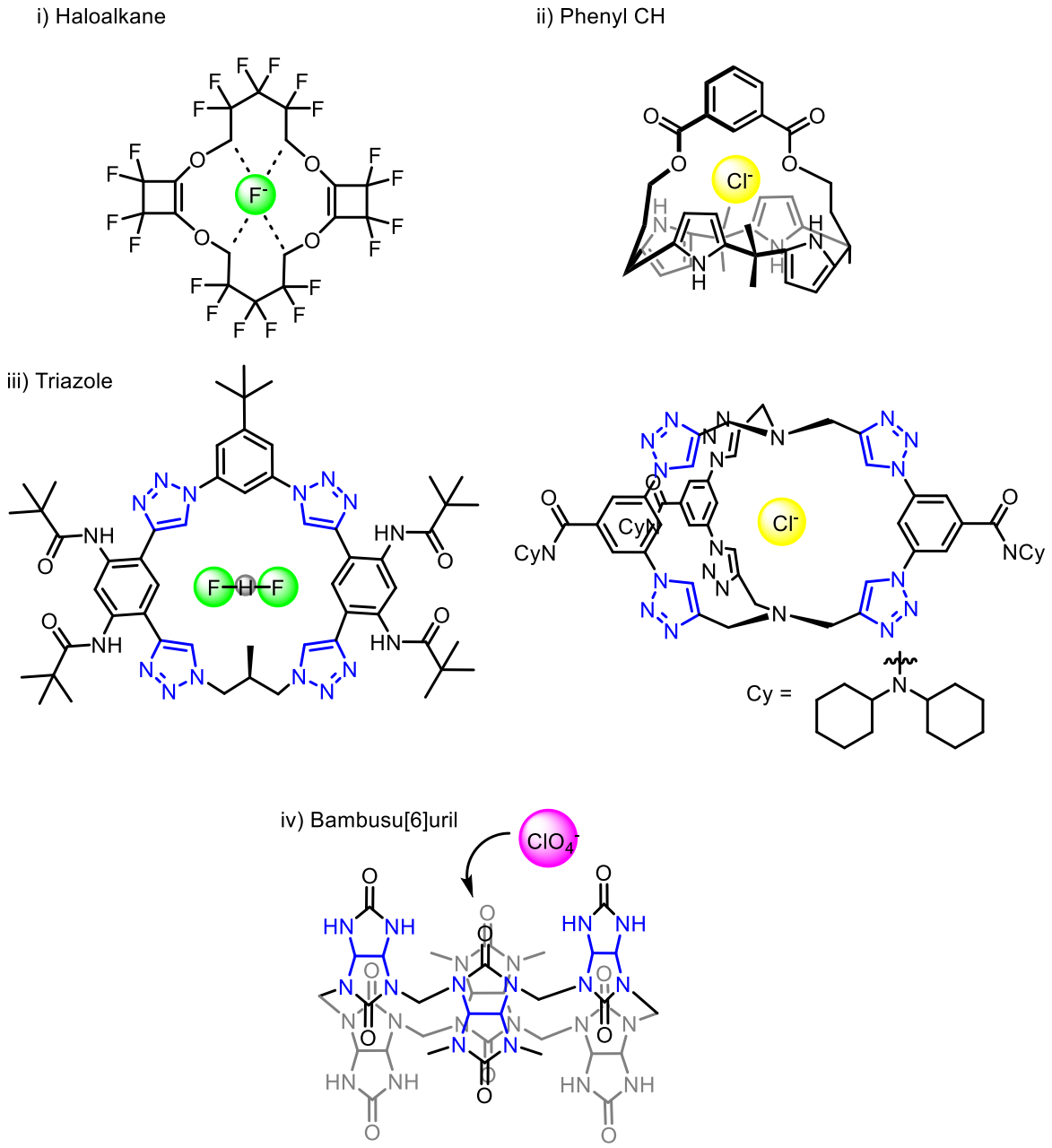

Figure 13. Neutral CH-based anion receptors. i) Farnham and Dixon's fluorinated ether macrocycle[66], ii) Sessler and Hay's strapped calix[4]pyrrole,[67] iii) Flood's triazolophane macrocycle[68] binding HF_2 and cryptand with strong affinity to Cl^-[69] with iii) Sindelar's Bambusu[6]uril.[70]

Cationic C-H Anion Receptors

Cationic CH···A^- interactions are characterised by strong electrostatic contributions, in particular imidazolium motifs have a positive partial charge between the nitrogen atoms.[71] Amendola and co-workers synthesised a tripodal imidazolium receptor which binds Cl^- within the tripod cavity (Figure 14i).[71] An x-ray crystal structure revealed three short CH···A^- contacts from the tripodal arms and 5

long CH interactions from neighbouring methylene units. The receptor appended with electron withdrawing pentafluoro benzene substituents displayed strong binding of Cl^- in competitive CD_3CN/D_2O mixtures. The positively charged triazolium motif has also been exploited for anion recognition studies. In Pandey and co-workers' on-going interest in steroid-based receptors, they incorporated two triazolium motifs as anion binding sites (Figure 14ii).[72] The meta-substituted macrocycle was found to have an affinity for F^- (560 M^{-1}) while its para-substituted cyclic analogue displayed an affinity towards $H_2PO_4^-$ (1100 M^{-1}) in $CDCl_3$. More recently, Kim and co-workers prepared a polyether linked calix[2]triazolium[2]arene structure that was shown to exhibit selectivity for $H_2PO_4^-$ in acetonitrile (Figure 14iii).[73]

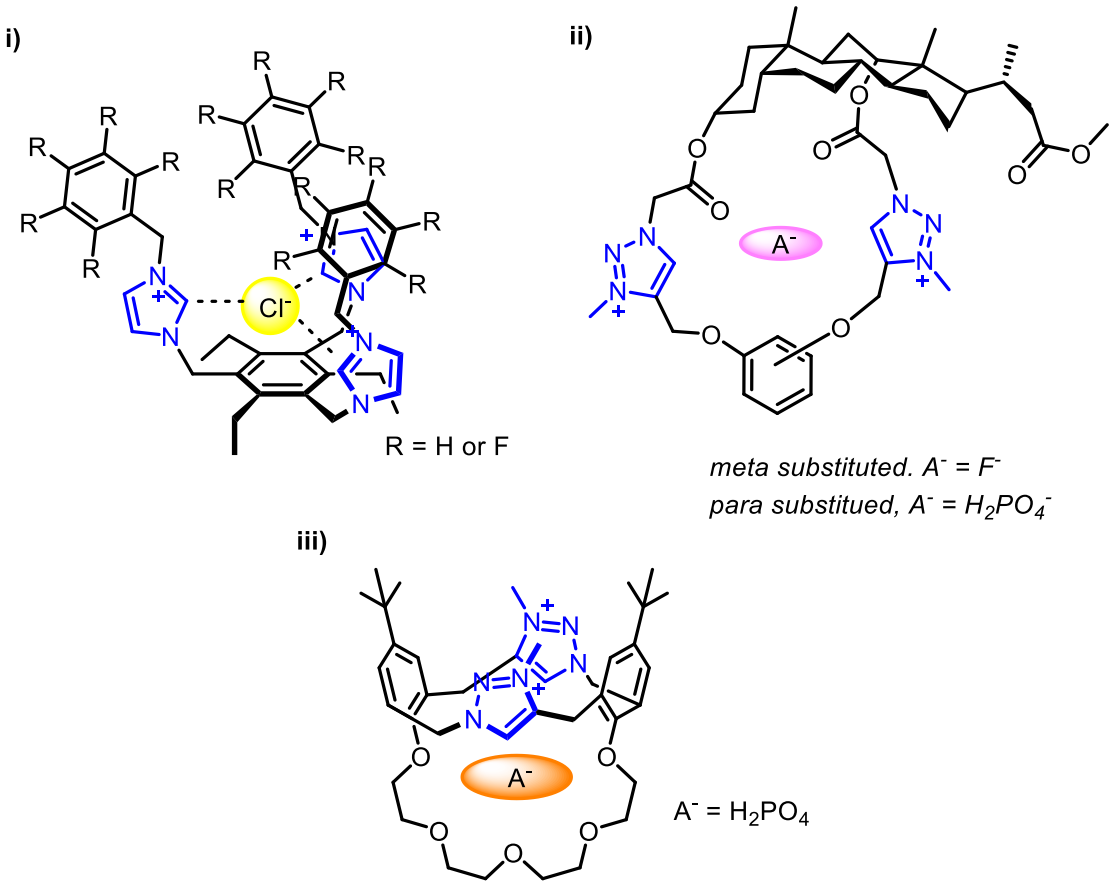

Figure 14. Cationic CH-based motifs in anion receptors. i) Amendola and co-workers imidazolium tripod, ii) Pandey and co-workers steroid-based triazolium macrocycle and iii) Kim and co-workers crown ether calix[2]triazolium[2]arene macrocycle.

1.4.4. Halogen Bonding Receptors

Originating in the areas of solid-state crystal engineering and materials chemistry,[21,46] halogen bonding (XB) has recently emerged as a promising and powerful non-covalent interaction for anion recognition. This σ-hole interaction is highly directional and of comparable strength to HB[21,22] (Section 1.3). Importantly, XB receptors have been found to exhibit stronger anion binding affinities compared to their hydrogen bonding (HB) analogues.[74–77]. This section will discuss anion receptors with halogen bond donor motifs bearing different electron-withdrawing functionalities such as neutral perfluoroarene and triazole units, cationic triazolium, imidazolium and metal-enhanced XB interactions.

Neutral XB Anion Receptors

Commonly used in solid state crystal engineering studies,[78–80] iodoperfluoroaryl derivatives have been employed in anion receptors (Figure 15).[81] One of the first examples was reported in 2005 by Resnati and Metrangolo using a heteroditopic XB tripodal host that binds NaI with an association constant of $2.6 \times 10^5\ M^{-1}$ in $CDCl_3$, 20-times more strongly than its perfluoroaryl analogue (Figure 15i).[82] Due to the para-position of iodine atom substituent, convergent XB interaction from all three arms of the tripod was not possible. Taylor and co-workers synthesised an ortho-substituted iodoperfluoroarene tripod where convergent XB resulted in the receptors' strong affinity towards halides ($Cl^- > Br^- > I^-$) in 1:1 host-guest stoichiometry (acetone-d_6) (Figure 15ii).[81]

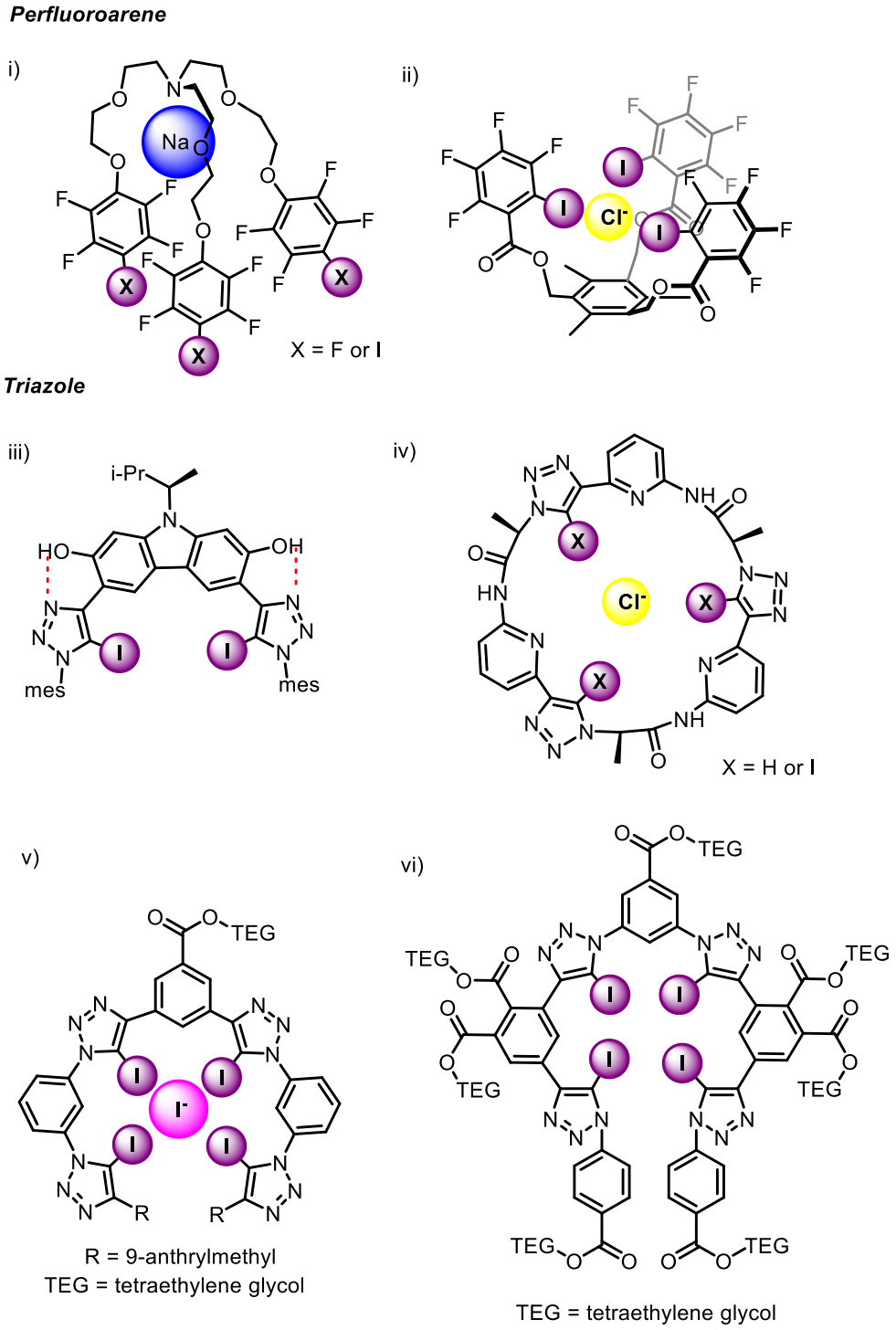

Figure 15. Neutral XB-donor anion receptors. Perfluoroaryl motifs i) Resnati's XB-tripod exhibiting ion-pairing effect from binding NaI.[82] ii)Taylor's preorganised XB tripod.[81] Triazole motifs such as iii) pre-organised bidentate triazole[83] iv) tridentate psudopeptide macrocycle[84] and v) tetradentate triazole receptor.[85]

Another popular XB anion binding motif is the 5-iodo-1,2,3-triazole, which has been widely employed due to its ease of synthesis via Cu(I)-catalysed azide-alkyne 1,3-dipolar cycloaddition

'click' reaction. A bidentate example employing iodotriazole units was reported by Schubert and co-workers studying the effect of preorganisation (Figure 15iii).[83] They found that the receptor with preorganised iodotriazoles, due to intramolecular $N_{trz}\cdots HO_{carbazole}$ HB interactions, exhibited a strong increase in halide anion binding affinity relative to the analogous XB carbazole receptor without the phenolic functionality. A macrocyclic pseudopeptide with three iodotriazole units described by Kubik, displays a high affinity for Cl^- in a competitive solvent mixture, *log* K_a = 3.28 in DMSO-d_6 (with 2.5 % H_2O) (Figure 14iv) attributed to the rigidity of the macrocycle[84]. The foldamer type tetradentate XB receptor reported by Beer and co-workers, exhibited a preference for larger, softer anions =I^- > Br^- > Cl^- ≈AcO^- ≈ $H_2PO_4^-$ in $CDCl_3$ (Figure 15v).[85] Through the peripheral attachment of tetraethylene glycol (TEG) functional groups, the XB foldamer was demonstrated to be highly selective for binding I^- in pure water (Figure 15vi)[86], forming a dimeric 2:1 host-guest complex assembly stabilised *via* multiple convergent σ-hole···halide and hydrophobic interactions.

Positively charged XB Anion Receptors

The XB halo-imidazolium motif [87,88] was incorporated into anion receptor design by Ghosh and co-workers who investigated the anion binding properties of a tetracationic iodo-imidazolium receptor (Figure 16i).[89] Through ^{13}C NMR and ITC experiments a 1:2 host-guest stoichiometric binding in acetonitrile was determined where the strongest complex was formed with Cl^- (K_a = 1.35×10^6 M^{-1}). X-ray crystal structures confirmed the participation of two diagonal haloimidazolium group XB interactions with halides where C_{imi}-I···Br^- was found to be 3.117 Å (81 % of the vdW radii with an almost linear XB angle of 179.23°).

The pyrrole-dicationic iodotriazolium hybrid receptor featuring both XB and HB-motifs (Figure 16ii) is capable of the selective binding of tetrahedral oxoanions ($H_2PO_4^-$ and SO_4^{2-}) over halides in the competitive CH_3CN/H_2O 9:1 v/v solvent mixture, attributed to the wider XB bidentate bite angle that provides size complementary for the larger oxoanions.[90]

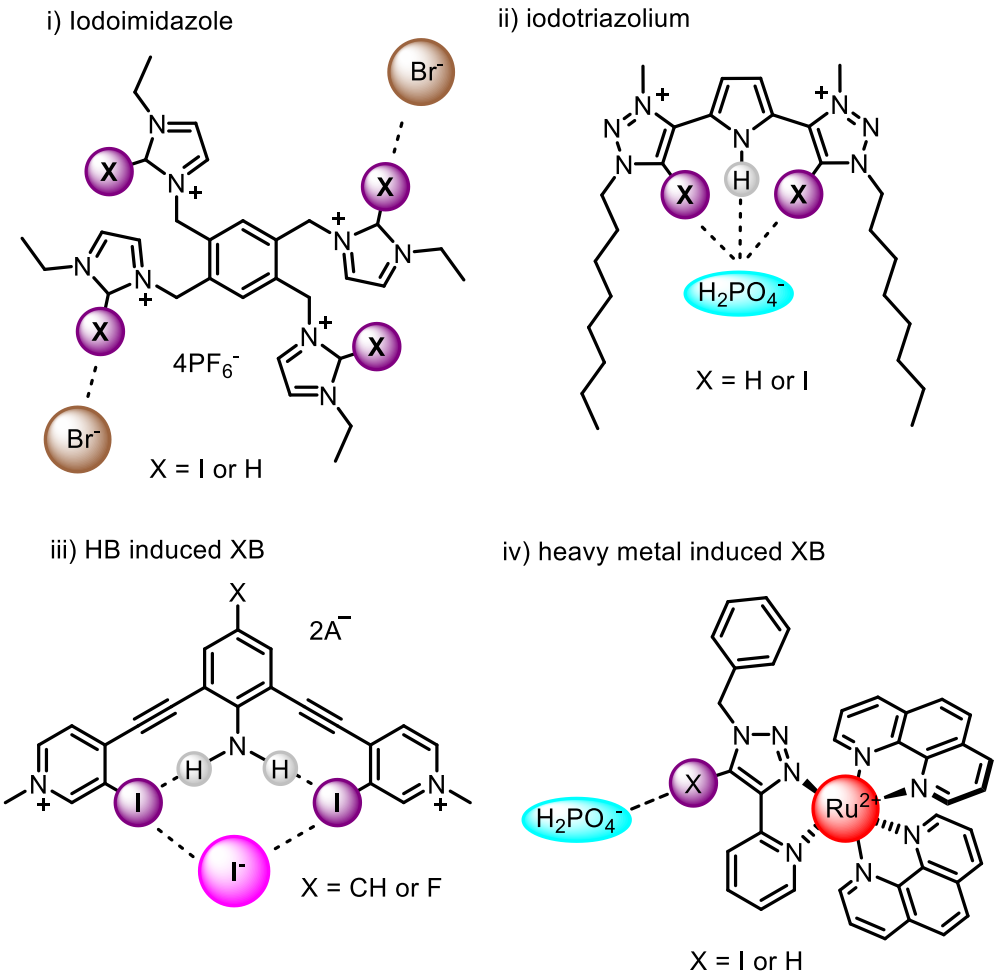

Figure 16. Cationic XB Anion receptors. i) Ghosh's tetrapodal cationic motif that binds Br- in a 1:2 host guest stoichiometry,[89] ii) Beer's hybride HB/XB receptor capable of binding $H_2PO_4^-$,[90] iii) Berryman's HB induced XB interactions leading to the formation of a 1:1 host-guest complex[91] and iv) Ghosh's Ru^{2+} enhanced XB interaction binding $H_2PO_4^-$ in a 1:1 host-guest complex.[92]

Other than cationic charge assisted enhanced XB, direct intramolecular hydrogen bonding to the halogen atom has been shown by Berryman and co-workers to further increase XB donor potency in an acyclic pyridinium receptor (Figure 16*iii*).[91] To prevent the rigid alkyne linked arms from freely rotating, the central phenyl group of the receptor is amine functionalised. Through DFT calculations, they found the augmented strength of the σ-hole to be attributable to HB induced XB (N-H···I) as evidenced through solid state crystal structures showing the $-NH_2$ substituent forming intramolecular HBs to both XB iodine donors with N···H···I distance to be 2.94 Å and 3.00 Å and angles of 168° and 170°. This effect is seen in the receptor's remarkedly increased affinity to halide binding where I^- has an association constant of 36 900 M^{-1} in a $CDCl_3/CD_3NO_2$ (2:3 v/v) solvent mixture. It has

previously been reported that complexation of Ru^{2+} enhances the acidity of the triazole proton rendering it an efficient anion binding motif with contributions from metal-enhanced second-sphere anion recognition mechanisms.[93–95] Ghosh and co-workers described a Ru^{2+} based receptor with a ligand containing iodotriazole motif (Figure 16 iv) that has an affinity towards $H_2PO_4^-$ (K_a = 1.94 × 10^5 M^{-1} in DMSO), as determined by monitoring anion binding induced perturbation of the MLCT emission band.[92]

1.4.5. Chalcogen Bonding Receptors

The application of ChB in anion recognition is only beginning to be explored, with the first ever reported chalcogen motif used for anion binding involving a bidentate boryl-telluronium moiety as Lewis acidic sites (Figure 17i). Gabbai and co-workers determined the receptor to be F^- selective in methanol[96] (K = 750 M^{-1}). Subsequently, Zibarev and co-workers[97] reported crystal structures showing evidence of chalcogen bonding between 3,4-dicyano-1,2,5-telluradiazole, iodide and a $[K(18\text{-crown-6})]^+$ complex. Iodide association constants were found to be K_a = 6.8 × 10^5 M^{-1} in CH_2Cl_2 and 1.5 × 10^3 M^{-1} in CH_3CN *via* UV-Vis spectroscopy (Figure 17ii). At the same time, Taylor and co-workers developed a range of chalcogenadiazoles to study their potential as chalcogen bond donor units for anion binding (Figure 17iii).[98] In this detailed paper, a linear free energy relationship was reported between ChB bond donor ability and electrostatic potential of the chalcogen centre. The telluro receptor binds Cl^- selectively with an association constant to be 38 000 M^{-1} in THF. Matile and co-workers[99] utilised fused-thiophenes for anion transport studies. Focusing on the strongest Cl^- binding sulfone bridged bis-cyano receptor (Figure 17iv) (K_d = 1.13 ± 0.03 mM in THF), they determined a correlation between σ-hole bond strength and anion transport activity.

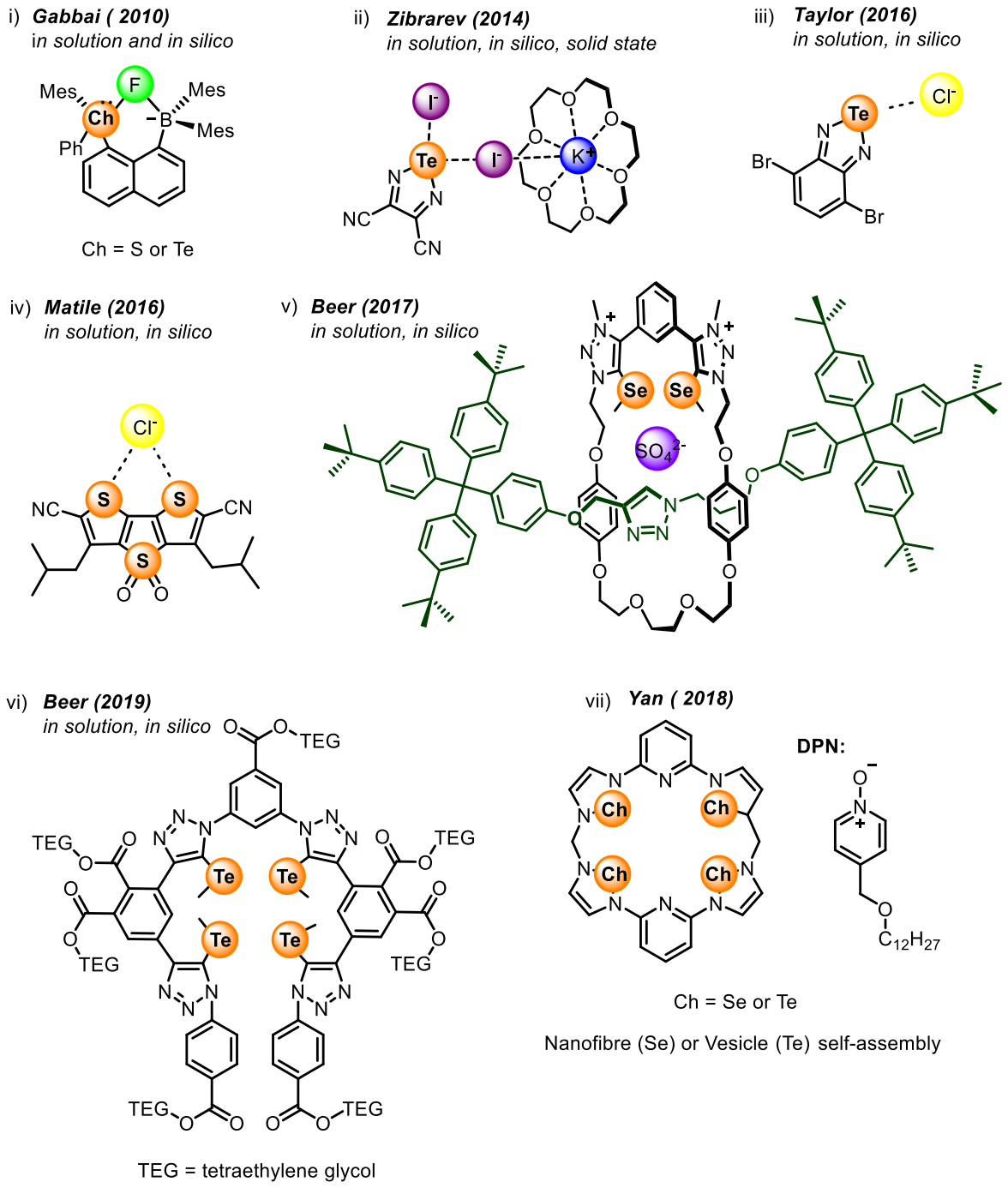

Figure 17. Chalcogen containing motifs for anion recognition.

More recently, Beer and co-workers[100] synthesised the first chalcogen containing neutral and dicationic interlocked structure where they demonstrate by ^{1}H NMR (acetone-d_6), X-ray crystal structure and DFT calculations that chalcogens are capable of acting as both Lewis basic donor ligands for metal cation binding (Cu^{+}) and as Lewis acids for anion binding via σ-hole interactions (Figure 17v). The Se-receptor has a strong affinity to SO_4^{2-} with an association constant of 3531

M^{-1} in 1:4 D_2O/acetone-d_6. The same group prepared the first neutral water-soluble tetra-tellurotriazole foldamer with selectivity for iodide (Figure 17*vi*).[86] Due to the large size of the -$TeCH_3$ binding motif, the coordinated halide anion is held above the plane of the receptor. ITC experiments carried out in pure H_2O and molecular dynamics simulations support a 2:1 stoichiometric host-guest complex for binding I^- (2.64×10^7 M^{-2} in H_2O) via multiple convergent ChB σ-hole interactions.

Self-assembly via chalcogen bonding has also been demonstrated where a selenium macrocycle interaction with a surfactant 4-dodecyl-pyridine N-oxide (DPN) results in the self-assembly of a nanofiber, while the tellurium macrocycle interaction with DPN produces the self-assembled structure of a bi-layered lipid-like vesicle in an organic-aqueous solution (1:2 v/v, THF/H_2O) (Figure 17 vii).[101] Both assembly processes were found to be reversible *via* competitive binding of halide ions.

Having received increasing attention in recent years, ChB has also found applications in organocatalysis,[102] for example the hydrogenation of quinolines with neutral ChB-receptors.[103]

1.5. Anion Sensing

In addition to the recognition of anions, it is also desirable for anion receptors to possess a reporter group, whereupon binding, a macroscopic response provides a detection mechanism for sensor applications. Optical reporter groups employed include pyrene (fluorescence response), transition metal centres (luminescence response) as well as ferrocene for electrochemical sensor appications.[104] Displacement assays have also been used successfully where the binding of the target anion leads to the displacement of a weakly coordinating fluorophore triggering an optical change.[105] Lastly, the irreversible chemodosimeter approach involves the receptor undergoing a chemical reaction with the anions.[106]

1.5.1. Optical and Electrochemical Anion Sensing

As mentioned above, common reporter groups integrated into anion receptor structural frameworks are the fluorescent pyrene and redox-active ferrocene motifs. Molina and co-workers have combined both in the ferrocene-napthalene dyad receptor (Figure 18i).[107] Fluoride binding in DMSO caused a significant fluorescent enhancement (12-fold) and a cathodic shift in the receptor's ferrocene/ferrocenium oxidation wave (190 mV). Another popular optical signalling strategy is through the assembly (or disassembly) of excimers which is often accompanied by significant changes in the fluorescence. Pyrene is a popular motif for this application where monomer fluorescence peaks consist of sharp signals between 350-425 nm while excimer fluorescence reveals a broad peak at *ca.* 480 nm. This was utilised in a pyrene-functionalised guanidinium receptor selective for pyrophosphate ($P_2O_7^{4-}$; PPi) where the bidentate binding of the anion leads to a 2:1 host-guest stoichiometry binding of the anion in methanol resulted in excimer formation (Figure 18ii).[108]

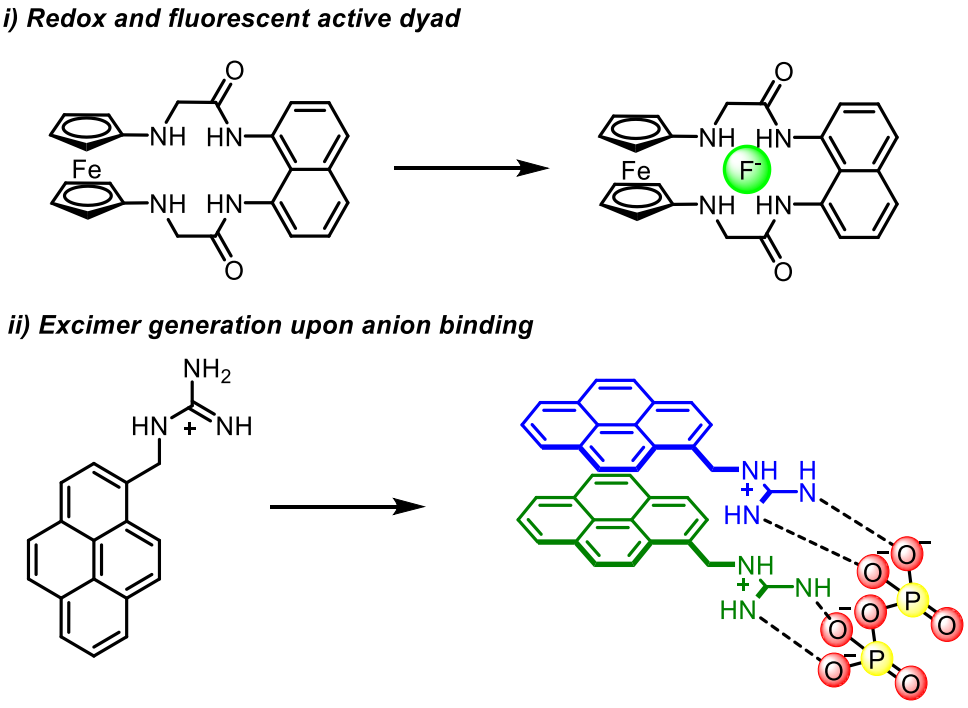

Figure 18. Reporter groups like ferrocene or pyrene/naphthalene can generate a redox or fluorescence response, respectively.

1.5.2. Displacement Assays

Indicator displacement assays involve the exchange of a dye indicator from the host upon anion binding causing an optical change in its photophysical properties. In a dinuclear Zn^{2+} colourimetric sensor (Figure 19), naked eye detection is due to the displacement of the pyrocatechol violet (PV) indicator where the complexed PV is blue and free PV is yellow-green.[105] Upon addition of pyrophosphate (PPi) anions, a 2:2 host guest complex is formed and the PV is released changing the solution to a yellow-green colour; the sensor is selective for PPi in MeCN/H_2O (8:2 v/v) solution.

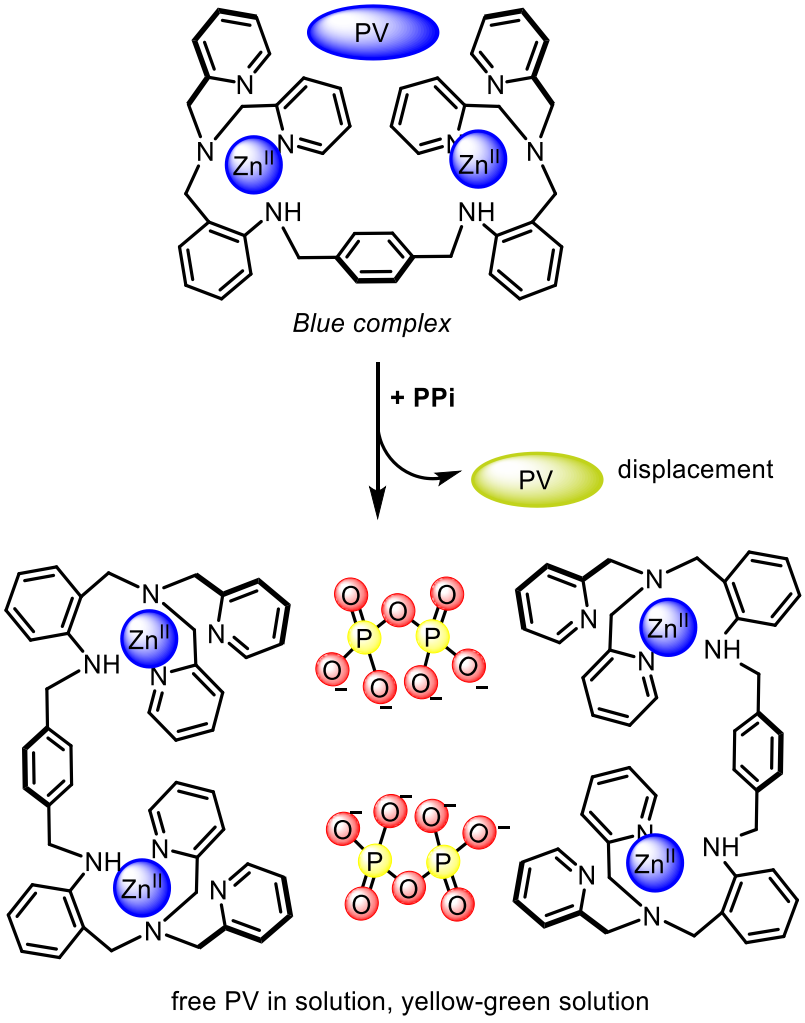

Figure 19. Indicator displacement assay of a dinuclear zinc complex, pyrophosphate (PPi) as anion guest and pyrocatechol violet (PV) as displaced dye indicator.[105]

1.5.3. Chemodosimeter Approach

Fluoride, in the form of TBAF, is commonly used in the deprotection of the trimethylsilyl-protected motif due to strong Si-F bond formation. A diketopyrrolopyrrole (DPP) dye with appended thiophene functionality capable of interacting with anions has been used as a F^- selective anion sensor (Figure 20i top).[109] Using TBAF as a deprotecting agent, the DPP receptor demonstrated a fluorescent change upon consumption of F^-. This reaction was tracked by its optical change where free F^- induces a blue spectral shift in fluorescence emission and absorption. Another chemodosimeter approach is the use of molecules with a high quantum yield like boron subphthalocyanine (Figure 20i bottom). Its axial position is easily substituted and upon replacing 4-hydroxybenzaldehyde with fluoride, fluorescence is quenched signalling the binding of fluoride ion in THF.[110] The chemodosimeter approach can also be used in rearrangement reactions, for example a cyanide-induced benzyl rearrangement reaction can be monitored *via* UV-Vis spectroscopy where a blue shift from 412 nm to 356 nm in methanol is caused by a change in structural conjugation (Figure 20i).[111]

i) ***Chemodosimeter for Fluoride***

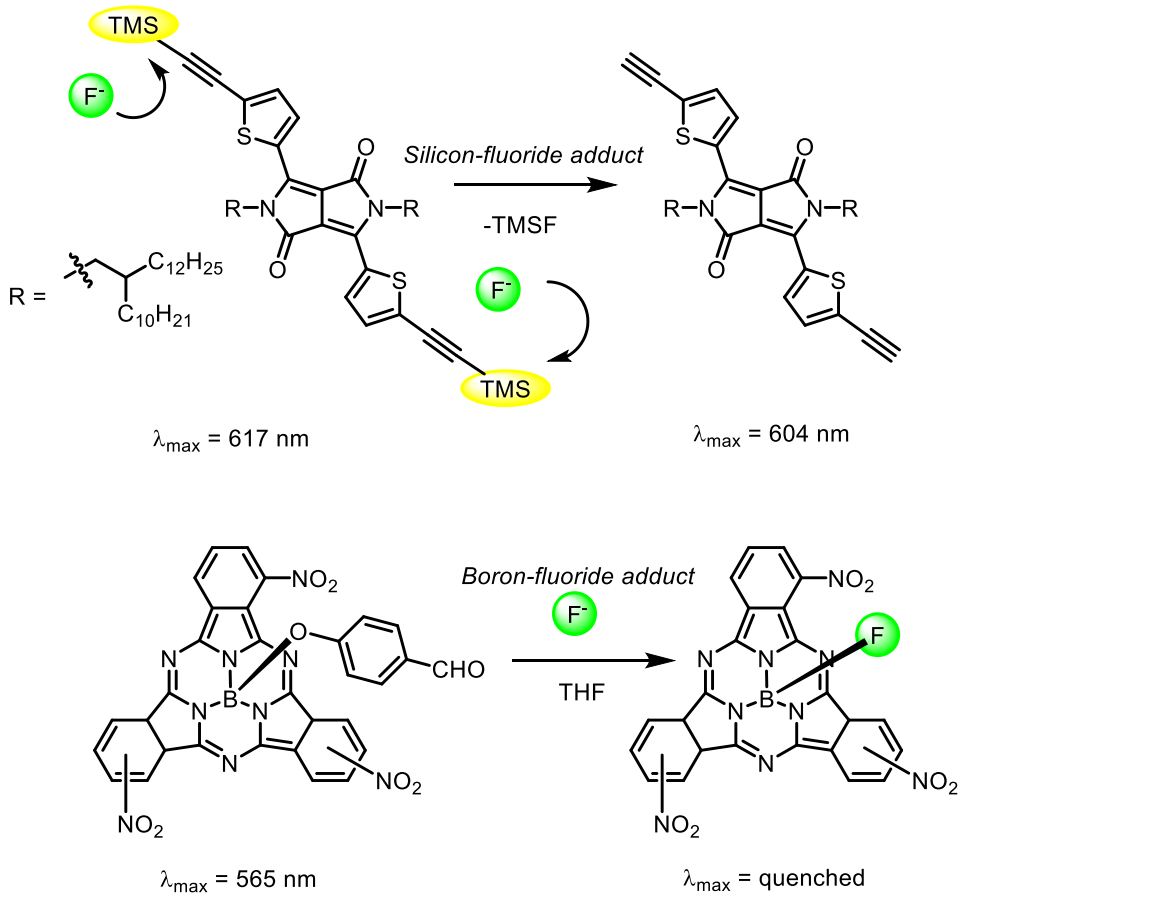

ii) ***Chemodosimeter for Cyanide***

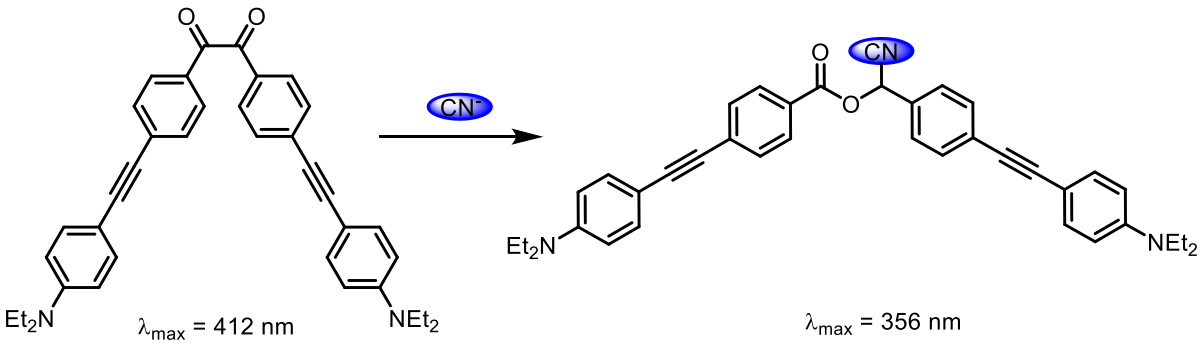

Figure 20. Chemodosimeter anion sensor examples binding fluoride and cyanide.

1.6. Strategies for the Synthesis of Mechanically Interlocked Molecules (MIMs)

1.6.1. The Mechanical Bond

The mechanical bond is the coming together of two or more components not by chemical bonds but by virtue of entanglement and interlocking. Such entities surround us in nature and can be found in proteins[112] as well as mitochondrial DNA[113] (DNA-[n]catenane or circular DNA) or even in technologies such as DNA nanoengineering.[114,115]

Relatively new in chemistry, mathematicians have been fascinated by knots and links for a very long time. Inspired by Lord Kelvin, mathematician Tait paved the way to the study of knots and the formulation of the mathematics of topology. Given the mathematical theory for interlocking systems, chemists seek the unique topology and cavity within these structures as a means to build synthetic receptors which have come to have very useful applications.

Mechanically interlocked structures can be prepared through various strategies. Two common structures are i) a catenane where two (or more) macrocycles are mechanically interlocked and ii) a rotaxane which involves an axle (usually stoppered by bulky groups to prevent extrusion of the macrocycle along the axle) and a macrocycle. Synthetic strategies to form these mechanically interlocked molecules (MIMs) involve the pre-formation of a pseudorotaxane, which upon using a variety of methodologies such as clipping, stoppering, slippage, shrinking, swelling and snapping, (Figure 21) affords the final mechanically bonded molecule. By *clipping* of a pseudorotaxane (e.g. via ring-closing methathesis), a [2]catenane is formed; where 2 is the number of entities that are mechanically interlocked. On the other hand, by *stoppering* both ends of a pseudorotaxane with bulky groups gives a [2]rotaxane. The bulky groups can also be modified by *shrinking* and/or *swelling* either chemically or via an external stimulus. Macrocycles can also be slipped (*slippage*) onto a pre-formed axle or it can be shrunk (*shrinking*) so it becomes small enough to prevent de-threading. *Snapping* is the formation of two halves of an axle within the macrocylic cavity while *clipping* is the closing of the macrocycle around an axle.

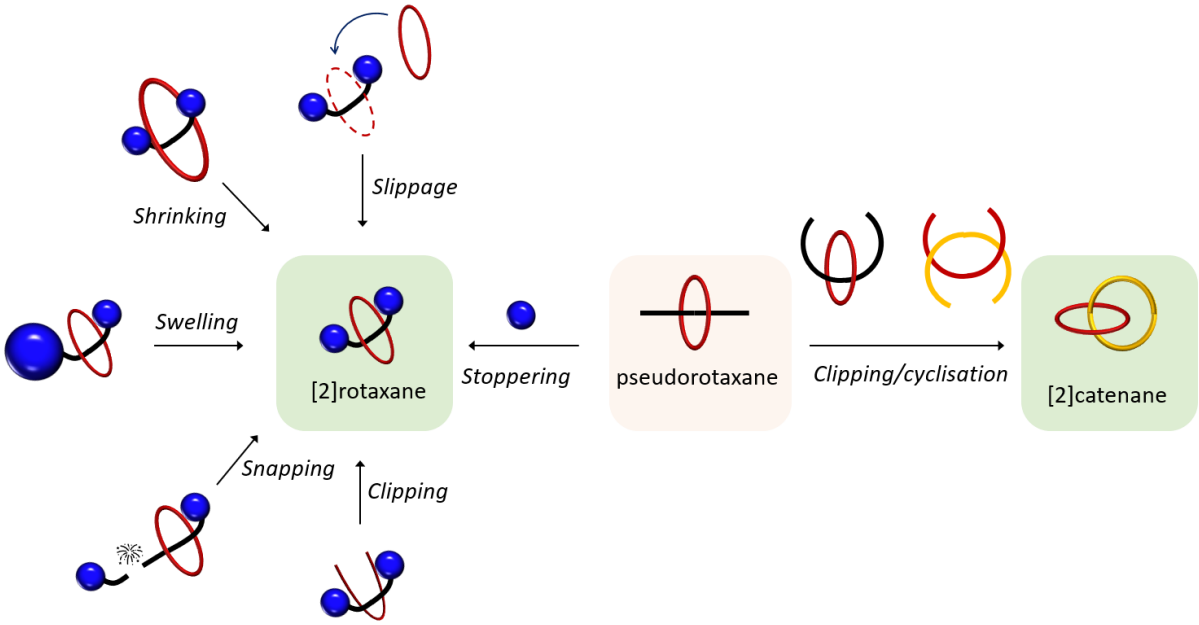

Figure 21. Various techniques for the synthesis of mechanically interlocked structures.

1.6.2. Pre-Template Synthesis Era

In 1960, Wasserman reported the first evidence of a mechanically interlocked structure between a cyclic acyloin and a cyclic hydrocarbon through statistical synthesis resulting in what he suggested was a topology similar to that of a catenane.[116] After the publication of "Chemical Topology" by Frisch and Wasserman, detailing the limitations of statistical methods, Schill & Lüttringhaus[117] synthesised and isolated a [2]catenane via covalent bond directed synthesis. Soon after, Harrison and Harrison isolated the first [2]rotaxane which they tried to name hooplane.[118] The isolation of these mechanically interlocked structures were the first evidence that such structures could indeed be achieved synthetically, however, the multiple steps taken gave extremely low yields.

1.6.3. Template-Directed Synthesis

The use of template-directed strategies to assemble the two components of a pseudorotaxane has greatly improved the synthetic yield of MIMs. This has been achieved by metal cation coordination, donor-acceptor interactions, hydrogen bonding, anion binding and hydrophobic interactions. The following sections discuss the different types of templates employed and the plethora of architectures obtained as a result.

1.6.4. Metal Cation Templates

The first example of a metal cation template used for the formation of mechanical bonds was introduced by Sauvage and co-workers in 1983. As noted earlier in Figure 2, binding a Cu(I) ion to two phenanthroline ligands gave an orthogonal, tetrahedral metal complex, which upon undergoing a double ring clipping ether reaction afforded the [2]catenane in a yield of 27% (Figure 22i).[4] Subsequently, a single ring clipping Grubbs' catalyst ring-closing metathesis reaction improved the [2]catenane yield up to 92% yield (Figure 22ii).[119] Since then a variety of transition metal cation templates with a range of stereochemical ligand fields such as square planar (Pt^{2+})[120], octahedral (Ru^{2+})[121], trigonal bipyramidal (Zn^{2+})[122] and linear (Au^{+})[123] have been utilised to form a variety of interlocked structures of different topologies.

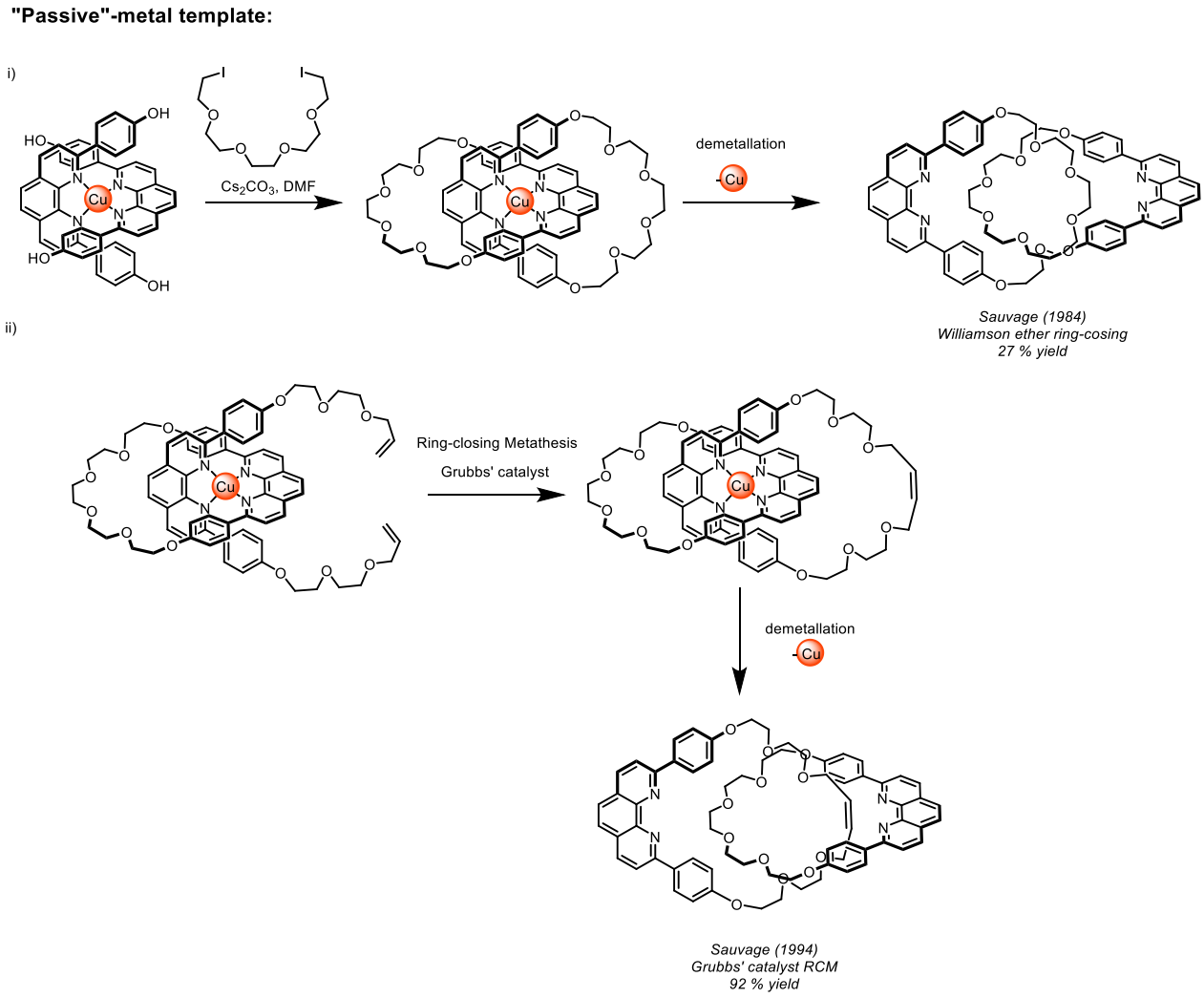

Figure 22. "Passive" metal template using Cu(I)-species to bring precursors orthogonal to each other

Lanthanide *f*-block metals have also been used to template MIMs. Taking advantage of their high coordination numbers of either 8 or 9, Beer and co-workers[124] incorporated a lanthanide complexed DOTA† within a macrocyclic structural framework (Figure 23i). Employing the lanthanide-N-oxide pyridine interaction to assemble a pseudorotaxane, a stoppering reaction afforded the [2]rotaxane in 20% yield.

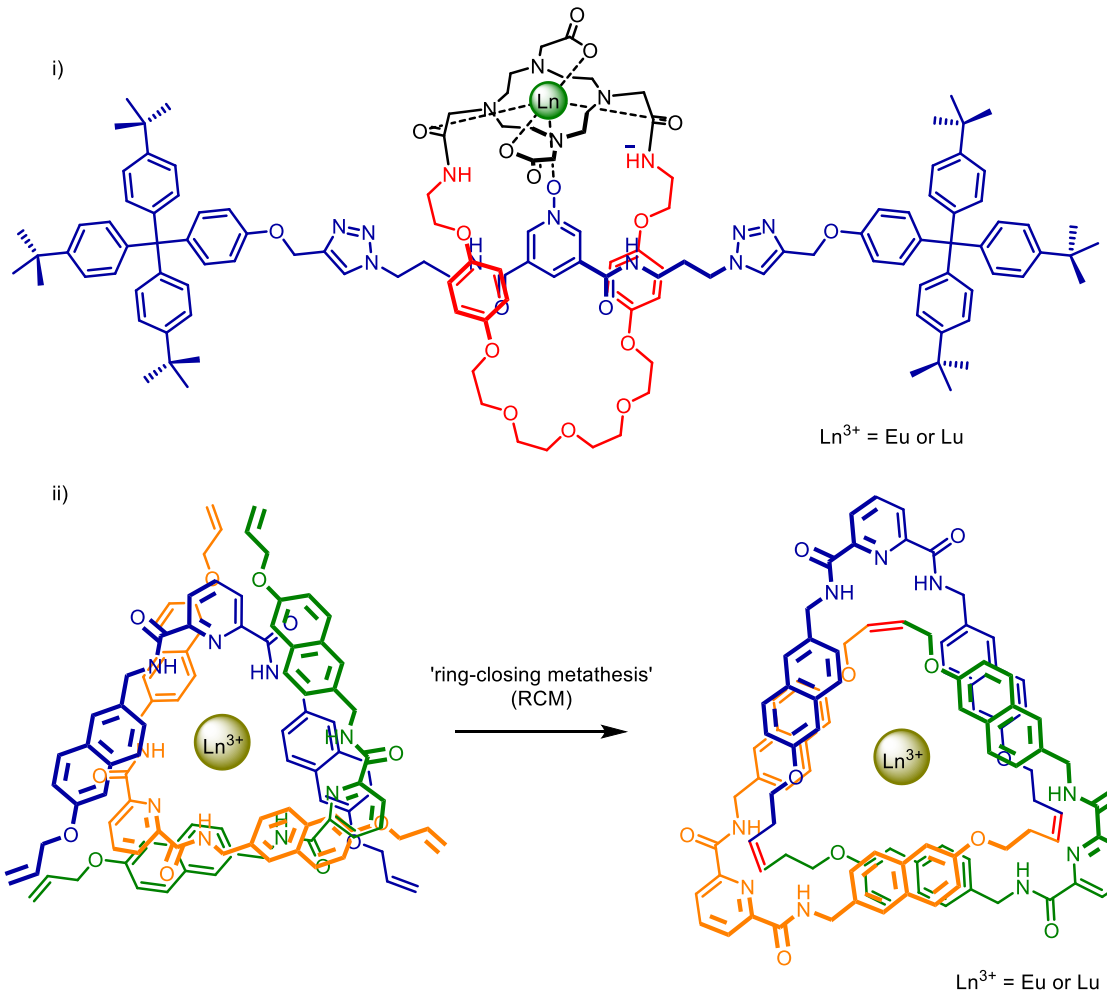

Figure 23. Lanthanide (III) cation templated interlocked structures.

A molecular knot was synthesised using a lanthanide cation as a template. The initial formation of a ML_3 complex containing three 2,6-diamidopyridine ligands with alkene functionalised end-groups,

† DOTA = 1,4,7,10-Tetraazacyclododecane-1,4,7,10-tetraacetic acid is a frequently used metal chelator known for stabilising lanthanide ions for medical applications such as contrasting agent.

followed by Grubbs' catalysed ring-closing metathesis (RCM) gave the trefoil knot product (Figure 23ii).[125]

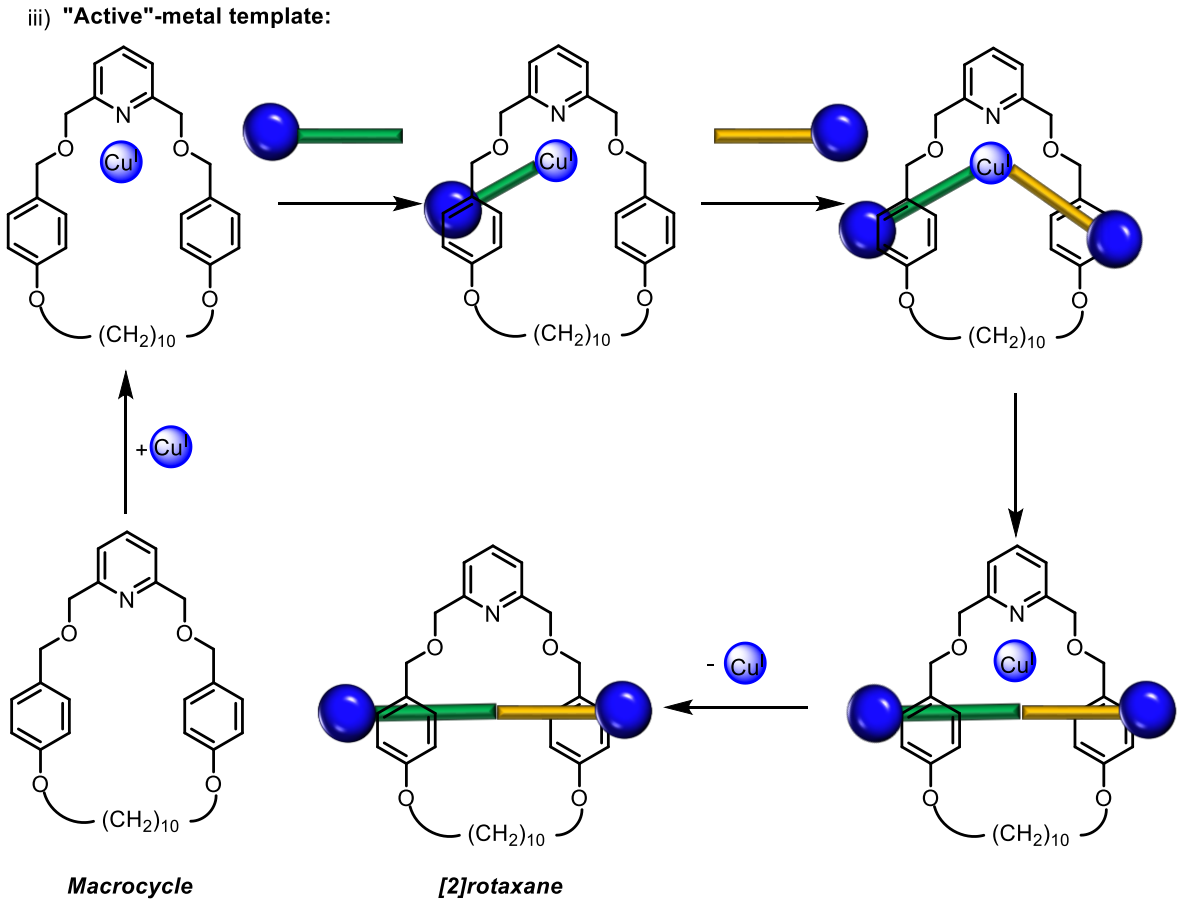

Figure 24. "Active" metal template via Cu^{I}-catalysed azide-alkyne cycloaddtion reaction. Schematic illustration of the principle of CuAAC-AMT for rotaxane synthesis, where Cu(I) (green ball) binds in the cavity of a macrocycle (red shape) as a template for coordinating an alkyne stopper group to carry out carry out the 'click' reaction.

In addition to using a transition metal cation template to coordinate precursor components in what has been coined a "passive" sense, the metal can also be used to act as a catalyst for mechanical bond formation. This active metal template (AMT) approach was first demonstrated by Leigh and co-workers, using the highly regioselective Cu(I)-catalysed reaction between terminal alkynes and azides to produce 1,3-substituted triazole axle functionalised [2]rotaxanes with yields of up to 94 %.[126] This requires the endotopic binding of a Cu(I) species within the macrocycle, thus allowing the cycloaddition reaction between an azide-appended stopper and alkyne-appended stopper to take place within the macrocyclic cavity (Figure 22iii).

1.6.5. Organic Cation Templates

Organic cation templates take advantage of a range of non-covalent interactions such as aromatic donor-acceptor interactions and hydrogen bonding, for MIM precursor assembly.

Stoddart's seminal work on the first molecular shuttle employed the now-famous 'blue-box' 4,4'-bipyridinium based macrocycle precursor forming donor-acceptor interactions around a hydroquinone functional group on the axle (Figure 2).[5] Ring-closing of the 'blue-box' around the hydroquinone functional group on the axle afforded the molecular [2]rotaxane shuttle. Later on, Stoddart and co-workers synthesised the five ring 'Olympiadane', where two tris(1,5-dioxynapthalene)[51]crown-15 are interlocked with three 4,4'-bipyridinium (methyl viologen or paraquat) macrocycles to form a [5]catenane, once again taking advantage of donor-acceptor interactions for the two-step self-assembly of this supramolecular structure (Figure 25i). Since then Olympiadane formed from DNA components have also been synthesised.[127]

Stoddart first described secondary ammonium cations to be capable of forming interpenetrated assemblies of macrocyclic crown ethers *via* a combination of electrostatics and polyether - hydrogen bonding interactions.[128] For example, Qu and co-workers reported the synthesis of a hetero[4]rotaxane consisting of an axle component with benzo[21]crown-7 (B21C7) terminal groups with interpenetrating ammonium stoppers and a central ammonium station interlocked with a dibenzo[24]crown-8 (DB24C8) macrocycle component, prepared in 54% yield (Figure 26i).[129]

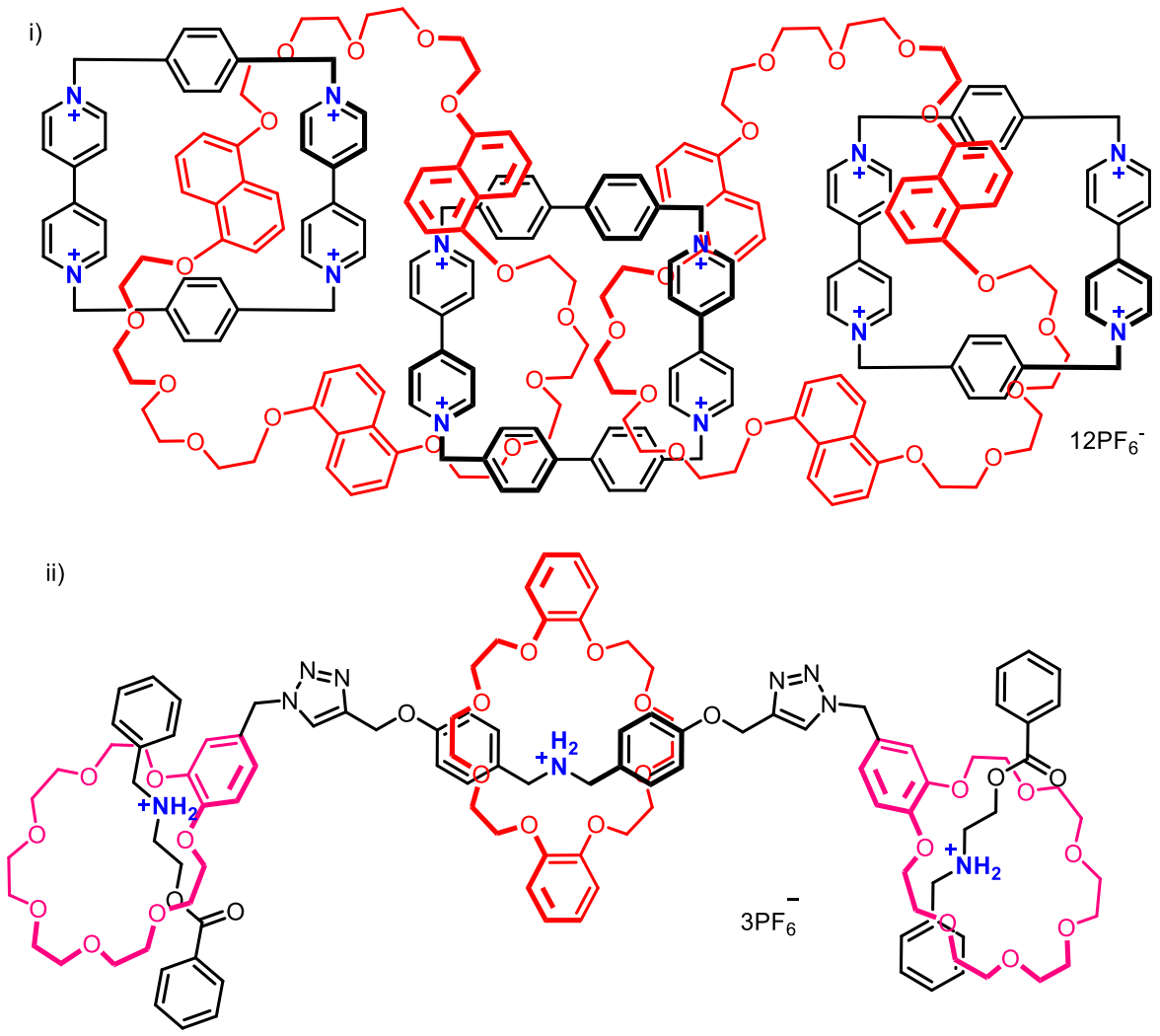

Figure 25. i) Leigh's Olympidane [5]catenane assembled via donor-acceptor interactions between paraquat and hydroquinone.[130] ii) Qu's Hetero[4]rotaxane synthesised via secondary amine template.[129]

Loeb and co-workers reported an asymmetric [3]rotaxane synthesised via a combination of HB between axle pyridinium linked ethyl C-H protons and crown ether macrocycles, and π-stacking of electron-rich catechol and electron-poor pyridinium rings (Figure 26i).[131,132] In an attempt to form molecular shuttles for solid state materials, Loeb and co-workers took advantage of the versatile benzimidazolium motif (Figure 26ii). When incorporated into a rigid H-shaped axle, it has the ability to adopt neutral, monocationic and dicationic states where the rate of molecular shutting of a macrocycle along the axle can be controlled by acid-base chemistry or lithium cation coordination. The formation of this [2]rotaxane molecular shuttle was achieved in a one-pot synthesis by mixing

the macrocycle and a cationic half-axle to form a pseudorotaxane stabilised by electrostatic and hydrogen bond interaction and condensation of the other half-axle to yield a neutral [2]rotaxane.[133]

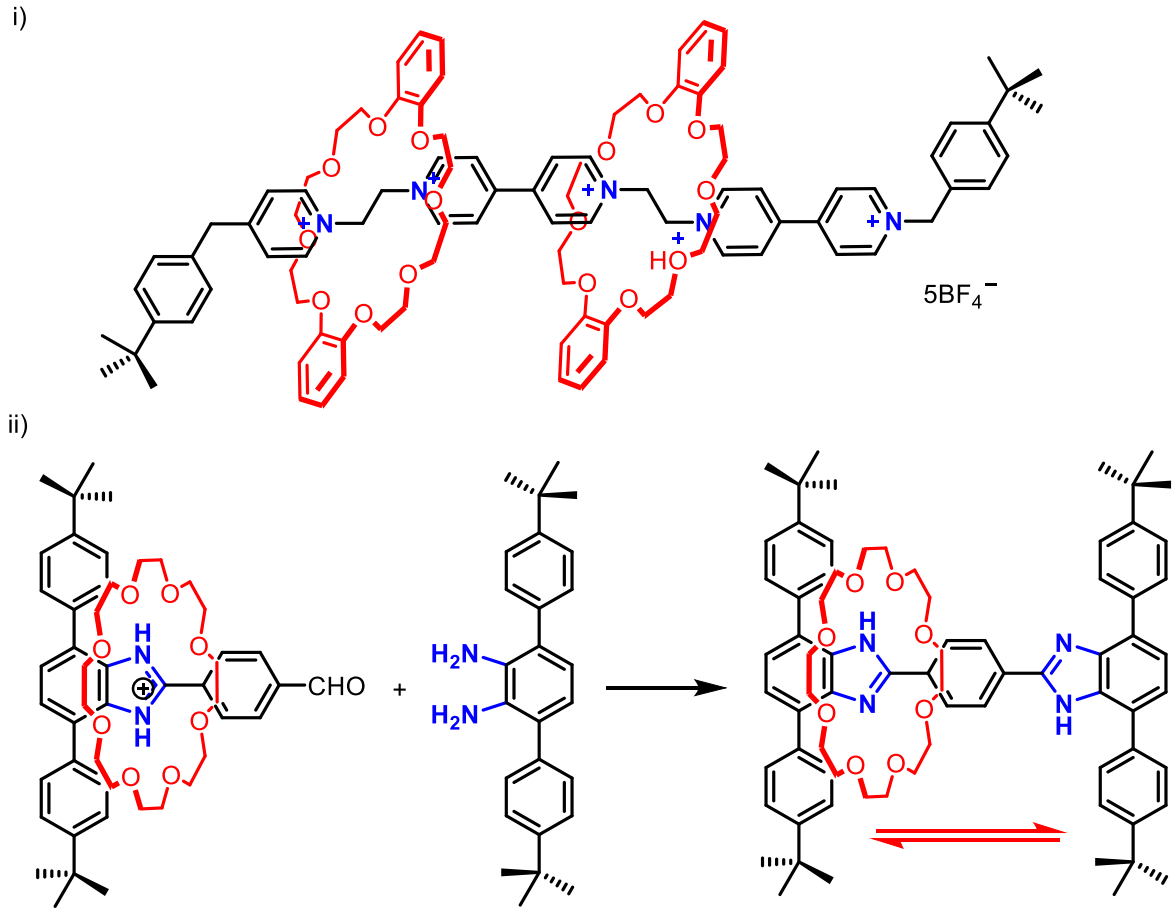

Figure 26. Loeb and co-workers' i) [3]rotaxane synthesised by threading DB24C8 via alkylpyridinium motifs[131,132,134] ii) [2]rotaxane molecular shuttle synthesised by threading DB24C8 onto an axle containing 2,4,7-triphenylbenzimidazolium.[133]

1.6.6. Anion Templates

The first anion templated interlocked structure was described by Vögtle and co-workers[135] who identified the high affinity between the secondary amides of tetralactam macrocycles serving as a HB-donor and an anionic phenolate stopper (Figure 27). Following addition of a stopper furnished with a bromobenzylic functional group, the resulting [2]rotaxane was isolated in 57% yield.

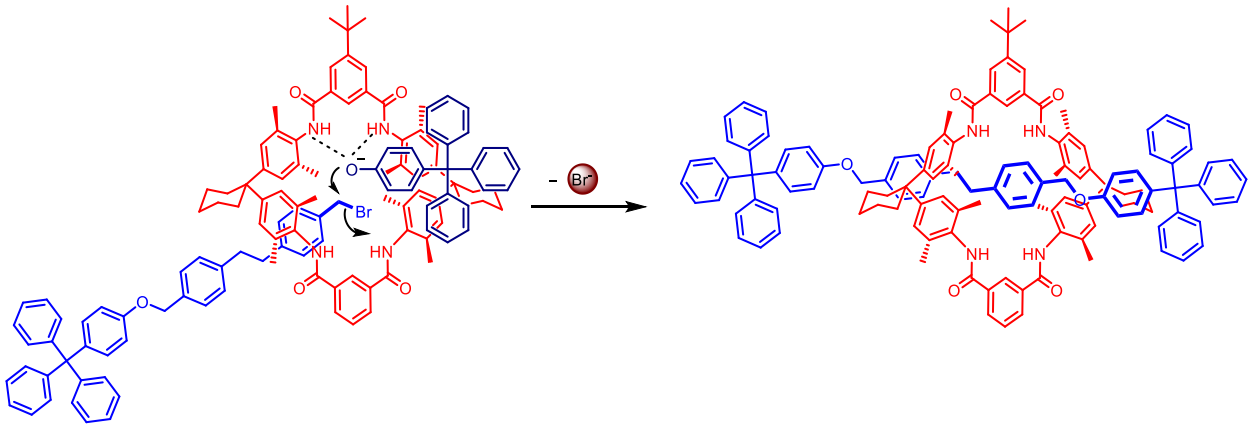

Figure 27. Anion templated [2]rotaxane via SN2 reaction between phenolate-stopper and bromobenzyl-stopper within the macrocycle cavity held in place via HBs from amide groups.

Taking inspiration from Sauvage's Cu(I)-passive metal template, Beer and co-workers reported using a coordinatively unsaturated chloride anion of a pyridinium ion pair to form a pseudorotaxane assembly with an isophthalamide containing macrocycle.[136–138] The solid state crystal structure revealed the chloride bound between the precursors through hydrogen bonding contributions from the respective pyridinium thread and macrocycle amide functional groups (Figure 28i).[136] Subsequently a chloride anion-templated [2]rotaxane was prepared via a Grubbs' catalysed RCM reaction (Figure 28ii). Importantly, after the removal of the template, the [2]rotaxane preserves its role as an anion receptor exhibiting selectivity for chloride.

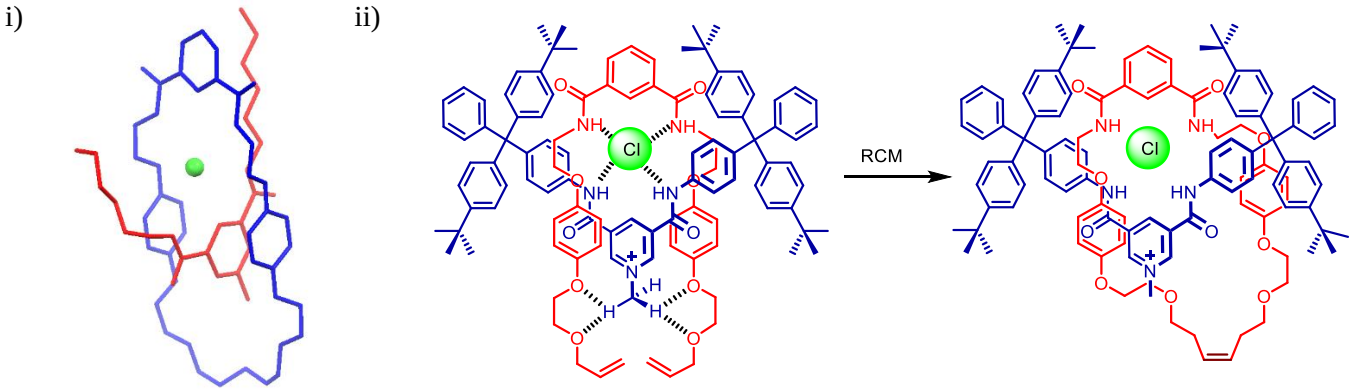

Figure 28. i) X-ray crystal structure of chloride-templated pseudorotaxane. ii) formation of chloride-templated [2]rotaxane by ring-closing methetasis of bis-alkene around the axle.

Interlocked structures can also be formed if the anion template is part of the axle. A cyanostar-shaped macrocycle was synthesised from cyanostillbene repeating units consisting of 5 internal HB-donors

(Figure 29). The solid-state structure revealed chiral π-stacked dimers and in solution the macrocycle has a high affinity for phosphate in 2:1 host-guest stoichiometry. Furthermore, a dialkyne-phosphate template was used to prepare a [3]rotaxane via a click stoppering reaction.

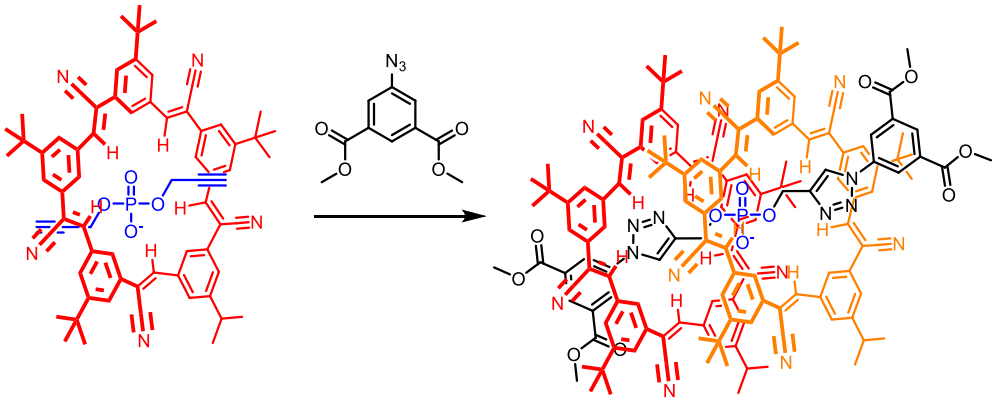

Figure 29. A cyanostar macrocycle used to prepare a [3]rotaxane via an anionic dialkyne-phosphate template.

1.6.7. Neutral Templates

MIMs can also be constructed using a neutral template approach such as hydrogen bonding and aromatic π- π donor-acceptor interactions. An example of the latter was described by Sanders and co-workers involving electron-rich naphthalene and electron-deficient diimide groups to construct a [2]catenane (Figure 30i).[139] Kaneda and co-workers synthesised the first Janus[2]rotaxane† where in aqueous solvent media, the cavity of α-cyclodextrin can accommodate azobenzene hydrophobic guest species (Figure 30ii). The favourable non-covalent interaction between α-cyclodextrin and azobenzene forms two pseudorotaxanes which can then undergo bis-azo coupling reactions where bulky naphthols act as stoppers.[140] In another examples, a bis-9-anthracene-terminated polyethylene glycol (PEG) chain is threaded through a α-cyclodextrin which upon irradiation can reversibly dimerize to interconvert between a [2]rotaxane and a [2]catenane (Figure 30iii).[141]

† Janus[2]Rotaxane refers to an interlocked structure whereby the axle contains a bulky stopper and a macrocycle on opposing sides. This macrocycle is then ring-closed around another axle forming a mechanically interlocked structure.

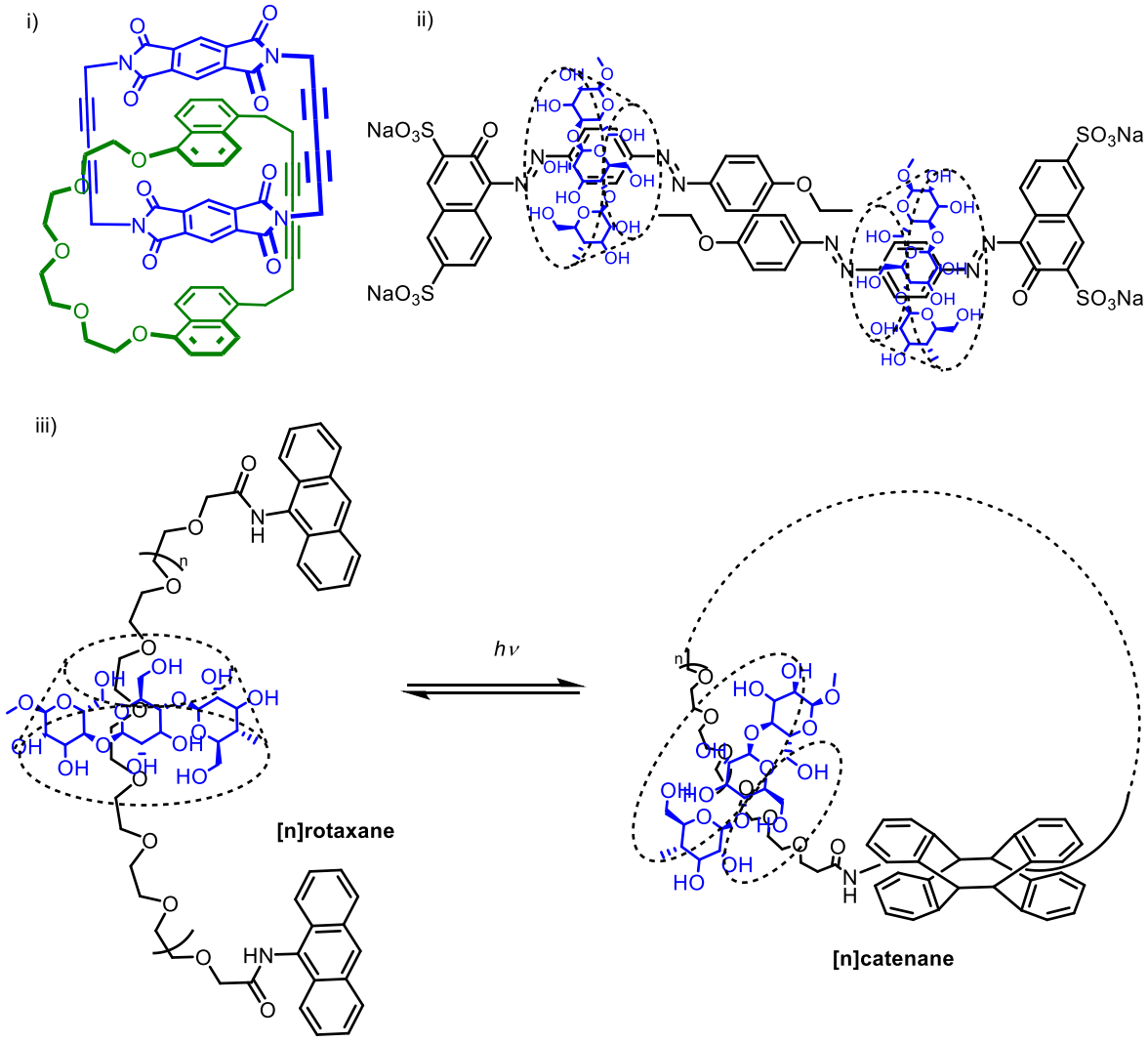

Figure 30. i) Assymetric [2]catenane formed by π-π interactions.[139] ii) First Janus [2]rotaxane.[140] iii) Photodimerisation of 9-anthracene to interconvert between a [2]rotaxane and [2]catenane.[141]

1.7. Applications of Mechanically Interlocked Molecules

The development of synthetic approaches have made MIMs more easily accessible (Section 1.6.3), allowing the synthesis of MIMs in sufficient quantities to be used in a variety of applications. The unique topology of the mechanical bond can be exploited in i) host-guest recognition and sensing, ii) drug delivery and biological applications, iii) catalysis and iv) nanomaterials, briefly discussed below.

Host-Guest Recognition and Sensing

The unique topological cavities of MIMs have been used for the molecular recognition and sensing of cation and anion guest species, enhancing selectivity compared to non-interlocked systems.[142] Recently, Goldup and co-workers reported a series of bipyridyl macrocycle component with triazole and pyridine axle containing [2]rotaxanes for the recognition of transition metal cations (Figure 31i).[143] Unusual coordination geometries enforced by the rotaxanes' binding cavities, altered the metals' redox properties and stability. For example, Cu-rotaxane complexes with 3-5 coordination numbers were formed and the pentadentate Cu-rotaxane revealed enhanced electrochemical reversibility in its $Cu^{2+/+}$ redox couple compared to its non-interlocked counterpart. Through UV-vis and ^{1}H NMR titrations, the authors concluded that the synergistic interplay between a sterically crowded binding site and the mechanical chelate effect was responsible for the unusually low coordination numbers in these transition metal rotaxane complexes. In another example, Smith and co-workers reported a chloride [2]rotaxane optical sensor consisting of a squaraine dye axle encapsulated within an anthracene tetralactam macrocycle (Figure 31ii).[144] Upon Cl^- binding in acetone, lateral displacement of the macrocycle along the axle caused a red-shift in fluorescence which was observable by the naked eye. MIMs as hosts can provide guest species with a shielded environment, changing the effect it can have on its surroundings

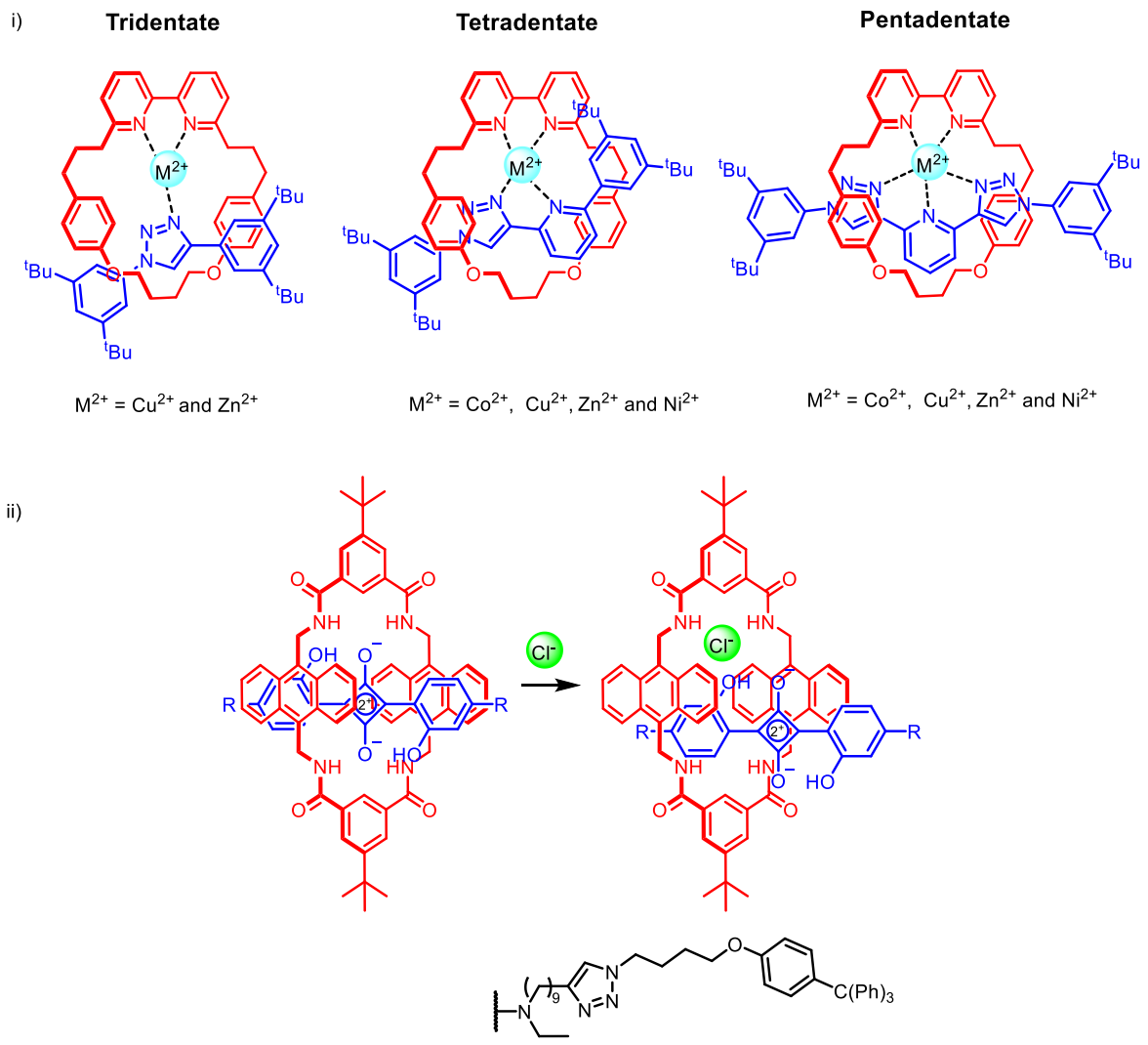

Figure 31. MIM hosts for recognition and sensing of anionic guest species. i) Goldup's Pt(II)-[2]rotaxane and ii) Smith's [2]rotaxane optical sensor shuttle.

Biological Applications

The use of synthetic chemistry as a vessel for drug delivery is a highly established field. In the process of drug delivery, the integrity of the active drug has to be kept, the delivery vessel has to have low toxicity and the 'delivery' efficiency is a bonus. Papot and co-workers developed a biocompatible [2]rotaxane consisting of a few structural components that address these factors (Figure 32i). Each of these components plays a part in delivering the anti-cancer drug paclitaxel into the cancer cell (in rat plasma) which was demonstrated by confocal microscopy and toxicity screening.[145]

Synthetic biomimetics are also impressive such as the one exemplified by Leigh and co-workers where a [2]rotaxane is capable of sequenced peptide synthesis (Figure 32ii). The axle contains three stations appended by β^3-amino acid building blocks and as the macrocycle moves along the axle, it 'picks' up the amino acid resulting in precisely controlled peptide sequencing.[146] This "molecular machine" was operated for 7 days in which the peptide sequencing was performed in DMF in the presence of triethylamine.

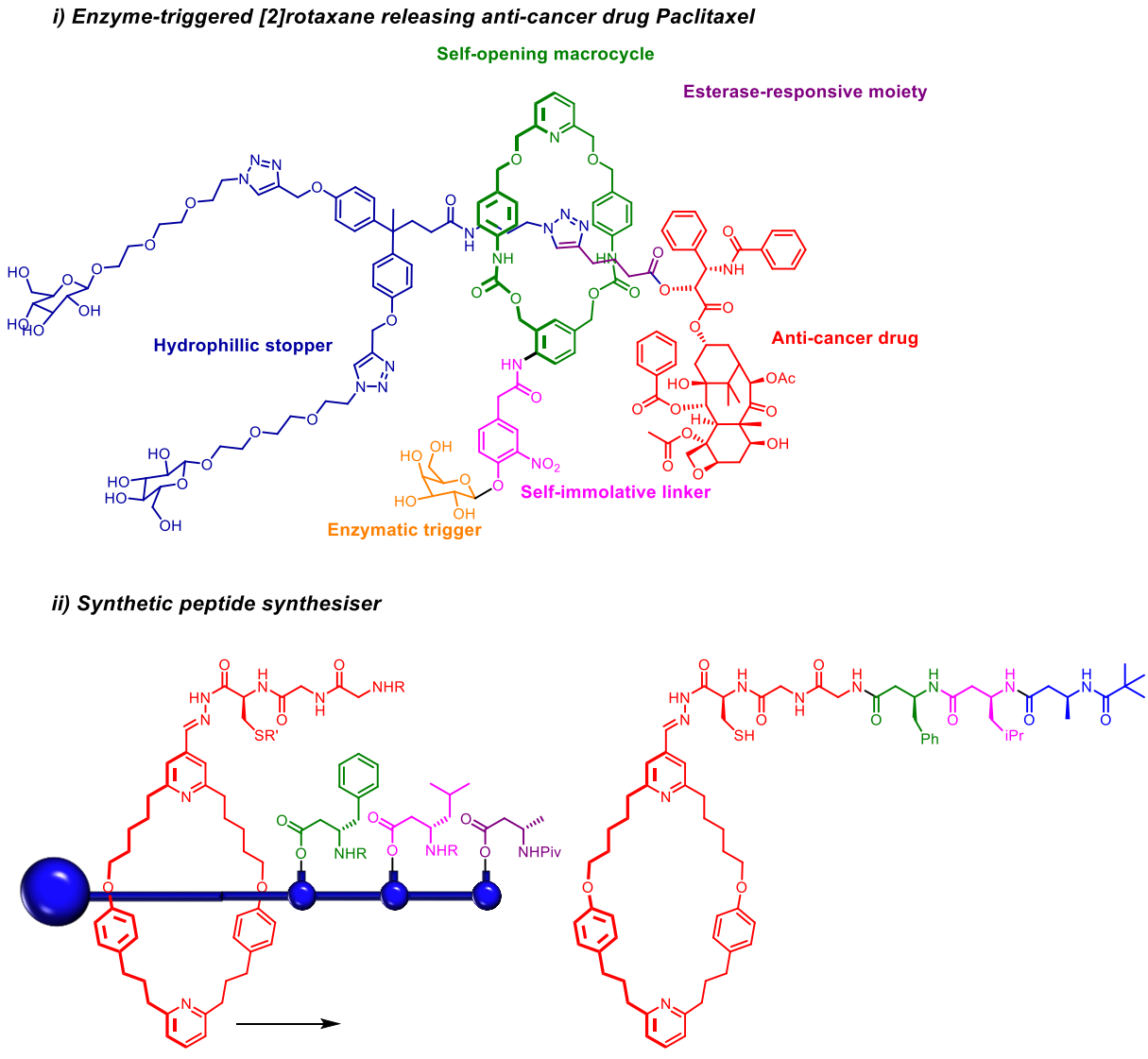

Figure 32. i) [2]rotaxane as an anti-cancer drug delivery vessel. ii) Synthetic 3-station peptide synthesiser.

Catalysis

MIM catalysts can provide steric control by virtue of its mechanical bond therefore providing stringent formation of desired catalytic product. Takata and co-workers reported the first catalytically active rotaxane in the mediation of a benzoin reaction in good yield with reasonable enantioselectivity demonstrating steric restriction stemming from mechanical bond for enantioselective catalysis to occur (Figure 33i).[147] Polylactide has received attention in the recent years as a biodegradable and recyclable polymer. Williams and co-workers have recently used a novel [2]rotaxane for the isoselective synthesis of polylactide *via* ring opening from *rac*-lactide. They observed a correlation between macrocycle-axle translocation rate with polymerisation selectivity where steric-access and monomer coordination sites were controlled (Figure 33ii).[148]

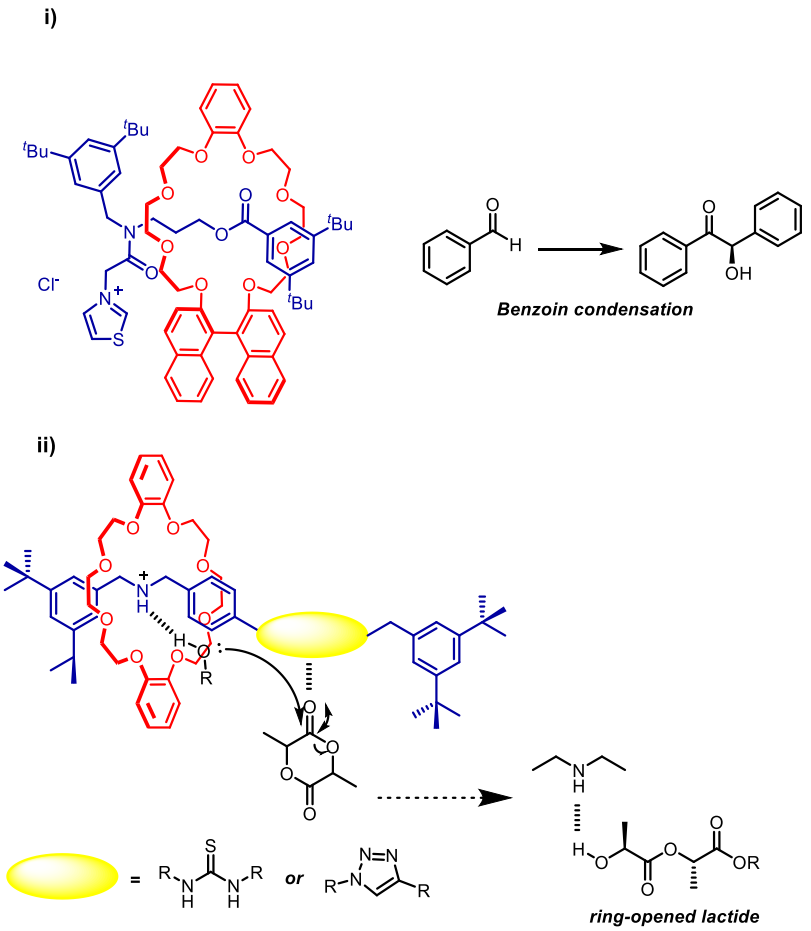

Figure 33. [2]rotaxane involved in lactide ring-opening reaction.

Nanotechnology

Due to the unique topology MIMs can offer, nanomaterials incorporated into such structures can have vastly different properties. Single-walled carbon nanotubes (SWNTs) have unique mechanical and electronic properties that are desirable as semiconducting materials or as bioscaffolds.[149] When SWNTs are used as an axle component of a rotaxane (Figure 34), the material's physical properties were shown to display up to 200% improvement in Young's modulus and tensile strength[150]. This area of chemistry is not new however, techniques are still being developed to fully characterise and study these materials.

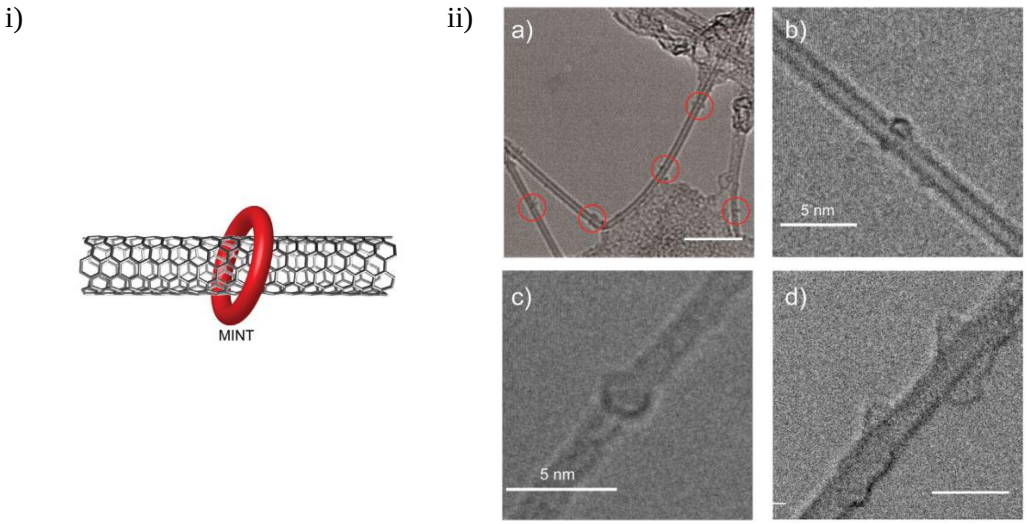

Figure 34. i) Mechanically interlocked single-walled carbon nanotube (MINT). ii) TEM images of macrocycles around SWNTs.

1.8. Aims and Objectives of the Thesis

Although the field of anion supramolecular chemistry has expanded enormously during the past few decades, the application of σ-hole interactions for anion recognition applications is under-developed (see Sections 1.4.4 and 1.4.5). This thesis aims to further understand the fundamentals stemming from anion binding halogen bonding and chalcogen bonding σ-hole interactions. This is investigated through new synthetic methods utilised for the preparation of novel σ-hole donor host molecules and elucidation of their solution phase anion binding properties in competitive solvents. In addition, rare halogen bond interactions will be discussed with the aim of creating new templating methods for the synthesis of MIMs.

Chapter 2 focuses on the synthesis of novel chalcogen bonding receptors and a detailed study of their anion binding thermodynamic properties. The second half of this chapter investigates synthetic routes to incorporate halogen and chalcogen bonding motifs into MIM structural frameworks.

Chapter 3 explores the synthesis of chiral XB rotaxanes consisting of BINOL macrocyclic and axle components. Thereafter, the synthesis and chiral recognition properties of a XB BINOL motif incorporated into acyclic foldamer and macrocyclic receptors are discussed.

Chapter 4 explores the potential of pyridine containing macrocycles and rotaxanes to stabilise XB iodonium species and discusses attempts to prepare MIMs via an iodonium template approach.

2 | σ-Hole Receptors for Anion Recognition

A σ-hole is an electron deficient region found on Group 14-17 elements (tetrel, pnictogen, chalcogen and halogen atoms) when they are covalently bound to an electron-withdrawing group (Refer to Chapter 1 for further details). The σ-hole is capable of forming non-covalent interaction(s) with Lewis bases. This chapter will discuss the thermodynamic properties of the lesser studied chalcogen bond – anion interaction, focussing on the incorporation of chalcogen bonding (ChB) and halogen bonding (XB) donor groups, alongside HB motifs, into acyclic, macrocyclic and MIM receptors for comparative anion binding investigation.

2.1. Cationic Chalcogen Bonding Acyclic and Macrocyclic Receptors[†]

Chalcogen bonding (ChB) is the attractive non-covalent interaction between an electron-deficient divalent Group 16 element (S/Se/Te) and a Lewis base arising from electrophilic σ-holes on the chalcogen atom.[151] Like halogen bonding (XB), its more well-studied sister σ-hole interaction involving heavy Group 17 elements (Br/I),[152] ChB displays comparable binding strengths to the ubiquitous hydrogen bonding (HB) with more stringent directionality, allowing for greater precision in three dimensional spatial control of host-guest binding. Nonetheless, there are important differences between XB and ChB interactions. Most notably, while XB is restricted to an optimal R-X···B angle of *ca*. 180º, the multivalent nature of chalcogen atoms allows more than one σ-hole to be present on the donor atom, resulting in a greater geometric diversity of interactions with Lewis bases.[33,46] ChB differs electronically from XB, being influenced not only by the intrinsic greater electropositivity of chalcogen donor atoms compared to halogens, but also by the cumulative effects of the number and spread of σ-holes, coupled with the nature of covalently bonded substituents. Although these unique attributes of ChB have been exploited in recent applications such as crystal engineering,[153] pharmaceutics,[154] catalysis,[103,155,156] self-assembly processes[157,158] and materials design,[159] solution-phase ChB host-guest recognition investigations remain extremely scarce.[160] In particular, only a handful of ChB receptor systems for anion binding, including acyclic,[46,86] macrocyclic and rotaxane[100] examples have been reported to date.

While several cationic Se-based ChB receptors are known,[46] the weakness of the C-Te bond (bond energy c.a. 200 kJ mol^{-1})[161] makes it susceptible to oxidation[162] and metal insertion reactions.[163–165] Thus, despite their potential for strong ChB interactions, cationic Te-based receptors are extremely rare,[96] with a recent example of the application of a dicationic Te-based chalcogen bond donor as a catalyst in a nitro-Michael reaction reported by Huber and co-workers.[166,167] This is the first

[†] Work done for Chapter 2 – section 2 has been published. *Chem. Eur. J.* **2018**, 24, 14560 – 14566. DOI:10.1002/chem.201803393

dicationic Te-based chalcogen bond donor that was found to be stable under ambient conditions with crystallographic evidence confirming its structure. The few reported functional neutral Te-based anion binding receptors tend to incorporate the chalcogen atom into aromatic heterocycles such as tellurophenes[98] or tellurodiazoles[97] for enhanced stability.

With the objective of gaining a greater insight into the nature of the ChB receptor-anion interaction, this section will discuss the synthesis of a novel robust monocationic tellurium-based ChB donor motif **2.5$_{Te}$** comprised of exocyclic divalent Te donor atoms covalently linked to a strongly electron-withdrawing 3,5-bis(triazole) pyridinium group (Scheme 1). The inherent stability of **2.5$_{Te}$** enabled the thermodynamic properties of ChB-halide anion binding in polar aprotic and wet protic organic solvent media to be determined. In comparison with acyclic and macrocyclic Se-based receptors **2.6$_{Se}$, 2.11$_{Se}$,** (Scheme 2) acyclic hydrogen bonding **2.5$_{H}$** and fluorine triazole functionalised **2.6$_{F}$** receptor analogues (Figure 35), the thermodynamic data helps to rationalize how the interplay between ChB receptor, anion guest and solvent medium affects halide binding selectivity and affinity trends.

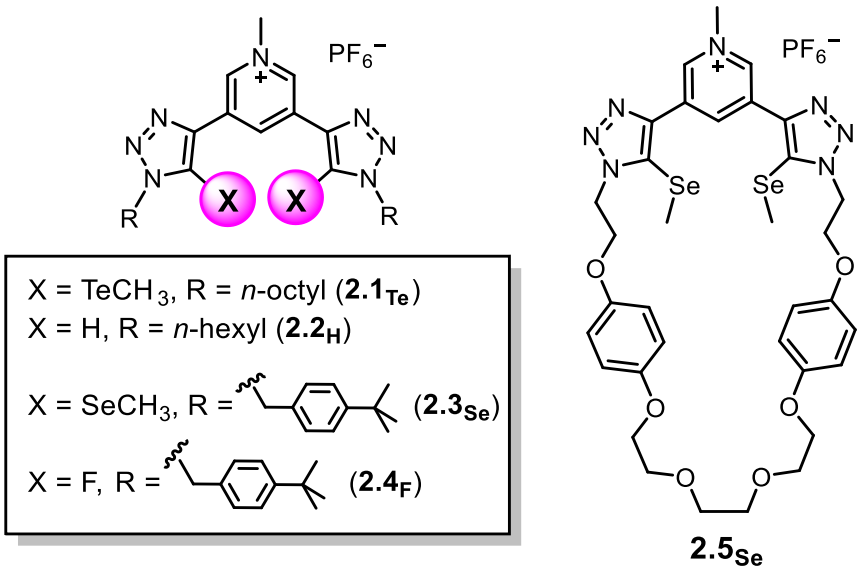

Figure 35. Anion receptors studied in Section 2.1.

2.2. Synthesis of Acyclic and Macrocyclic Receptors

The acyclic receptors **2.1**$_{Te}$ and **2.3**$_{Se}$ were constructed using copper(I)-catalysed azide-alkyne cycloaddition (CuAAC) reactions, either directly from 3,5-bis(ethynyl)pyridine[168] in a 'one-pot' reaction or from the corresponding iodoalkyne[169] in a 'two-pot' reaction in relatively good yields. Following this, the methylchalcogeno-triazoles were generated by aromatic nucleophilic substitution (SNAr) of the iodotriazoles (**2.6**$_{I}$, **2.7**$_{H}$ and **2.8**$_{I}$) by reactive methylchalcogenide anions generated *in situ* from methyllithium and the elemental chalcogen (Se/Te). While methylseleno-triazoles were previously accessed[100] using a two-step procedure,[170] the use of THF as solvent allowed them to be directly formed in synthetically viable yields in one step from iodotriazole precursors. *N*-Methylation of pyridine units in the neutral receptor precursors **2.9**$_{Te}$ and **2.10**$_{Se}$ using iodomethane, followed by anion exchange with aqueous NH_4PF_6 afforded **2.1**$_{Te}$ and **2.3**$_{Se}$ in good yields of and 84% respectively. (Scheme 1)

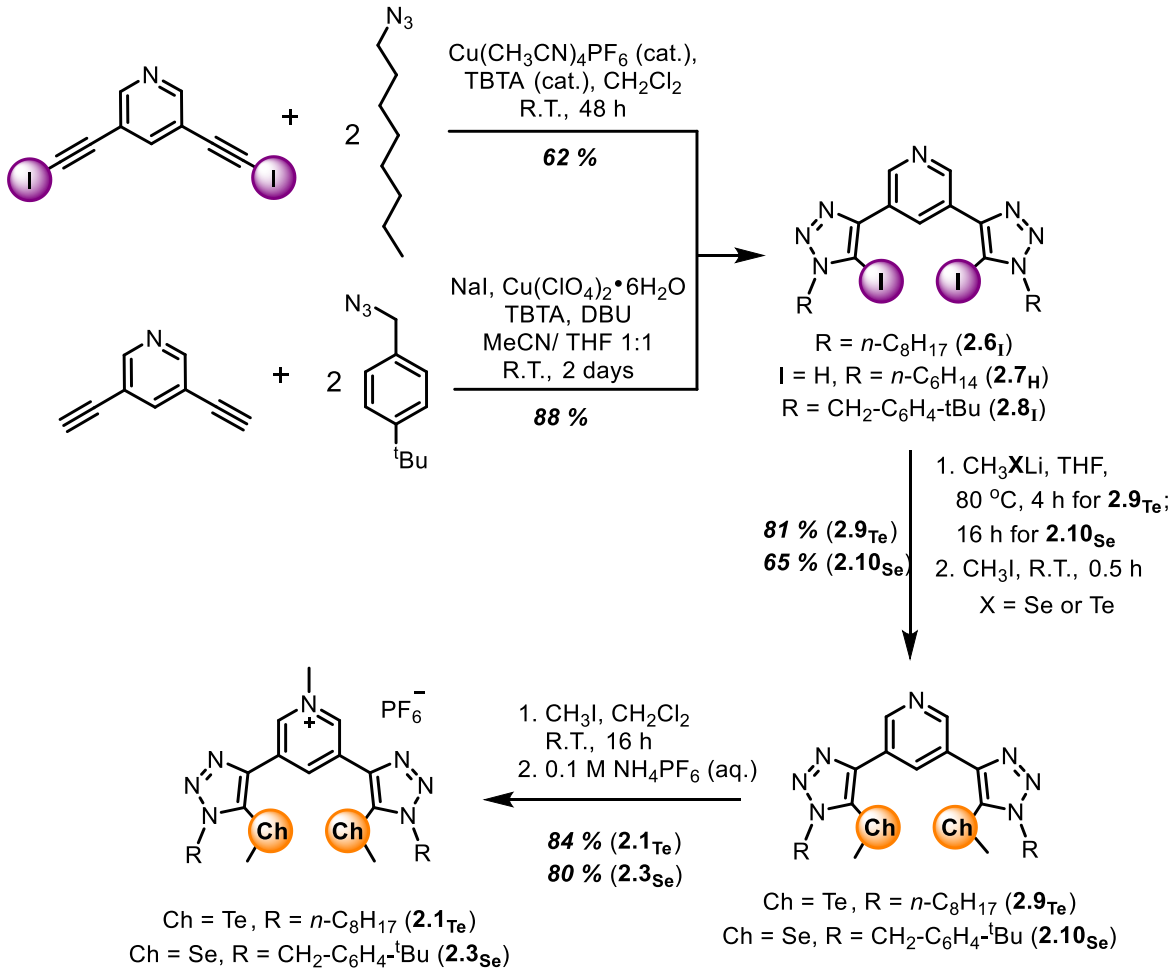

Scheme 1. Synthesis of acyclic ChB receptors.

This approach was then adopted to construct the structurally more elaborate macrocycle **2.5$_{Se}$**.[†] Using a methoxymethyl (MOM)-protected hydroquinone derivative, a CuAAC 'Click' reaction afforded bis-iodotriazole **2.11**, which was converted to bis(methylseleno-triazole) **2.12** by reaction with *in situ* generated lithium methylselenide. MOM-deprotection under acidic conditions afforded the free bis-phenol **2.13**, and S_N2 ring-closing with triethylene glycol bis-tosylate afforded neutral macrocycle **2.14** in 26% yield. The target cationic macrocycle **2.5$_{Se}$** was prepared by methylation with iodomethane, then washed vigorously with an aqueous solution of NH_4PF_6 to afford macrocycle in 56% yield. For all receptors, ^{1}H NMR characterisation confirmed the exclusive methylation of the

[†] Due to the lability of the C-Te bond, synthesis of the analogous Te-containing macrocycle proved challenging and could not be isolated in sufficient quantities for detailed anion binding studies.

central pyridine functionality, whilst ^{125}Te and ^{77}Se NMR spectroscopy ascertained the presence of the ChB donor atoms.

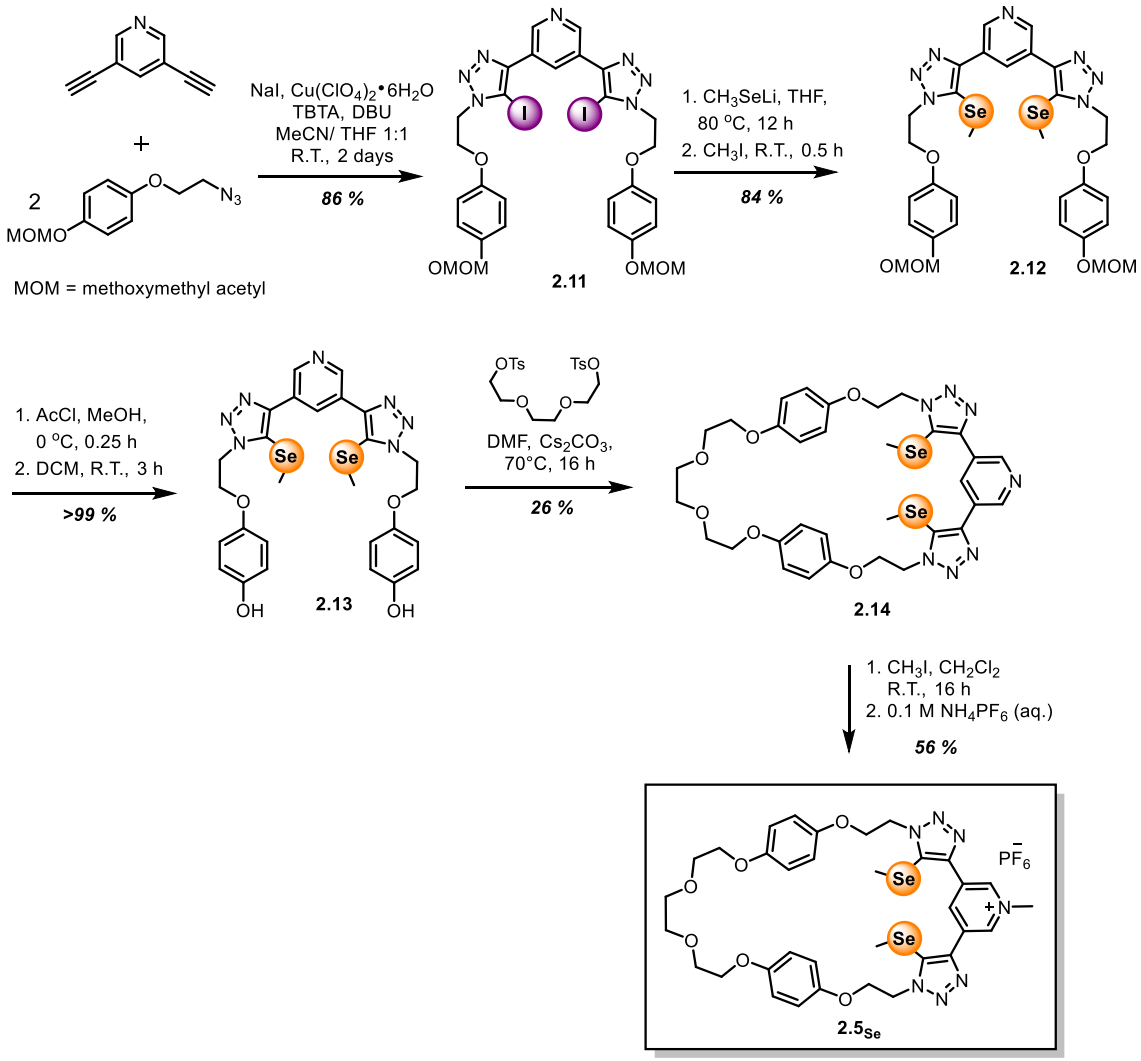

Scheme 2. Synthesis of Se-containing macrocycle ***2.5*** $_{Se}$.

A control receptor bearing fluorotriazole motifs not capable of halogen bonding was synthesised. Adapting from previously reported synthetic procedure[170], **2.8**$_{I}$ dissolved in acetonitrile and an aqueous solution of potassium fluoride was placed in a microwave reactor. The crude reaction was extracted with chloroform and subsequent purification by silica gel column chromatography afforded **2.8**$_{F}$ in 52% yield. To yield the cationic receptor, **2.8**$_{F}$ was dissolved in iodomethane and subsequently subjected to a series of aqueous wash. The combined organic layer was dried over $MgSO_4$ and solvent removed in vacuo to afford pure control receptor **2.4**$_{F}$ in 82% yield.

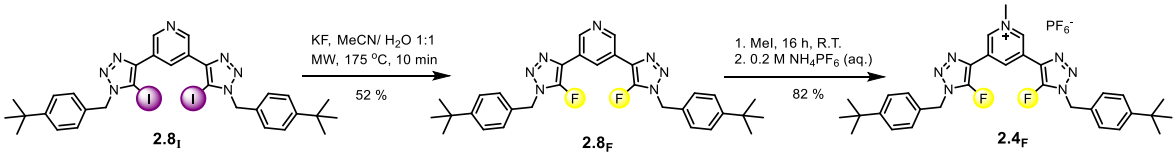

Scheme 3. Synthesis of control receptor 2.4$_F$.

2.3. Anion Binding Studies of Cationic Chalcogen-containing Receptors

2.3.1. Anion Binding in Acetonitrile

The anion binding behaviour of receptors **2.1$_{Te}$**, **2.3$_{Se}$** and **2.5$_{Se}$** were first probed by ^{1}H NMR titration experiments in CD_3CN. The addition of tetrabutylammonium (TBA) chloride to **2.1$_{Te}$** elicited large downfield shifts of the signals arising from the internal pyridinium aromatic proton (H_a) and the $TeCH_3$ moieties (Figure 36i), whilst giving negligible perturbations of protons H_b and H_d even after 10 equivalents of Cl^-. Notably, significant downfield shifts of the $TeCH_3$ groups were also observed upon anion addition (Figure 36ii). In contrast, no perturbations of any of the proton signals arising from the octyl chains (e.g. H_c) were seen throughout the titrations. These observations strongly imply that the Cl^- guest is binding in the vicinity between the Te ChB donor groups. By monitoring the shifts of H_a, non-linear regression analysis of the titration data using the WinEQNMR2 software[171] determined anion association constants (K_a) shown in Table 1. For comparison, binding affinities were also determined for the HB receptor analogue (**2.5$_H$**).[172] See appendix A1 for titration protocol.

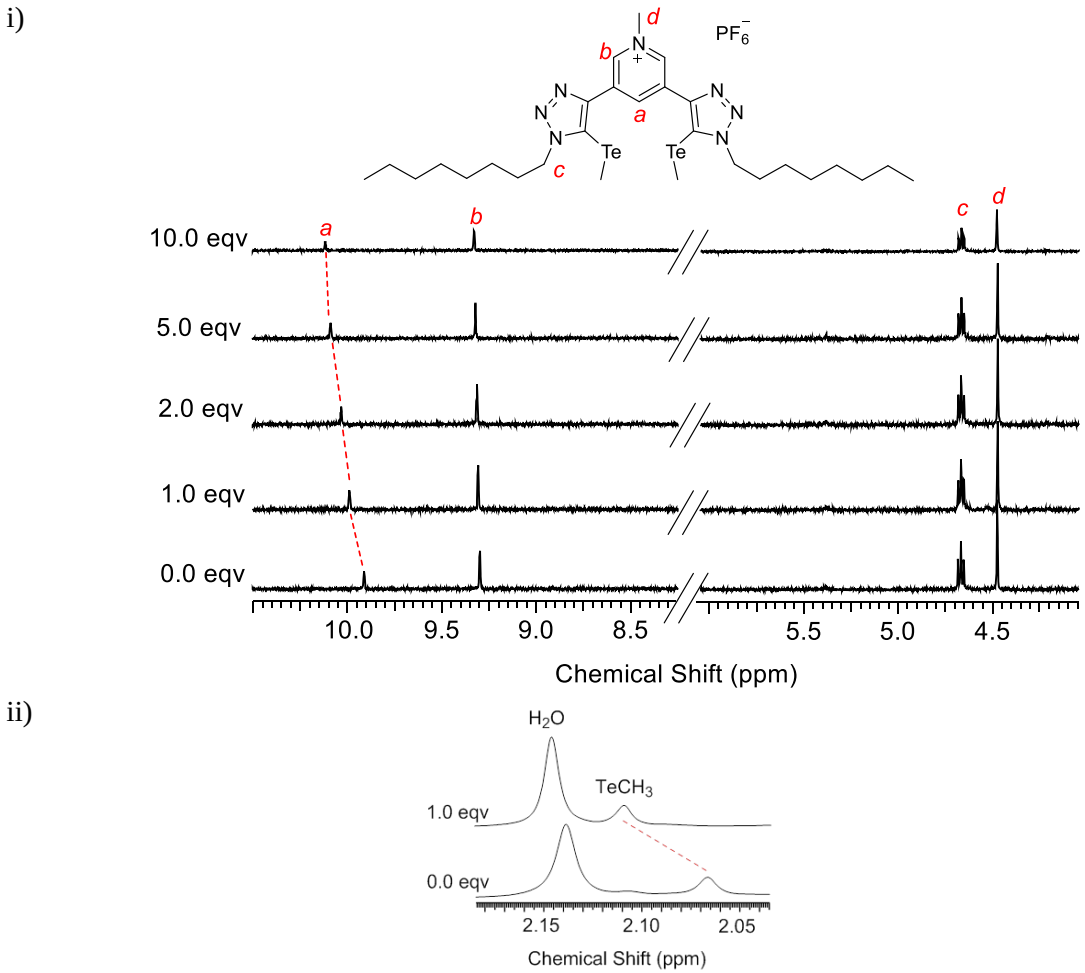

*Figure 36. i) Partial ^{1}H NMR spectra of **2.5$_{Te}$** in the presence of increasing quantities of Cl^- ([**2.5$_{Te}$**]= 1.0 mM, CD_3CN, T = 298 K). ii) Partial ^{1}H NMR spectra of $TeCH_3$ proton shifts after 1.0 eqv of Cl^-.*

The ChB receptor **2.1$_{Te}$** exhibits appreciable affinities for a range of anions of differing charge densities and geometries (Table 1). It is noteworthy that by replacing the $TeCH_3$ units with hydrogen atoms in receptor **2.2$_H$**, all anion binding affinities are significantly reduced in magnitude. Contrasting anion affinity preferences between the ChB and HB receptors include **2.1$_{Te}$** binding all the halides more strongly than acetate, whereas **2.2$_H$** displays a higher affinity for acetate over the heavier halides bromide and iodide. While this may be a consequence of the contrasting directionalities of ChB and HB, these observations also suggest that ChB-mediated anion binding may be less sensitive to anion basicity than HB interactions. For the halides, while anion affinities for both **2.1$_{Te}$** and **2.2$_H$** decrease in order of charge density (Cl^- > Br^- > I^-), **2.1$_{Te}$** showed a larger enhancement in anion affinity relative to **2.2$_H$** with the softer and more lipophilic heavier halides, I^- and Br^- (Table 2). ChB receptors show augmented binding affinities in the heavier halides compared to HB receptor, possibly due to enhanced 'soft-soft' interactions. However, a strong association was

observed between **2.1$_{Te}$** and $H_2PO_4^-$, showing an initial host-guest 2:1 binding (K_{21}) stoichiometry that became 1:1 (K_{11}) at higher anion concentrations (Figure 37). In contrast, $H_2PO_4^-$ addition to **2.2$_H$** resulted in precipitation of the host-guest complex. The significant differences in anion recognition properties between **2.1$_{Te}$** and **2.2$_H$** give a strong indication that ChB interactions dominate the binding of anions by **2.1$_{Te}$**.

*Table 2. Association constants (K_a/ M^{-1}) of **2.1$_{Te}$** and **2.2$_H$** with different anions in CD_3CN at 298 K.[a]*

Anion	K_a/ M^{-1}	
	2.1$_{Te}$	**2.2$_H$**
Cl^-	652 (13)	263 (8)
Br^-	503 (16)	106 (3) [b]
I^-	305 (11) [c]	59 (2) [b]
CH_3COO^-	269 (9)	198 (6)
N_3^-	330 (22)	92 (3)
$H_2PO_4^-$	K_{21} = 411 (40) [c] K_{11} = 1530 (138)	- [b,d]

*[a] Values of K_a determined using the WinEQNMR2 software[171] by monitoring the internal proton H_a for **2.1$_{Te}$** and the triazole aromatic proton for **2.2$_H$** using a 1:1 host-guest binding model unless otherwise stated; Errors (±) in parentheses; [host] = 1.0 mM. CD_3CN, T = 298 K); [b] Values previously reported in ref. [172] ; [c] $TeCH_3$ protons monitored instead of H_a; [d] precipitation of host during titration.*

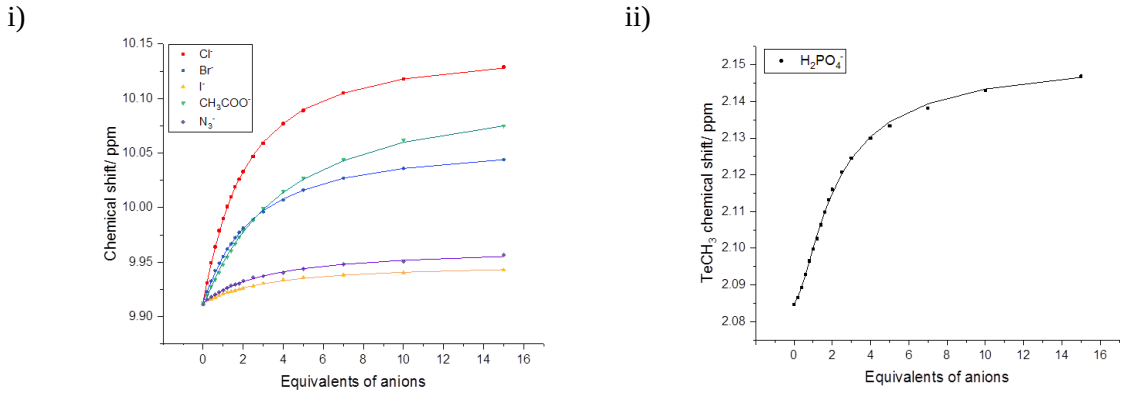

*Figure 37. Changes in the chemical shifts of (A) internal pyridinium aromatic proton H_a of receptor **2.1$_{Te}$** with increasing quantities of Cl^-, Br^-, I^-, CH_3COO^-, N_3^- and (B) $TeCH_3$ protons for $H_2PO_4^-$ in CD_3CN*

([1.Te] = 1.0 mM, T = 298 K). For the $H_2PO_4^-$ titration, the $TeCH_3$ protons gave significantly better fit with a 2:1 host-guest binding model than H_a

Further evidence of strong involvement of ChB in anion coordination was observed from the large upfield shifts of the tellurium receptor's ^{125}Te NMR signals ($\Delta\delta$ = -9.9 ppm) upon addition of 1.0 equivalent of Cl^-, which is consistent with the donation of electron density from Cl^- into the C-Te σ* orbital (Figure 38).[100]

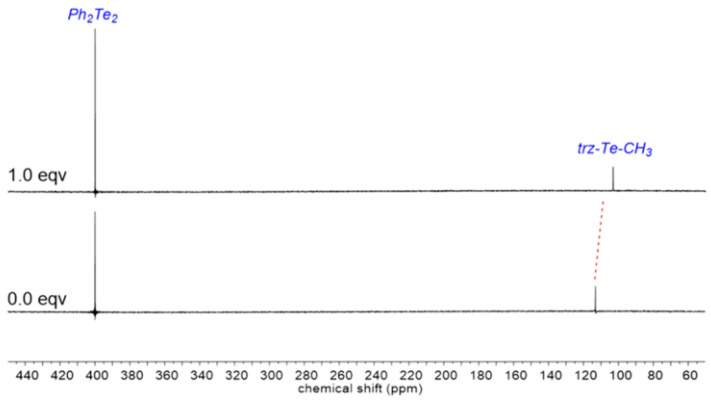

*Figure 38. Partial ^{125}Te NMR spectra of **2.1$_{Te}$** in the presence of 0.0 and 1.0 eqv of Cl^- in d_6-acetone ([**2.1$_{Te}$**] = 4.0 mM, T = 298 K,). A saturated internal standard of diphenyl ditelluride was used for referencing (d_6-acetone, δ 400 ppm). $\Delta\delta_{Te}$ = -9.9 ppm upfield.*

2.3.2. Solvent Effects on Anion Binding

The significant anion affinities exhibited by **2.1$_{Te}$** in CD_3CN prompted us to determine the ChB receptor's anion binding properties in a range of solvent media of varying competitiveness. Analogous ^{1}H NMR titration experiments in d_6-acetone revealed large downfield perturbations of only the H_a and $TeCH_3$ proton signals of **2.1$_{Te}$.** This indicated that despite the weaker charge screening in acetone (dielectric constant ε = 20.7) compared with acetonitrile (ε = 37.5), which could favour electrostatically-driven binding in the vicinity of the cationic pyridinium nitrogen atom, Te-mediated ChB was still dominating the anion recognition. More than an order-of-magnitude enhancement in the K_a values were seen with Cl^- and I^- in acetone (Table 3) when compared to acetonitrile (Table 2). On the other hand, more competitive solvents such as d_6-DMSO resulted in

considerably weaker Cl^- binding, whilst no detectable binding was observed in CD_3OD (Table 3). It is noteworthy that **2.1$_{Te}$** showed noticeably weaker Cl^- anion affinity compared to the XB pyridinium-3,5-bis(iodotriazole) receptor analogue (K_a = 387 M^{-1}) in d_6-DMSO.[172] Although tellurium is more electropositive than iodine, the significant discrepancy observed in this case may be due to a combination of the increased steric bulk of the larger $TeCH_3$ ChB-donor groups, the more diffuse σ-holes on the divalent Te atom compared to the monovalent XB-donor iodine atom,[38] and the potential electron-donating nature of the methyl group covalently bonded to Te reducing the electron-deficiency of its σ-hole.

2.3.3. Anion Binding in the Presence of D_2O

The presence of water in an organic solvent has been shown to be detrimental to the anion affinities of HB[173] and XB[174] hosts, attributed to the increased energetic demands required to overcome anion hydration for binding to occur. To directly compare the effects of solvent hydration on ChB-mediated anion binding, ^1H NMR titration binding studies were also performed with **2.1$_{Te}$** in CD_3CN/ D_2O 99:1 v/v and the resulting host-guest 1:1 stoichiometric association constants are summarised in Table 3 with binding isotherms shown in Figure 39. Compared to the K_a values determined in dry CD_3CN (Table 3), the presence of just 1% water by volume in the solvent resulted in a significant reduction of all anion affinities with the extent of magnitude decrease mirroring the anion's hydration energies ($H_2PO_4^-$ > Cl^- > Br^- > I^-).[24]

Table 3. Anion association constants of 2.1_{Te} and 2.2_{H} in different solvents. [a]

Anion	2.1_{Te} K_a (M^{-1})			2.2_{H} K_a (M^{-1})
	d_6-acetone	d_6-DMSO	CD_3CN/ D_2O 99:1	CD_3CN/ D_2O 99:1
Cl^-	$> 10^4$ [b]	43 (3)	122 (1)	79 (3)
Br^-	-[c]	-[d]	183 (4)	62 (2)
I^-	3528 (54)	-[d]	139 (1)	44 (1)
$H_2PO_4^-$	-[d]	-[d]	100 (2)	-[c]

*[a] Values of K_a determined using the WinEQNMR2 software[171] using a 1:1 host-guest binding model; Errors (±) in parentheses; [host] = 1.0 mM. CD_3CN, T = 298 K). [b] ^1H NMR titration of Cl^- with receptor **2.1_{Te}** in d_6-acetone were carried out at 298, 308 and 318 K, giving $K_a > 10^4$ M^{-1} in each case. [c] precipitation of the host-guest complex observed during titration; [d] not performed.*

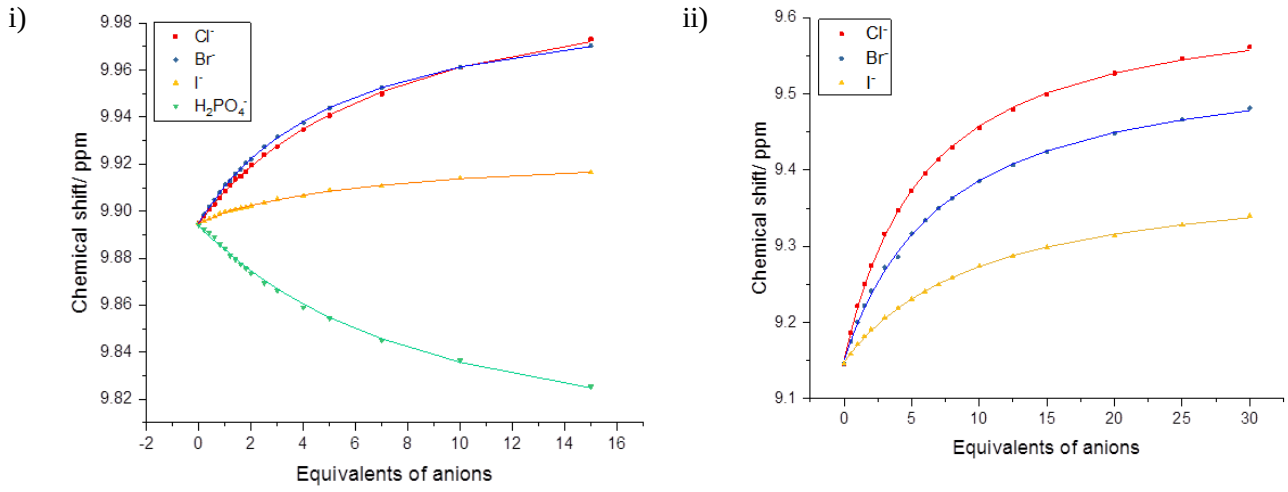

*Figure 39. i) Changes in the chemical shifts of internal pyridinium aromatic proton H_a of receptor **2.1_{Te}** with increasing quantities of anions in CD_3CN/ D_2O 99:1 v/v ([**2.1_{Te}**] = 1.0 mM, T = 298 K). ii) Changes in the chemical shifts of triazole protons of receptor **2.2_H** with increasing quantities of anions in CD_3CN/ D_2O 99:1 v/v ([**2.2_H**] = 1.0 mM, T = 298 K).*

As a consequence, **2.1$_{Te}$** exhibits comparable affinities for all anions studied, albeit with a slight preference for Br^-. The Hofmeister bias of binding the heavier, less-hydrated halides in wet solvent media closely mirrors the behaviour observed for XB host systems,[175] highlighting the similarity between both sister σ-hole interactions, and contrasts with the binding preferences of HB donor hosts. This is clearly illustrated by the K_a values determined for **2.2$_H$** with the halides in CD_3CN/ D_2O 99:1 v/v (Table 3), which show a distinct anti-Hofmeister bias (K_a of $Cl^- > Br^- > I^-$).

Summarising the anion binding results, overall (a) **2.1$_{Te}$** binds anions more strongly than its HB analogue **2.2$_H$** under identical solvent conditions, this is especially the case with the heavier halides bromide and iodide; (b) the nature of the solvent significantly influences the stability of the chalcogen-bonded host-guest complexes, where the strongest associations are observed in aprotic organic media of lower polarity (d_6-acetone > CD_3CN > d_6-DMSO > CD_3OD); and (c) in wet solvent media (CD_3CN/D_2O 99:1) **2.2$_{Te}$** displays the Hofmeister bias of favouring the binding of the heavier halides.

2.3.4. Chalcogen Atom Effects on Anion Binding

Having ascertained the anion binding properties of **2.1$_{Te}$** in a variety of solvents, the effects of substituting the Te ChB-donor atom with Se was investigated using receptors **2.3$_{Se}$** and **2.5$_{Se}$**. As no evidence of binding with Cl^- was found using **2.5$_{Se}$**, in CD_3CN, halide binding studies were performed in the less competitive d_6-acetone. In this solvent, the addition of Cl^- to acyclic receptor **2.3$_{Se}$** elicited *downfield* perturbations of the signals arising from the external aromatic proton H_b and the pyridinium methyl group H_c, concomitantly giving an *upfield* shift of H_a (Figure 40), which is in stark contrast to Cl^- binding by **2.1$_{Te}$** shown in Figure 36.[†]

[†] Lack of perturbations of signals arising from the $tBuArCH_2$-groups (i.e.H_d, H_e and H_f) show that they are not interacting with Cl^- nor involved in any significant desolvation processes accompanying anion binding. The possibility of the different terminal groups of 2.Se and 1.Te accounting for any differences in anion binding behaviour can thus be ruled out.

Similarly, iodide addition only caused small proton perturbations in the pyridinium region of **2.3$_{Se}$** (Figure 41). By fitting the titration data to a 1:1 host-guest stoichiometric binding model, **2.3$_{Se}$** was found to form the strongest complex with the more charge-dense Cl^- (K_a = 419 M^{-1}) compared to iodide (K_a = 190 M^{-1}) (Figure 41 & Figure 42).

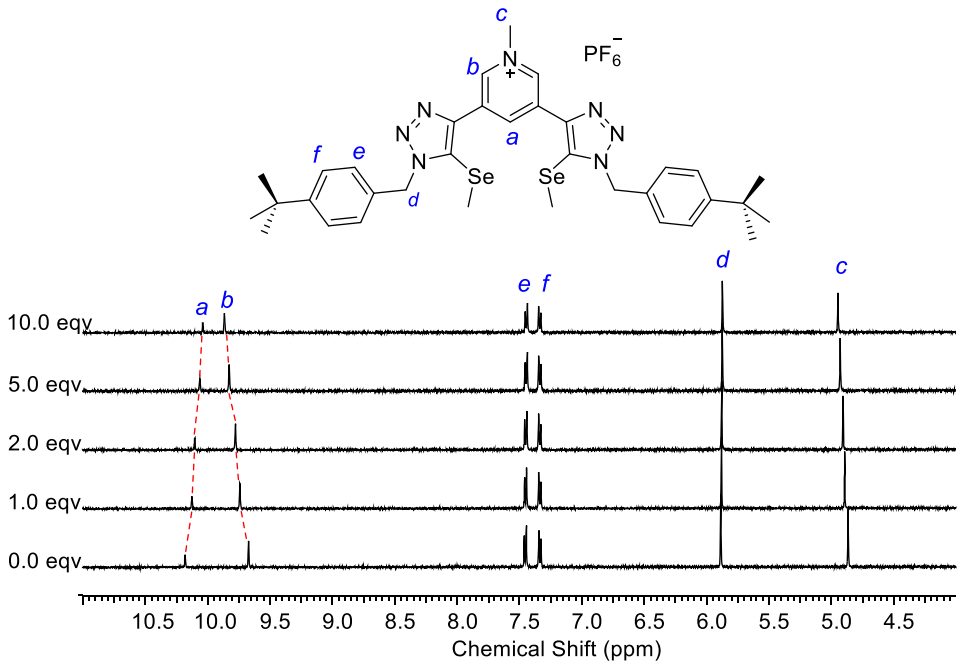

*Figure 40. Partial ^{1}H NMR spectra of **2.3$_{Se}$** in the presence of increasing quantities of Cl^- in d_6-acetone ([**2.3$_{Se}$**] = 1.0 mM, T = 298 K).*

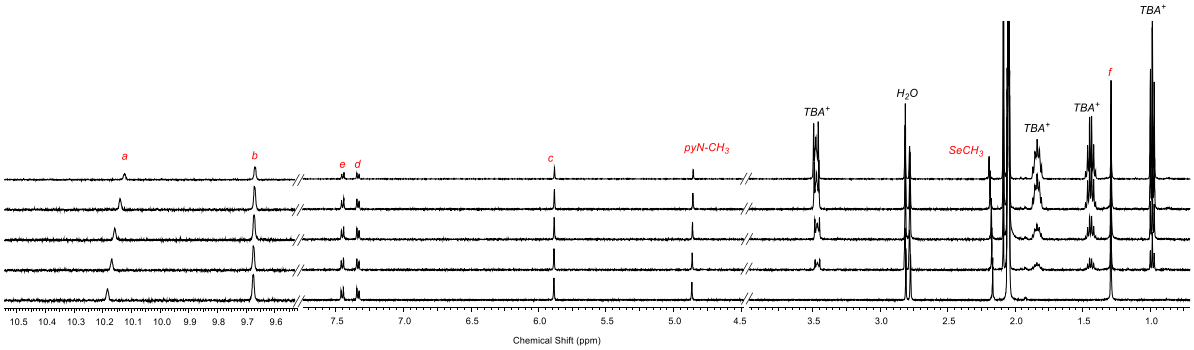

*Figure 41. Partial ^{1}H NMR spectra of **2.3$_{Se}$** in the presence of increasing quantities of I^- in d_6-acetone ([**2.3$_{Se}$**] = 1.0 mM, T = 298 K).*

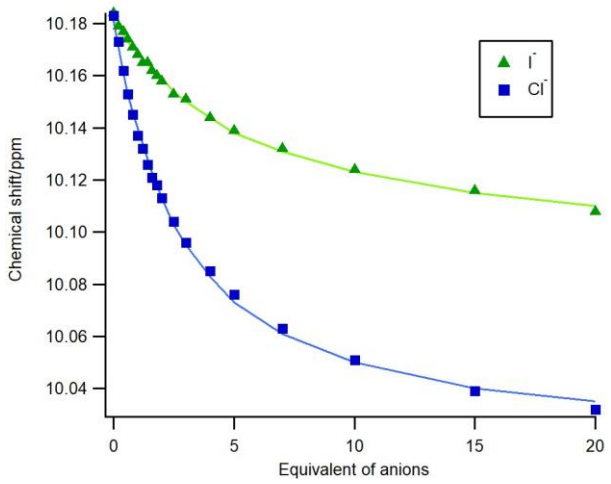

*Figure 42. Changes in the chemical shifts of internal protons (H_a) of receptor **2.3$_{Se}$** with increasing quantities of Cl^- and I^- in d_6-acetone ([**2.3$_{Se}$**] = 1.0 mM, T = 298 K).*

Similar signal perturbations were also observed with the pyridinium-bis(methylseleno-triazole) moiety of macrocycle **2.5$_{Se}$**, whilst the rest of the macrocycle signals showed no appreciable shifts (Figure 43i). These observations suggest that Cl^- is not binding in the cleft between both $SeCH_3$ units but is predominantly interacting in the vicinity of the cationic pyridinium nitrogen atom of both receptors, possibly driven by Coulombic attraction and HB interactions with H_b and H_c. Indeed, the possibility of competing HB or to a much lesser extent, anion-π interactions, between anions and cationic aromatic receptor frameworks bearing XB donor groups has been recently demonstrated by Huber and co-workers,[176] providing support for this mode of interaction between Cl^- and **2.3$_{Se}$** /**2.5$_{Se}$**.

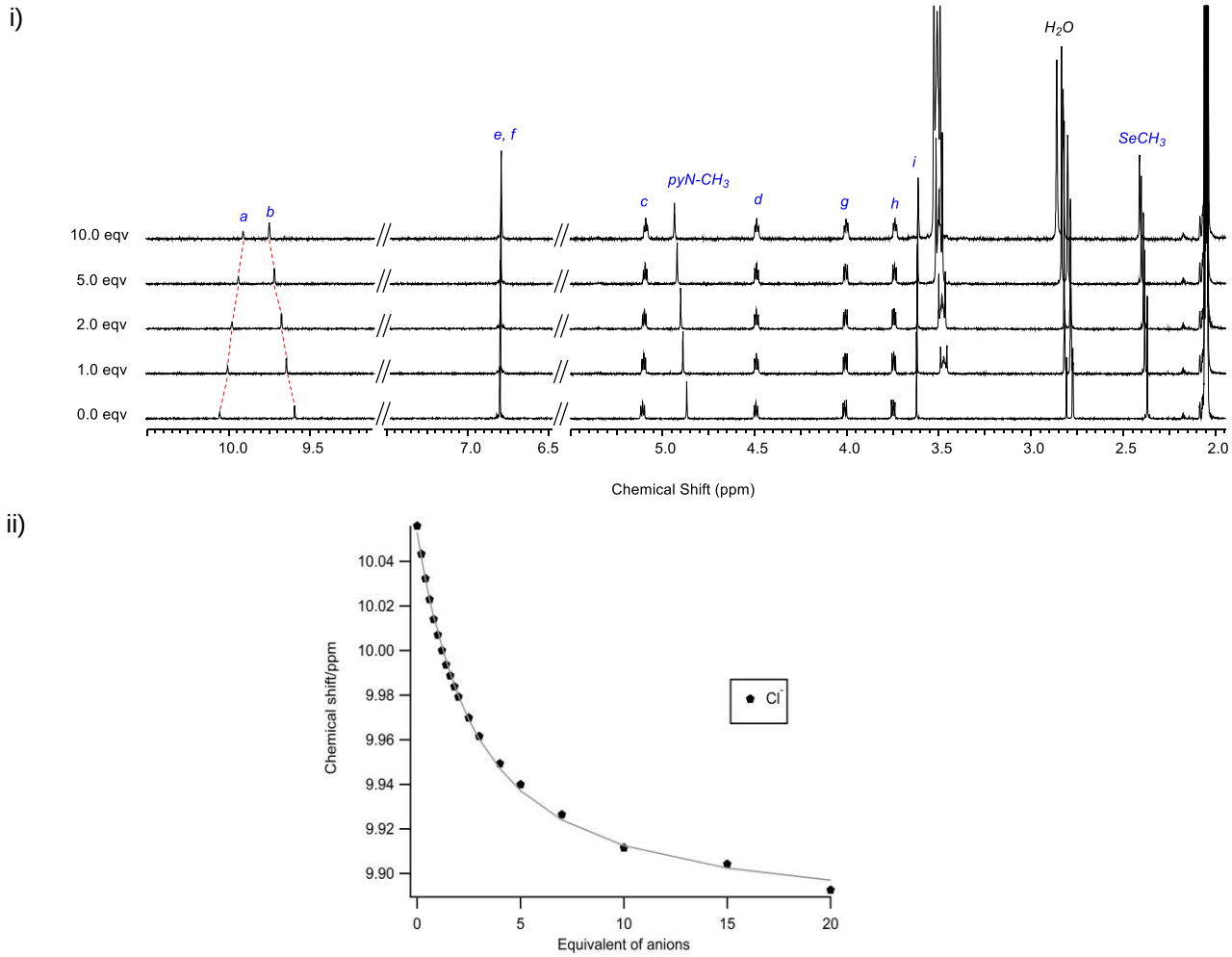

*Figure 43. i) Partial ^{1}H NMR spectra of macrocycle **2.5$_{Se}$** in the presence of increasing quantities of Cl^- in d_6-acetone ([**2.5$_{Se}$**] = 1.0 mM, T = 298 K). ii) Changes in the chemical shifts of pyridinium protons of macrocycle **2.5$_{Se}$** with increasing quantities of Cl^- in d_6-acetone ([**2.5$_{Se}$**] = 1.0 mM, T = 298 K)*

To provide further evidence, an analogous Cl^- titration experiment under identical conditions with the bis-fluorotriazole acyclic host analogue **2.4$_F$** was undertaken. Significant downfield shifts were seen for only H_b and H_c immediately adjacent to the cationic pyridinium nitrogen atom (Figure 44i). Furthermore, the similar Cl^- association constants determined for **2.5$_{Se}$** (K_a = 450 ± 23 M^{-1}) and **2.4$_F$** (K_a = 411 ± 21 M^{-1}), obtained by monitoring the downfield shifts of H_b, as well as the very small perturbations of the $SeCH_3$ ^{77}Se signals ($\Delta\delta_{Se}$ = +1.1 ppm over 10.0 equivalents of Cl^-) for **2.3$_{Se}$**, lends further support that Se-mediated ChB interactions play only a minor role in the halide anion association of **2.3$_{Se}$** and **2.5$_{Se}$** (Figure 44iii).

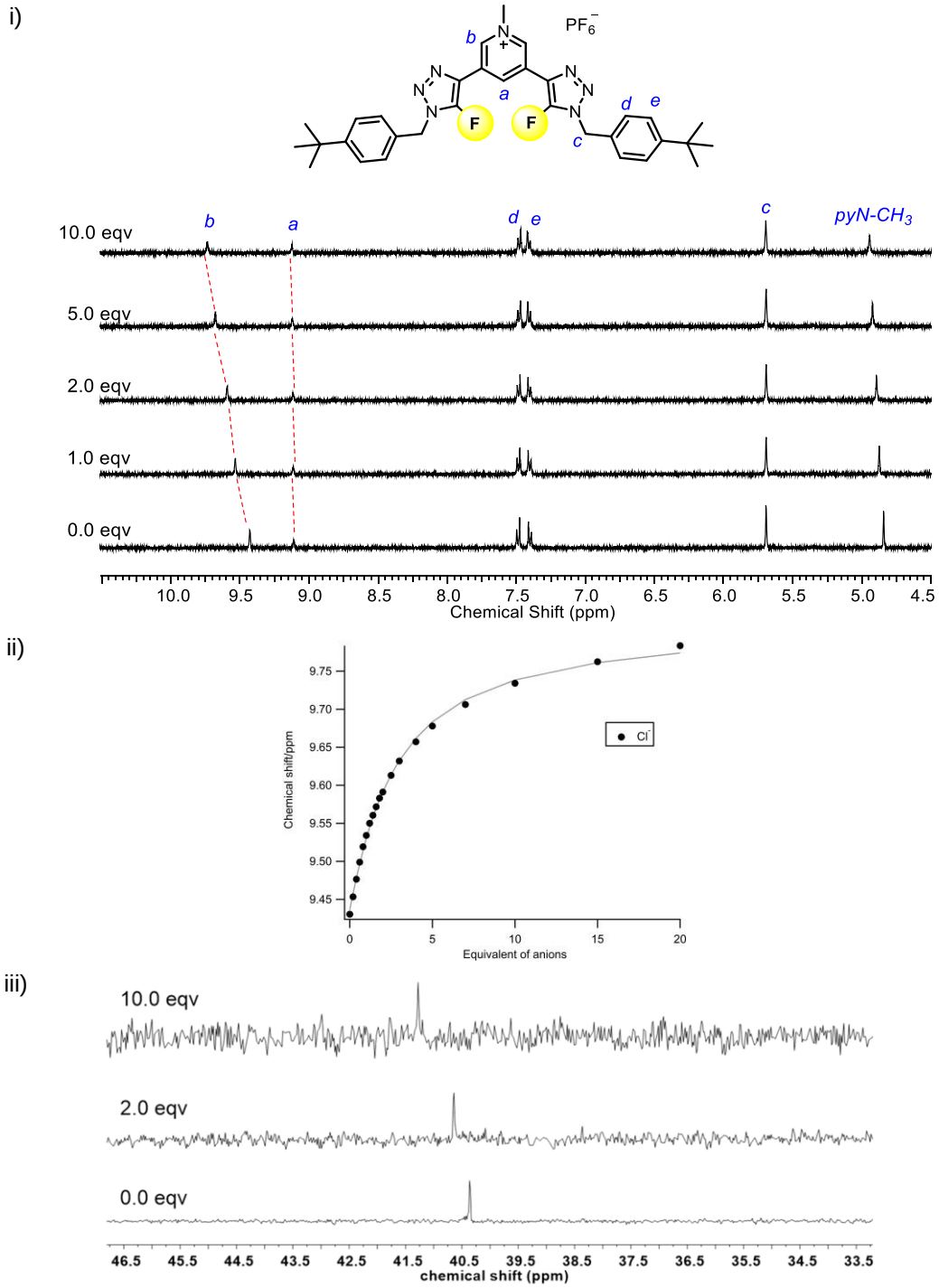

*Figure 44. i) Partial ^{1}H NMR spectra of **2.4$_F$** in the presence of increasing quantities of Cl$^-$ in d_6-acetone ([**2.4$_F$**] = 1.0 mM, T = 298 K). ii) Changes in the chemical shifts of pyridinium protons of receptor **2.4$_F$** with increasing quantities of anions in d_6-acetone ([**2.4$_F$**] = 1.0 mM, T = 298 K). iii) Partial ^{77}Se NMR spectra of **2.3$_{Se}$** in the presence of 0.0, 2.0 and 10.0 eqv of Cl- in d_6-acetone ([**2.3$_{Se}$**] = 4.0 mM, T = 298 K). A saturated internal standard of diphenyl diselenide was used as a reference peak (d_6-acetone, δ 453 ppm). ΔδSe = +1.1 ppm downfield.*

Although one may expect that the ChB donor properties of Se-based receptors to be inferior to Te-containing analogues owing to the reduced polarizability of Se, the weakness of the ChB-anion

interactions with **2.3$_{Se}$** and **2.5$_{Se}$** is surprising, considering that cationic methylseleno-triazolium (direct N^3-methylation on the triazole)[100] and divalent chalcogeno-benzimidazolium motifs[155] are potent ChB donors in both the solid state and in solution. Clearly, polarisation of neutral methylseleno-triazoles with a central cationic pyridinium unit is insufficient to render the σ-holes on Se electron-deficient enough for strong anion interactions.

2.4. Thermodynamic Contributions to Anion Binding

The thermodynamic enthalpic and entropic contributions behind the ChB halide anion binding trends were elucidated by variable-temperature (VT) ^{1}H NMR titration experiments. Measurements were performed at temperatures spanning at least 40 K to determine K_a values in dry and wet CD_3CN as well as d_6-acetone. Evidence of anion association was observed to weaken with increasing temperatures. Notably, **2.1$_{Te}$** did not show any evidence of thermal decomposition at temperatures as high as 338 K even in the presence of water, a testament to its thermal and chemical stability (Figure 45). †

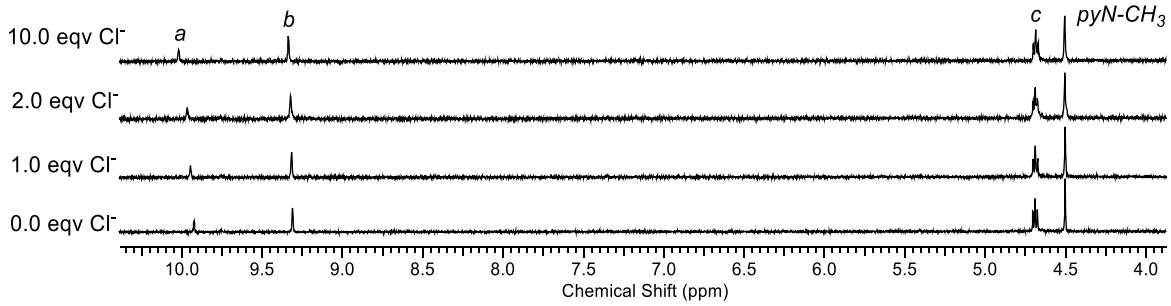

*Figure 45. Partial ^{1}H NMR spectra of **2.1$_{Te}$** at 338 K in the presence of increasing quantities of Cl^- in CD_3CN ([**2.1$_{Te}$**] = 1.0 mM) where H_a is the internal pyridinium proton and H_b is the external pyridinium protons. Note the absence of receptor decomposition at 338 K.*

† For all host systems, halide guests and solvent conditions studied, plots of $\ln K_a$ against T^{-1} gave excellent linearity (|Pearson's R| > 0.99) indicating negligible changes in overall heat capacity of the system over the temperature range studied due to enthalpic invariance ($C_p = dH/dT$).

2.4.1. Elucidating Thermodynamic Properties of Chalcogen Receptors

Association constants (K) gathered from VT ^{1}H NMR titrations allow the enthalpic (ΔH) and entropic (ΔS) term to be determined *via* the van't Hoff equation:[†]

$$\ln K = -\frac{\Delta H^0}{R}\frac{1}{T} + \frac{\Delta S^0}{R}$$

Plotting ln K against $\frac{1}{T}$, gives, $-\frac{\Delta H^0}{R}$ as the gradient, and $\frac{\Delta S^0}{R}$ as the intercept of the linear[‡] fit.

Hence the change in enthalpy (ΔH) will determine the type of van't Hoff plots obtained, where $\Delta H > 0$ (negative gradient) represents an endothermic reaction while $\Delta H < 0$ (positive gradient) represents an exothermic reaction.

The van't Hoff plots obtained for receptor **2.1$_{Te}$**, **2.2$_{H}$**, **2.3$_{Se}$** and **2.5$_{Se}$** in various solvents are shown in Figure 46. From the plot gradients, the exothermic and endothermic trends can be observed. VT titration measurements carried out in dry and wet CD_3CN resulted in receptors **2.1$_{Te}$** and **2.2$_{H}$** having positive gradients which suggests exothermic binding events while Se-containing receptors have negative gradients suggesting endothermic binding events. As seen from Figure 46, all van't Hoff plots gave excellent line of best fit by its calculated Pearson's R value > 0.99. By using the Gibbs' free energy equation, $\Delta G = \Delta H - T\Delta S$, the thermodynamic halide binding data (ΔG, ΔH and $T\Delta S$) is collected in Table 4 and represented visually in Figure 47.[ǂ]

[†] R is the ideal gas constant (8.314 $JK^{-1}mol^{-1}$)

[‡] A linear van't Hoff plot assumes that enthalpy and entropy are constant with temperature changes where any non-linearity (first-order approximation) suggests that different species has different heat capacities.

[ǂ] Binding isotherms and associations constants can be found in Appendix A2.

i)

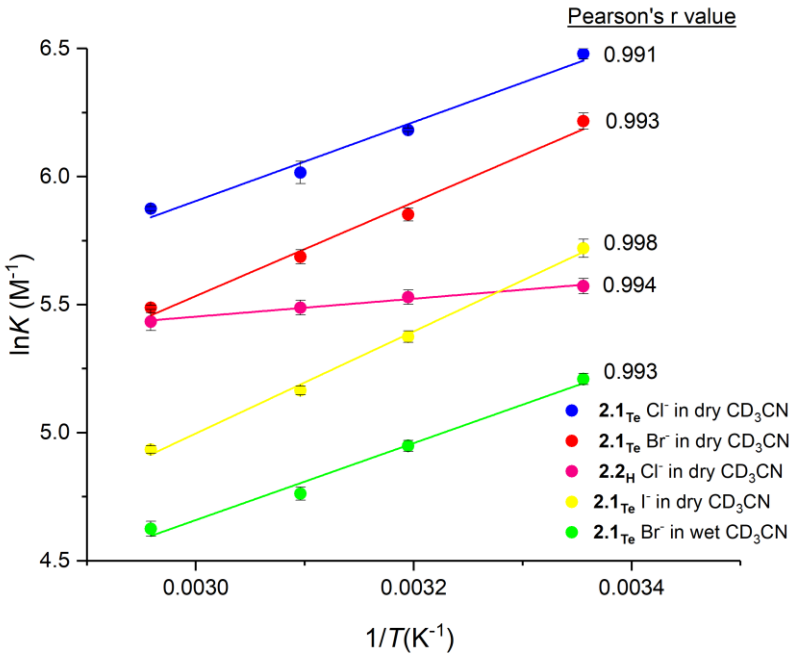

ii)

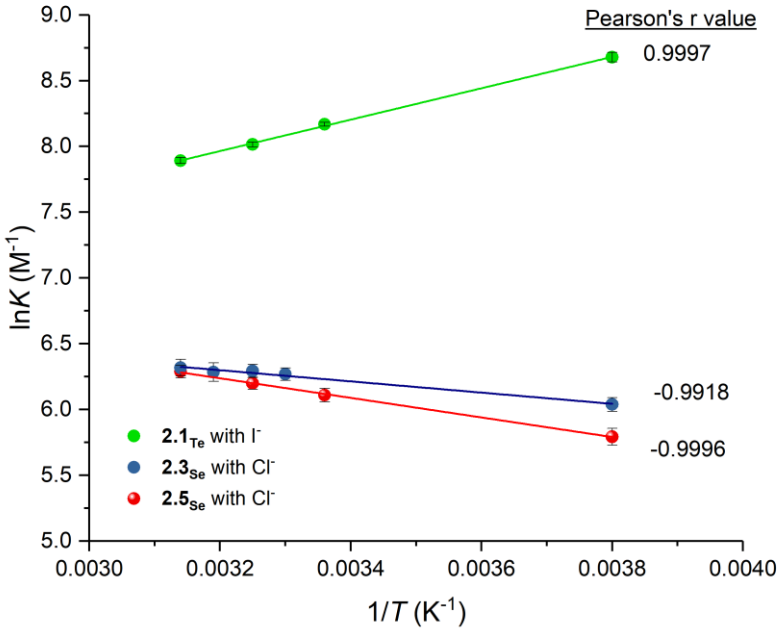

*Figure 46. van 't Hoff plots showing the changes of association constant (K_a (M^{-1}) i) **2.1$_{Te}$** and **2.2$_H$** with different halides at different temperatures (T (K)), determined using VT ^{1}H NMR titration experiments. Errors (±) of K are indicated as error bars ([host] = 1.0 mM, solvent = CD_3CN or CD_3CN/D_2O 99:1). ii) **2.3$_{Se}$** and **2.5$_{Se}$** with different halides at different temperatures (T (K)),*

determined using VT ^{1}H NMR titration experiments. Errors (±) of K are indicated as error bars ([host] = 1.0 mM, solvent = d_6-acetone).

Table 4. Thermodynamic parameters (ΔG, ΔH and TΔS) for halide binding by receptors ***2.1$_{Te}$, 2.2$_H$, 2.3$_{Se}$*** *and* ***2.5$_{Se}$*** *in various solvent mixtures.* [a]

S/N	Host	Solvent	Anion	Δ*G*/ kJ mol^{-1}	Δ*H*/ kJ mol^{-1}	TΔS/ kJ mol^{-1}
1		CD_3CN	Cl^-	-16.1	-12.8	+3.2
2		CD_3CN	Br^-	-15.4	-15.2	+0.1
3	**2.1$_{Te}$**	CD_3CN	I^-	-14.2	-16.6	-2.4
4		d_6-acetone	I^-	-20.2	-9.9	+10.3
5		CD_3CN/ D_2O 99:1	Br^-	-12.9	-12.5	+0.4
6	**2.2$_H$**	CD_3CN	Cl^-	-13.8	-2.9	+10.9
7	**2.3$_{Se}$**	d_6-acetone	Cl^-	-15.4	+3.6	+19.0
8	**2.5$_{Se}$**	d_6-acetone	Cl^-	-15.1	+6.2	+21.3

[a] Errors for individual titrations <10%; [host] = 1.0 mM

2.4.2. ChB-mediated Binding of Halides

In CD_3CN, the ChB-mediated binding of halides to **2.1$_{Te}$** (Table 4, entries 1-3) was found to be strongly dominated by enthalpy in all cases. This is especially the case with bromide and iodide which exhibit significantly larger exothermic enthalpic values than chloride. Interestingly, whereas the binding of chloride is also entropically favourable, an almost negligible entropic contribution is observed for Br^- and entropy is disfavoured for I^-. Clearly, the reduction in binding affinity observed with the heavier halides is driven solely by the increasingly unfavourable entropic contributions. It has been previously demonstrated computationally that interactions between ChB donors and the heavier, 'softer' and more polarisable halides possess greater covalency/charge-transfer character,[100] which may partly account for the increasing exothermic contribution observed for Te-bromide and Te-iodide chalcogen bond formation. It is interesting to note that a similar trend of more exothermic binding compensated by greater loss in entropy (although Δ*S* was favourable in all cases) in the binding of Cl^-, Br^- and I^- was previously reported with iodoimidazolium XB hosts.[177] Nonetheless, the varying extents of halide desolvation during the anion binding process may also partly contribute towards the thermodynamic trends observed.

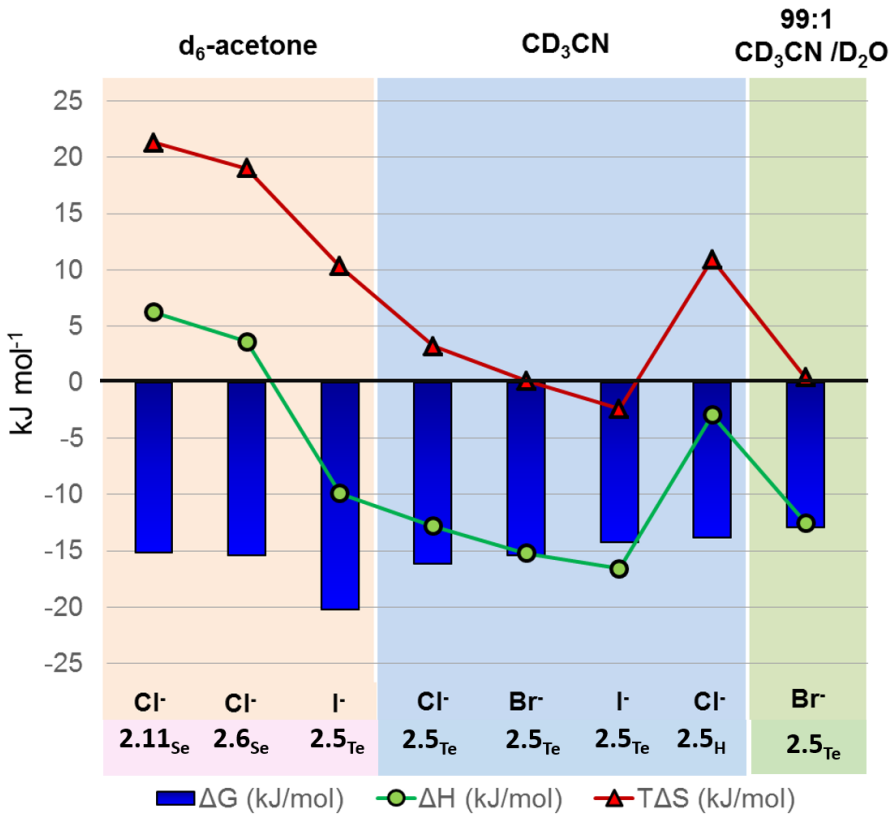

Figure 47. Thermodynamic parameters of receptors ***2.1*** $_{Te}$, ***2.2*** $_{H}$, ***2.3*** $_{Se}$ *and* ***2.5*** $_{Se}$ *in various solvent mixtures to halide guests.*

2.4.3. Influence of Solvent

As shown in Table 4, dramatic enhancements in the Cl^- and I^- affinities of $\mathbf{2.1_{Te}}$ was found in d_6-acetone compared with CD_3CN. Due to the very strong association of Cl^- ($K_a > 10^4$ M^{-1}), thermodynamic binding parameters could not be determined accurately using ^1H NMR van't Hoff analysis. Nonetheless, $\mathbf{2.1_{Te}}$-I^- binding in d_6-acetone was observed to be driven by favourable enthalpic and entropic contributions (Table 4, entry 4), in contrast to binding in CD_3CN (Table 4, entry 3) which was exclusively enthalpically-driven. Surprisingly, the greater iodide affinity observed in d_6-acetone was not reflected in a larger exothermic enthalpy value; indeed, the exothermic magnitude is significantly diminished. Instead, the augmented affinity results from a favourable entropy increase. This unexpected result is difficult to rationalise, given that both solvents

have similar Gutmann donor/acceptor numbers[178] ($DN_{acetone}$ = 17.0 > $DN_{acetonitrile}$ = 14.1), ($AN_{acetone}$ = 12.5 < $AN_{acetonitrile}$ = 19.3) and free energies of iodide solvation.[179] Nonetheless, these observations may be a consequence of changes in the solvent structure following host-guest binding. In the liquid phase, theoretical simulations have revealed that acetone[180] exhibits smaller degrees of short-range molecular ordering than acetonitrile,[181] with the latter adopting L-shaped and head-to-tail antiparallel configurations between neighbouring molecules. Upon binding between I^- and **2.1$_{Te}$**, the released CD_3CN molecules undergo a greater extent of re-ordering compared with d_6-acetone, giving rise to a greater entropic penalty. A similar reasoning has been invoked to account for the exothermic, but entropically-disfavoured anion binding in solvents exhibiting a degree of structural-ordering such as water[182] and chloroform.[183]

The van't Hoff analysis of Br^- binding by **2.1$_{Te}$** in CD_3CN/ D_2O 99:1 *v/v* (Table 4, entry 5) proved insightful in elucidating the thermodynamic origins of the reduced anion affinities observed in the presence of water (Table 3). Compared to pure CD_3CN (Table 4, entry 2), Br^- binding in the wet solvent retained the dominance of the enthalpic driving force over entropy, despite reducing the exothermic magnitude ($\Delta\Delta H$ = -2.7 kJ mol^{-1}). This observation is consistent with previously reported computational findings on the effects of halide hydration on ChB binding:[100] the binding of hydrated halide anions brings the associated water molecules in its hydration shell into close proximity with the Te atoms, which disrupt the Te···Br^- ChB interactions. At the same time, the stronger D_2O···Br^- interactions compared with CD_3CN, reflected by the large acceptor number of D_2O (AN = 54.8),[178] makes desolvation enthalpically unfavourable. These factors in combination may manifest in the diminished exothermicity observed.

2.4.4. Differences Between ChB- and HB-mediated Anion Binding.

To understand the unique aspects of ChB-mediated anion binding, the thermodynamic parameters for the binding of Cl^- to **2.2$_H$** were determined (Table 4, entry 6). Although Cl^- binding was driven favourably by both enthalpy and entropy in CD_3CN, the entropic term dominates for **2.2$_H$**, accounting

for nearly 80% of the free energy of binding. In contrast, **2.1$_{Te}$**···Cl^- binding was mostly dominated by enthalpy (Table 4, entry 1). A favourable entropic contribution to binding of anions to HB receptors in polar aprotic solvents with significant hydrogen bond basicity[184] such as acetonitrile[185–188] has been attributed to desolvation of the Lewis acidic host binding site during anion complexation.[173] The difference in thermodynamic signature with **2.1$_{Te}$** may suggest that its ChB-donor binding cavity is less extensively desolvated during anion binding. As the process of desolvation is inherently endothermic, this may also partly account for a much smaller exothermic binding contribution observed for **2.2$_{H}$** compared to **2.1$_{Te}$**. Similarly, Cl^- binding by **2.3$_{Se}$** and **2.5$_{Se}$** in d_6-acetone was found to be driven exclusively by entropy (Table 4, entries 7 and 8), in stark contrast with that for I^- binding by **2.1$_{Te}$** in the same solvent (Table 4, entry 4). As mentioned previously, the Se atoms are insufficiently polarised by the cationic pyridinium-bis(triazole) receptor framework to allow strong ChB interactions with the halides, with the consequence that halide binding by **2.3$_{Se}$** and **2.5$_{Se}$** is predominantly electrostatically-driven, unlike the ChB interactions primarily responsible for I^- binding by **2.1$_{Te}$**. The large entropic driving force observed in each case is thus consistent with extensive host-guest desolvation upon anion association, whilst the absence of strong directional bonding interactions (e.g. HB) formed between **2.3$_{Se}$** and **2.5$_{Se}$** with Cl^- results in the lack of any favourable enthalpic contribution. Nonetheless, although the **2.5$_{Se}$**···Cl^- interaction is more favourable entropically, this is offset by a larger unfavourable endothermic enthalpy, resulting in almost identical Cl^- affinities for the Se receptors. Although this difference in thermodynamic signature is likely a consequence of the structural differences between **2.3$_{Se}$** and **2.5$_{Se}$**, no significant macrocyclic effect is observed which may be due to the exocyclic association of Cl^- on the periphery of the macrocycle **2.5$_{Se}$**.

2.4.5. Concluding Remarks

The synthesis of novel cationic ChB-based acyclic and macrocyclic anion receptors, that importantly are stable at ambient and alleviated temperatures, allowed the elucidation of their anion binding thermodynamic properties *via* VT ^{1}H NMR titrations. The stability of macrocycle **2.5$_{Se}$** encouraged a subsequent investigation into the integration of ChB-donors into interlocked hosts which is

presented in the last section of this chapter (Section 2.7.1). In an effort to provide more insights into σ-hole anion interactions, the following sections discuss hybrid XB-HB (Section 2.5) and ChB-HB structures (Section 2.7.3) for anion recognition that contain thioamide HB binding motifs.

2.5. Hybrid XB-HB Interlocked Structures Containing Thioamides

Thioamides are known to possess more acidic protons than their amide counterparts and have been incorporated into receptors as anion binding motifs.[22,173,188,189] It has been reported that isosteric substitution of an amide HB donor with a thioamide donor results in increased anion binding affinity due to lone pair (n) $n \rightarrow \pi^*$ electronic delocalisation.[190] For example, Jurczak and co-workers, developed a range of acyclic pyrrole-based amide and thioamide receptors for anion recognition in DMSO/0.5% H_2O solvent mixture.[188] A comparison of the binding constants found the thioamide receptors exhibited a stronger affinity towards benzoate and chloride anions than their amide analogues. Also Bowman-James and co-workers have shown polythioamide macrocycles to display higher affinity for $H_2PO_4^-$, HSO_4^- and F^- in DMSO compared to the cyclic amide analogues.[191]

The synthesis of a novel thioamide macrocycle **2.22** (Scheme 5) was inspired by the reported significant evidence of halide anion - halogen bond covalency in a mixed HB/XB [2]catenane $\mathbf{2.17_{XB}}$[172] consisting of XB bis-iodotriazole pyridinium **2.15** and HB isophthalamide macrocycle $\mathbf{2.16_{CH}}$ components (Scheme 4). Using a Cl^- template strategy and ring-closing metathesis (RCM) of vinyl-appended XB pyridinium precursor **2.15** and isophthalamide macrocycle $\mathbf{2.16_{CH}}$ with Grubb's II catalyst (10% wt), [2]catenane $\mathbf{2.17_{XB}{\cdot}Cl}$ was isolated in 41% yield. The catenane exhibited very strong Br^- and I^- affinity ($K_a > 10^4\ M^{-1}$) in a competitive aqueous-organic solvent mixture (10:45:45 $D_2O/CDCl_3/CD_3OD$). Importantly, this XB/HB catenane proved to be far more potent and selective for the heavier halides when compared to the HB [2]catenane $\mathbf{2.17_{HB}}$.[192] It was of interest to investigate the influence of HB donor ability on the anion recognition properties of a target thioamide macrocycle containing XB/HB catenane analogue.

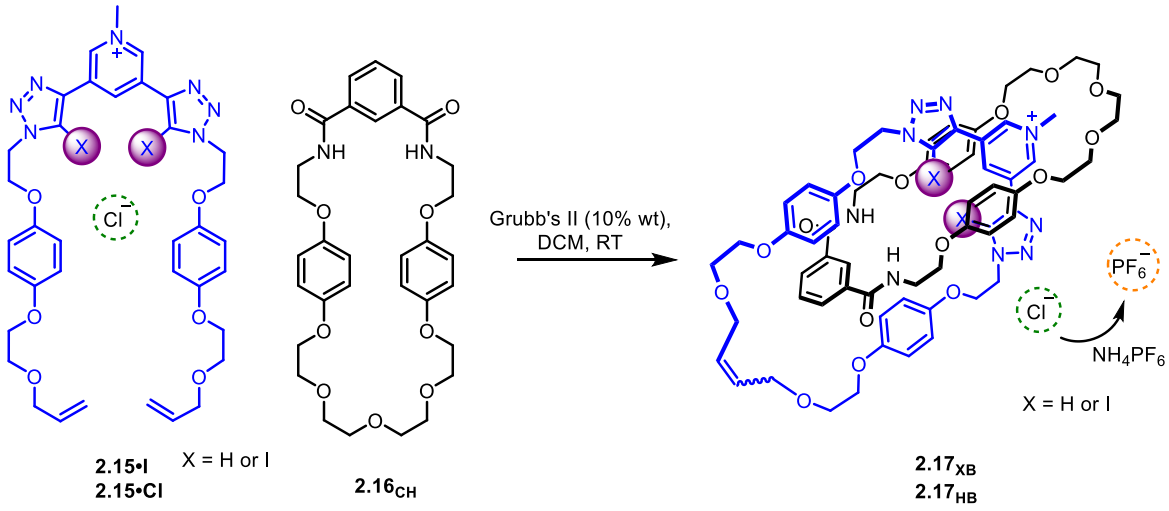

2.15•I
2.15•Cl

2.16_{CH}

2.17_{XB}
2.17_{HB}

Scheme 4. Previously reported mixed HB/XB [2]catenane 2.17.[172,192]

2.5.1. Synthesis of Thioamide Macrocycle

The synthesis of the target thioamide macrocycle **2.22** was achieved *via* the initial preparation of previously reported isophthalamide macrocycle **2.16**[136] (Scheme 5). *t*-Bu-isophthalic acid chloride **2.19** was synthesised from the corresponding commercial acid **2.18** *via* reaction with oxalyl chloride and a catalytic amount of DMF and used immediately without further purification. Reduction of bis-azide **2.20**[193] using hydrazine monohydrate in the presence of 10% Pd/C afforded the bis-amine macrocycle precursor **2.21** in 84% yield. High dilution conditions were used for amine condensation of precursors $\mathbf{2.19_{t\text{-}Bu}}$† and **2.21** in the presence of triethylamine in dry DCM to give macrocycle $\mathbf{2.16_{t\text{-}Bu}}$ in 38% yield after chromatographic purification. The amide groups of $\mathbf{2.16_{t\text{-}Bu}}$ were then converted to thioamides using the mild thionating Lawesson's reagent to give macrocycle **2.22**. Evidence of full conversion to thioamides was confirmed by IR spectroscopy. The characteristic amide carbonyl C=O bond stretch of $\mathbf{2.16_{t\text{-}Bu}}$ at *ca.* 1660 (± 20) cm^{-1} (as a strong band) was replaced by the thioamide C=S stretch at 1117 cm^{-1} in agreement with literature observations.[194]

† Instead of isophthalic acid, t-butyl isophthalic acid was used to increase solubility of final macrocycle.

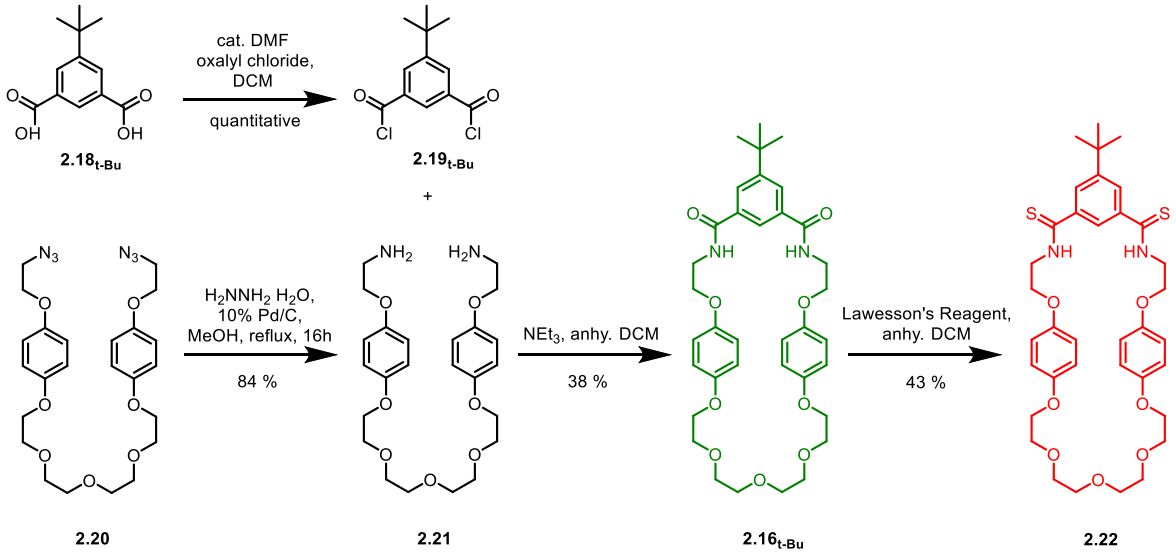

*Scheme 5. Synthesis of thiophthalamide macrocycle **2.17**.*

Small and poorly diffracting crystals of macrocycle **2.22** were obtained by slow evaporation of acetone in water. The crystal suffered considerable beam damage during data collection using synchrotron radiation, and hence relatively low-quality data were obtained. Nevertheless, the structure of the macrocycle was unambiguously determined showing unequivocal evidence of the thioamide functionalities present. (See Appendix B – for further details)

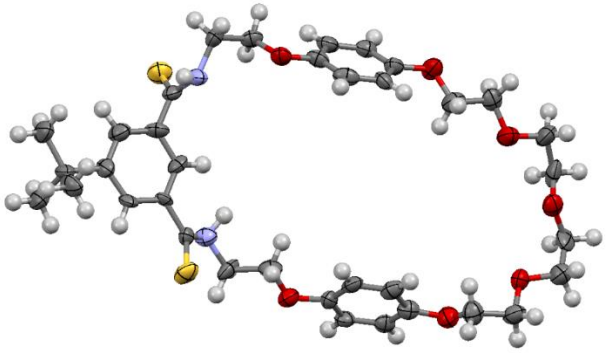

*Figure 48. X-ray crystal structure of macrocycle **2.22**. Thermal ellipsoids are displayed at the 50% probability level. Red = Oxygen; Blue = Nitrogen; Yellow = Sulfur.*

2.5.2. ^{1}H NMR Anion Binding Studies of Thioamide Macrocycle

Preliminary ^{1}H NMR anion titration studies were carried out in d_6-acetone and more competitive D_2O/d_6-acetone mixtures to compare the anion binding abilities of the thioamide macrocycle **2.22** with the amide-containing macrocycle analogue **2.16**. Generally, upon addition of halide anions to **2.22**, large downfield perturbations of the macrocycle's protons $H_{1,2,3}$ were observed (Figure 49). Splitting and downfield shifts were also seen for hydroquinone protons $H_{6,7}$ as well as some minor shifts in CH_2 protons $H_{4\text{-}11}$. These observations suggest the halide anion is binding within the macrocycle's bis-thioamide cleft[138] with iodide eliciting the smallest shifts (ie. $\Delta\delta_{H2}$ = 0.12 ppm after 10.0 equivalents of I^-). Nonlinear regression analysis of the ^{1}H NMR titration data using the WinEQNMR2 software[171] monitoring the shifts of proton H_2 determined 1:1 host-guest stoichiometric association constants summarised in Table 5.

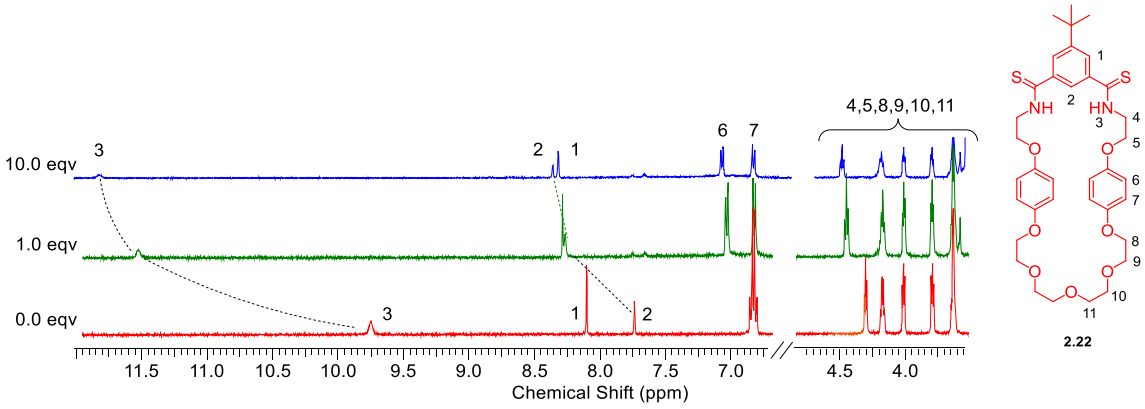

*Figure 49. Partial ^{1}H NMR spectra of **2.22** upon addition of 0.0, 1.0 and 10.0 eqv of TBACl in d_6-acetone. ([**2.22**] = 1.5 mM, Temperature = 298 K)*

In d_6-acetone, as was anticipated, the thioamide macrocycle **2.22** binds chloride (K_a >10^4 M^{-1}) much more strongly than amide macrocycle counterpart **2.16**$_{t\text{-Bu}}$ (K_a = 2560 M^{-1}, Table 5). Halide binding for **2.22** was found to follow the selectivity trend Cl^->Br^->I^-, dictated by charge density/relative size match, as observed with **2.16**$_{t\text{-Bu}}$. The binding of acetate (AcO^-) resulted in a 1:2 host-guest binding stoichiometry which may be attributed to a poorer geometry and size match with the macrocycle

binding site. In summary, as expected, thioamide-containing **2.22** proved to be the more effective HB-donor and anion receptor, consistent with previously reported observations.[195,196]

Analogous ^{1}H NMR titration experiments of **2.22** with Cl^- were conducted in more competitive D_2O/d_6-acetone solvent mixtures. In 2% D_2O/ d_6-acetone the association constant magnitude decreased significantly to K_a = 373 M^{-1} which was further reduced in progressively higher percentage of D_2O solvent mixtures, where no binding was observed in 10% D_2O. This is attributed to the increasing competition of Cl^- hydration.

*Table 5. Association constants, K_a (M^{-1}) for thioamide macrocycle (**2.22**) and isophthalamide macrocycle (**2.16$_{t\text{-}Bu}$**) with anions as tetrabutylammonium salts. [a]*

Anions	**2.16$_{t\text{-}Bu}$** [a,b] **K_a(M^{-1})**	**2.22**[a] **K_a(M^{-1})**			
	d_6-acetone	d_6-acetone	2% D_2O in d_6-acetone	5% D_2O in d_6-acetone	10% D_2O in d_6-acetone
Cl^-	2560	>10^4 (1557)	373 (3)	45 (1)	–[c]
Br^-	470	1216 (11)	–[d]	–[d]	–[d]
I^-	50	76 (2)	–[d]	–[d]	–[d]
AcO^-	–[d]	K_1 = 3559 (44) K_2 = 837 (13)	45 (3)	–[d]	–[d]

*[a] ^{1}H Titrations were carried out in the solvents indicated and WinEQNMR2[171] was used to determine the association constants using a 1:1 host-guest stoichiometric ratio for halides and a 2:1 host-guest ratio for acetate (AcO^-). (Errors in parentheses < 10%, [**2.22**] = 1.5 mM, Temperature = 298 K). b) Association constants previously reported ref[138]. c) no binding. d) titrations not conducted*

2.5.3. Anion Template Synthesis of Thioamide-XB-[2]Catenane

Anion templation has been exploited for interlocked rotaxane and catenane construction *via* strong intermolecular interactions.[197] As thioamide macrocycle **2.22** has a high affinity for binding Cl^-, as evidenced from ^1H NMR titration studies discussed in the previous section, this halide affinity was employed to template the formation of an unprecedented thioamide XB-[2]catenane. Using CuAAC click reaction conditions, the reaction of 3,5-bis-iodoethyne pyridine[198] with two equivalents of azide-alkene derivative **2.23**[192] in the presence of $Cu(MeCN)_4PF_6$ catalyst in dry, degassed THF afforded the bis-iodotriazole product **2.24** in a high yield of 84% (Scheme 6). Pyridine *N*-methylation of **2.24** using excess iodomethane and anion exchange of the resulting iodide salt **2.15·I** by repeated washing with 0.1 M NH_4Cl (aq) gave the chloride salt **2.15·Cl**. An equimolar mixture of the macrocycle precursor **2.15·Cl** and thioamide macrocycle **2.22** was dissolved in dry DCM and stirred at room temperature for 30 minutes, before ring closing metathesis (RCM) Stewart-Grubbs catalyst (10% wt/wt) was added to afford the target catenane **2.25·PF_6** in 34% isolated yield after preparative TLC purification and anion exchange to the non-coordinating PF_6^- salt (Scheme 6). The XB thioamide-based [2]catenane (**2.25·PF_6**) was fully characterised using ^1H, ^{13}C, ^{19}F, ^{31}P, 2D ROESY NMR spectroscopy as well as high-resolution ESI mass spectrometry (MS).

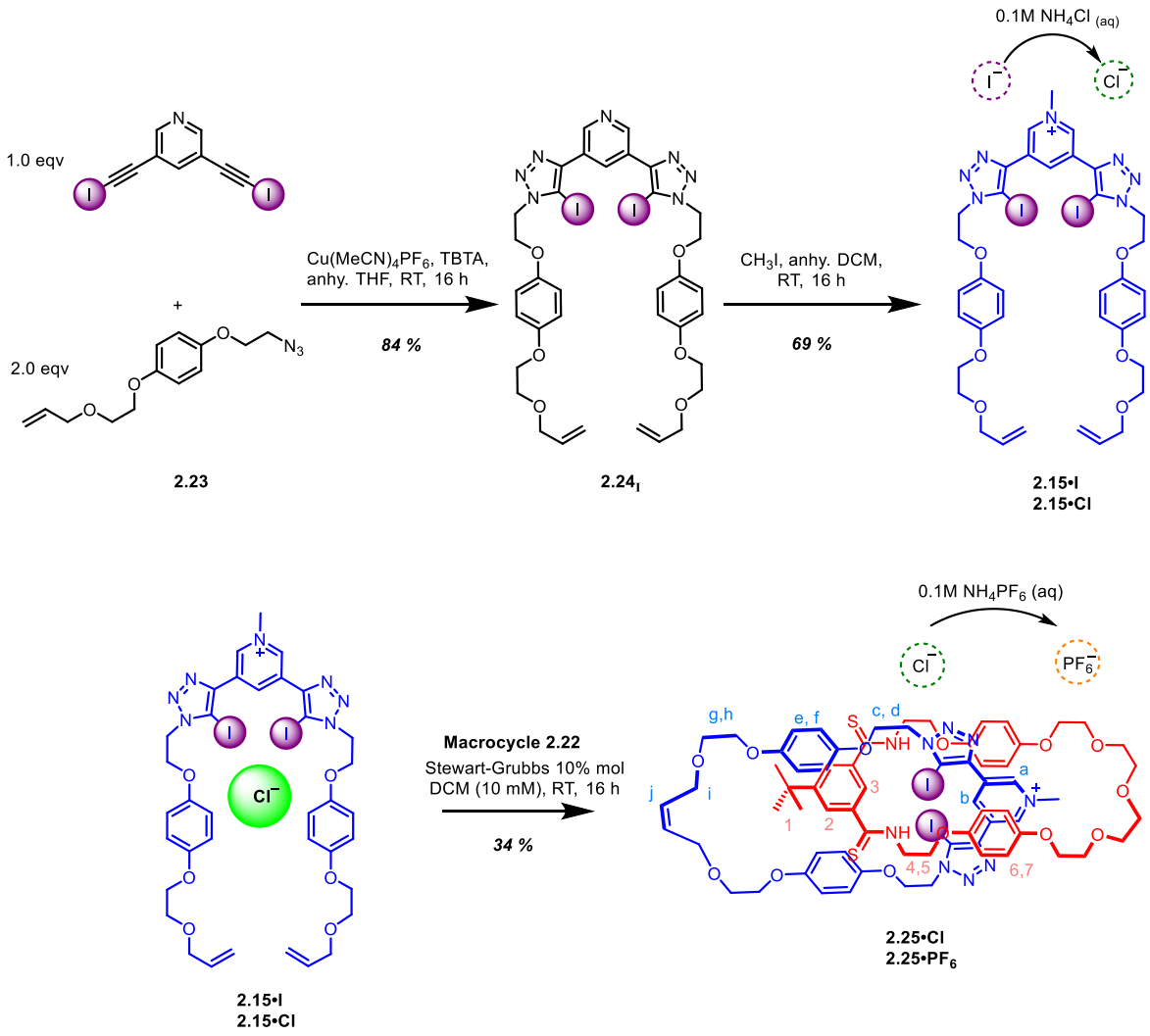

Scheme 6. Synthesis of thioamide-[2]catenane ***2.25·PF6.***

Crystals suitable for X-ray diffraction structural analysis were obtained by slow diffusion of diethyl ether into a solution of **2.25·Cl** in $CDCl_3/CD_3OD/D_2O$ (45:45:10 *v/v/v*) Significant positional disorder was observed on the polyether chains of one of the interlocked macrocycles, one of the iodine atoms, the chloride anion as well as the tert-butyl group, as manifested in enlarged prolate displacement ellipsoids. However, these disordered regions were successfully modelled and refined using partial occupancies over two sites. [2]Catenane **2.25·Cl** crystallised in *C*2/*c* with 1:1 host-guest ratio. Nonetheless, the halogen bonding interactions between one of the iodotriazoles units and Cl^- were clearly evident from the crystal structure. The XB interaction I···Cl^- has a measured distance of 2.971 Å (Red contact as shown in Figure 50), which is *ca.* 74% the sum of the van der Waals radii with bond angles of 173°, while the other I···Cl^- has a measured distance of 3.627 Å revealing

an asymmetric binding of Cl^- between the two iodotriazole motifs. Weaker HB interactions (blue contacts as shown in Figure 50) are also evident between hydrogens from thioamide protons, internal *t*-butyl benzene protons and Cl^-. Despite the presence of the S atom with the potential to form chalcogen bonds, no evidence of S···Cl^- interaction were observed, Cl^- binding is dominated by HB and XB interactions. Furthermore, π-π interactions can be seen from the stacking of the pyridinium motif between the aromatic hydroquinone groups. (See Appendix B – for further details)

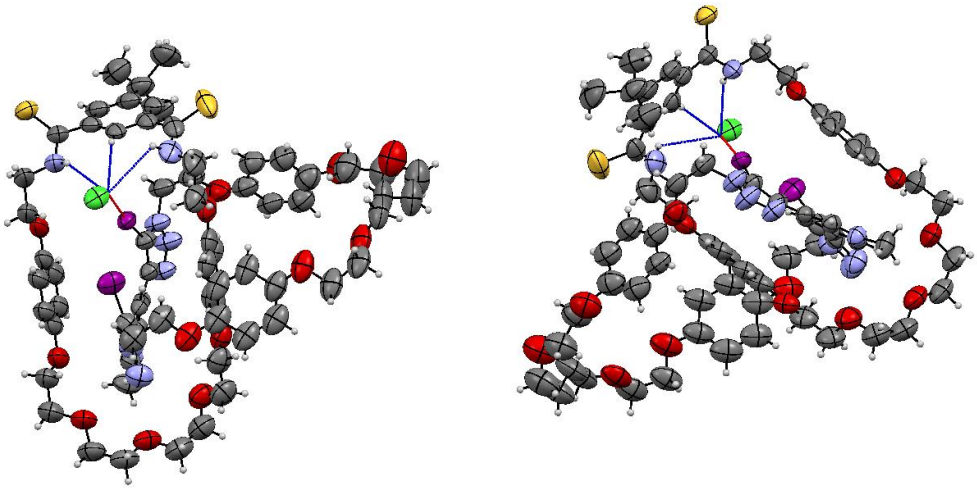

Figure 50. X-ray crystal structure showing the major component of catenane ***2.25·Cl*** *viewed at different angles. Thermal ellipsoids are displayed at the 50% probability level.*

Comparing the ^{1}H NMR spectra of macrocycle **2.22** and [2]catenane **2.25·PF_6** revealed significant proton perturbation differences (Figure 51i), where downfield shifts in aromatic protons $H_{1,2}$ and splitting of thioamide proton H_3 were observed. Significant upfield shifts and multiple splitting of the hydroquinone protons $H_{6,7}$ were observed upon formation of the [2]catenane due to aromatic π-stacking of the electron-rich hydroquinone and electron deficient pyridinium groups in close proximity. The interlocked nature of the catenane was also evidenced by 2D ROESY where through space interactions between pyridinium protons $H_{a,b}$ with hydroquinone protons $H_{6,7}$ were observed (Figure 51ii).

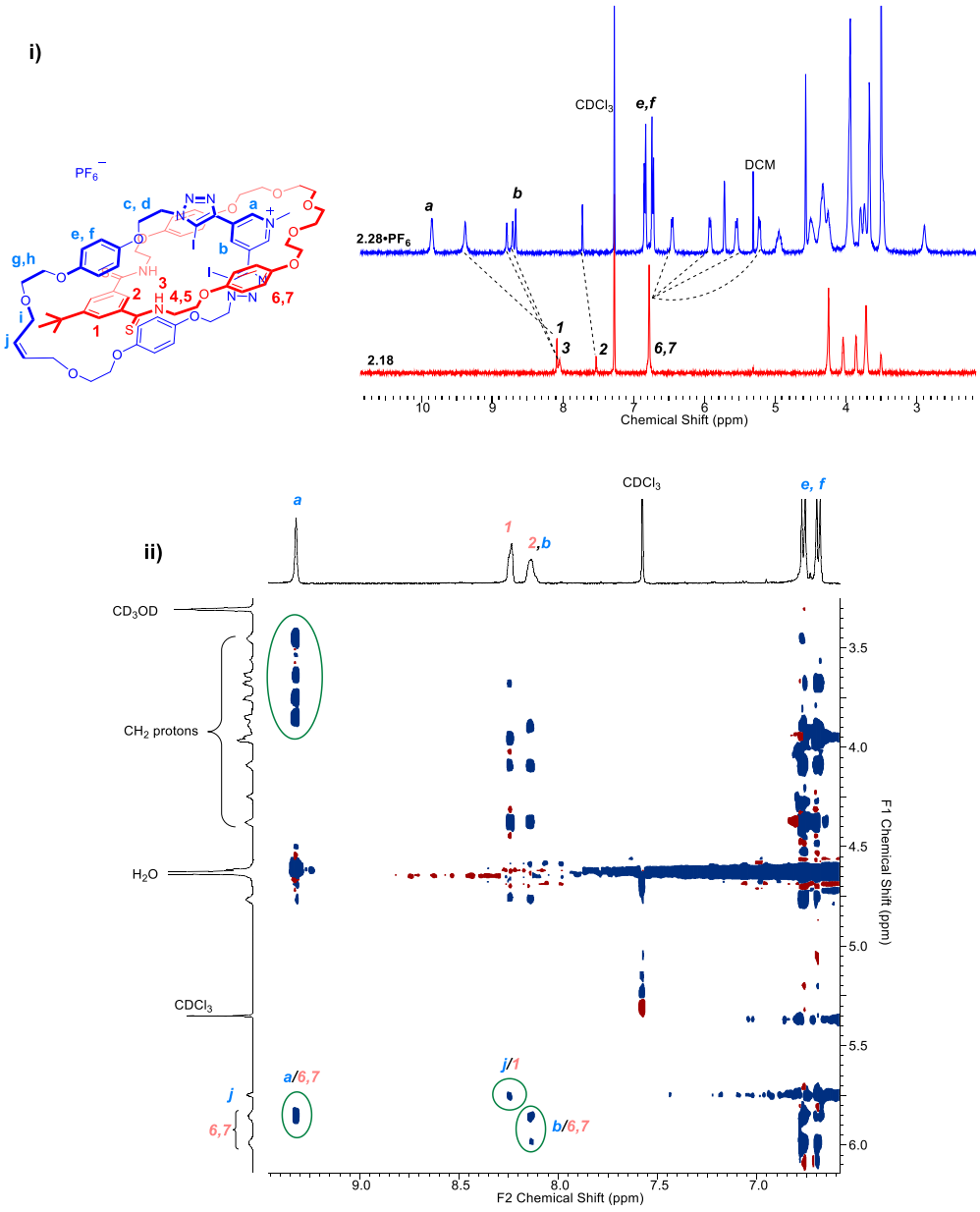

*Figure 51. i) Partial ^{1}H NMR spectra of thioamide macrocycle **2.22** and **2.25·PF$_6$** obtained in $CDCl_3$ solution. ii) 2D ROESY spectra of **2.25·PF$_6$** in 1:1 $CDCl_3$/CD_3OD solvent mixture.*

2.5.4. ^{1}H NMR Anion Titration Studies of Thioamide-XB [2]Catenane

Anion association constants were obtained by undertaking ^{1}H NMR anion titration experiments of the catenane with tetrabutylammonium salts in the competitive $CDCl_3/CD_3OD/D_2O$ (45:45:10 v/v) solvent mixture and monitoring changes in the chemical shifts of the internal proton H_b on the

pyridinium ring of the catenane host **2.25·PF$_6$** (Figure 52). Upon addition of aliquots of anions, evidence for binding was observed from the considerable upfield shifts of proton H_b. Iodide binding caused the largest perturbations in proton H_b ($\Delta\delta$ = 0.69 ppm after 10.0 equivalents of I^-) followed by bromide and chloride. No binding was observed for oxoanions acetate (AcO^-) and dihydrogen phosphate ($H_2PO_4^-$), probably due to the unfavourable geometric match of the respective trigonal planar and tetrahedral-shaped anions with the cavity of the catenane. Linear anion azide (N_3^-) and bent anion nitrite (NO_2^-) were also able to elicit significant proton perturbations for 1:1 stoichiometric host-guest association constants as determined by the WinEQNMR2 software[171] (Table 6). The observed Hofmeister bias in aqueous solvent mixtures for halides may be due to greater ease of halide desolvation for the heavier halides and has been previously observed.[18,175,199,200]

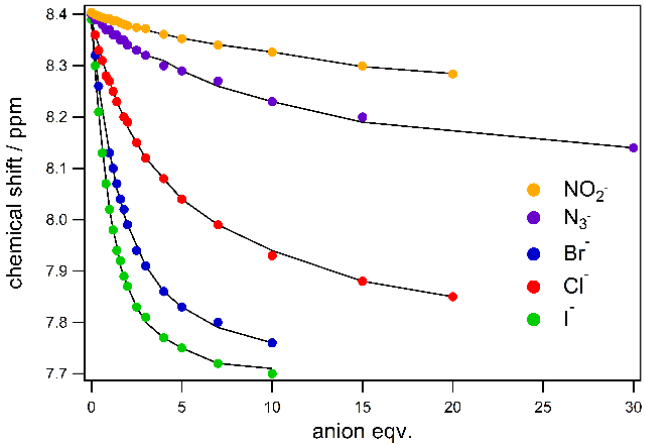

*Figure 52. Changes of the NMR chemical shifts of proton Hb on catenane **2.25·PF$_6$** with respect to the equivalent of anions added. Experimental data (solid markers) and fitted isotherms (solid lines) are shown.*

Table 6. Anion association constants, K_a (M^{-1}) for catenanes ***2.25·PF₆*** and ***2.17·PF₆***

Anion	**2.25·PF$_6$** [a]	**2.17·PF$_6$** [a, b, c]
		K_a**(M^{-1})**
Cl^-	295 (6)	1850 (224)
Br^-	869 (35)	$>10^4$
I^-	2061 (60)	$>10^4$
AcO^-	–[d]	–[d]
$H_2PO_4^-$	–[d]	–[d]
N_3^-	99 (5)	–[e]
NO_2^-	71 (4)	–[e]

a) ^{1}H NMR titrations were carried out in competitive $CDCl_3/CD_3OD/D_2O$ (45:45:10 v/v) solvent mixture and association constants were fit to a 1:1 model using WinEQNMR2 with errors in parentheses (> 15%), [2.25·PF$_6$] = 1.0 mM, Temperature = 298 K) b) Association constants obtained from ref[172]. c) Errors were found to be less than 10%. d) no binding. e) not conducted.

Thioamide macrocycle **2.22** was demonstrated to have relatively more potent HB donors in comparison to amide analogue **2.16**. Hence, it was expected that the thioamide-containing [2]catenane **2.25·PF$_6$** would exhibit enhanced binding affinity when compared to its similar[†] amide-containing [2]catenane **2.17·PF$_6$**.[172,175,195] However, the halide association constant values of the analogous isophthalamide catenane **2.17·PF$_6$** (Table 6) are higher in the same competitive solvent mixture $CDCl_3/CD_3OD/D_2O$ (45:45:10). Both XB catenanes display a Hofmeister bias ($I^->Br^->Cl^-$) in halide selectivity. It appears that the interactions between the competitive aqueous-organic solvent medium and the relatively more acidic thioamides of **2.25·PF$_6$** are stronger thus reducing the catenane's affinity for halides.

[†] Structurally similar [2]catenanes **2.25•PF$_6$** and **2.17•PF$_6$** differs by a ^{t}Bu group on the HB macrocycle, however this should not have any significant difference on the association constants measured.

2.6. Thioamides for Active-Metal Template Strategy

In biological systems, sulphur-based ligands originating from amino acids such as cysteine are often found coordinated to metal centres, as in zinc finger proteins and/or enzymes.[201] They are known to readily form coordination complexes with a variety of *d*-block metal cations.[202] Thioamides in particular bind Cu(I) through S-Cu interactions.[203] With this in mind, when incorporated into a macrocycle, there is the potential for the thioamide motif to be exploited for the active-metal template (AMT) synthesis of MIMs as discussed in Chapter 1 Section 3.3.1. This could be achieved using Cu(I) catalysed alkyne-azide cycloaddition (CuAAC), where the Cu(I) catalyst is bound in an endotopic fashion to thioamide macrocycle **2.22** as shown in Scheme 7. This section investigates the use of a thioamide based macrocycle in AMT synthesis of mixed XB-HB and ChB-HB donor rotaxanes for anion recognition.

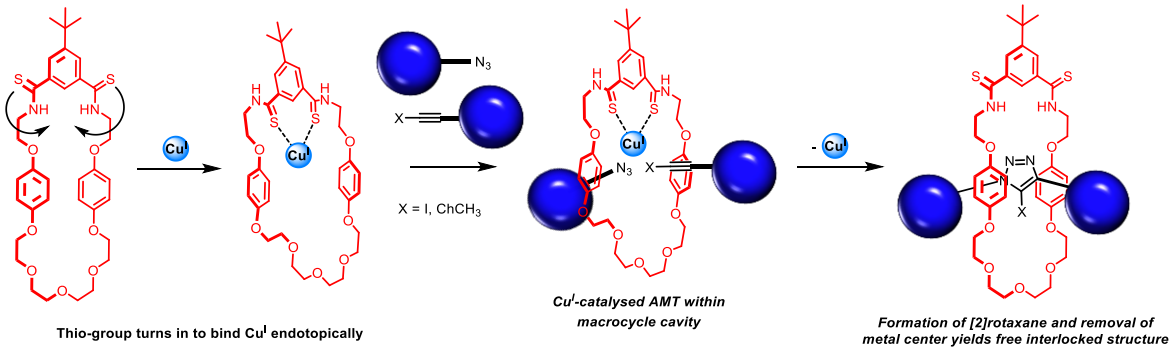

Scheme 7. Proposed Cu(I) coordination via thiol functional group within the macrocyclic cavity suitable for Cu(I)-catalysed AMT to afford final interlocked structure.

2.6.1. Attempted Synthesis of a Thioamide-XB[2]Rotaxane

The binding of Cu(I)[⌜] to macrocycle **2.22,** a pre-requisite for CuAAC-AMT, was investigated by UV-Vis titration in dichloromethane. Considerable changes were observed with a decrease of the

[⌜] $Cu(MeCN)_4PF_6$ was used and solvent was degassed using N_2(g) for at least 30 mins before use.

peak at *ca.* 287 nm and the appearance of a shoulder at *ca.* 350 nm with an isosbestic point at 304 nm. Significant colour change was also observed when increasing concentrations of Cu(I) were added to **2.22** (Figure 53).

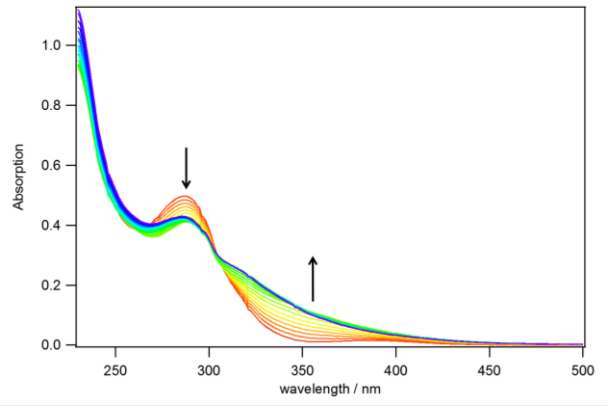

*Figure 53. UV-Vis titration of **2.22** (concentration = 50 µM). Upon aliquot addition of $Cu(MeCN)_4PF_6$ in dichloromethane, spectral changes from 0.0 eqv (red) to 3.0 eqv (blue)*

Binding of Cu(I) complex was also investigated by ^{1}H NMR titration of macrocycle **2.22** in acetone-d_6 (Figure 54). Significant proton perturbations and peak broadening in protons H_1 and H_2 were observed suggesting Cu(I)-interaction with the macrocycle. However, it was not possible to deduce the mode of Cu(I) coordination or to determine quantitative association constant data.

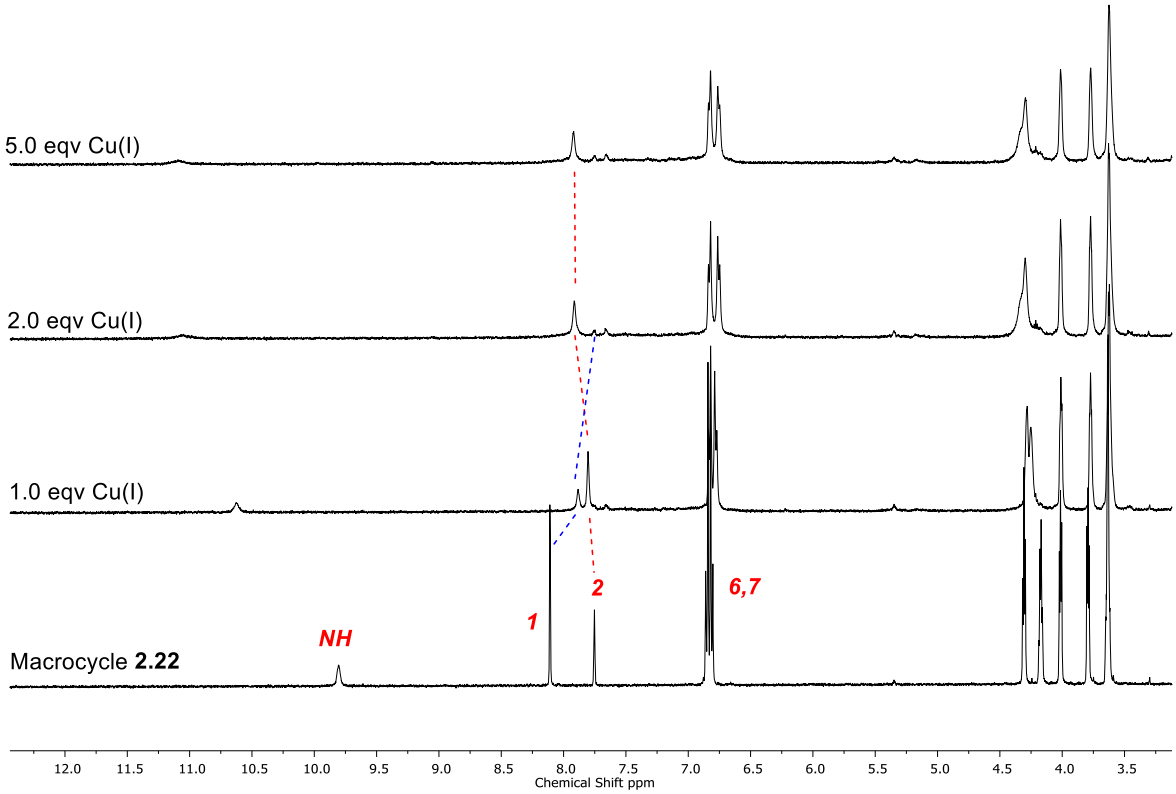

*Figure 54. Partial ^{1}H NMR spectra of macrocycle **2.22** in the presence of increasing quantities of $Cu(MeCN)_4PF_6$ in d_6-acetone ([**2.6**$_{se}$] = 1.0 mM, T = 298 K).*

Encouraged by the possibility of Cu(I)–binding by macrocycle **2.22**, the attempted synthesis of mono and bis-CuAAC 'click' triazole axle containing rotaxanes was undertaken (Scheme 8). Applying AMT conditions to equimolar mixtures of macrocycle **2.22** and $Cu(MeCN)_4PF_6$ in dry, degassed dichloromethane, excess amounts of the appropriate alkyne **2.27** (proto- or iodoalkyne) or bis-alkyne **2.28**, and stopper azide **2.26** were added sequentially and the reactions monitored by ESI-MS. Rotaxane **2.29$_H$** was detected by ESI-MS at 1836.0 m/z $[M + Na]^+$ however efforts to purify the interlocked structure by preparatory thin layer chromatography were challenging and the target rotaxane could not be isolated. Reaction attempts to synthesise the XB-analogue rotaxane **2.29$_I$** also failed to afford any evidence of interlocked product. Rotaxane **2.30** was not detected by ESI-MS measurements, instead, peak at 1302.9 m/z corresponding to the axle $[M + H]^+$ was observed suggesting the Cu(I) catalytic species was not being endotopically coordinated within the macrocycle, which is crucial for AMT mechanical bond formation.

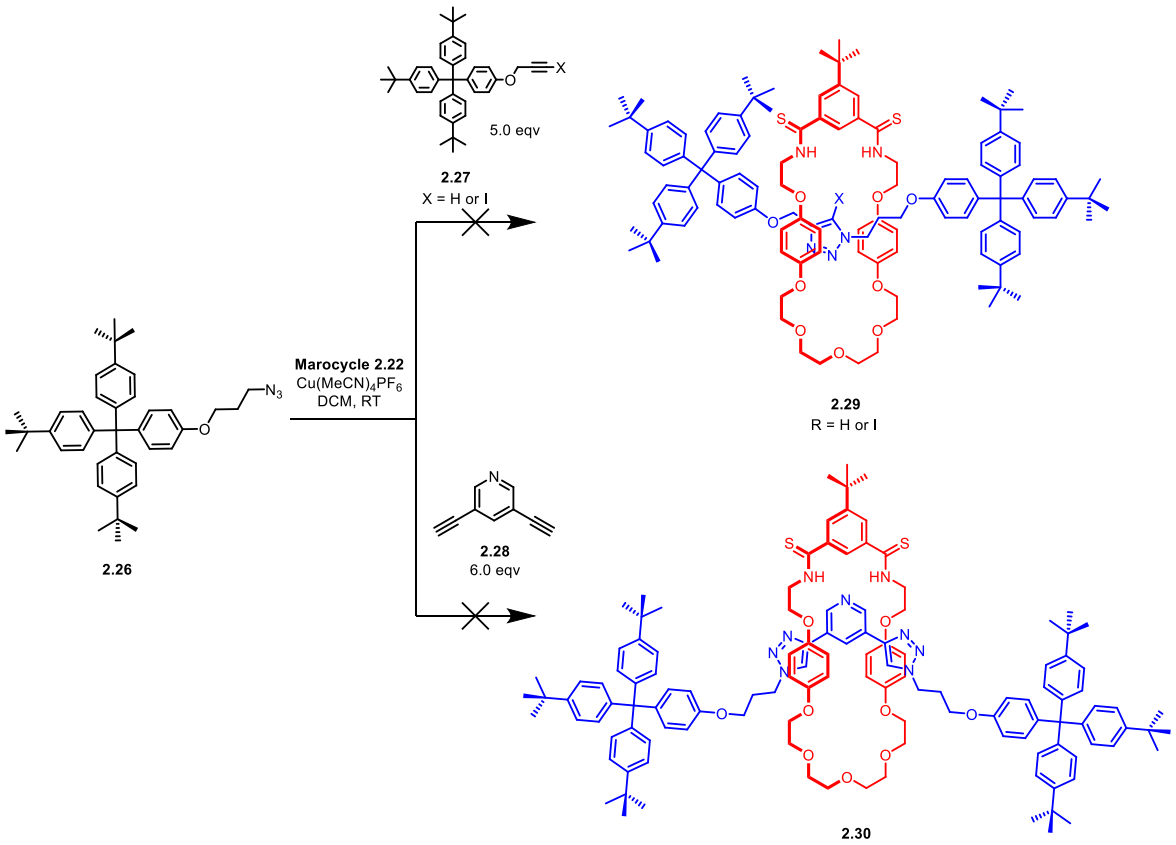

*Scheme 8. Attempted AMT synthesis of rotaxanes **2.29** and **2.30**.*

2.7. Towards ChB-containing Hybrid Sigma-Hole MIMs

ChB-based anion receptors are rare let alone the incorporation of such motifs into interlocked host structures. The first such examples were reported by the Beer group[100] in 2017 where macrocycles containing Se or Te motifs were shown to be capable of acting as both Lewis acid ChB donors and Lewis basic ligands for anion binding and the endotopic binding of Cu(I) respectively. This subsequently led to the successful synthesis of neutral Se[2]rotaxane **2.31$_{Se}$** and Te[2]rotaxane **2.31$_{Te}$** *via* active-metal template (AMT) in 56 and 46% yields respectively as well as the tricationic analogue, Se[2]rotaxane **2.32^{3+}** (Figure 55). Unfortunately the attempted synthesis of a tricationic Te[2]rotaxane^{3+} resulted in lability issues upon methylation of the macrocycle at the triazole position leading to the difficulty of isolating a pure sample of Te[2]rotaxane^{3+}. To overcome this issue, post-rotaxane methylation can occur by replacing the macrocyclic benzene-spacer with pyridine allowing *N*-methylation to still yield a final +1 cationic MIM.

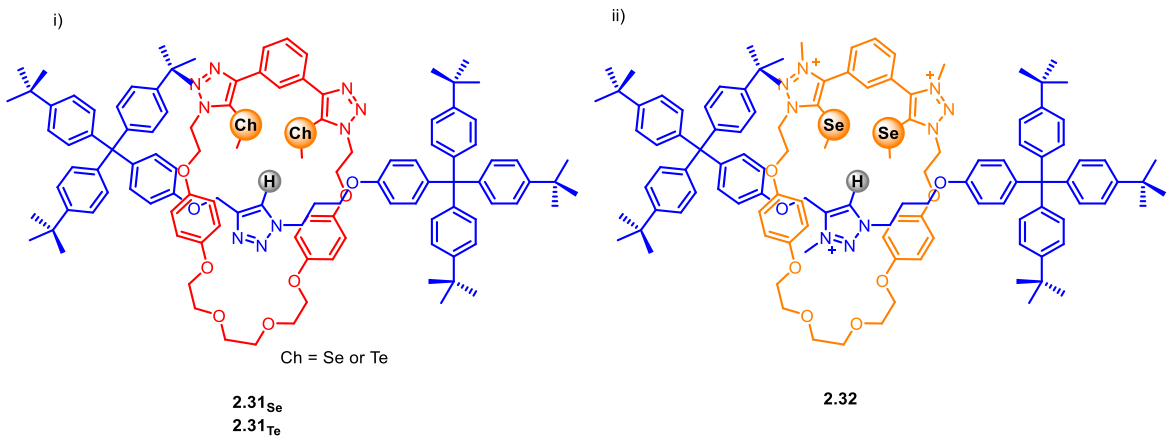

Figure 55. First example of hydrid mixed ChB/HB-donor groups in [2]rotaxane. i) neutral Se[2]rotaxane ***2.31Se*** *and Te[2]rotaxane* ***2.31Te*** *ii) tricationic Se[2]rotaxane^{3+} (counter-anions omitted) reported by Beer and co-workers.*[100]

Building on this work, this section explores the synthesis of hybrid XB/ChB and HB/ChB rotaxane receptors for anion binding investigation.

2.7.1. Attempted Synthesis of ChB-based MIMs

Hybrid interlocked systems containing both XB and ChB donor motifs for anion recognition have never been reported. The successfuly synthesised Se-based macrocycle **2.5Se** (Section 2.2) was found to be a suitable candidate in the synthesis of target hybrid XB/ChB MIMs (Scheme 9).

Active Metal Template (AMT) Approach

Efforts were undertaken to synthesise a cationic [2]rotaxane using the Cu(I)-catalysed AMT approach. AMT conditions were employed for the attempted synthesis of [2]rotaxane **2.33** (Scheme 9). An equimolar quantity of Cu(I) and macrocycle **2.5Se** were dissolved in DCM following which stopper-azide **2.26** and stopper-alkyne **2.27I** were added. Although no evidence of the desired interlocked [2]rotaxane **2.33** was observed by MS, macrocycle **2.5Se** was recovered after purification of the crude material.

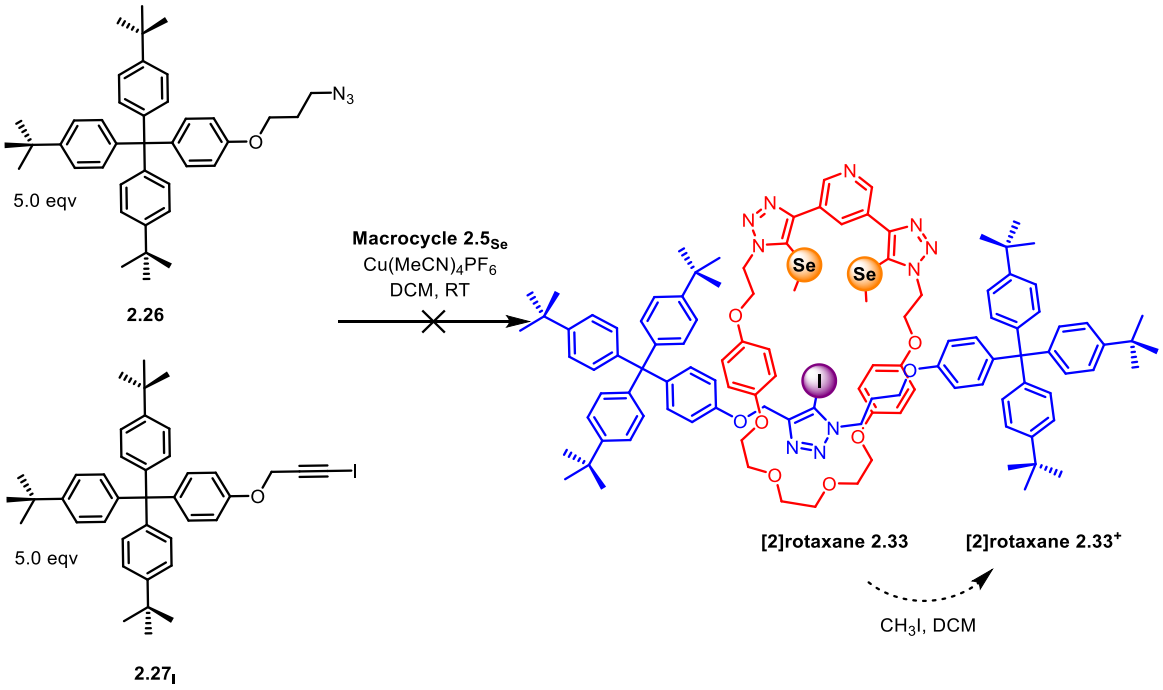

*Scheme 9. Attempted synthesis of monocationic [2]rotaxane **2.33**$^{+}$.*

Anion Template Approach

Having failed in the attempt to form rotaxane **2.33** using AMT conditions, the anion template method was employed for the formation of [2]catenane **2.34** where chloride was used to template bis-amine **2.21** macrocycle precursor around cationic macrocycle **2.5$_{Se}$** to favour a ring closing amide condensation step (Scheme 10). Monocationic macrocycle **2.5$_{Se}$·Cl** and bis-amine **2.21** were dissolved in DCM before triethylamine and acid-chloride **2.19$_{CH}$** were added sequentially and the reaction was monitored *via* MS. Evidence of [2]catenane **2.34** ([M+H]$^{+}$ 1396.4 m/z) and isophthalamide macrocycle **2.16$_{CH}$** ([M+H)$^{+}$ 595.6 m/z) was observed, however purification using preparatory thin layer chromatography consistently gave only trace amounts of the desired [2]catenane and isophthalamide macrocycle **2.16$_{CH}$**.

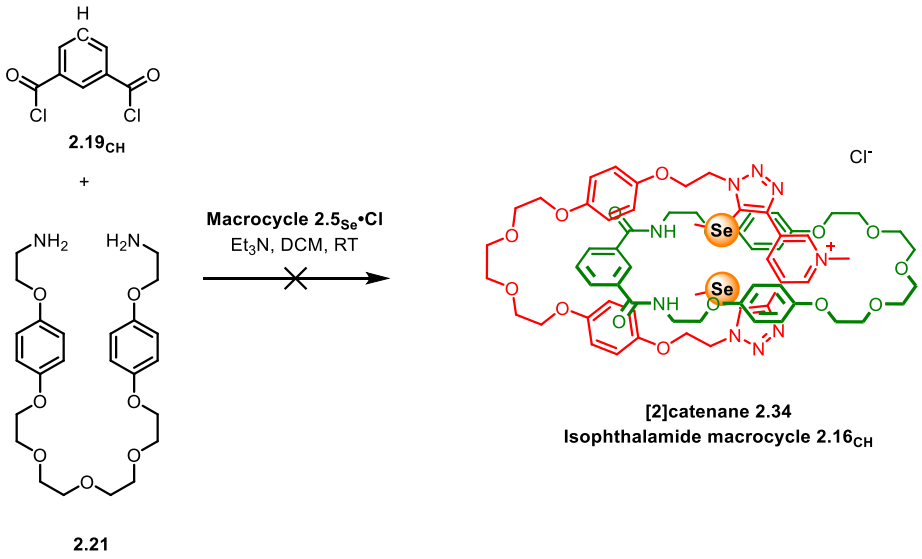

Scheme 10. Attempted synthesis of monocationic [2]catenane 2.34⁺.

One might attribute the low yield of [2]catenane on steric grounds, with the steric bulk of the $SeCH_3$ groups preventing the interpenetrative assembly of precursors. However, anion binding studies (Section 2.3) suggest that macrocycle **2.5$_{Se}$** is not able to bind Cl^- through Se chalcogen bonding in an endotopic fashion but rather *via* pyridinium electrostatic interactions leading to exotopic binding, which would prove ineffective for [2]catenane **2.34** formation.

2.7.2. Attempted Synthesis of Te-based Macrocycle

As the use of macrocycle **2.5$_{Se}$** failed to produce any MIMs (Section 2.7.1), attempts were made to synthesise the Te-analogue of macrocycle **2.5$_{Te}$** where its stronger ChB interactions can be utilised in the subsequent formation of MIMs *via* the AMT or anion template approach. A similar approach as in the synthesis of its Se-analogue (Section 2.2) was employed to obtain precursors **2.12$_{Te}$** and **2.13$_{Te}$** (Scheme 11).

Bis-iodotriazole **2.7** was converted to bis(methyltelluro-triazole) **2.12$_{Te}$** by reaction with *in situ* generated lithium methyltelluride followed by the addition of iodomethane in DCM (10% *v/v*). MOM-deprotection under acidic conditions afforded the free bis-phenol **2.13$_{Te}$**. S_N2 ring-closing with triethylene glycol bis-tosylate was monitored by MS and purification *via* preparatory thin layer chromatography afforded a range of products including mono-Te macrocycle **2.14$_{Te/H}$**, (4%), proto-

macrocycle **2.14$_{H/H}$** (3%) as well as the desired macrocycle **2.14$_{Te}$** (5%). Methylation of macrocycles **2.14$_{Te/H}$**, **2.14$_{H/H}$** or **2.14$_{Te}$** in a solution of 10% iodomethane in dichloromethane (*v/v*) resulted in the decomposition of starting material evidenced by ^{1}H NMR spectroscopy. This once again exposed the lability of C-Te bond which has been shown in multiple examples throughout the chapter.

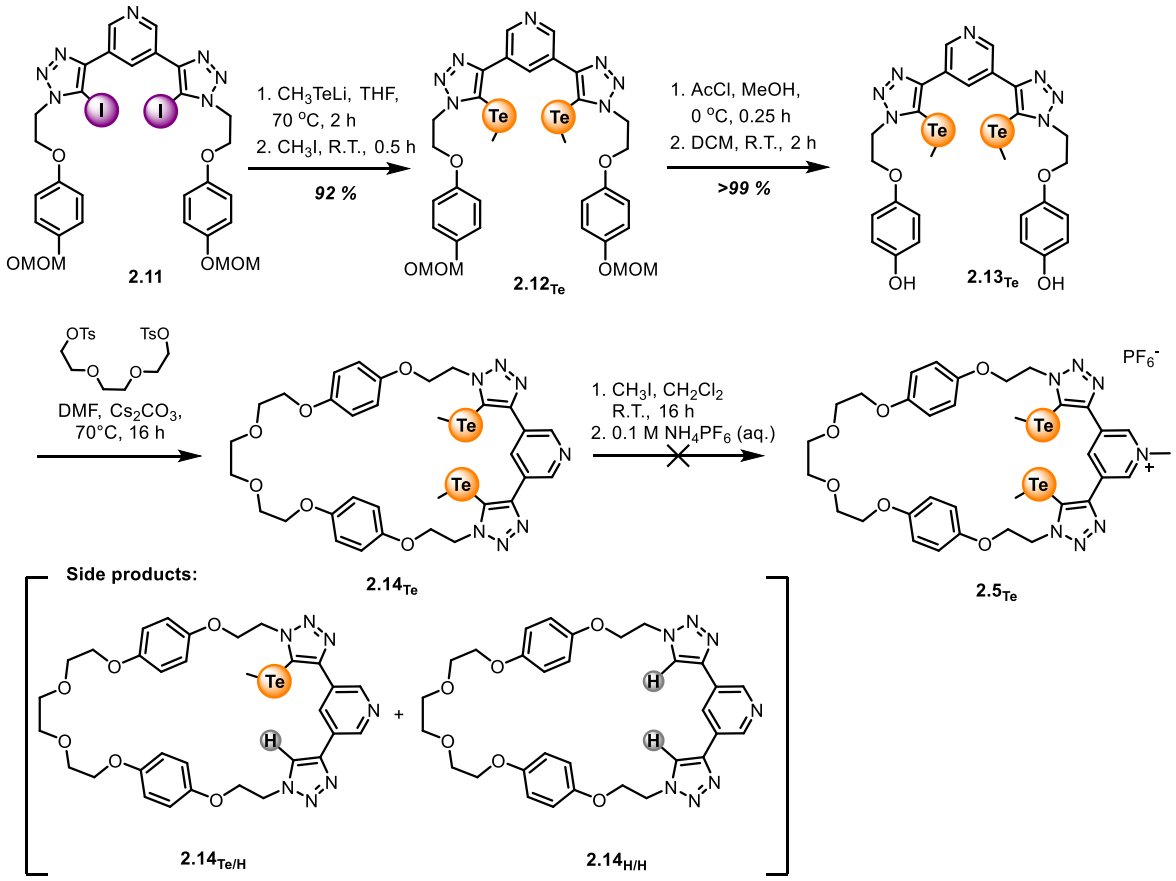

Scheme 11. Attempted synthesis of macrocycle bearing Te-CH$_3$ motifs.

2.7.3. Attempted Synthesis of Cationic ChB/HB Interlocked Receptors

Encouraged by the previously reported potency of ChB rotaxanes for anion binding,[100] and the success of the [2]catenane (**2.25·PF$_6$**) containing thioamide functionalities in Section 2.5.3, a cationic pyridinium-bis-tellurotriazole ChB donor motif was synthesised in an attempt to obtain a cationic thioamide-ChB-[2]catenane.

The triazole-containing bis-alkene **2.24$_I$**[172] was converted to bis(methyltelluro-triazole) alkene **2.24$_{Te}$** by reaction with *in situ* generated lithium methyltelluride followed by addition of iodomethane in DCM (10% *v/v*) (Scheme 12). Purification of the crude product by silica gel column chromatography afforded **2.24$_{Te}$** in 64% yield. To obtain the cationic analogue, **2.24$_{Te}$** was dissolved in a solution of 10% iodomethane in dichloromethane (v/v). Subsequently, the product was repeatedly washed with 1 M NH_4PF_6 (aq) affording **2.15$_{Te}$·PF$_6$** in 82% yield. The ^{1}H NMR spectrum of **2.15$_{Te}$·PF$_6$** revealed the presence of the $TeCH_3$ units at 2.07 ppm as well as signals at -11.2 ppm in ^{13}C NMR and 113.4 ppm in ^{125}Te NMR spectra which is a consequence of the highly electropositive Te atom. The high yield and stability in solution for studies *via* NMR spectroscopy reveals the robustness of **2.15$_{Te}$** as a Te-donor suitable for further solution studies, therefore steps were taken to carry out synthesis of a Te[2]catenane.

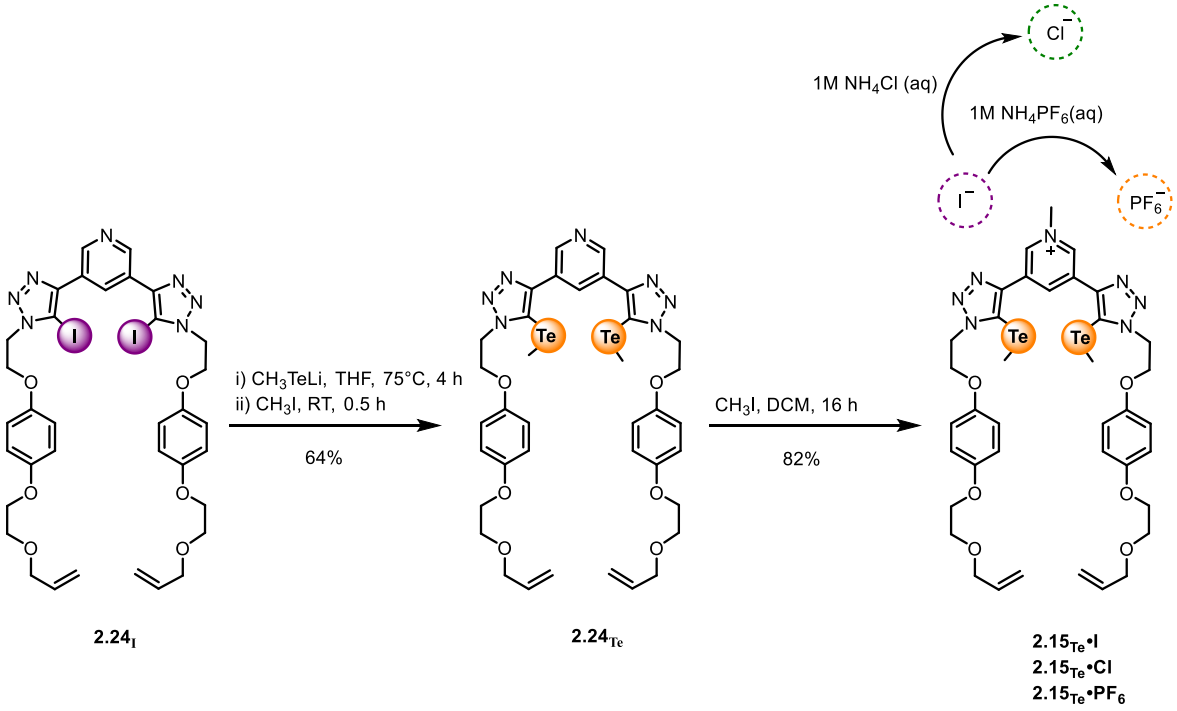

Scheme 12. Synthesis of novel Te-containing bis-vinyl macrocycle precursor ***2.25$_{Te}$.***

Having been successful in the synthesis of [2]rotaxane **2.25** (Section 2.5.3) by using a chloride anion template followed by RCM using Grubbs' catalyst, this method was once again employed in the attempted synthesis of the thioamide-containing bis-methyltellurotriazole[2]catenane **2.35**. The synthesis of target Te[2]catenane **2.30** employed RCM reaction between a novel Te-containing bis-

vinyl macrocycle precursor **2.15$_{Te}$** and a HB-macrocycle **2.22** (thioamide) or **2.16** (isophthalamide) using a Cl^- template (Scheme 13). To an equimolar mixture of **2.15·Cl** and macrocycle **2.22** dissolved in DCM, RCM Stewart-Grubbs catalyst (10% *wt/wt*) was added. The reaction was monitored by MS and evidence of [2]catenane **2.35** at 1606.5 m/z $[M+H]^+$, macrocycle **2.22** at 705.3 m/z $[M+H]^+$ and ring-closed **2.15** macrocycle at 924.2 m/z $[M+H]^+$ was found. It was encouraging that evidence of the formation of target [2]catenane **2.35** was observed in MS, however, isolation of the product was challenging due to the formation of only trace amounts of [2]catenane.

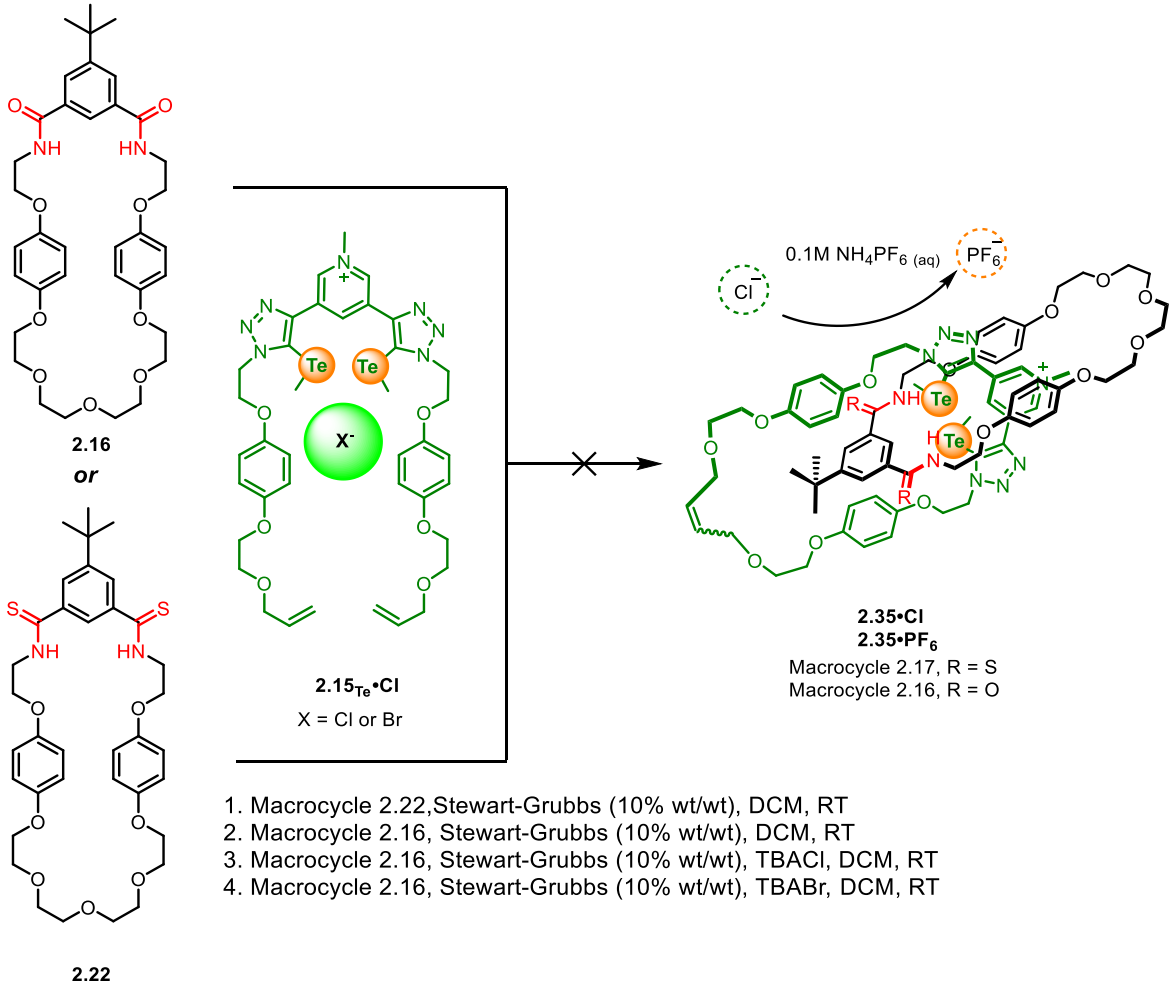

*Scheme 13. Attempted synthesis of monocationic thioamide-Te[2]catenane **2.35**.*

As thioamide-[2]rotaxane **2.25** was found to be a less efficient anion receptor than its amide-analogue [2]rotaxane **2.17**, isophthalamide macrocycle **2.16** was used in the synthesis of the bis-methyltellurotriazole[2]catenane instead. The reaction (Scheme 13) was attempted three more times with isophthalamide macrocycle **2.16**. The first attempt followed the same protocol where an

equimolar mixture of **2.15$_{Te}$·Cl** and macrocycle **2.16** were dissolved in DCM, followed by the addition of RCM Stewart-Grubbs catalyst (10% *wt/wt*). MS showed the formation of the target [2]catenane ([M+H]$^+$,1574.5 m/z), macrocycle **2.16** ([M+H]$^+$, 673.3 m/z) and ring closed **2.15$_{Te}$** ([M+H]$^+$, 924.2 m/z). Purification efforts using preparatory thin layer chromatography did not yield the desired [2]catenane **2.35** as it was produced in quantities too low to be isolated. The second attempt was a repeat of the first attempt with the addition of TBACl and the third attempt involved using the less charge dense bromide anion (as TBA salt) as an anion template instead. MS evidence using additional Cl$^-$ template found the target [2]catenane ([M+H]$^+$, 1574.5 m/z), pseudorotaxane ([M+H]$^+$, 1602.5 m/z), **2.15$_{Te}$** ([M+H]$^+$, 952.2 m/z) and ring closed (or potentially homo catenane) **2.15$_{Te}$** ([M+H]$^+$, 924.2 m/z) (Figure 56). No evidence of any significant product was found when Br$^-$ was used as a template suggesting weak or no binding of Br$^-$ by precursor **2.15$_{Te}$**

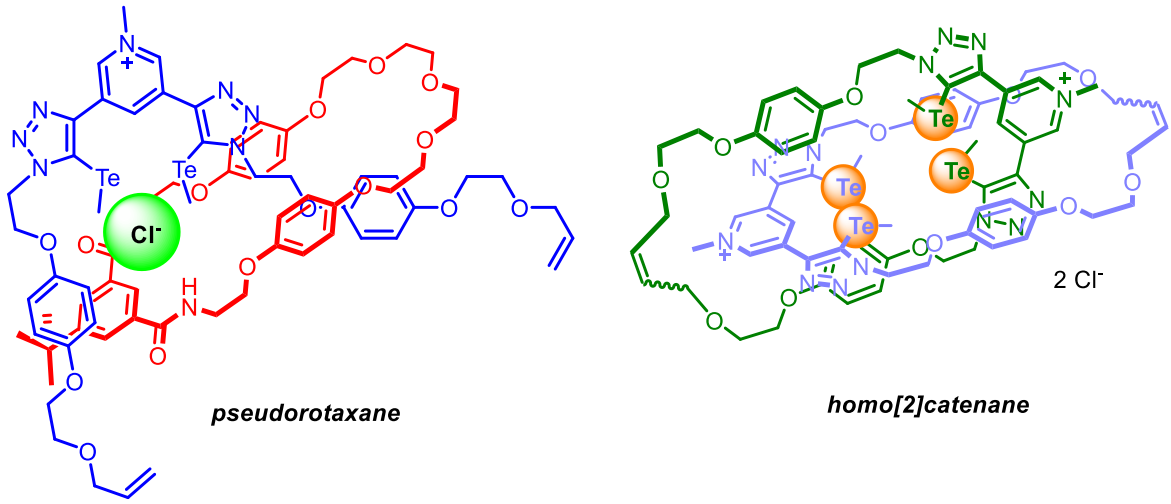

Figure 56. Molecular structured of MS detected pseudorotaxane and homo[2]catenane.

2.8. Conclusions

This chapter discussed the synthesis of chalcogen and halogen bonding receptors, investigating their anion binding thermodynamic properties as well as attempts to discover new synthetic pathways leading to XB/ChB interlocked molecular structures.

Section 2.1 investigated the synthesis of a novel and stable cationic tellurium-based ChB-donor motif capable of binding a wide range of anions strongly. These features enabled the thermodynamic origins of ChB-mediated anion binding to be elucidated for the first time, giving an insight into the nature of this poorly understood σ-hole interaction. Fundamental thermodynamic aspects of chalcogen bonding anion recognition were determined through van't Hoff analysis of NMR data in various solvent media. Compared with its HB analogue, the augmented anion affinities of ChB-donor $\mathbf{2.1_{Te}}$ in acetonitrile are characterised by a strong, predominantly enthalpic driving force. Nonetheless, the importance of entropy is evident as it appears to dictate ChB-mediated anion binding trends in many instances, including the diminishing binding affinities of the heavier halides in acetonitrile and the stronger association observed in 'less competitive' aprotic solvents such as acetone. Preliminary studies in protic wet organic solvent media reveal bromide binding by $\mathbf{2.1_{Te}}$ to be, again, enthalpically favoured. Interestingly, replacement of the Te ChB-donor groups with Se in the pyridinium host framework appeared to largely negate the ChB contributions.

A novel thioamide macrocycle **2.22** was synthesised where its enhaced binding strength of chloride, compared to the cyclic amide analogue, was used in the Cl- template synthesis of a XB-[2]catenane $\mathbf{2.25{\cdot}PF_6}$. Surprisingly, anion association constants determined via ^{1}H NMR titration studies undertaken in competitive $CDCl_3/CD_3OD/D_2O$ (45:45:10 v/v) solvent mixture revealed the presence of the thioamide motif instead decreased the potency of [2]catenane $\mathbf{2.25{\cdot}PF_6}$ as an anion receptor in comparison to the amide [2]catenane analogue. This was attributed to competition from strong solvent-receptor interactions resulting from the more acidic protons of the catenane's thioamide macrocycle component.

Attempts were made to exploit thioamide macrocycle **2.22** for use in the AMT synthesis of interlocked structures. Employing AMT click CuAAC reaction conditions the target [2]rotaxanes were not produced in sufficient amounts to be isolated, indicating inefficient Cu(I) endotopic binding by the thioamide macrocycle. Efforts were also made to prepare a cationic thioamide-ChB-[2]catenane using a novel vinyl-appended bis-tellurotriazole pyridinium macrocycle precursor $\mathbf{2.15{\cdot}Cl}$. However, the desired Te[2]catenanes could not be isolated.

2.8.1. Potential Future Work

The attempted synthesis of methylchalcogen-triazole interlocked structures resulted in only MS trace evidence of the desired products, suggesting inefficient association between the anion template and chalcogen bond donor. Since chalcogens are capable of multivalency, the number of σ-holes and importantly their strength and position can be tuned.[98] For example, molecular ESP calculations for F_2C=Se reveal a single σ-hole at the pole position of the double bonded chalcogen atom, unlike $(F_3C)_2$Se where two σ-holes are present (Figure 57).[204]

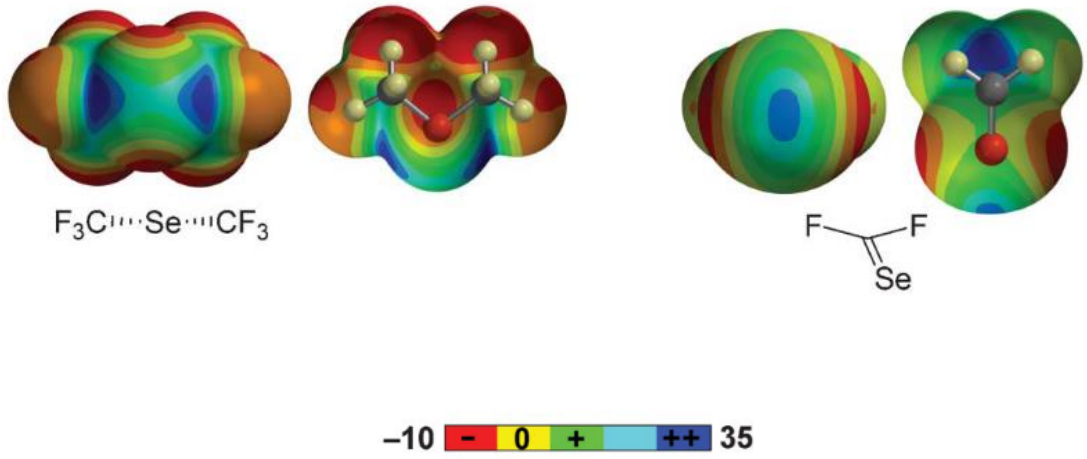

Figure 57. Molecular ESP surfaces of chalcogen molecules reported by Fontera and co-workers.[204] $(F_3C)_2$Se was found to have 2 σ-holes with electrostatic potential of 32 kcal mol^{-1} while F_2C=Se single σ-hole has a measured center of 17 kcal mol^{-1}.

When incorporated into anion receptor design, the single σ-hole found in F_2C=Se could provide stringent control and directionality, creating potential avenues for exploration. Basic computational modelling was performed on two hypothetical C=Se ChB donor motifs integrated into 5- and 6-membered cyclic urea ring motifs (Figure 58) and linked to a 3,5-substitued pyridinium core to evaluate their potency for use in anion recognition. Geometry optimisations and single-point calculations were carried out using the B3LYP method and basis sets with 6-21G++ level of theory for C, H, N, O atoms and aug cc-pVTZ-PP level of theory for Se atoms. All computational models reflect electrostatic potential on the 0.001 au molecular surface where blue is the most electropositive and red is the most electronegative. See appendix C for computational protocol.

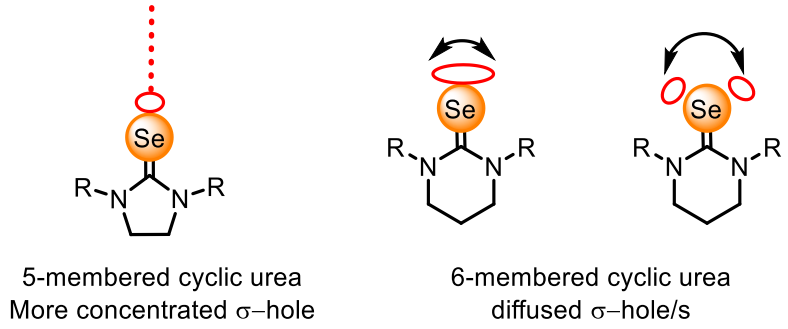

Figure 58. 5-membered and 6-membered cyclic urea motifs with hypothesised area of electropositivity (red circles).

The computation investigations conducted on receptor **2.38** (Figure 59) revealed the cationic pyridinium motif to be the most electropositive with $V_{s,max}$ = +103.78 kcal mol^{-1} while the σ-hole generated at the end of the C=Se bond elongation was found to be +42 kcal mol^{-1}.

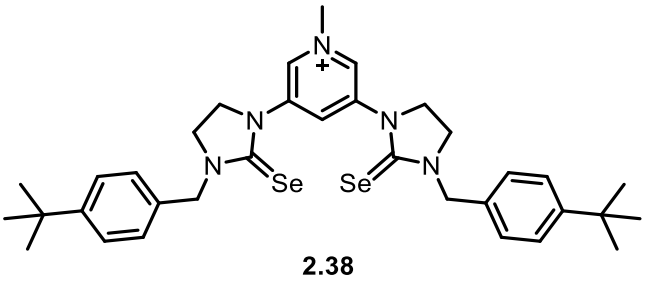

2.38

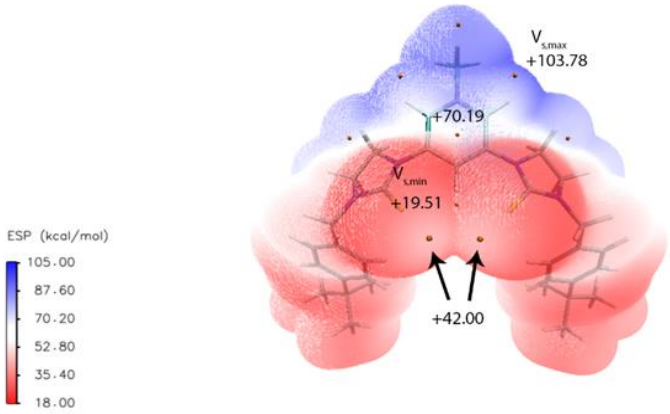

*Figure 59. Electrostatic potential on the 0.001 au molecular surface of cationic methylseleno-urea acyclic **2.38** (molecular structure shown) where locally most electron negative and positive points of the surface are shown as $V_{s,max}$ and $V_{s,min}$ respectively; in kcal/mol. ESP colour scale is in the bottom left.*

Molecular electrostatic potential (MEP) calculation of receptor **2.39** was also conducted showing the back and front views of the surface (Figure 60). Analogous to receptor **2.38**, the electropositive contribution from the pyridinium motif is greater than σ-hole contributions. The σ-holes in both receptors are observed to be singular which supports the hypothesis that C=Se generates a single area of electropositivity. However, the strong electrostatic contribution from the pyridinium group, would likely dominate anion binding, as observed with acyclic receptor **2.3**$_{Se}$. Taking this into account, the tellurium receptor analogues should be targeted instead to ensure ChB made a significant contribution to the anion recognition process.

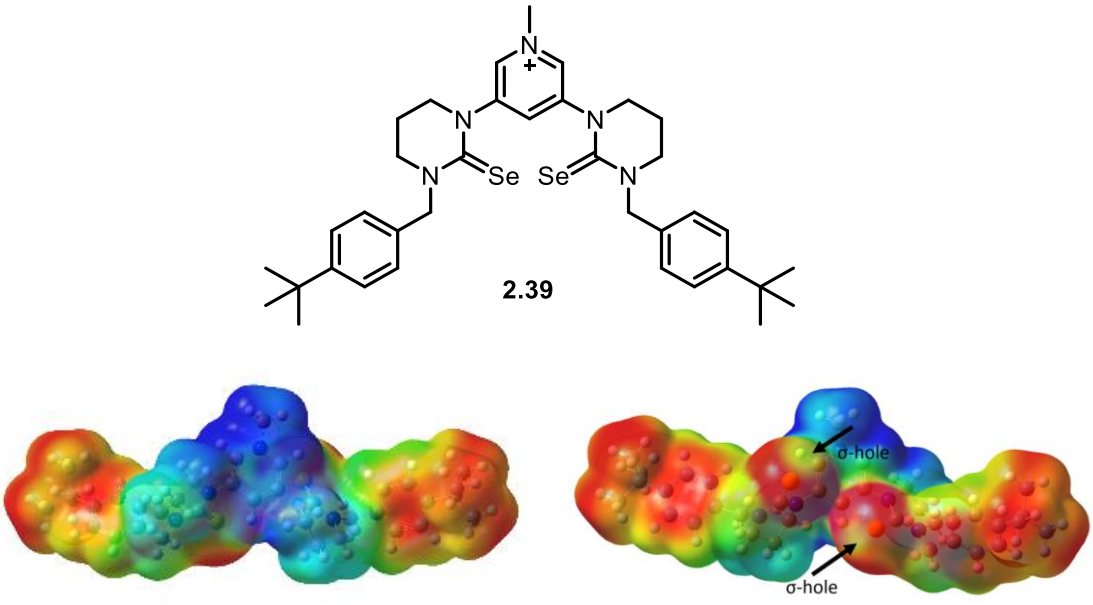

*Figure 60. Molecular structure of cationic methylseleno-triazole receptor **2.39** and MEP on the 0.001 au molecular surface where blue is most electropositive and red is most electronegative.*

Very recently, Huber and co-workers synthesised an acyclic dicationic Te-based receptor reportedly stable under ambient conditions,[166] while Beer and co-workers reported the synthesis of the tellurotriazole motif directly from a CuAAC reaction between azide and telluro-alkyne precursors.[86] Future work should consider exploiting these new synthetic methodologies to easily incorporate Te chalcogen donors into various structural frameworks leading to efficient hosts for anion recognition.

3 | BINOL Motifs for Chiral Anion Recognition and Sensing

3.1. Nature of Chiral Recognition

Chirality can be found everywhere in nature, from the spirals of a snail's shell to our very own left and right hand, which are mirror images of each other, where one is non-superimposable on the other. Biologically important amino acids occur in the *L*-configuration (19 out of 20 amino acids), while naturally occurring sugars form in the *D*-configuration, is in itself, a mystery and is one of the many questions about the origin of life.[205,206] Chiral recognition has biological and physiological importance,[207] for example α-alkoxyalkyl anions are involved in the synthesis of chiral alcohols that are used as pharmaceutical drugs[208] and are bioactive natural products.[209] They also have industrial use in analytical chemistry such as chiral chromatography[210] with applications in the flavour and perfume industry.[211] The role and awareness in chirality has slowly unfolded over years of scientific research. From the discovery of chiral molecules by Louis Pasteur in 1848 for the isolation of sodium ammonium tartrate isomers,[212] to the infamous pharmaceutical drug Thalidomide[∂] in the 1950s, the need for chiral recognition has been more important than ever.

[∂] Discovered in the 1950s, Thalidomide was prescribed to pregnant women to help suppress morning sickness. However, this caused birth defects in infants often leading to death. Investigation into Thalidomide revealed the R-isomer to have therapeutic effects while the S-isomer does not promote therapeutic effects but instead is the cause of these birth defects.

Chiral compounds are non-superimposable molecules whereby their spatial arrangement of atoms around a chiral centre is unique. The most common form of chirality arises from stereogenic centres (or otherwise termed point chirality), for example a sp^3 carbon atom with four different substituents has no improper axis of rotation (S_n) which includes a plane of symmetry and an inversion centre (*i*) (Figure 61i). In addition, axial, planar and helical chirality is also possible. Axial chirality is commonly found in substituted biaryl compounds such as biphenyls or binapthyls in which rotation about their aryl-aryl bond is restricted by bulky substituents (Figure 61ii). Usually found in metallocenes, planar chirality consists of two dissymmetric rings that are not allowed to rotate about the connecting bond (Figure 61iii). Helical chirality arises from a molecule containing a stereogenic axis and can be induced by steric strain forcing the molecule to adopt a helical twist (Figure 61).[213]

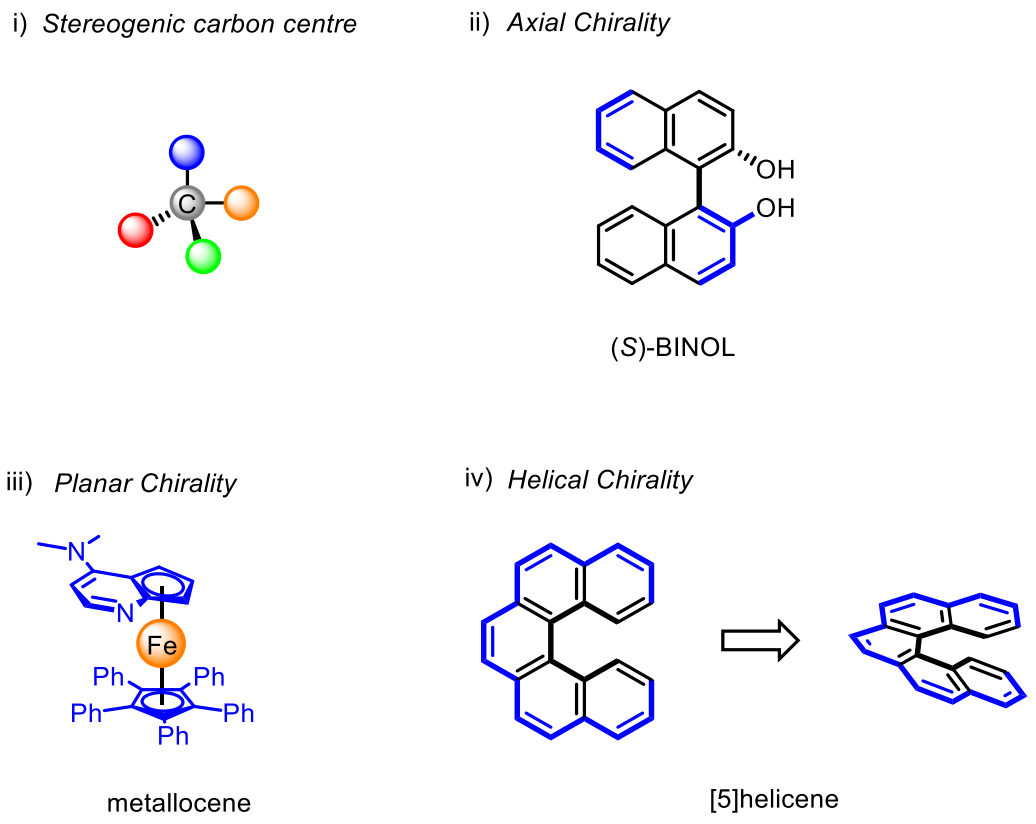

Figure 61. Common types of chirality arising from i) stereogenic carbon centres, ii) axial chirality in (S)-BINOL, iii) planar chirality in metallocenes and iv) helical chirality in polyaromatic rings.

According to the three-point attachment model by Easson and Stedman in 1933, in order for a receptor to discriminate between two enantiomeric species, the binding pocket should interact with at least three configuration-dependent points of a guest molecule (Figure 62i).[214] This was the first

proposal of a specific receptor interaction with a chiral drug molecule. However, a study by Mesecar and Koshland on isocitrate dehydrogenase found the same three binding interaction in D- and L-isocitrate, proving the lack of robustness in the three-point attachment model.[215] This led them to propose the four-location model in which a fourth binding site needs to be considered for proper discrimination between isomers (Figure 62ii).[216] These models are based on assumptions that binding happens at one stereocentre. The binding of guests with more than one stereocentre can be explained by the stereocentre recognition (SR) model in which interaction of substituents at each stereocentre is considered, thus providing a more general scope for explaining chiral recognition.[217] The SR model (Figure 62iii) predicts that a substrate with N stereocentres distributed along a single chain requires a minimum of N + 2 substrate interactions distributed over all stereocentres *ie*. substrate with 1 stereocentre requires 3 points of interaction per stereocentre.[217] Other factors to consider include conformational changes, non-covalent interactions, steric hindrances and repulsive interactions that the molecular host and/or guest can experience.[215,218] In an analogy given by Wainer,[219] where he states that chiral recognition could similarly be described using the induced-fit model† (Figure 62iv), isomers of a chiral molecule can experience the same kind of interactions but differ in enantiomer conformation energy changes to achieve optimum interactions.[220] Wainer illustrated this point by the calculation of conformational change in energy upon optimal binding interactions between chiral isomers of benoxaprofen and its enzyme. It was found that (R)-benoxaprofen-enzyme complex has a conformational-induced binding energy 250 cal mol^{-1} higher than its favoured (S)-isomer.[219]

† The induced-fit model proposes that enzyme-substrate interaction induces conformational changes in the enzyme that strengthen the binding event.

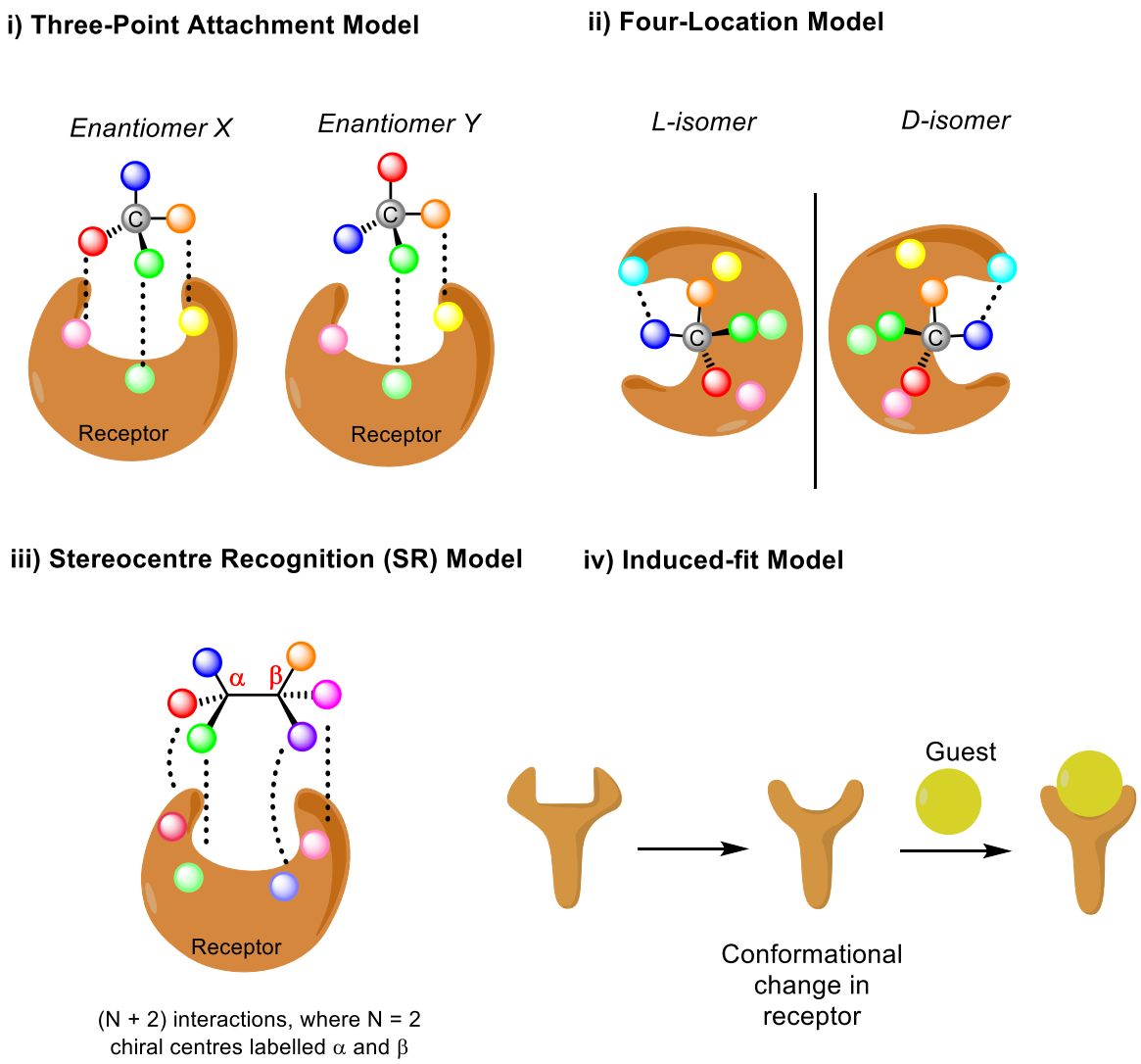

Figure 62. Chiral binding mechanisms described by different models.

The next sections will discuss briefly biotic chiral receptors (Section 3.1.1) as well as abiotic receptors (Section 3.1.2) including MIMs (Section 3.2) developed in an effort to understand the fundamentals of chiral anion recognition perfected by nature.

3.1.1. Enantiospecific Guest binding in Nature

Biologically important substrates are inherently complex, and the use of models introduced above struggle to fully explain the binding mechanism of chiral biotic receptors and guests. More often than not, these guest molecules possess more than one stereogenic centre. A popular case study to explain the enantiospecific binding of a guest with more than one stereogenic centre is the binding of isocitrate in isocitrate dehydrogenase (IDH). Isocitrate has two stereogenic centres and hence can

exist in the form of *L*-isocitrate (1*S*, 2*R*) (Figure 63i) or *D*-isocitrate (1*R*, 2*S*) (Figure 63ii), while IDH is the enzyme responsible for catalysing the oxidative decarboxylation of isocitrate. Both isocitrate isomers are bound in the active site of IDH when no metal is present, however catalytic activity is lost when L-isocitrate is bound. IDH interacts with four locations of isocitrate across the two stereogenic centres. L-isocitrate interacts with IDH residues at -OH and -COO^- functional groups at carbon atom 1 and -COO^- and -CH_3COO^- functional groups at carbon atom 2 (Figure 63i). However, in the presence of Mg^{2+}, only *D*-isocitrate is bound due to the change in interaction of OH functional group at carbon atom 1 with the metal ion instead of Arg119 (Figure 63ii).

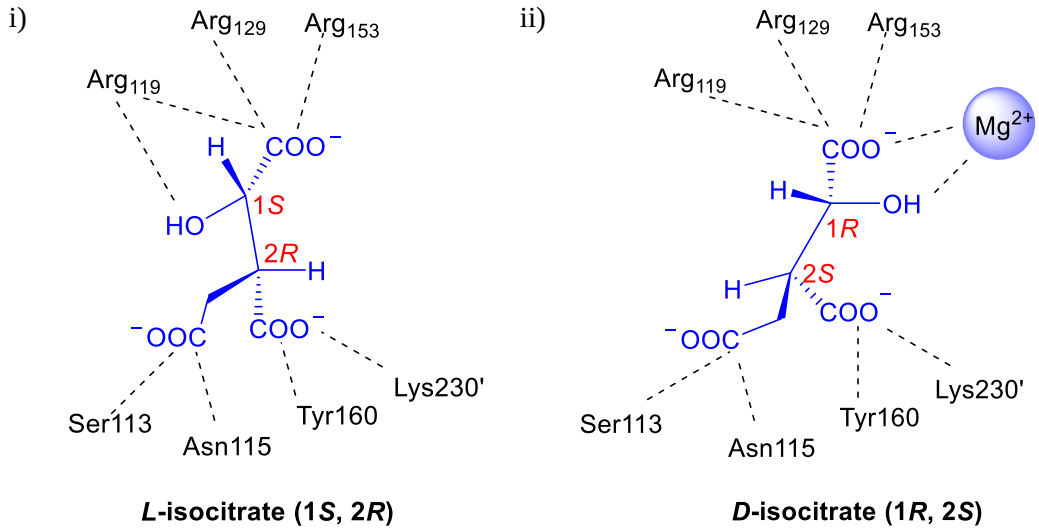

iii)

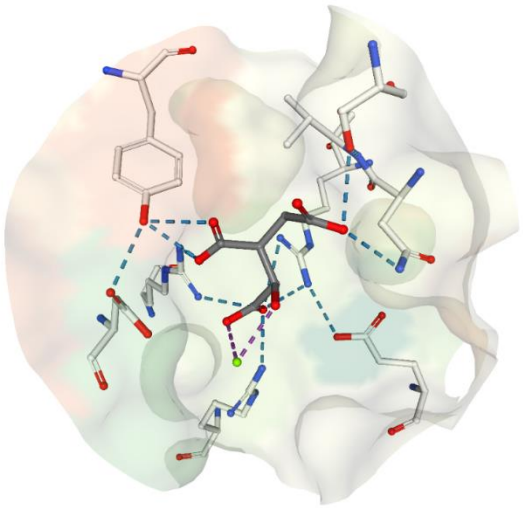

Figure 63. Isocitrate (blue) showing interactions (dashed lines) with residues in isocitrate dehydrogenase (IDH). i) L-isocitrate (1S, 2R) interacting with IDH in the absence of Mg^{2+} and ii) D-

isocitrate (1R, 2S) interacting with IDH in the presence of Mg^{2+}. iii) Crystal structure of IDH with complexed D-isocitrate-Mg^{2+} PDB ID: 1CW7.[221]

The enantiospecificity of IDH for *D*-isocitrate originates from the interaction with Mg^{2+} where the difference lies in the fourth point of interaction providing insights into the pedantic mechanisms of a biotic anion receptor. By studying naturally occurring host-guest interactions, abiotic anion receptors can be developed to be more efficient.

3.1.2. Synthetic Receptors for Enantioselective Anion Recognition

Nature has developed extraordinary enantioselectivity important in many biological processes. However, this is challenging to replicate in synthetic receptors for chiral recognition due to the difficulty in designing receptors with specific binding cavity spatial alignments. To achieve chiral recognition, receptors need to possess an intrinsic chirality in close proximity to the binding site which is achieved by incorporating chiral functional groups such as sugars,[222] amino acids[223] or any chiral molecule as part of the receptor molecular structure.

A commonly used approach is the incorporation of amino acids such as Jiang and co-worker's proline-based receptors containing phenylboronic acid groups for the chiral recognition of glucose enantiomers, studied in a mixture of organic/aqueous buffer (Figure 64i).[223] The *L*-receptor was found to exhibit a preference for *L*-glucose binding in 1:1 (v/v) MeOH/NH_3–NH_4Cl (0.05 M pH 10.0) buffer. Further investigation of monosaccharide (mannose, xylose and galactose) binding by the receptor found no significant chiral recognition properties, demonstrating the impressive selectivity of the receptor for glucose attributed to the stabilisation of a cyclic like structure between the receptor and guest (Figure 64i).

Another popular motif employed to impart chirality in receptors is 1,1'-bi-2-napthol (BINOL). For example, BINOL-incorporated macrocycle (Figure 64ii) was found to selectively form 1:1 stoichiometric complexes with phenylglycine and phenylalanine in $CDCl_3$ as evidenced through ^1H

NMR qualitative extraction studies.[224] The authors further studied the enantiodiscrimination by chiral HPLC and found the *S*-macrocycle displayed a preference for *D*-phenylglycine binding with 91.8% *ee*. The X-ray crystal structure of the host-guest complex shows three hydrogen bonds between three sulphonamide groups (two carbazoles and one BINOL) and carboxylic group of the guest. A series of BINOL-based macrocycles of differing ring size (Figure 64iii)[21] found the smallest sized macrocycle displayed the greatest enantioselectivity† for *D*-NAc-Phe (K_a = 318 M^{-1}, α = 1.70) via ^{1}H NMR titration experiments carried out in 0.5 % D_2O in acetone-d_6, while the larger and more flexible macrocycles exhibited low enantioselectivity.

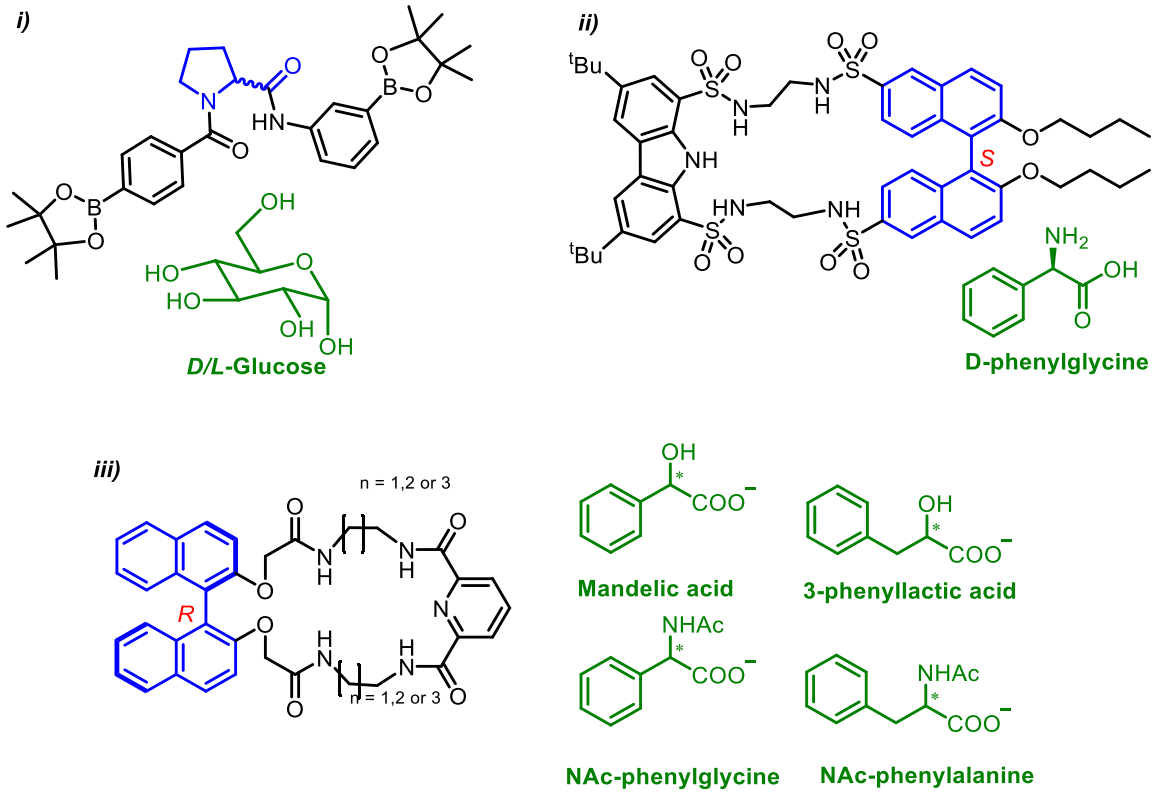

Figure 64. Synthetic chiral receptors for chiral anion recognition.

† Enantioselectivity (α) for an isomer can be obtained by comparing the binding constants (K) where $\alpha = K_R/K_S$

3.1.3. Mechanically Interlocked Structures for Chiral Guest Recognition

MIMs can offer unique topology arising from the mechanical bond providing highly specific spatial arrangement within the binding cavity for higher selectivity in chiral guests. Chiral mechanically interlocked structures can present themselves in two forms: i) due to the unique topology of the mechanical bond, spatial arrangement of substituents on macrocyclic and/or axle components can lead to isomerism[225] and ii) isomerism can arise from covalently linked chiral substituents like glucose stopper groups,[226] or incorporation of amino acid residues within the molecular framework.[227]

An example of i) is a [2]rotaxane consisting of an achiral axle and asymmetric macrocycle interconverting between enantiomeric co-conformations by shuttling of the macrocyclic component along the axle component upon addition of base (Figure 65).[228] This was observed through variable temperature ^{1}H NMR experiments (203 – 303 K, CD_2Cl_2) where the rotaxane was found to exist in a dynamic racemic mixture. The nonsymmetric environment around the macrocycle-shielded triazolium enabled enantioselective anion recognition to occur enabling Credi and co-workers to study any potential enantioselective properties as an anion receptor. Upon addition of (1S-(+)-10-camphorsulfonate (as its TBA salt) in CD_2Cl_2 large proton perturbations were observed for the axle unencircled triazolium proton while the macrocycle encircled triazolium proton is largely unaffected. They state that the stereogenic unit located far from the mechanical bond could arise from the folding receptor forming a ‘chiral pocket’.

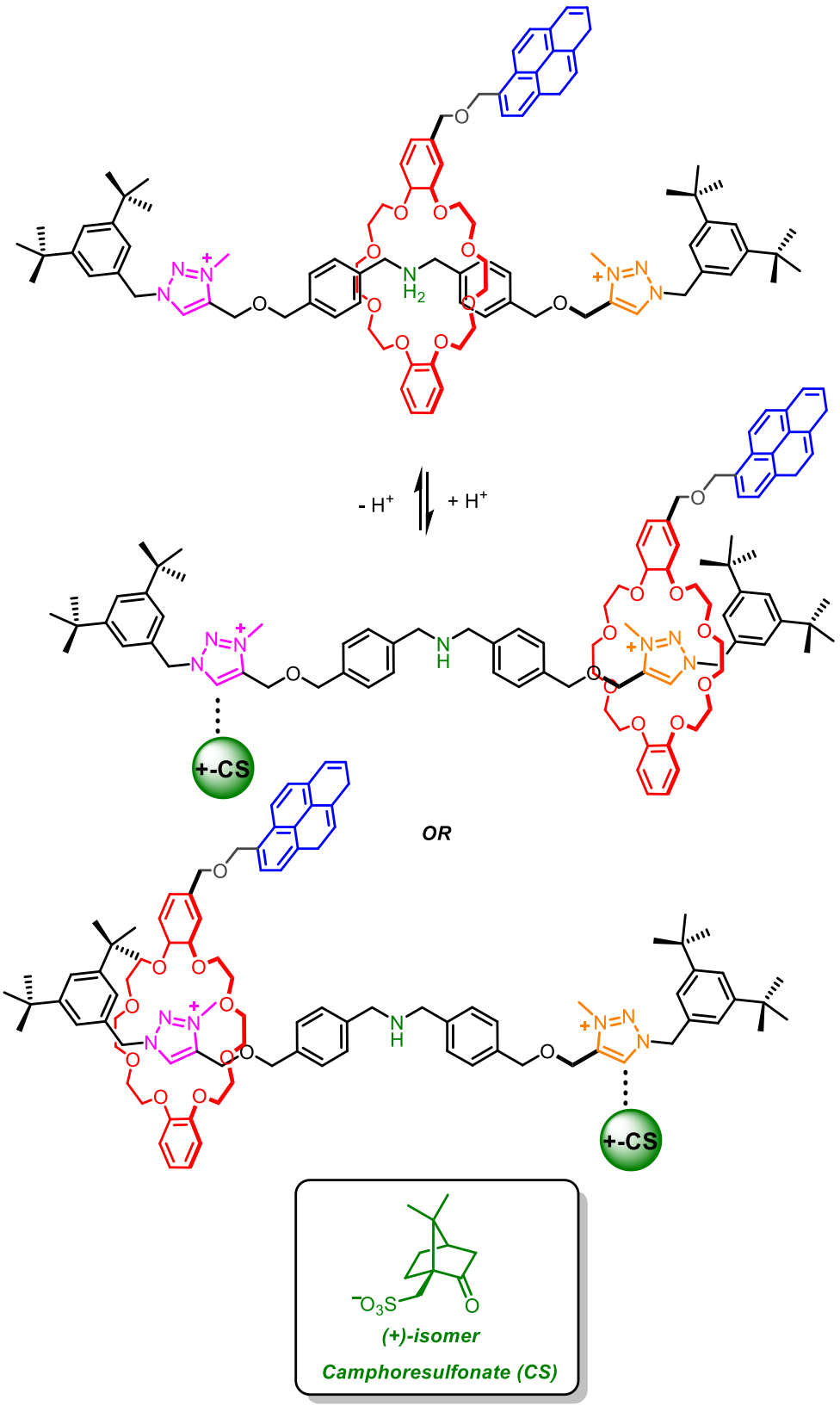

Figure 65. Mechanically interlocked receptors for chiral anion recognition. Shuttling [2]rotaxane where chirality arises from asymmetric macrocycle by virtue of the mechanical bond.[228]

An example of ii) is the use of a (S)-BINOL-phosphate derivative, where Niemeyer and co-workers synthesised the first [2]catenane containing chiral discriminating groups for binding dicationic guest molecules. Chiral anion titration studies monitored *via* ^{1}H NMR spectroscopy found favourable binding of *D*-isomers of (*R*)-lysine (5700 M^{-1}), (*R*)-arginine (8200 M^{-1}) and (*S*,*S*)-enantiomer of 1,2-diaminocyclohexane (15800 M^{-1}) in DMSO-d_6, exploiting the chiral catenane cavity for enantioselectivity.[229]

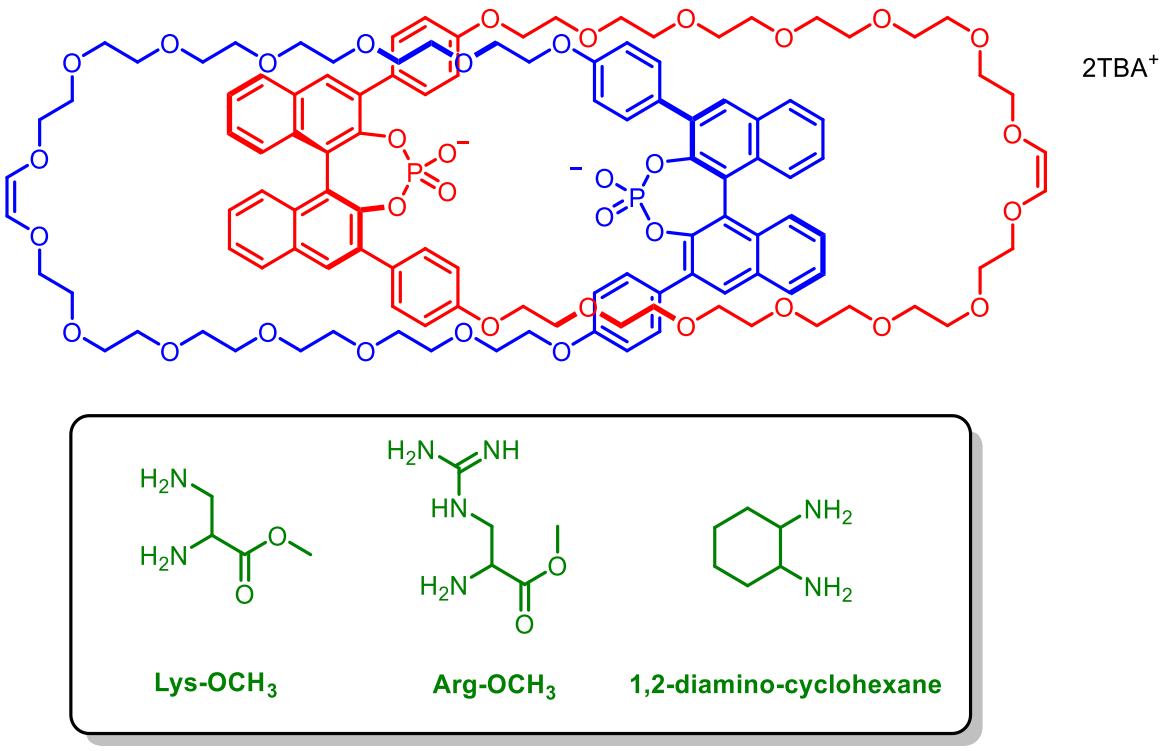

Figure 66. Enantiopure [2]catenane featuring two chiral (S)-BINOL-PO_4^{2-} motifs suitable for binding diamines used as 2HCl salts

There exists an array of examples exploring chiral MIMs in various applications taking advantage of HB binding motifs. However, application of XB-donor motifs in chiral anion recognition are rare and remains largely unexplored. Due to the nature of halogen bonding, incorporating XB-donor binding motif provides stringent geometric control of guests imparting higher directionality and linearity compared to their HB analogues. Thus far, only a few examples have employed XB-donor motifs (ie. iodotriazole) in acyclic[230,231], [2]rotaxane[227], [3]rotaxane[232] (discussed in Section 0) and foldamer-like[85] receptors capable of enantioselective discrimination of chiral anions. These

examples were reported by Beer and co-workers where chiral BINOL was employed as the chiral discriminating unit and iodotriazole unit as the chiral anion binding motif. An example is the chiral XB [2]rotaxane[227] (Figure 67) which consists of a chiral (*S*)-BINOL-macrocycle and a chiral symmetric axle component derived from (*S*)-serine residues with iodotriazole units as XB donor groups for anion recognition. Extensive ^{1}H NMR titration studies revealed the (*S*)-[2]rotaxane displayed enantioselectivity for (*S*)-isomer guest species, for example, binding of (*S*)-Pro (4298 M^{-1}) was *ca.* three times stronger than (*R*)-Pro (1465 M^{-1}) in acetone-d_6/D_2O (98:2 v/v), where proton perturbations suggested the chiral anion is bound in the space between the macrocycle and axle allowing the chiral units of both components to interact with the chiral guest species.

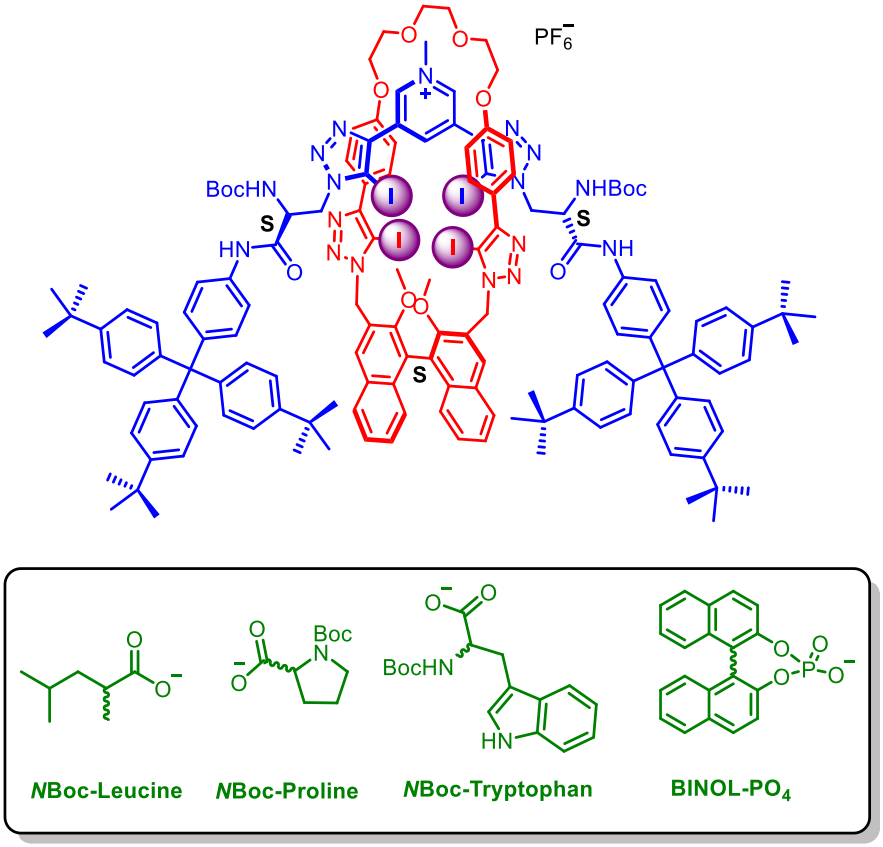

Figure 67. [2]rotaxane by Beer and co-workers with BINOL-motif (macrocycle) and S-serine containing axle as chiral discrimination units.[227] Note: Anions studied for each MIM are highlighted and boxed in green.

3.1.4. Chapter Aims

Halogen bonding donor motifs for chiral anion recognition purposes is currently underdeveloped with limited examples. XB can enhance the chiral recognition pathways through its stringent linear σ-hole interaction and steric bulk of the σ-hole donor motif in the binding cavity constraining the spatial environment thus leading to increased chiral discrimination. The rare examples of chiral XB MIMs have shown real promise in enantioselective anion recognition and are therefore important to explore further.

The overall aims of this chapter were to investigate synthetic pathways towards BINOL-containing receptors with mixed XB/HB and all-XB bond donors as chiral anion binding units. Axle and macrocyclic components were initially prepared with the ultimate objective of constructing novel XB/HB chiral rotaxanes. The second part of this chapter focuses on BINOL-based acyclic and macrocyclic XB hosts designed for dicarboxylate anion recognition.

3.2. BINOL-containing Structures for MIMs

BINOL has been used as a chiral discriminating unit in catenanes (Figure 66) as well as rotaxanes (Figure 67) for the enantioselective recognition of chiral anions. Readily available BINOL exists as axially chiral stereoisomers where rotation around the bridging C-C bond between two bulky naphthalene groups is hindered. Furthermore, BINOL is chemically stable in its pure enantiomeric forms (*R*)- and (*S*)- and is a fluorophore making it a versatile molecule.[233]

Herein, BINOL is used as a chiral discriminating unit in anion receptors (Section 3.2) as well as a fluorescent reporter group for anion sensing (Section 3.6). This section outlines the challenges faced in the synthesis of chiral BINOL-containing axles and macrocycles, and eventually the attempted synthesis of chiral MIMs where anion template and AMT methods were employed. Potential target MIMs designs shown in Figure 68 aim to provide insights into the role of BINOL in enantioselectivity. This involves bis-BINOL XB donor containing axle components (Section 0) and MIM rotaxanes with chiral and achiral macrocyclic components.

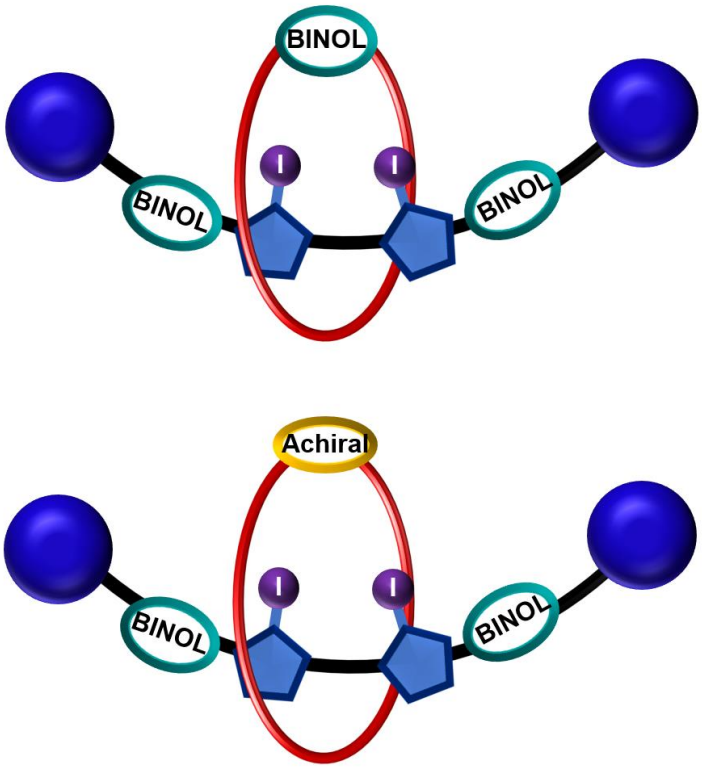

Figure 68. Target MIMs with chiral discriminating BINOL functionality and iodotriazole anion binding motif

3.2.1. BINOL-containing XB Axle Component

Axles stoppered with large bulky *tert*-phenyl stoppers were designed with various spacer groups (R, Figure 69) to study the importance of proximity between the XB anion binding 3,5-bis-iodotriazole pyridinium motif and the BINOL-chiral discriminating group. Attempts were made to synthesise axles with ethyl (**3.1**), propyl (**3.2**) and para-xylene (**3.3**) spacer units (Figure 69).

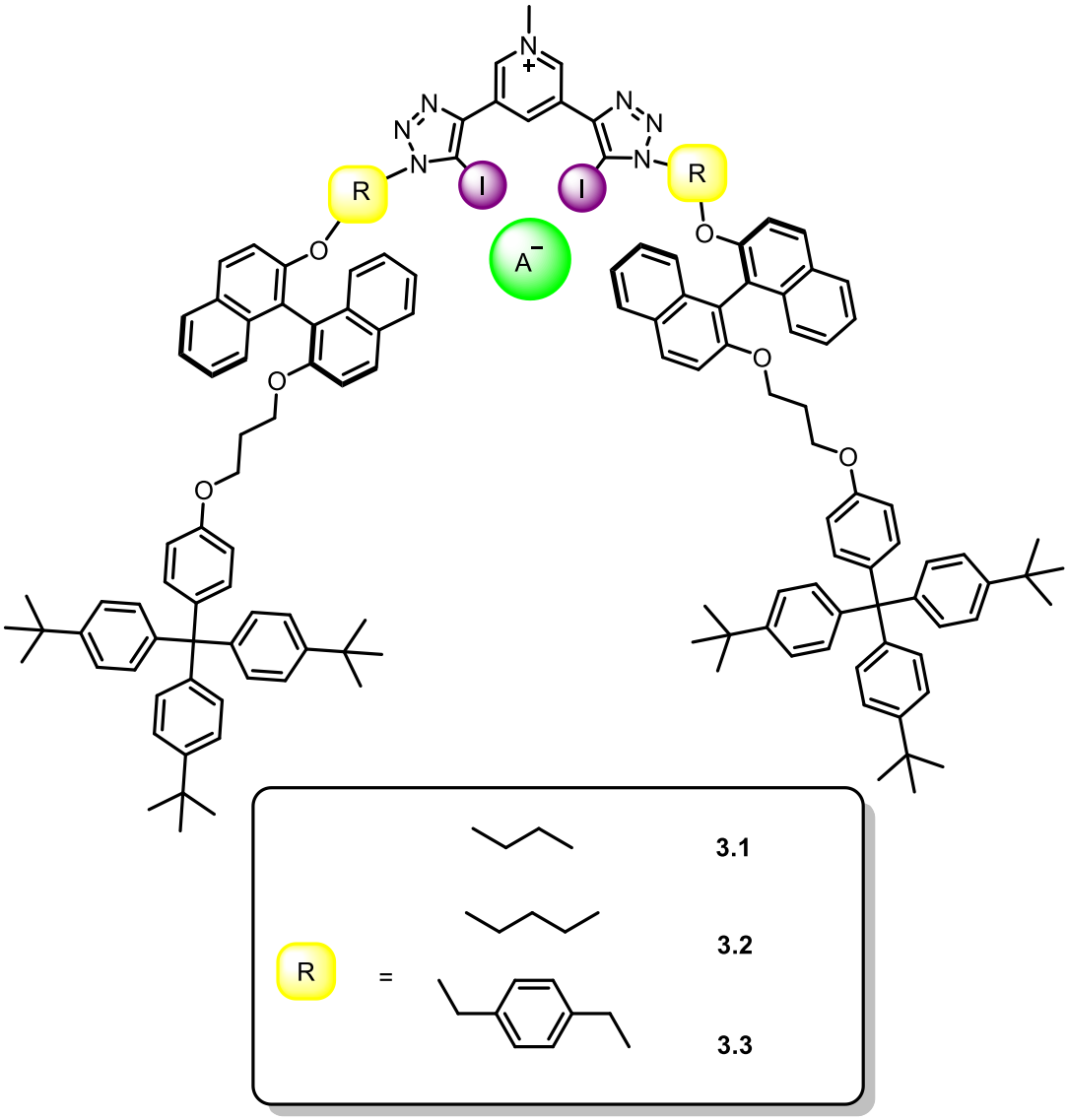

Figure 69. Target chiral XB axles with differing spacers (R) between iodotriazole and BINOL motifs.

The various synthetic routes undertaken in an effort to prepare the alkyl-spaced axles **3.1** and **3.2** are outlined in Scheme 14. *Route 1*: The reaction of bromine functionalised stopper **3.4**[234], with (*S*)-BINOL **3.5** under basic conditions afforded stopper-(*S*)-BINOL **3.6** in 85 % yield. A Mitsunobu

reaction between **3.6**, 2-chloroethanol, PPh_3 and DEAD gave compound **3.7** after column chromatography purification in an isolated yield of 46% yield. Attempts to carry out azidation of **3.7** with sodium azide were unsuccessful, resulting only in starting materials, and thus the synthesis of axle **3.11** could not proceed. The failed synthesis of **3.8** was surprising; repeating the reaction in the presence of potassium iodide also gave no evidence of product formation by MS analysis. *Route 2*: A new synthetic route was undertaken for the synthesis of axle **3.12** with the longer propyl alkyl spacer. The propyl chain also allowed safe synthesis of azide-propyltosylate[126] which on reaction with stopper-(*S*)-BINOL **3.6** under basic conditions afforded **3.9** in very good yields after purification *via* column chromatography.

As a general procedure, CuAAC 'click' reaction can occur via two reaction pathways: i) 'one-pot' click reaction or ii) 'two-pot' click reaction whereby the former involves the reaction between a proto-alkyne and terminal azide while the latter involves the reaction between an iodo-alkyne and terminal azide. Attempts using both types of 'click' reaction were carried for the synthesis of axle **3.19**. 'One-pot' CuAAC reactions of azide **3.25** with 3,5-bis(ethynyl)pyridine[168] and 'two-pot' CuAAC reactions with the corresponding bis-iodoalkyne[169] were undertaken in a range of solvents such as THF, DCM or THF/MeCN mixtures, and at elevated temperatures (up to 40˚C). Surprisingly, no evidence for the formation of axle **3.12** was observed by ESI-MS analysis of the reaction mixtures. However, reaction *via* 'one-pot' click revealed evidence for the formation of mono- 'clicked' products (Scheme 14) with MS signals at m/z = 1041.6 and m/z = 1167.5 corresponding to the mono-prototriazole and mono-iodotriazole product respectively. *Route 3*: As these CuAAC click reactions in the final step to form the desired axle failed, a new synthetic route *via* S_N2 reaction was designed. Firstly, a 'two-pot' CuAAC reaction was carried out to synthesise compound **3.10**. The reaction of 3,5-bis(iodoethynyl)pyridine in DCM with $Cu(CH_3CN)_4PF_6$, TBTA followed by the addition of azide-propyltosylate[126] gave compound **3.10** in 59 % yield after purification by precipitation in methanol. Thereafter, **3.10** and two equivalents of stopper-(*S*)-BINOL **3.6** were stirred with caesium carbonate in acetonitrile and the reaction monitored by TLC. While complete consumption of starting materials was observed by TLC, no evidence of the target axle was found by MS analysis.

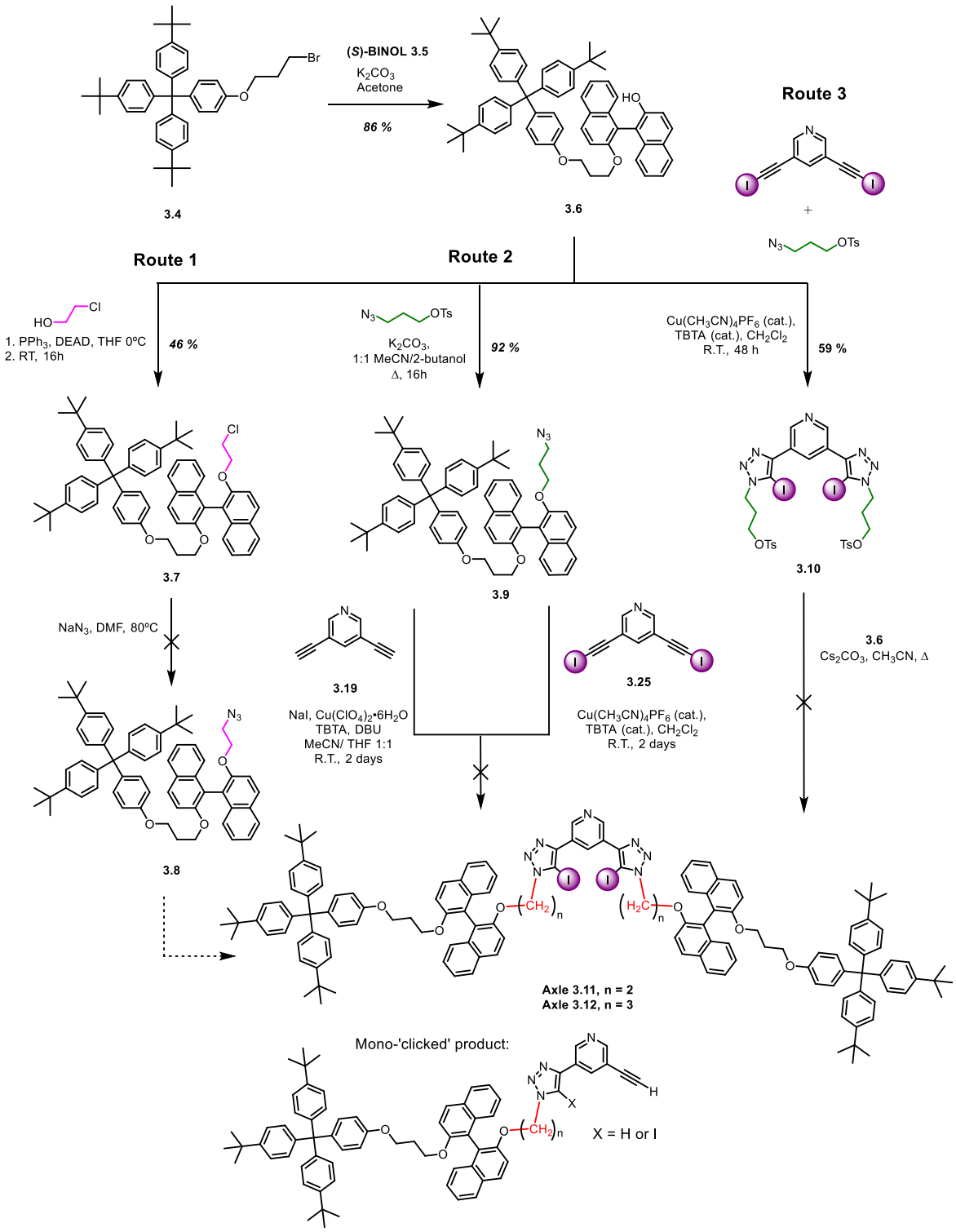

*Scheme 14. Attempted synthesis of (S)-BINOL containing chiral axles **3.11** and **3.12**.*

The preparation of the target xylene spaced axle **3.16**$_S$ was achieved via the synthetic route outlined in Scheme 15. Stopper-BINOL **3.6**$_S$ derivative,[28] was reacted with a large excess of dibromo-xylene under basic conditions to give **3.13**$_S$ in 90 % yield after purification *via* column chromatography.

The azide analogue **3.14$_S$** was prepared in 97% yield by stirring **3.13$_S$** with NaN_3 in DMSO. Subjecting two equivalents of **3.14$_S$** and one equivalent of bis(ethynyl)pyridine to 'one-pot' click reaction conditions, the reaction was monitored by MS. MS analyses of the crude material found signals at m/z = 2332.0 and 1103.6 corresponding to axle **3.15$_S$** and mono-'clicked proto product respectively. Purification of crude material using column chromatography afforded neutral axle **3.15$_S$** in 58% yield. Axle **3.15$_S$** was then reacted with an excess of methyl iodide and subsequent anion exchange to the PF_6^- salt, gave cationic axle **3.16$_S$** in 64 % yield. ^{1}H NMR characterisation confirmed the exclusive methylation of the central pyridine functionality, whilst ^{19}F and ^{31}P NMR spectroscopy ascertained the presence of the PF_6^- anion. MS analysis found peaks at m/z = 2345.9 corresponding to the cationic axle **3.16$_S$**. Analogous synthetic procedures using the corresponding (*R*)-BINOL derivative of **3.6$_R$** afforded the corresponding target **3.16$_R$** axle in similar overall yield. (see Chapter 6 for characterisation of axle **3.16**)

[L] Synthesis starts from enantiopure S-BINOL or R-BINOL, hence enantiopurity is assumed to be 99 % according to commercially available BINOL.

[Γ] Herein, letter subscript nomenclature of molecular structure refer to chirality of isomers. i.e. subscript S indicates *S*-isomer and subscript R indicate *R*-isomer.

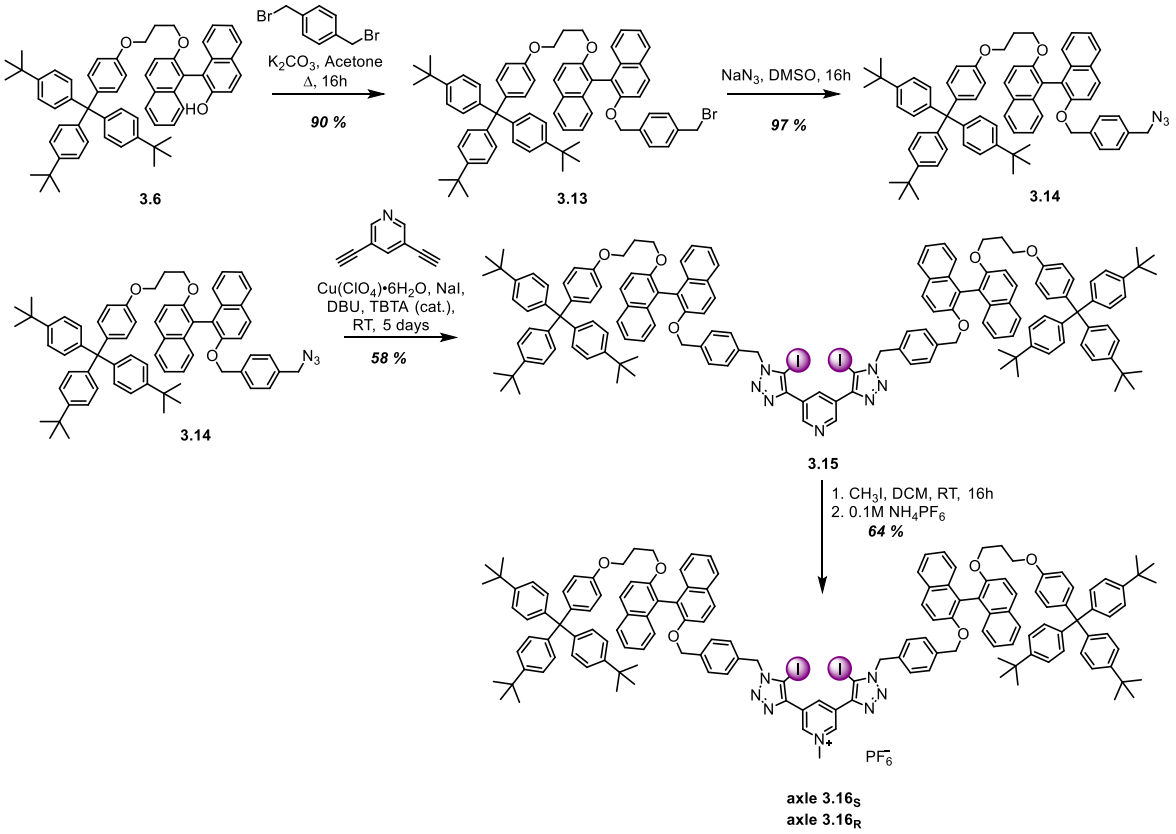

*Scheme 15. Synthesis of XB **3.16**$_S$ and **3.16**$_R$ axle enantiomers.*

3.2.2. Chiral Macrocyclic Receptors

(*S*)-BINOL-containing macrocycles were designed with XB and HB donor motifs for anion binding. Macrocyclic receptors **3.8**, **3.16** and **3.13** containing amide, thiourea and iodotriazole motifs respectively, were targeted (Scheme 16 & Scheme 17)

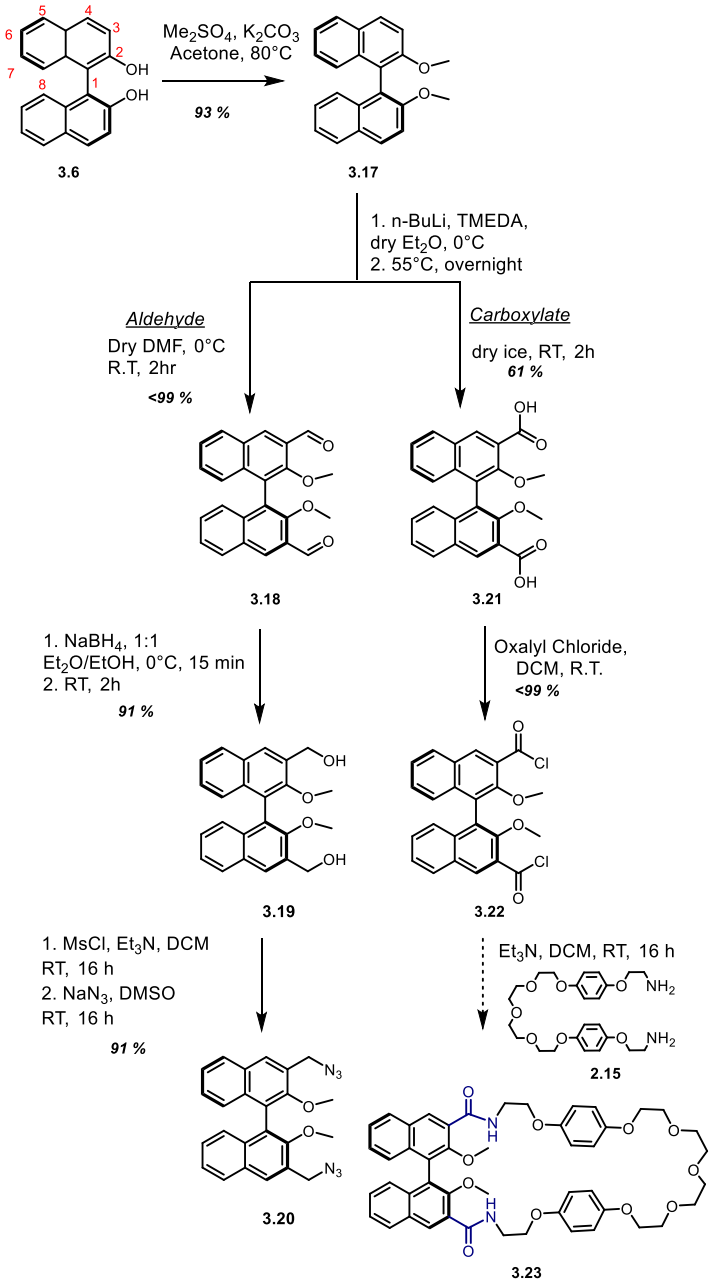

*Scheme 16. Synthesis of macrocycle precursor **3.20** and attempted synthesis of macrocycle **3.23**.*

Starting from enantiomerically pure (*S*)-BINOL **3.6**, methylation of hydroxyl groups at the 2,2'-positions using dimethyl sulfate afforded 2,2'-methoxy-(S)-BINOL **3.17** in 93% yield (Scheme 16). Ortholithiation of **3.17** and subsequent quenching with DMF or CO_2 (from dry ice) gave bis-aldehyde **3.18** in near quantitative yield and bis-carboxylic acid **3.21** (61 % yield) respectively. Bis-aldehyde **3.19** was reduced to the bis-alcohol **3.22** and subsequently reacted *via* a mesylate intermediate to afford bis-azide **3.20** in 91 % yield. Dicarboxylic acid **3.21** was subjected to an excess of oxalyl

chloride to generate its acid chloride analogue **3.22** which was used immediately in the anion template synthesis of interlocked structures described in the following Section 3.3.

Macrocyclic precursor **3.25** was obtained in 69% yield by 'one-pot' CuAAC reaction between bis-azide **3.20** and MOM-protected alkyne **3.24** (Scheme 17).[227] Subsequent acid deprotection of the MOM protecting-group afforded bis-phenol derivative **3.26** and macrocycle formation was carried out under high dilution conditions *via* Williamson ether synthesis with bis-tosylate **3.27** and excess Cs_2CO_3. Cesium carbonate here not only acts as a base but the 'cesium effect' also reduces oligomerisation. Purification *via* column chromatography afforded macrocycle **3.28** in a modest 11% yield.[227]

Reduction of bis-azide **3.20** using hydrazine monohydrate and 10% Pd/C afforded bis-amine **3.29** in 75% yield (Scheme 17). Using an excess of thiophosgene and base, the bis-thiocyanate derivative **3.30** was isolated in 64% yield. Under high dilution conditions, the condensation reaction of **3.30** and bis-amine **2.15** in dry dichloromethane gave the desired crude macrocycle **3.31**, evidenced by MS 789.9 m/z corresponding to the [macrocycle + H]$^+$ adduct. However, efforts to isolate **3.31** using chromatographic methods failed, possibly due to poor solubility and low yield of cyclic product. An attempt to prepare a non-chiral analogue of the thioamide macrocycle containing biphenyl instead of BINOL derivative was also carried out, however, once again the macrocycle could not be isolated because of solubility issues and poor yield (Scheme 4).

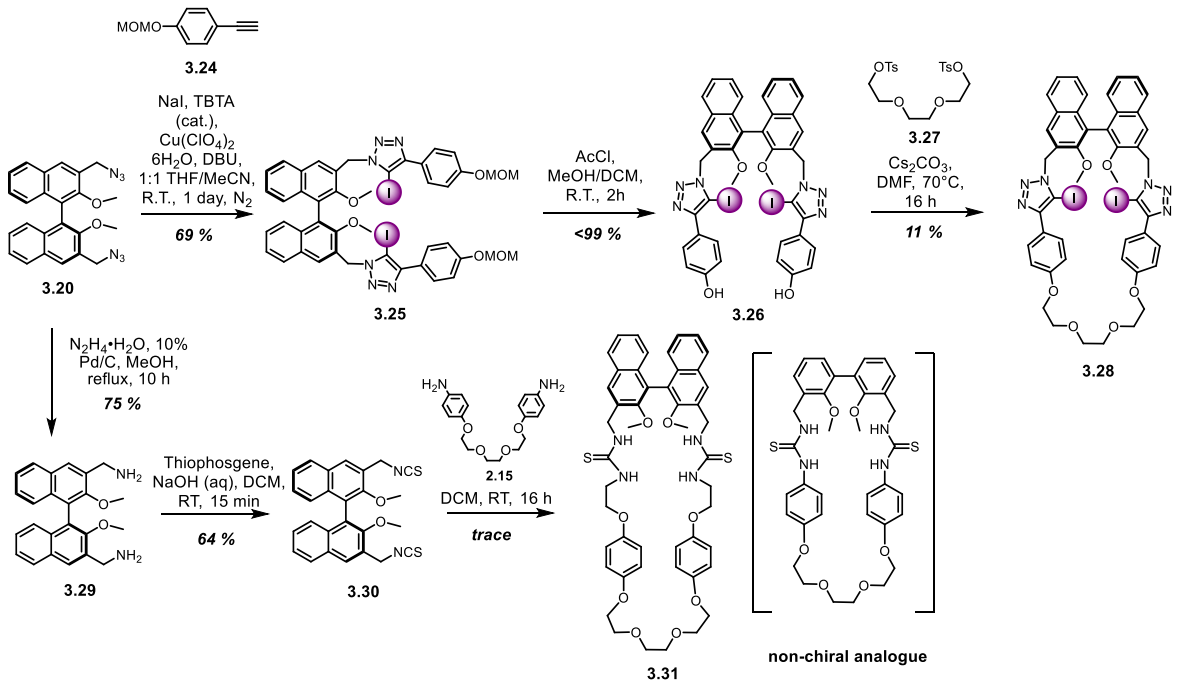

*Scheme 17. Synthesis of XB macrocycle **3.3.28** and thiourea macrocycle **3.31**.*

Having successfully prepared the novel chiral BINOL-containing axles **3.16** and macrocycle **3.23,** attempts were made to construct MIMs.

3.3. Anion Template Synthesis of Chiral Interlocked Structures

The novel chiral XB axle component $\mathbf{3.16_{S/R}}$ successfully prepared in Section 0 enabled anion template methods to be investigated for the construction of chiral MIMs. Firstly, anion exchange of the $\mathbf{3.16_S{\cdot}PF_6}$ axle to the corresponding chloride salt $\mathbf{3.16_S{\cdot}Cl}$ was achieved *via* washing with 0.1M NH_4Cl solution (0.1 M). Axle $\mathbf{3.16_S{\cdot}Cl}$ was then used in ensuing anion template reactions.

The preparation of [2]rotaxane $\mathbf{3.32_S}$ and the attempted synthesis of an all-BINOL [2]rotaxane $\mathbf{3.33_S}$ are outlined in Scheme 18. To a solution of $\mathbf{3.16_S{\cdot}Cl}$ in basic dichloromethane, macrocycle precursors bis-amine **2.15** and bis-acid chloride **2.13** were added sequentially. ESI analysis of the crude reaction mixture revealed the desired [2]rotaxane $\mathbf{3.32_S}$ at m/z = 2941.4 (Scheme 18A). The

crude reaction was purified by preparative TLC to afford [2]rotaxane **3.32**$_S$ in 4% yield which was characterised by ^{1}H NMR spectroscopy.

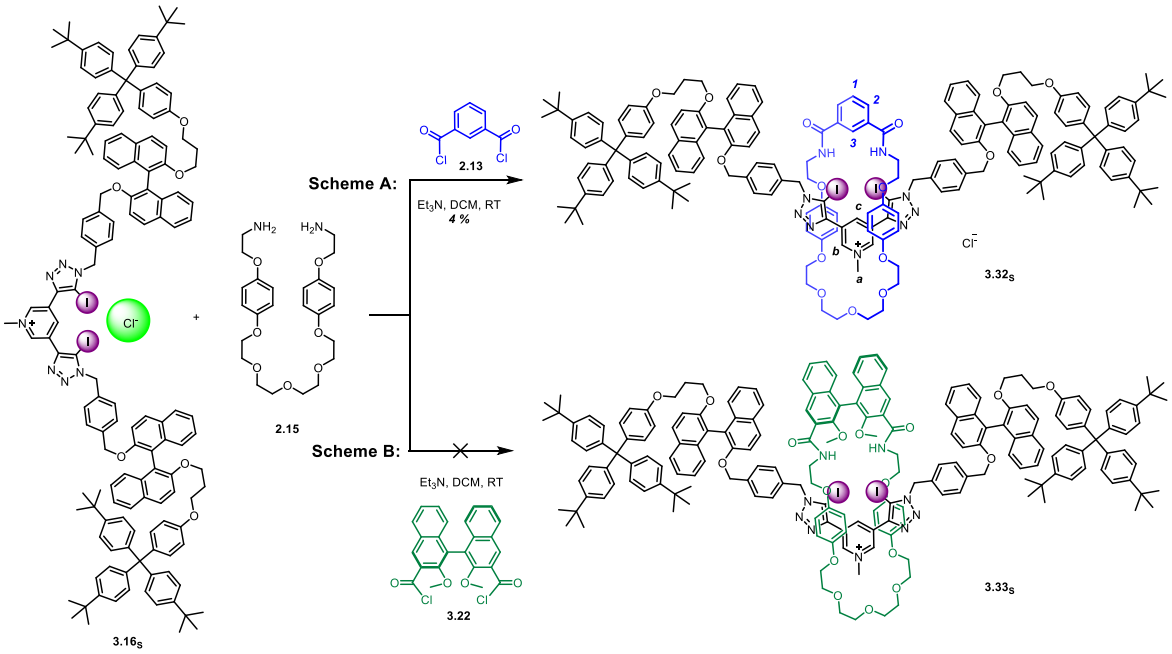

Scheme 18. Synthesis of target chiral [2]rotaxanes via a chloride-template method.

Figure 70 compares the ^{1}H NMR spectra of free axle **3.16s** with the [2]rotaxane product **3.32**$_S$ in 1:1 $CDCl_3/CD_3OD$ solvent mixture. The free macrocycle was insoluble in this solvent mixture therefore a direct comparison could not be made. However, protons $H_{8\text{-}11}$ corresponding to the macrocycle polyether chains are diagnostic of the presence of the macrocyclic component. Large perturbations of the axle component's pyridinium H_c and H_b protons were observed indicative of shielding and de-shielding interactions. Typically in related [2]rotaxanes, these result from aromatic donor-acceptor π-π stacking interactions between the electron-rich macrocycle hydroquinone groups and electron-deficient pyridinium leading to upfield perturbations and increased splitting in the hydroquinone protons. This phenomenon is not observed here presumably due to the many aromatic proton signals present which in turn make proton assignments more challenging.

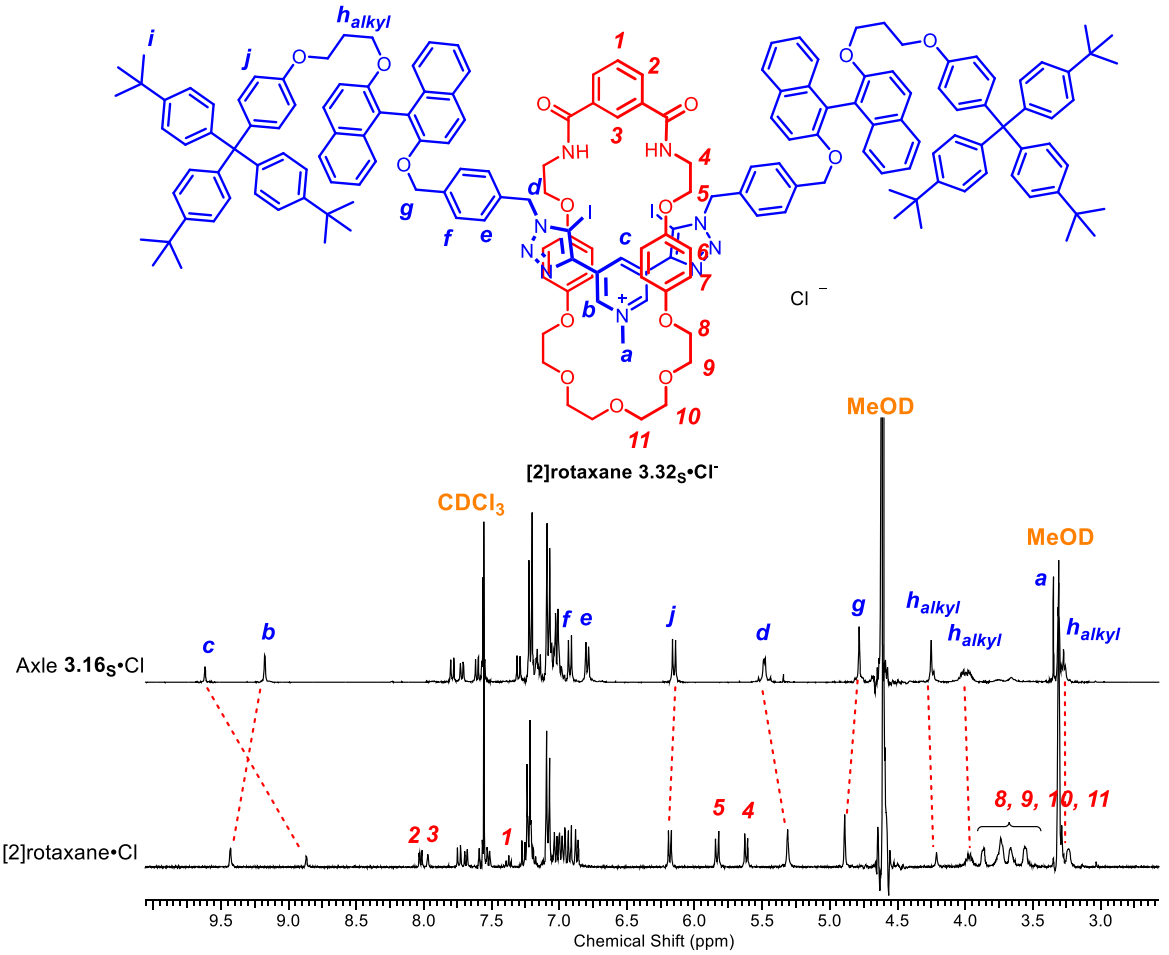

*Figure 70. Partial ^{1}H NMR spectra of [2]rotaxane **3.32** compared to free macrocycle and free axle **3.16$_S$** in $CDCl_3/CD_3OD$ (1:1 v/v). Note: Macrocycle ^{1}H NMR was measured in acetone-d_6 due to solubility issues in $CDCl_3/CD_3OD$ (1:1 v/v) therefore proton perturbations cannot be compared directly.*

Attempts to obtain a ^{1}H-^{1}H ROESY spectrum in 1:1 $CDCl_3/CD_3OD$ solvent mixture unfortunately, did not provide conclusive evidence of rotaxane formation due to the very small quantity of rotaxane isolated. However, preliminary 2D-DOSY experiments showed the rotaxane existed as a single species instead of separate macrocyclic and axle components. Where species are not interlocked, diffusion rates would differ due to the large difference in hydrodynamic radii. The small amount of [2]rotaxane isolated precluded anion binding studies being undertaken.

An analogous chloride anion template clipping synthetic procedure was undertaken to prepare an all-BINOL rotaxane **3.33$_S$** (Scheme 18B). Axle **3.16$_S$·Cl** and bis-amine **2.15** were dissolved in a dichloromethane solution of NEt_3. Following which, BINOL-containing bis-acid chloride **3.22** was

added to the reaction. Mass spectrometry analysis of the crude reaction mixture indicated formation of the macrocycle (853.4 m/z $[M+Na]^+$) and [2]rotaxane (3177.6 m/z $[M+H]^+$). However, attempts to isolate the interlocked product *via* chromatographic methods failed, most likely due to only a trace amount being formed. This maybe a consequence of steric interactions between the bulky (*S*)-BINOL units of acid chloride **3.22** and axle hindering the chloride anion from acting as an efficient template for mechanical bond formation.

Finally, an ambitious condensation reaction between acid chloride **3.22** and bis-amine **2.15** in the presence of macrocycle $\mathbf{3.28_S}$ to prepare chiral [2]catenane $\mathbf{3.34_S}$ was carried out (Scheme 6). However, no evidence of target [2]catenane were observed by MS analysis, again possibly due to unfavourable steric interactions.

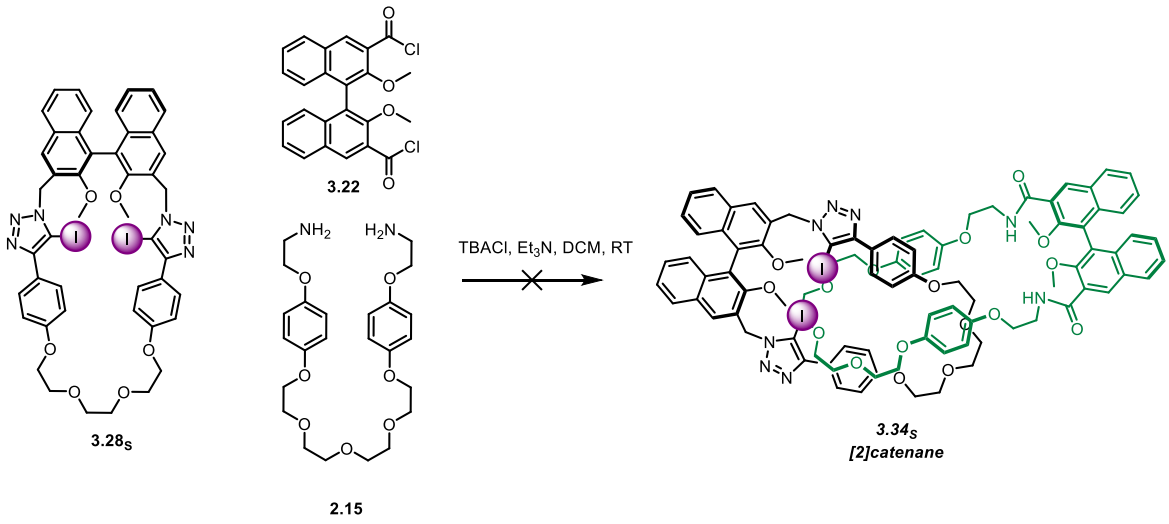

Scheme 19. Attempted synthesis of an HB/XB chiral [2]catenane ***3.34S.***

3.4. Attempted Active Metal Template Synthesis of Chiral Rotaxane

Macrocycle $\mathbf{3.28_S}$ has previously been used in the AMT synthesis of the chiral rotaxane shown in Figure 7. An attempt to prepare a novel chiral rotaxane $\mathbf{3.35_S}$ via an analogous AMT synthetic procedure was undertaken (Scheme 7). Excess amounts of 3,5-iodoethynylpyridine (4.0 equivalents) and stopper-azide $\mathbf{3.14_S}$ **(**8.0 equivalents) were added to an equimolar DCM solution of macrocycle

3.28$_S$ and $Cu(CH_3CN)_4PF_6$ and the reaction was monitored *via* TLC and MS. Disappointingly, no evidence of interlocked product was detected after 7 days. Only recovered macrocycle and axle **3.15**$_S$ components were isolated from the crude reaction mixture, suggesting mechanical bond formation was sterically disfavoured by the bulky BINOL units of the stopper-azide **3.14**$_S$.

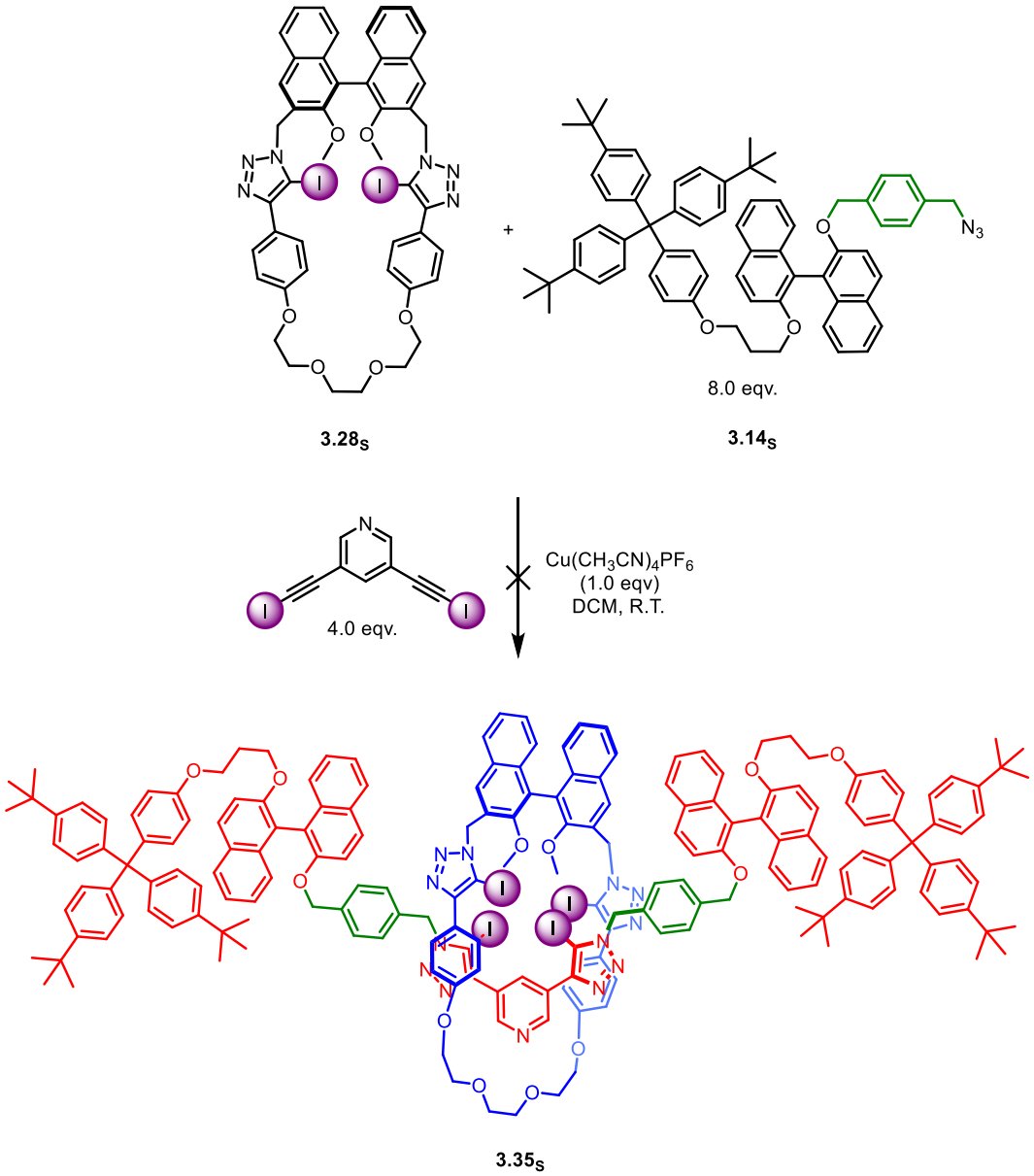

Scheme 20. Attempted synthesis of [2]rotaxane ***3.35***$_S$.

3.5. ^{1}H NMR Chiral Anion Binding Studies of Axle 3.16$_S$

The enantioselective anion binding behaviour of chiral axle **3.16$_S$** was investigated by ^{1}H NMR titration experiments. Initial studies conducted in pure acetone-d_6 found association constants to be $>10^4$ M^{-1}, too strong for accurate quantitative data being obtained. Hence, titrations were performed in the more competitive 3% D_2O/acetone-d_6 solvent mixture. Chiral anions studied included biologically important amino acid derivatives (NBoc-leucine, NBoc-proline and NBoc-tryptophan) and BINOL-derived phosphate (BINOL-PO_4^-) commonly used in asymmetric catalysis experiments. Anion binding isotherms were obtained by titrating aliquots of tetrabutylammonium (TBA) salts (Figure 71, synthesis of TBA salt preparation can be found in Chapter 6), monitoring changes in the chemical shift of the internal proton H_b on the pyridinium ring of the axle (Figure 72).

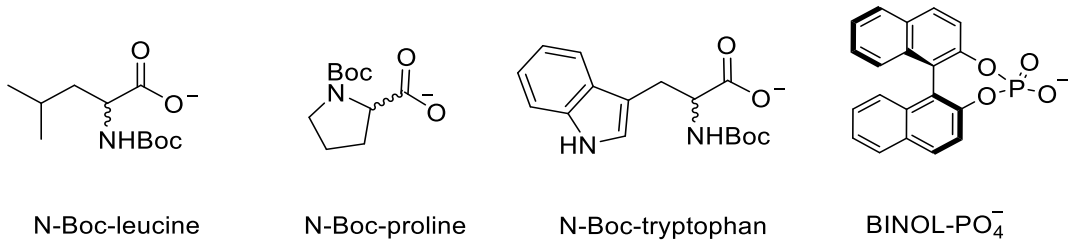

Figure 71. Chiral anions studied in this section as their tetrabutylammonium salts.

Typically the addition of anions to axle **3.16$_S$** showed evidence for binding, seen from significant *downfield* shifts of pyridinium proton H_b, with (*R*)-Pro causing the largest perturbations ($\Delta\delta$ = 0.17 ppm after 10.0 equivalents) while *upfield* shifts from pyridinium-CH_3 protons H_c were also evident ($\Delta\delta$ = 0.10 ppm after 10.0 equivalents) (Figure 72). By fitting the titration data (Figure 73) to a 1:1 host-guest stoichiometric binding model using OriginPro software[235], anion association constants were determined and are summarised in Table 7.

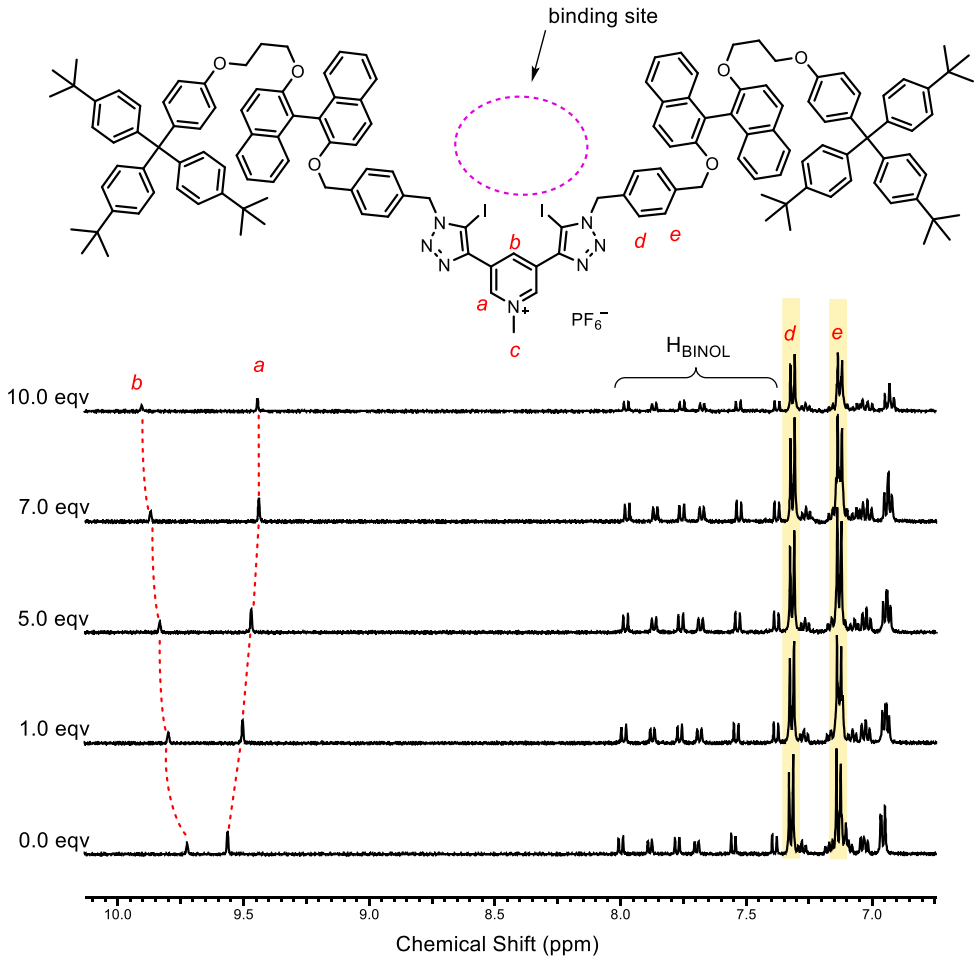

*Figure 72. Partial ^{1}H NMR of axle **3.16$_S$** with aliquots of TBA R-Pro in 3% D_2O in Acetone-d_6. [**3.16$_S$**] = 1.0 mM, Temperature = 298 K*

Axle **3.16$_S$** was found to display affinity for (*R*)-Pro (K_a = 990 M^{-1}) and (*S*)-Pro (K_a = 1020 M^{-1}) with no discernible differences between the enantiomeric guest species. (Table 7) Likewise, (*R*)-Trp (K_a = 760 M^{-1}) and (*S*)-Trp (K_a = 817 M^{-1}) were bound with similar affinity and no enantioselectivity. These observations suggest the BINOL chiral discriminating groups are too far away from the XB anion binding site to induce significant enantioselectivity.[227] However, **3.16$_S$** apparently exhibits a preference for (*R*)-Leu (K_a = 1394 M^{-1}) compared to (*S*)-Leu (K_a = 506 M^{-1}), with enantioselectivity of 0.36, which is the opposite stereochemical preference reported in a related acyclic BINOL receptor.[231] Future computational modelling investigations may be able to explain the promising chiral discrimination for (*R*)-Leu. During the titration experiments with BINOL-PO_4^-, precipitation problems unfortunately negated quantitative binding data from being obtained. Chiral anion binding

studies with cationic axle **3.16$_R$** were not undertaken due to the lack of enantioselectivity exhibited by axle **3.16$_S$**.

Table 7. Association constants, K_a (M^{-1}) for 3.16$_S$ with chiral anions as tetrabutylammonium salts and amino acids are Boc-protected.[a]

Anions[a]	**N-Boc-*D*-anion** *R*-isomer	**N-Boc-*L*-anion** *S-isomer*	ξ[c]
Proline	990 (53)	1020 (47)	1.03
Tryptophan	760 (36)	817 (43)	1.07
Leucine	1394 (245) [d]	506 (17)	0.36
BINOL-PO$_4$	[b]	[b]	

*^{1}H Titrations were carried out in 3 % D_2O in acetone-d_6 and non-linear curve fit function[235] applied using OriginPro 2017 software was used to determine the association constants using a 1:1 host-guest stoichiometric ratio. (Adjusted R^2 are >0.99 except for (R)-Leu with R^2=0.97, [**3.16$_S$**] = 1mM, Temperature = 298 K).* [b] *precipitation observed during titration.* [c] *Enantioselectivity, ξ = K_s/K_r where K is the association constants for its respective (S)- or (R)-enantiomer.*

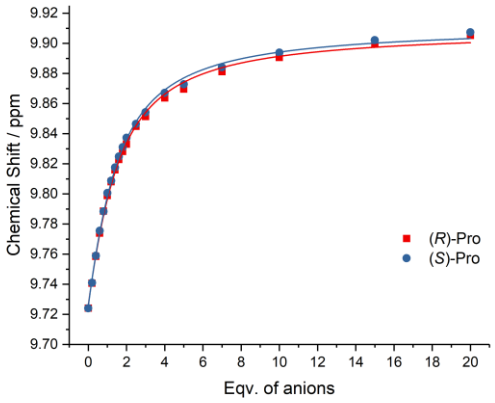

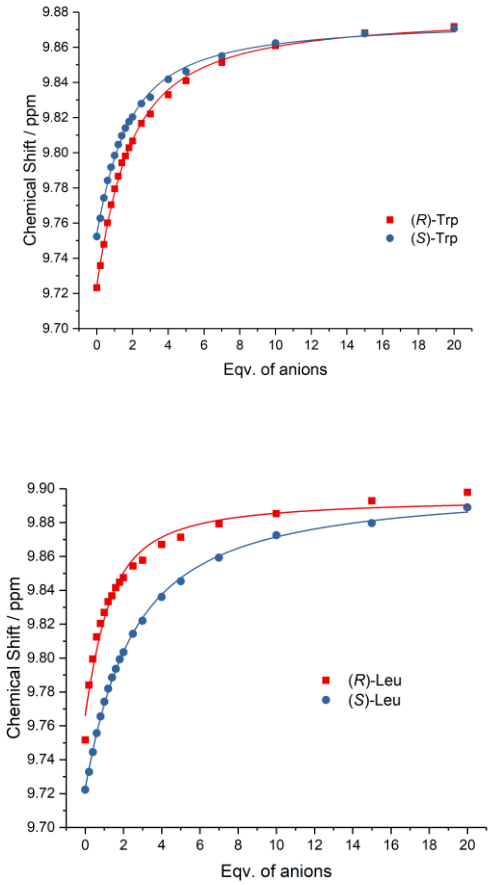

*Figure 73. Changes of the NMR chemical shifts of proton H_b on **3.16$_S$** with respect to the equivalent of anions added. Experimental data (solid markers) and fitted isotherms (solid lines) are shown.*

3.6. Chiral Acyclic and Macrocyclic Tetra-iodotriazole Containing Receptors for Anion Recognition

Rotaxane, catenane[236] and foldamer[86] XB receptors that contain tetra-iodotriazole donor motifs have been shown to be potent hosts for anions in competitive aqueous solvent media. A recent example reported by Beer and co-workers describes a chiral [3]rotaxane, with a (*S*)-BINOL axle component, capable of stereo- and geometric dicarboxylate anion isomer guest discrimination through convergent XB and HB donor units (Figure 74).[232] Specifically, the [3]rotaxane was able to bind (*S*)-Glu with an impressive enantioselectivity of 5.7 and a geometric selectivity for fumarate of 4.4 over maleate by forming 1:1 stoichiometric host-guest complexes in an organic-aqueous solvent mixture

($CHCl_3/CH_3OH/H_2O$ 60:39:1 *v/v/v*). As a follow-up to this work, this section discusses the synthesis of novel chiral acyclic and macrocyclic XB receptors with four iodo-triazole donor motifs covalently linked by two chiral BINOL groups. Through the integrated exploitation of BINOL, and in the case of the acyclic receptor systems, additional pyrene organic fluorophore substituents, the anion binding properties of these chiral tetra-iodotriazole receptors are investigated using fluorescence spectroscopy.

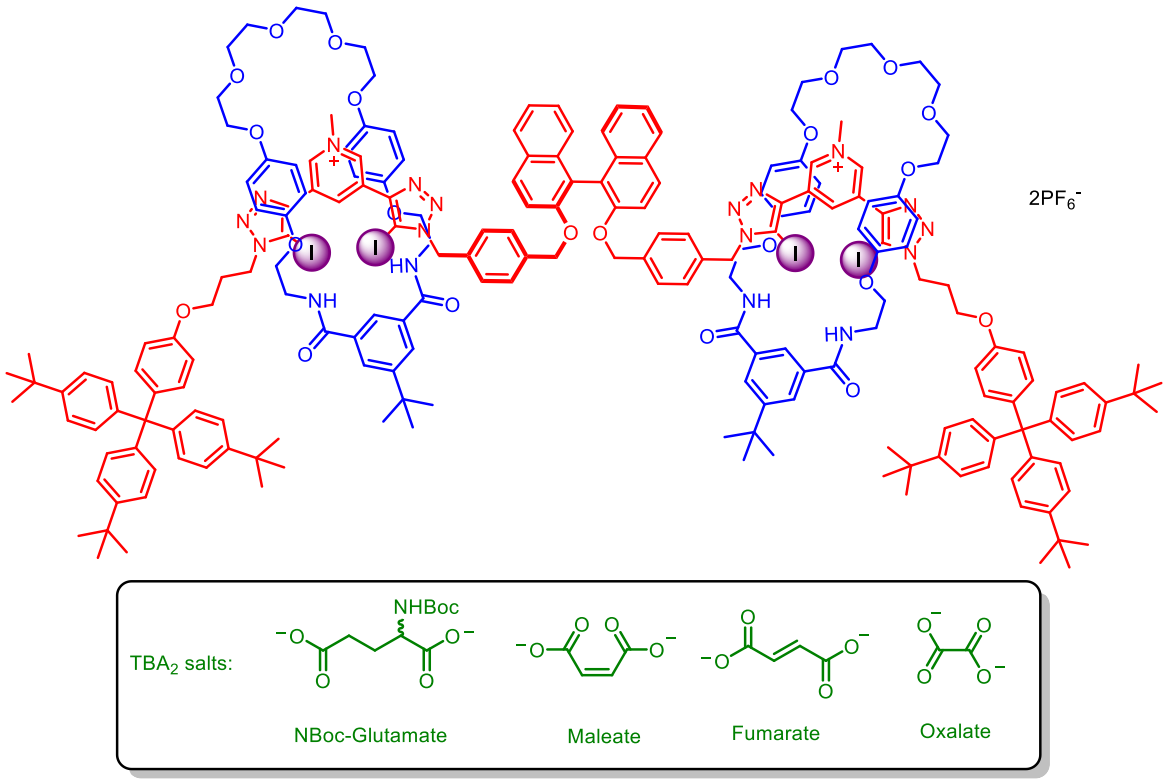

Figure 74. [3]rotaxane with convergent HB and XB donor units for chiral and geometric isomer anion discrimination.

3.6.1. Tetra-iodotriazole Pyrene Acyclic Receptor

Design and Synthesis of Acyclic Receptor

Target acyclic receptor **3.40** consists of solubilising ester functional groups, chiral discriminating BINOL units, iodotriazole anion binding motifs and organic fluorophore, pyrene (Figure 75). Solubilising groups were needed to overcome solubility issues of tetraiodotriazole motifs, while pyrene functionality allows the receptor to act as an anion optical sensor.

Pyrene monomers possess high fluorescent quantum yields[237] and have characteristic sharp emission signals at ca. 370-400 nm.[238] However, when these monomers come close to each other (< 10 Å), a characteristic broad excimer emission at longer wavelength, *ca.* 425–550 nm, is commonly observed.[40,239] The designed anion sensing mechanism (Figure 75), operates by receptor **3.40** undergoing a conformational change upon chiral dicarboxylate anion recognition via cooperative XB interactions. This leads to the receptor's two terminal pyrene groups being proximal to each other resulting in excimer emission.

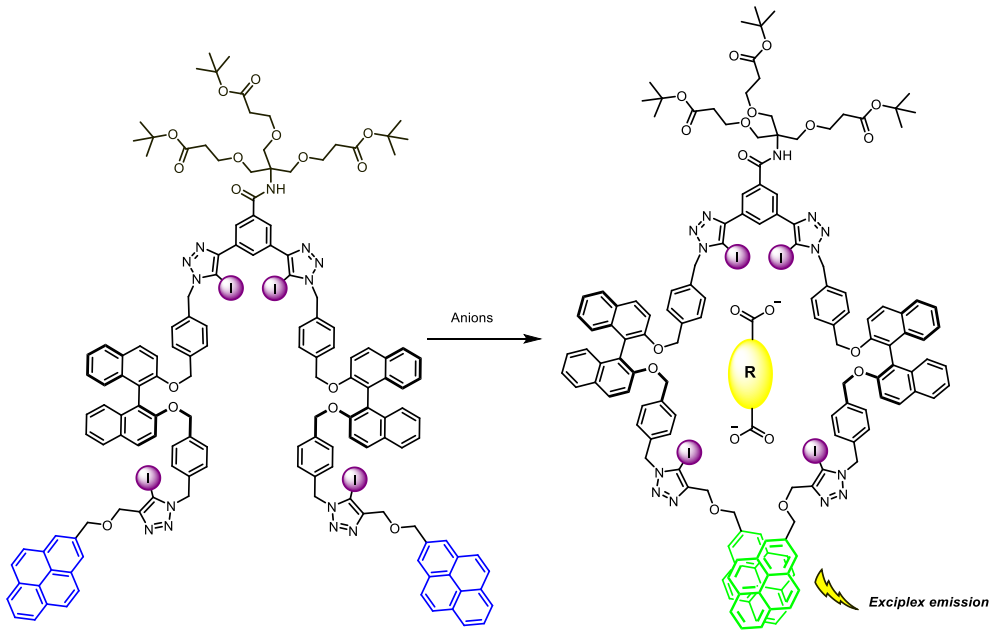

*Figure 75. Design of chiral receptor **3.40** and proposed binding mechanism upon addition of dicarboxylate anions.*

Receptor precursor **3.38** was synthesised using CuAAC reaction conditions (Scheme 21). A large excess of BINOL-bis-azide **3.37**[232] was dissolved in a solution of $Cu(CH_3CN)_4PF_6$ and TBTA (cat.) in THF, followed by the addition 3,5-bis(iodoethynyl)pyridine **3.36** appended with ester solubilising groups. Both $\mathbf{3.38_{R/S}}$ precursor compounds were isolated in good yields.

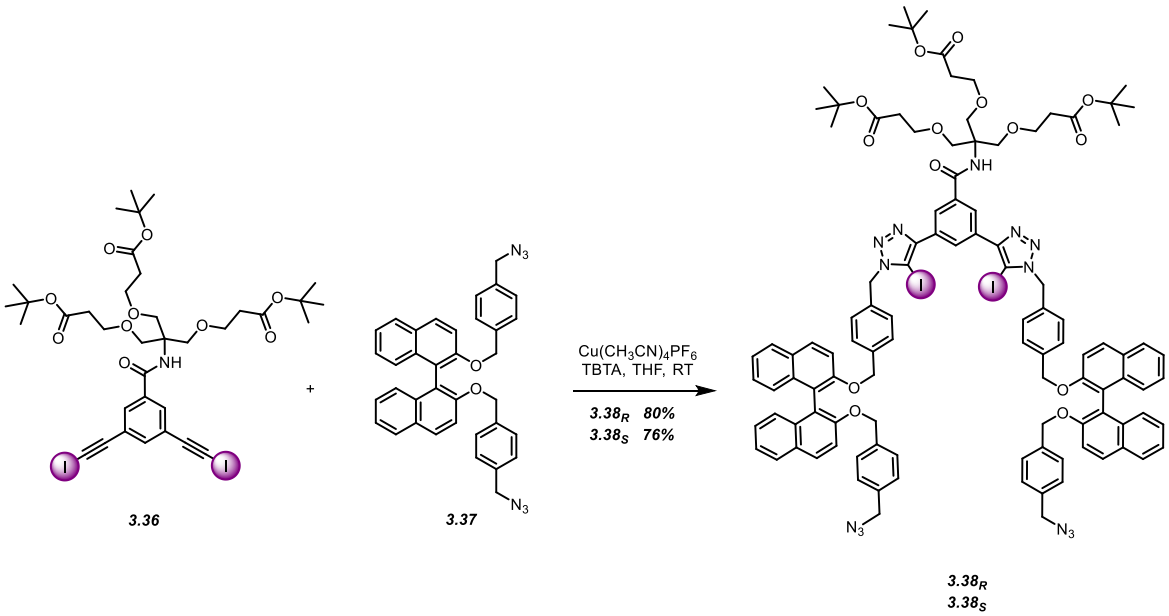

*Scheme 21. Synthesis of precursor **3.38** using Cu(I)-catalysed azide-alkyne cycloaddition reaction between an iodoalkyne **3.36** with appended solubilising ester functional groups and bis-azide **3.37** with chiral functionality incorporated.*

The target XB receptors $\mathbf{3.40_S}$ and $\mathbf{3.40_R}$ were prepared *via* reaction of **3.38** with two equivalents of pyrene-iodoalkyne $\mathbf{3.39_H}$ or pyrene-protoalkyne $\mathbf{3.39_I}$ using respectively 'one-pot' and 'two-pot' CuAAC reaction conditions (Scheme 22). Both reaction pathways gave similar yields and both receptors were characterised by ^{1}H, ^{13}C NMR and ESI-MS.

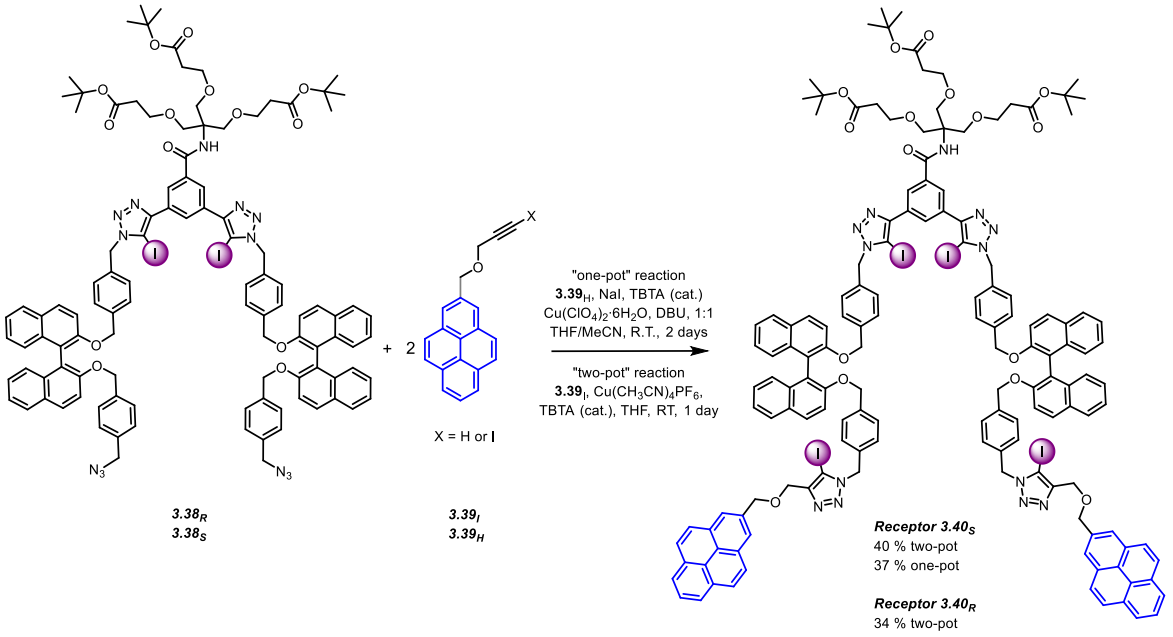

*Scheme 22. Synthesis of acyclic receptor **3.40**$_S$ and **3.40**$_R$ using CuAAC 'one-pot' or 'two-pot' reaction.*

Fluorescence Anion Titration Studies of Pyrene-containing Receptor

UV/Vis absorption and emission spectra of receptors **3.40**$_S$ and **3.40**$_R$ were measured in acetonitrile. Pyrene absorption band maxima (Figure 76 – blue spectra) originating from π-π* transitions are observed at 276, 326 and 341 nm, while the BINOL absorption lies hidden under the pyrene absorption bands due to the significantly smaller molar extinction coefficient (pyrene in cyclohexane, ε = 54 000 cm^{-1}/M; BINOL in $CHCl_3$, ε = 6510 cm^{-1}/M). The anion binding behaviour of both receptors **3.40**$_S$ and **3.40**$_R$ was investigated by fluorescence spectroscopy in acetonitrile with an excitation wavelength of λ = 341 nm. Pyrene monomer fluorescence is characterised by its sharp vibronic bands and are labelled as band I (375 nm), band II (379 nm, shoulder), band III (385 nm), band IV (395 nm) and band V (414 nm) which are attributed to π- π* transitions (Figure 76 – green spectra).[239] It is characteristic for band I to exhibit a higher fluorescence intensity than band III when spectra are recorded in a polar environment like acetonitrile.[240,241] Unexpectedly, both **3.40**$_S$ and **3.40**$_R$ fluorescence spectra display monomer (377 & 395 nm, Figure 76 – shaded blue) and excimer emission (487 nm, Figure 76 – shaded pink) This suggests some degree of rigidity in the receptor

structure possibly imparted by the BINOL motif which puts the pyrene chromophores in close proximity even in the absence of anions.

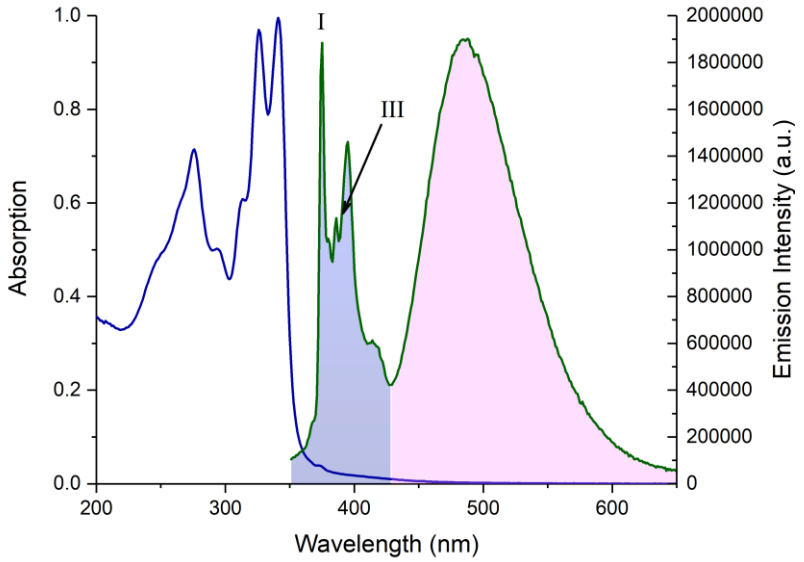

*Figure 76. Photophysical measurements of Receptor **3.40**$_S$ showing UV-Vis absorption spectrum (blue line - left axis) and fluorescence spectrum (green line - right axis) in acetonitrile. Fluorescence arising from pyrene monomeric units (blue shaded area under curve) and excimer units (pink shaded area under curve) were observed. λ_{ex} = 341 nm*

The addition of anions typically resulted in a decrease in excimer fluorescence concomitant with an increase in monomer fluorescence intensity (Figure 77 and Figure 79). It has been reported that vibronic band intensities of pyrene *monomer* fluorescence are solvent dependent. Due to coupling of electronic and vibronic states, *monomeric* bands III and I are highly sensitive to the polarity of the surrounding micro-environment in which the relative fluorescence intensity of bands r = III/I is usually a measure of *local polarity* about the fluorophore.[239,240,242] In polar solvents such as acetonitrile r = 0.57, while in non-polar solvents like *n*-hexane r = 1.65.[240] By comparing the relative intensities of bands III/I before and after anion titration, insights of the receptor's microenvironment may help explain the fluorescence decay pathways from *monomer* excited states. For example, the relative intensity r = III/I of the the free receptor r_{host} = 0.6, whereas after addition of Cl^-, $r_{host + guest}$ = 1.11. (Figure 77 – Receptor **3.40**$_S$ Cl^-) This indicates that upon halide anion binding the hydrophobic environment around the receptor increases. Similar trends are also observed upon

addition of bromide, iodide and carboxylate anions (Figure 77 and Figure 79). The addition of I^- induced the largest decrease in pyrene excimer fluorescence intensity by 77 % while Br^- and Cl^- were found to be reduced by 63 and 53 % respectively. The relative quenching of the excimer fluorescence upon halide addition correlates with the 'heavy-atom' effect in the following order $I^- > Br^- > Cl^-$.[243,244] Interestingly, the increase in monomer fluorescence appears to be the largest with Cl^- (Figure 77).

Receptor **3.40$_S$**

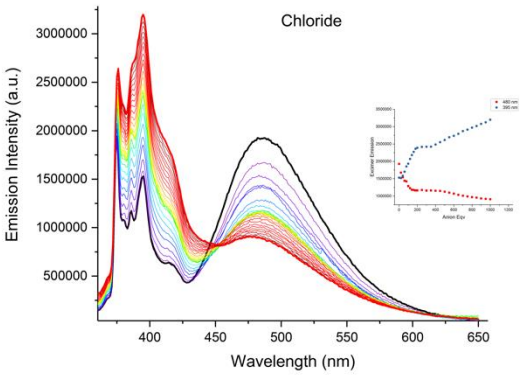

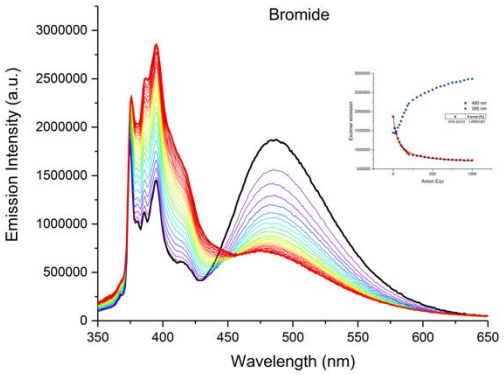

Receptor **3.40$_R$**

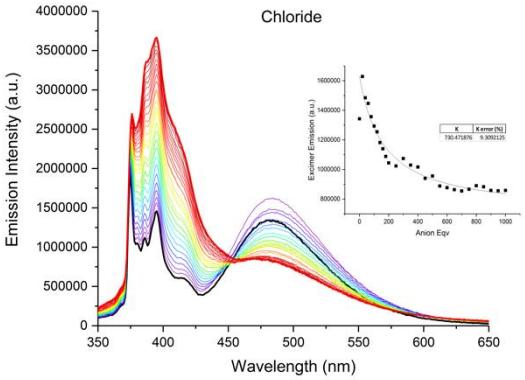

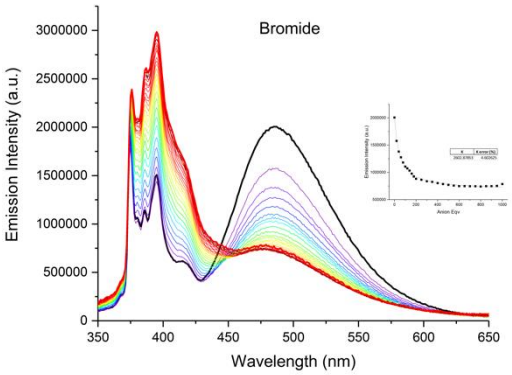

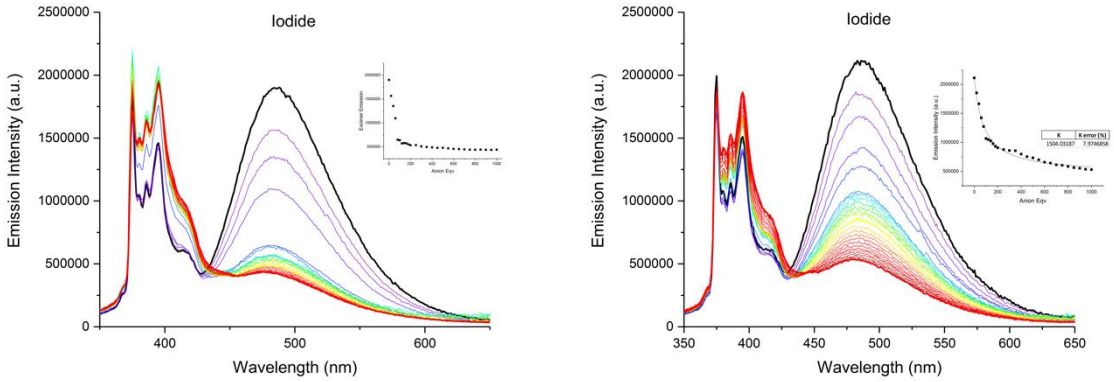

Figure 77. Fluorescence spectrum of receptor ***3.40S*** *and* ***3.40R*** *(Black line) with increasing concentration of TBA anions (red line). ([host] = 8.3 µM. acetonitrile, λ_{ex} = 341 nm, T = 298 K) Inset: Excimer fluorescence maxima at each titration point.*

This 'hydrophobic' sensing phenomenon was noted by Shimizu and co-workers who studied the influence of TBA salts on the solvophobic interactions of molecules in organic solvents. They designed molecular 'balances' where the intramolecular interaction between two non-polar surfaces determined a *folded* and *unfolded* conformation (Figure 78).[245] It was found that upon addition of Cl^- to the molecular balance in acetonitrile, they observed a 2-fold increase in folding of the molecular balance† measured by ^1H NMR spectroscopy. The anion-induced solvophobic effect strengthening could lead to an increase in the polarity of acetonitrile, similar to that of methanol. By testing a series of common TBA salts, they found that the more charge dense anion (eg, Cl^-) produces a larger acetonitrile solvation energy, enhancing the solvophobic effect through change in bulk solvent properties. Having hypothesised that, a likely scenario that causes the drastic change in fluorescence may occur through the change in environment surrounding pyrenes resulting in pyrene arms folding into an overall enclosed receptor due to hydrophobicity.

† Concentration of molecular balance is independent to salt effects.

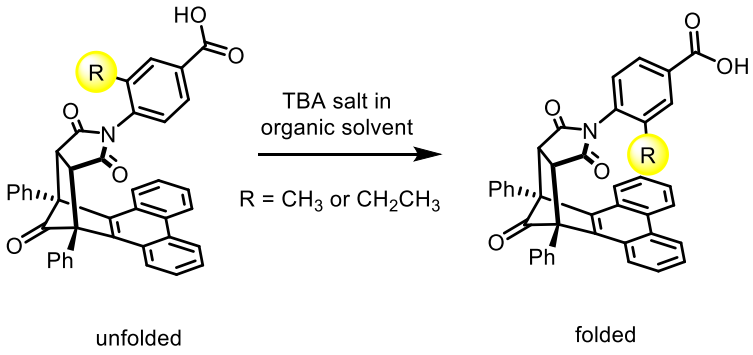

Figure 78. Molecular balance conformational change from its unfolded to folded state due to anion-enhanced solvophobic effects in organic solvents. [245]

By fitting the titration data monitoring the receptors' excimer emission to a 1:1 stoichiometric host-guest model using non-linear regression (BindFit[235]), anion association constants were determined (Table 8). Association constants of receptor **3.40$_R$** obtained from monitoring excimer emission reveals preference for Br^- (K_a = 2604 M^{-1}) over I^- (K_a = 1504 M^{-1}) and Cl^- (K_a = 730 M^{-1}) (Table 8). Receptor **3.40$_R$** selectivity for Br^- could be a result of host-guest size complementary.

*Table 8. Association constants (K_a/ M^{-1}) of Receptors **3.40$_S$** and **3.40$_R$** with different anions in acetonitrile at 298 K.*[a]

Anions	Receptor 3.40$_S$	Receptor 3.40$_R$
Chloride	–[b]	730 (5%)
Bromide	1935 (4%)	2604 (4%)
Iodide	–[b]	1504
(*R*,*R*)-Tartrate	1916 (10%)	2560 (8%)
(*S*,*S*)-Tartrate	1540 (7%)	1258 (6%)
Phthalate	836 (3%)	1000 (3%)
Isophthalate	730 (3%)	747 (6%)
Terephthalate	–[b]	1712 (13%)

[a] Values of K_a determined using BindFit.[235] Errors (%) in parentheses; [host] = 8.3 µM. acetonitrile, T = 298 K); [b] BindFit analysis of titration data could not determine K_a.

Chiral and geometric dicarboxylate anion titration data obtained from monitoring excimer emission (Figure 79) were also fitted to a 1:1 stoichiometric host-guest model using non-linear regression (BindFit[235]) to determine association constants shown in Table 2. Notably, a degree of enantioselectivity was observed with receptor **3.40$_R$** forming a stronger association with (*R*,*R*)-

tartrate (K_a = 2560 M^{-1}) in comparison with the (*S*,*S*)-tartrate enantiomer (K_a = 1258 M^{-1}). Receptor **3.40$_S$** also displays this preference, although the difference in binding strengths between the tartrate enantiomers is less marked. Of the geometric isomer dicarboxylate guest species, **3.40$_R$** exhibits greater affinity for linear terephthalate (K_a = 1713 M^{-1}) followed by phthalate (K_a = 1000 M^{-1}) then isophthalate (K_a = 747 M^{-1}). A similar trend was observed for receptor **3.40$_S$** with phthalate binding being stronger than isophthalate. Structural configuration is hard to determine *via* fluorescence spectroscopy and further studies needed to be carried out.

Receptor 3.40$_S$ **Receptor 3.40$_R$**

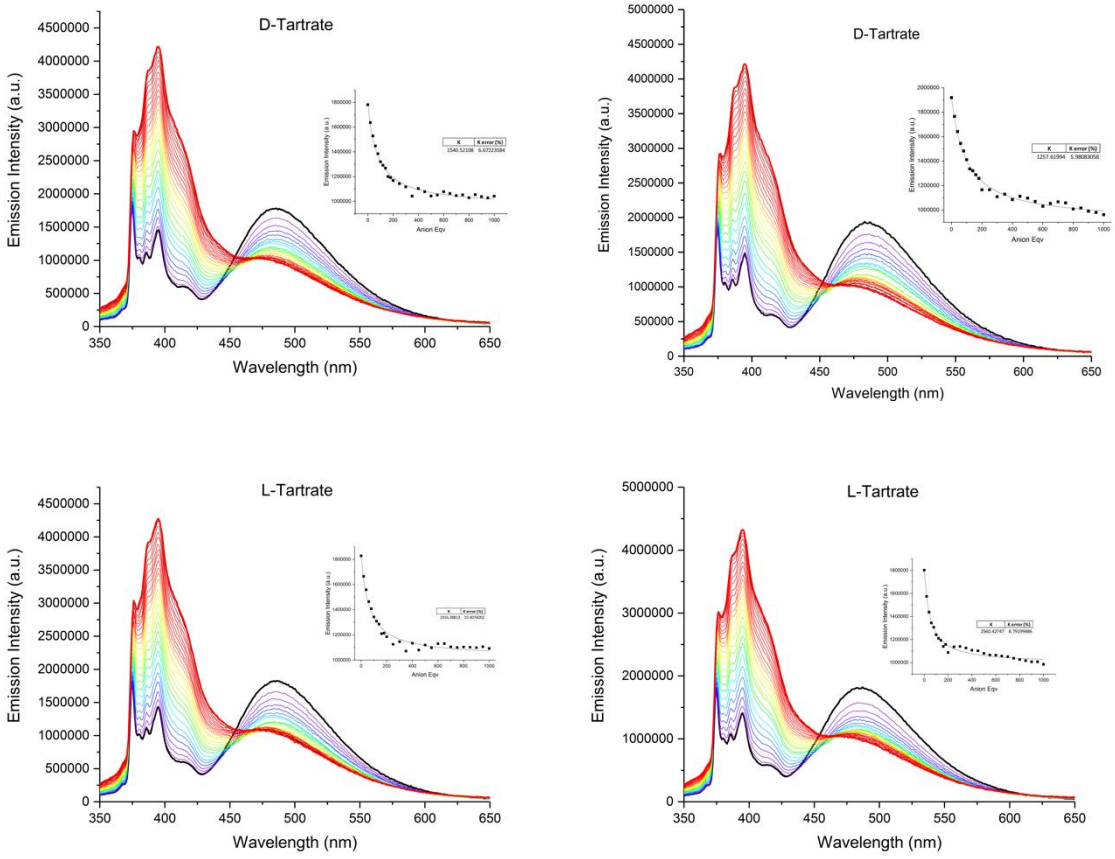

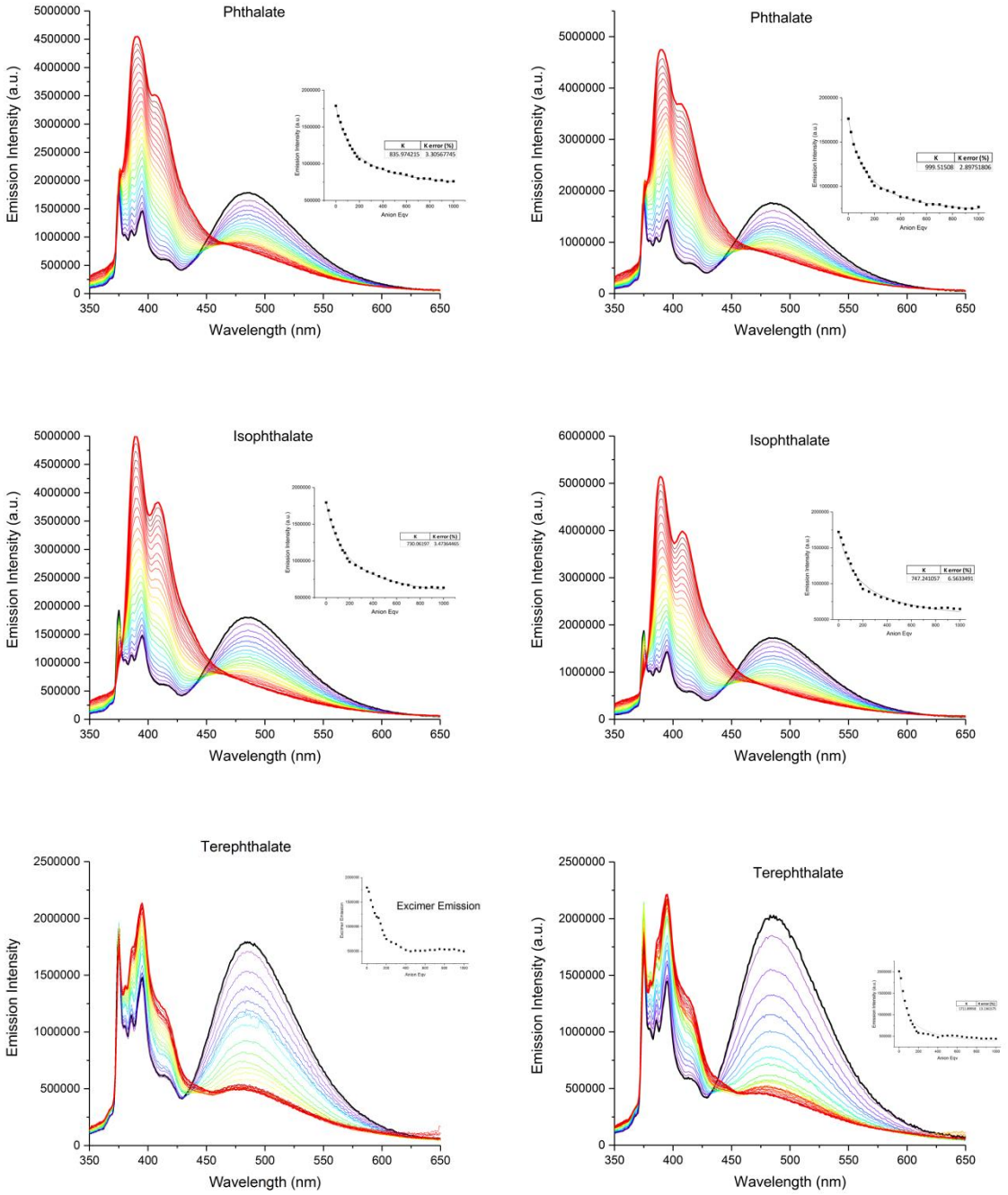

Figure 79. Fluorescence spectrum of receptor ***3.40S*** *and* ***3.40R*** *(Black line) with increasing concentration of* TBA_2 *dicarboxylates (red line). ([host] = 8.3 µM. acetonitrile,* λ_{ex} *= 341 nm, T = 298 K) Inset: Excimer fluorescence maxima at each titration point.*

3.6.2. Tetra-iodotriazole Macrocycle Receptor

Macrocycle Synthesis

Macrocycle **3.41$_{S/R}$** was synthesised by 'two-pot' CuAAC 'click' reaction under high dilution conditions (Scheme 23). The bis-azide functionalised precursor **3.38$_{S/R}$** was added to a solution of $Cu(CH_3CN)_4PF_6$ and TBTA in THF. Following which, 3,5-bis(iodoethynyl)pyridine was added slowly *via* syringe pump over 8 hours. The resulting crude reaction material was purified by preparatory TLC to afford macrocycles **3.41$_S$** and **3.41$_R$** in the same yield of 16%, characterised by ^1H, ^{13}C NMR spectroscopy and ESI-MS.

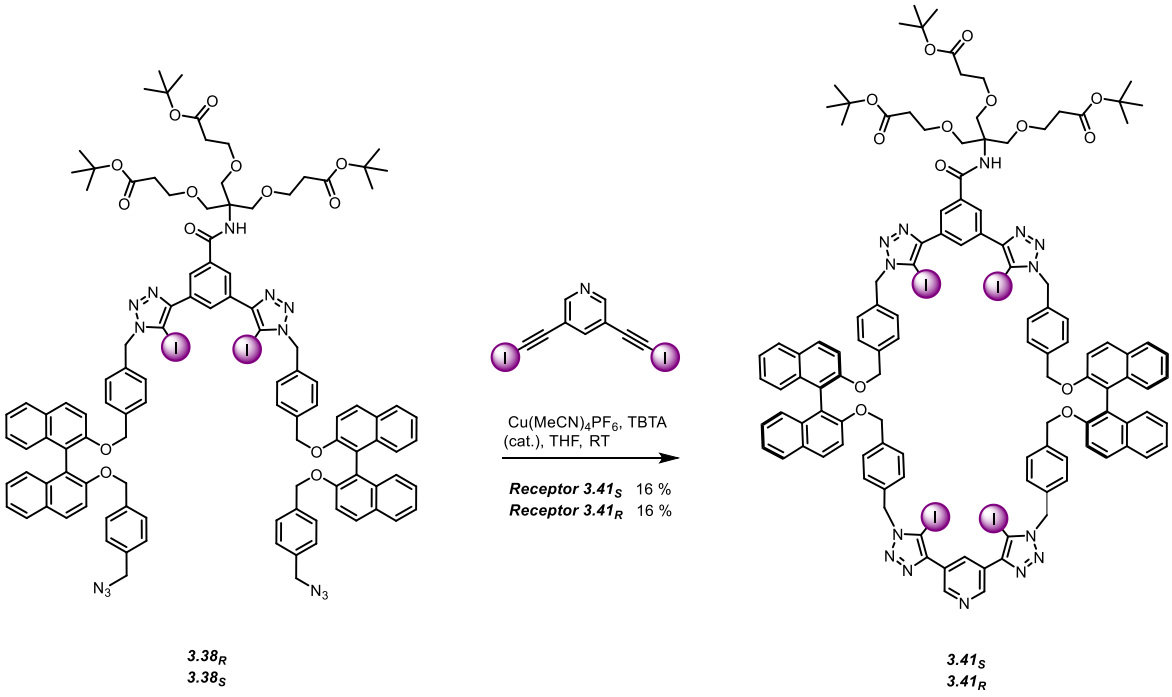

Scheme 23. Synthesis of tetra-iodotriazole macrocyclic receptor using a "two-pot" CuAAC reaction.

3.6.3. Anion Binding Studies of Macrocycle

^{1}H NMR Titration with chloride

The anion binding behaviour of macrocycle **3.41$_S$** was first probed by ^1H NMR titration in $CDCl_3$. The addition of tetrabutylammonium (TBA) chloride to macrocycle **3.41$_S$** elicited large downfield shifts of H_a corresponding to the internal pyridine proton (**Error! Reference source not found.**).

Concomitantly, upfield proton perturbations of H_g arising from the internal benzene proton were also observed, presumably due to some form of shielding effects from aromatic ring currents arising from a change in macrocyclic conformation upon Cl^- binding. Perturbations of other proton signals were insignificant. By monitoring the shifts of H_a, non-linear regression analysis of the titration data using the WinEQNMR2 software[171] determined a 1:1 host-guest stoichiometry anion association constant K_a = 99 (14) M^{-1}.

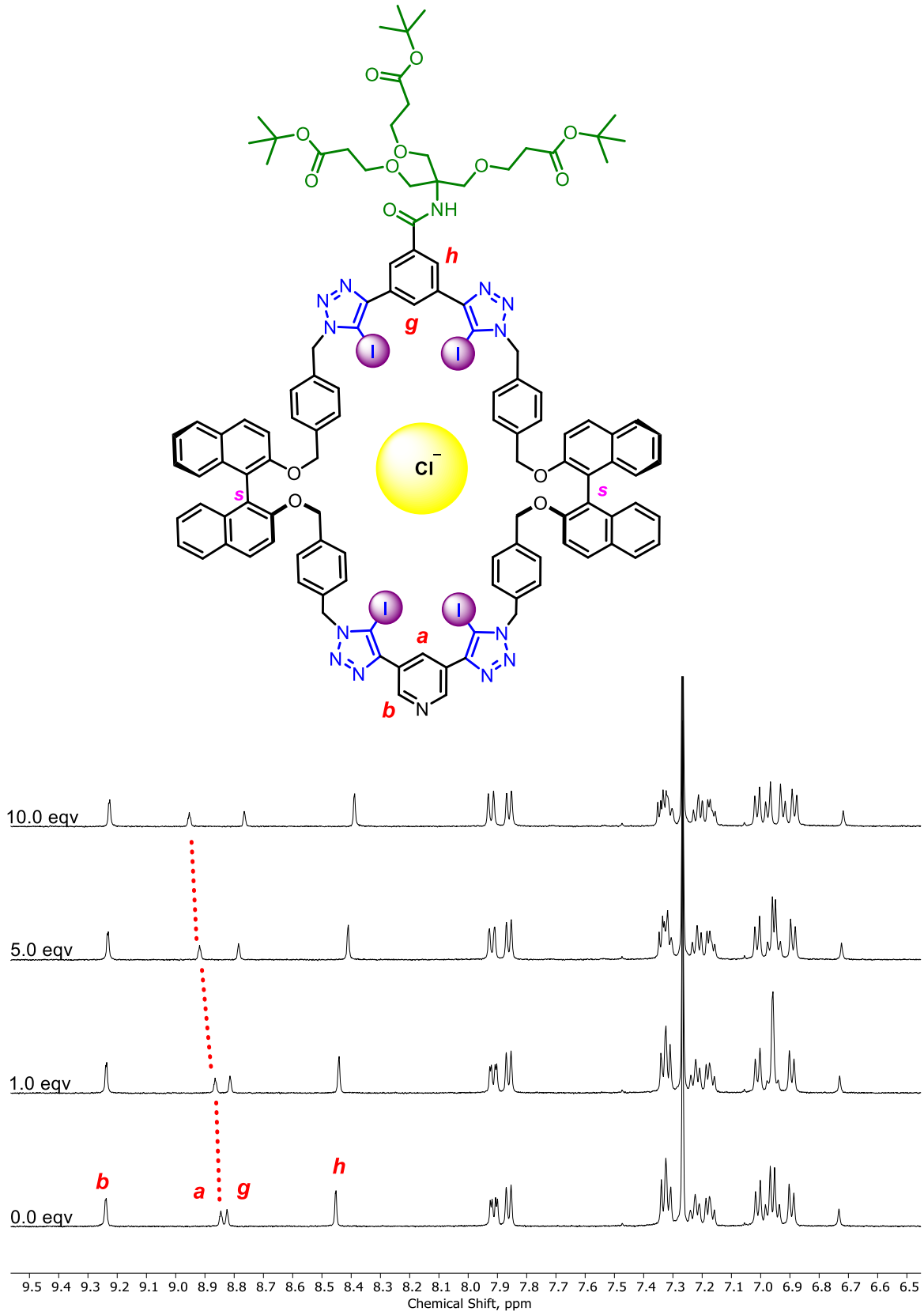

*Figure 80. Partial ^{1}H NMR spectra of tetraiodotriazole macrocycle **3.41$_S$** in the presence of increasing quantities of Cl^- ([**3.41$_S$**] = 1.0 mM, $CDCl_3$, T = 298 K).*

Fluorescence Anion Titrations

The BINOL motif is inherently fluorescent due to its aromatic conjugated system and its emission response is influenced by the dihedral angle between aromatic planes. Furthermore, BINOL containing anion receptors have been demonstrated to function as fluorescent sensors (Figure 74). To determine the anion recognition capabilities of macrocycle **3.41$_S$,** fluorescence titrations were carried out in acetonitrile[†] with halides, and chiral/geometric isomers of dicarboxylate anions. (Figure 81).

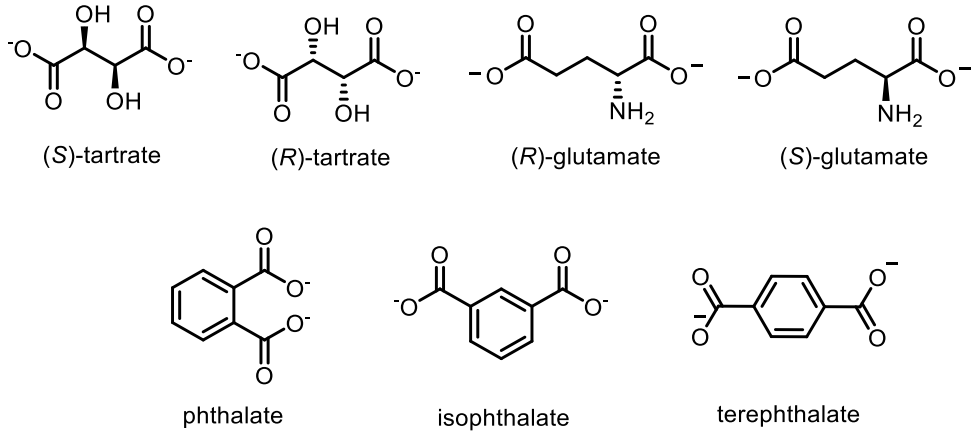

Figure 81. Anions (X) used as their TBA salts (TBA_2X): chiral anions such as (S)-/(R)-tartrate, glutamate and geometric dicarboxylates such as phthalate, isophthalate and terephthalate. (See Chapter 6 for TBA salt synthesis)

Absorption and emission spectra of macrocycle **3.41$_S$**[‡] revealed intense aromatic absorption stemming from π-π* transition < 300 nm while BINOL absorption was observed in the range of 325 – 340 nm. Excitation at 336 nm led to broad fluorescence with λ_{max} at 357 nm, similar to literature examples (Figure 82).[246]

[†] Fluorescence anion titrations were undertaken in acetonitrile, a solvent which displays a spectroscopic window that does not overlap with the photophysical properties of BINOL.

[‡] Absorption and emission spectra measured for macrocycle containing (R)-BINOL was the same as that of (S)-BINOL shown in Figure 82.

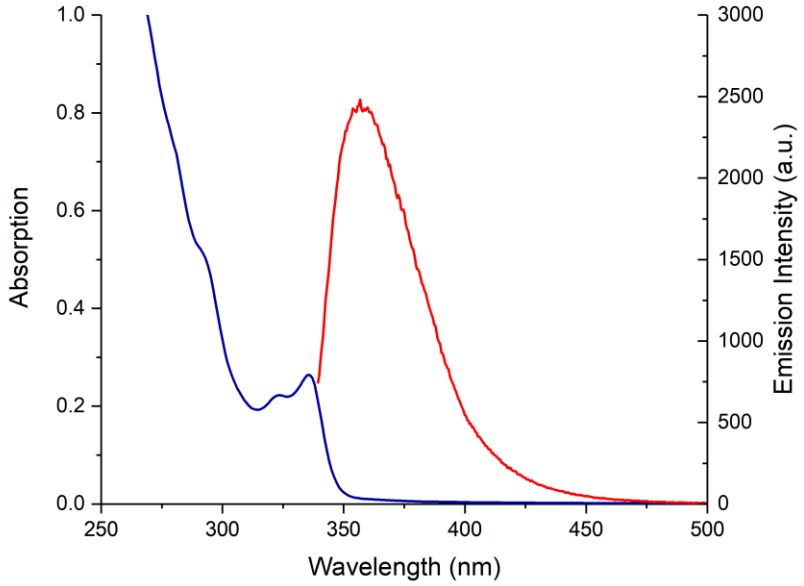

Figure 82. Photophysical measurements of receptor ***3.41*** $_S$ *showing UV-Vis absorption spectrum (blue line - left axis) and fluorescence spectrum (*λ_{ex} *= 336 nm, red line - right axis).*

The addition of TBA halides resulted in an initial significant increase in fluorescence intensity up to 20 equivalents, followed by a fluorescence intensity decrease with further equivalents added (Figure 83). This fluorescence response may tentatively be rationalised by a combination of conformational rigidification of the macrocycle upon halide binding, photo-induced electronic transfer (PET) quenching effects as well as angle changes of naphthyl group affecting BINOL fluorescence.

i)

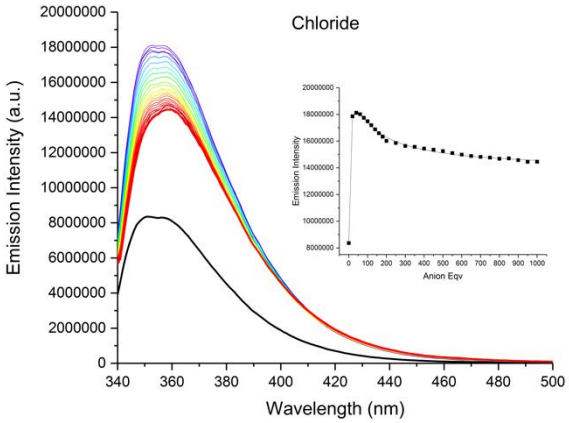

ii)

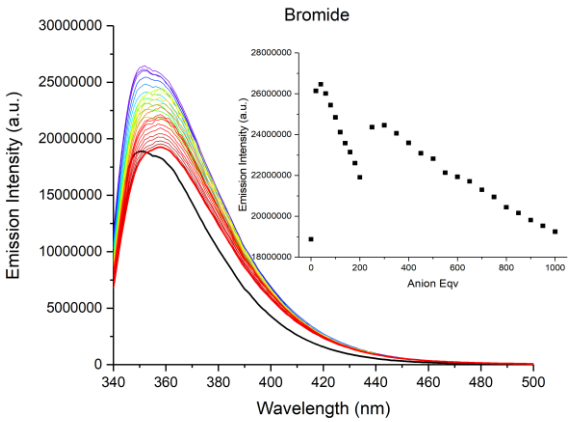

iii)

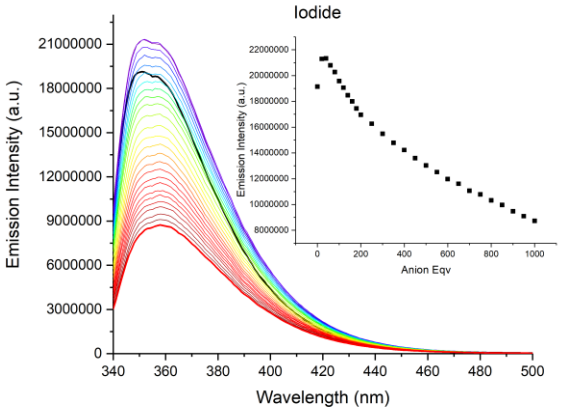

*Figure 83. Fluorescence spectra of macrocycle **3.41$_S$** (Black line) with increasing concentration of TBA i) chloride ii) bromide and iii) iodide. ([**3.41$_S$**] = 5 × 10^{-5} M, acetonitrile, λ_{ex} = 336 nm, T = 298 K). Inset: Plot of added anion eqv vs fluorescence maxima at each titration point*

The addition of up to 20 eqv of anions resulted in a fluorescence increase of *ca.* 40% for Cl^- and Br^-, while a fluorescence increase of *ca.* 12% was found for I^- (Figure 84). Further addition of halides of up to 1000 eqv resulted in a quenching of intensity of *ca.* 34%, 25% and 59% for Cl^-, Br^- and I^- respectively. The overall change of fluorescence intensity after 1000 eqv for Cl^- was -8% and I^-, -54%, while Br^- resulted in a modest 5% increase (see purple marker in Figure 84**).**

Analogous dicarboxylate anion titrations revealed similar trends where an initial increase in fluorescence was observed for up to 20 eqv, followed by a decrease with further addition (Figure

85). Fluorescence PET quenching by dicarboxylate binding to BINOL fluorophore functionalised anion receptors has been observed previously.[247,248]

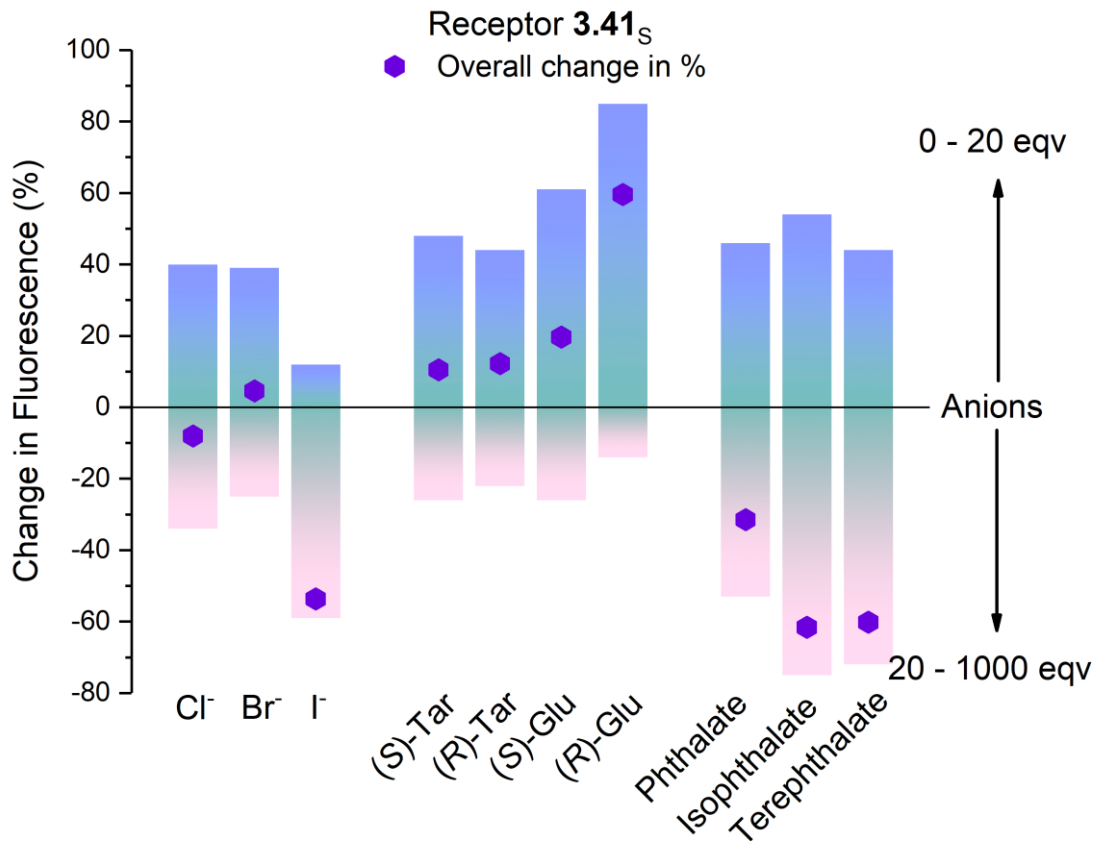

*Figure 84. Percentage change in fluorescence of receptor **3.41**$_S$ in acetonitrile upon addition of anions. For all anions tested, an increase in fluorescence was observed between 0–20[†] eqv while a decrease in fluorescence was observed between 20-1000[‡] eqv. Overall change in fluorescence indicated in purple marker. [†] See appendix D for table of values.*

Although the fluorescence titration data could not be analysed by BindFit for association constant determination, qualitative analysis of the percentage quenching **(**Figure 84) indicates a receptor preference for (*R*)-Glu (60%), isophthalate (-62%) and terephthalate (-60%) where overall changes in fluorescence (0-1000 eqv) were the largest. The quenching effect was greatest amongst the

[†] Percentage intensity increase calculated by taking difference between 0 eqv and 20 eqv fluorescence intensity at 357 nm.
[‡] Percentage quenching of intensity calculated by taking difference between 20 eqv and 1000 eqv fluorescence intensity at 357 nm.

geometric isomer dicarboxylates with phthalate, isophthalate and terephthalate quenching emission by 53, 75 and 72% respectively between 20-1000 eqv, whereas moderate decreases in fluorescence were observed with chiral dicarboxylate guest species. Interestingly, the overall change in fluorescence with all chiral dicarboxylates was an intensity enhancement which contrasts a fluorescence quenching effect observed with geometric dicarboxylates.

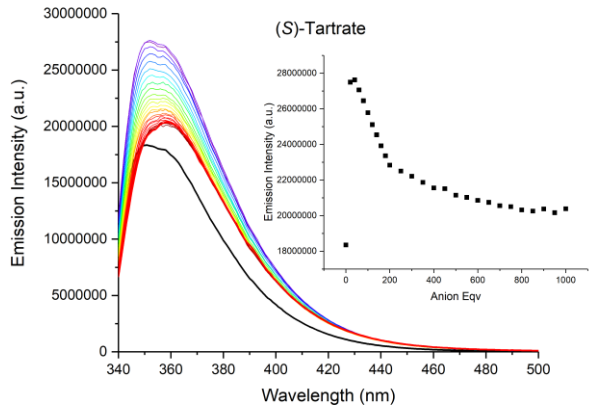

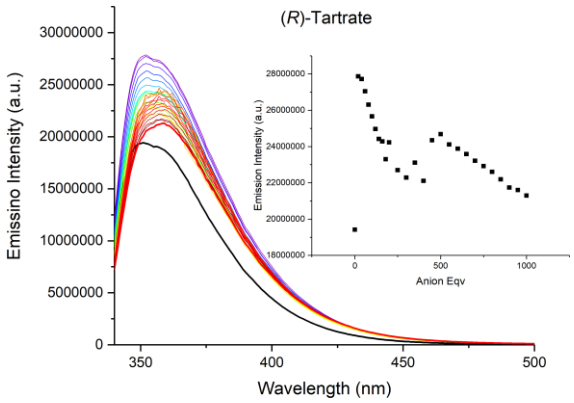

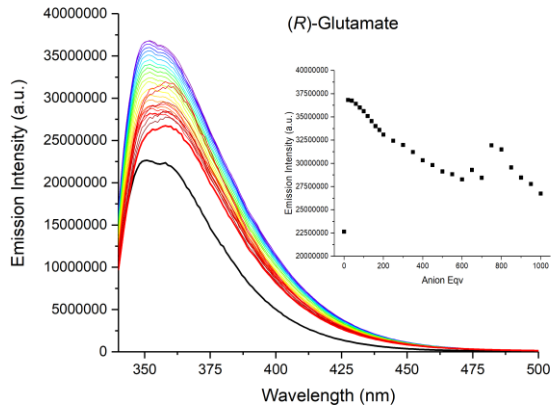

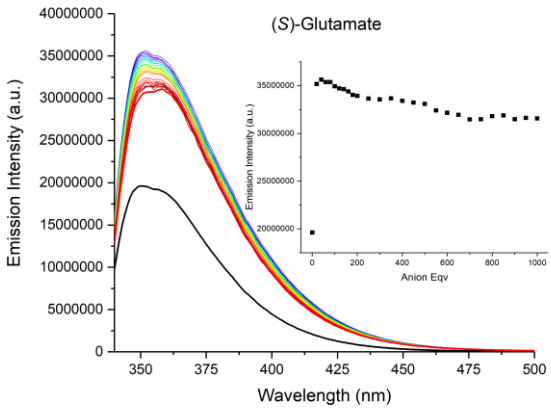

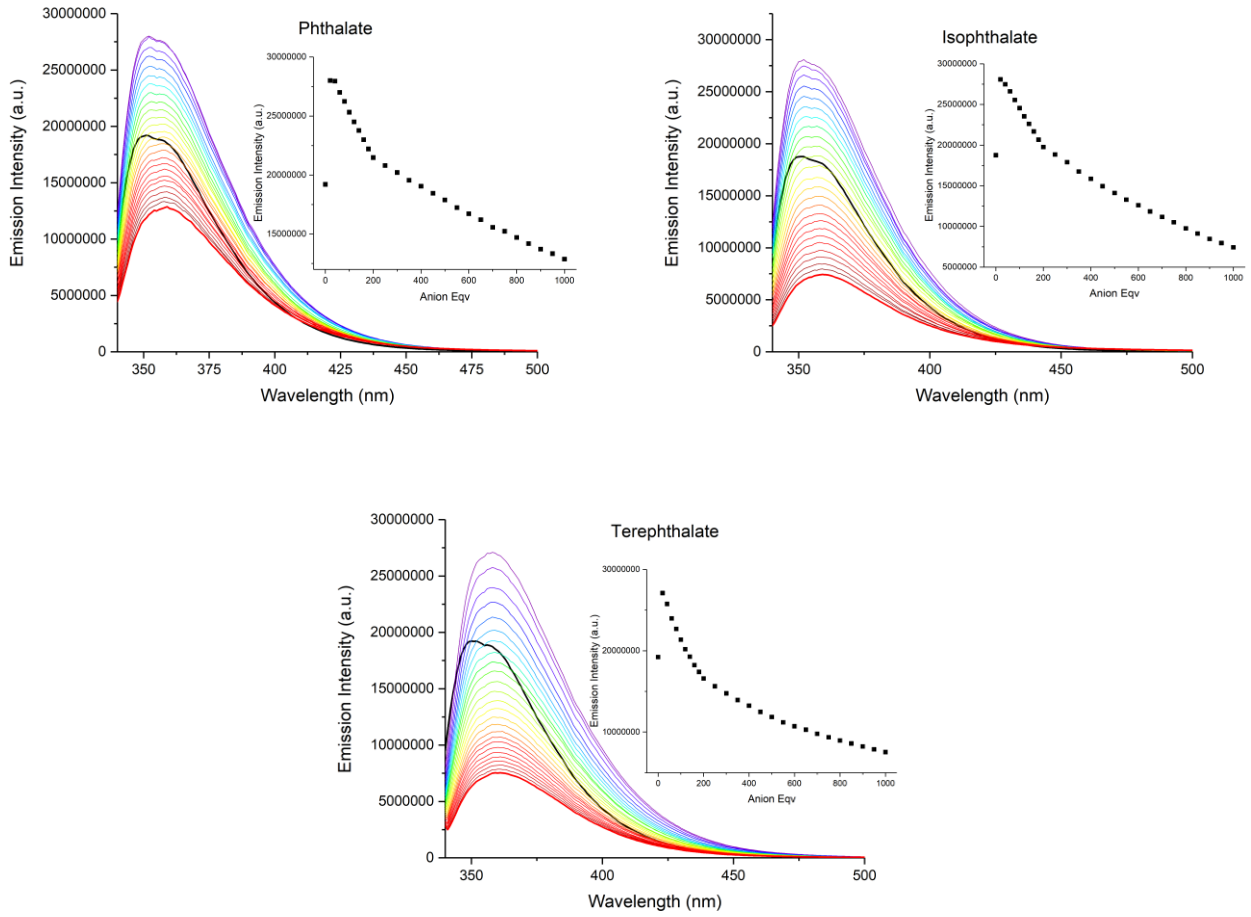

*Figure 85. Fluorescence spectra of macrocycle **3.41**$_S$ (Black line) with increasing concentration of TBA anions (red line). ([**3.41**$_S$] = 5 × 10^{-5} M, acetonitrile, λ_{ex} = 336 nm, T = 298 K). Inset: BINOL fluorescence maxima at each titration point.*

3.7. Conclusions and Potential Future work

The synthesis and chiral anion recognition studies of chiral XB receptors is discussed in this chapter. By incorporating the chiral BINOL motif into an axle component, attempts were made to synthesise interlocked host structures *via* anion and active metal template methodologies which proved to be challenging. Nonetheless, a [2]rotaxane **3.32**$_S$ was successfully synthesised albeit in low yields. Efforts then focused on the incorporation of BINOL motifs into acyclic and macrocyclic receptor host frameworks, that were shown to be capable of binding carboxylate guest species through four integrated iodotriazole binding motifs.

Chiral and geometric dicarboxylate anion titration data obtained from monitoring excimer emission of bis-pyrene terminally functionalised acyclic receptors **3.40$_R$** and **3.40$_S$** revealed both to exhibit a degree of enantioselectivity towards (*R*,*R*)-tartrate compared to its (S,S)-tartrate isomer. Amongst the geometric phthalate isomers, **3.40$_R$** displayed greater affinity for terephthalate, probably due to better matching host-guest size complementarity. Although significant perturbations of the BINOL fluorescence of macrocyclic receptor **3.41$_S$** were observed upon anion addition, unfortunately quantitative data could not be determined from the titration data.

3.7.1. Future Work

In future work, it would be interesting to further investigate the photophysical properties of the tetradentate XB acyclic and macrocyclic chiral receptors. Techniques such as ultrafast spectroscopy could provide insights into photophysical decay pathways between host and guest association. In combination with molecular modelling studies, host-guest conformational binding modes of dicarboxylate guest recognition could be determined.

4 | Mechanical Bond Formation using Iodonium Halogen Bonding Interactions

4.1. Haloniums

4.1.1. The 'other' Halogen Bond

Haloniums were first postulated by Roberts and Kimball in 1937 when they reported the mechanism of electrophilic addition of halogens to ethylenes to explain the observed diastereoselectivity.[249] The first isolation and structural evidence of a chloronium species was then reported by Kochi and co-workers.[250] Single crystals suitable for X-ray structure determination revealed an unsymmetrical cyclopropane chloronium bridge (C-Cl^+ bonds were found to be 2.08 Å and 1.92 Å) with a weakly coordinating counteranion ($SbCl_6^-$) (Figure 86i).

Similar compounds such as (bis-adamantylidene)bromonium triflate (Figure 86ii) and bis(*sym*-collidine)bromonium triflate (Figure 86iii) have been utilised as a Br^+ transfer agents for the halocyclisation of 4-penten-1-ol thereby transferring the halide to the product.[251]

In general, cationic haloniums have a formal charge of +1 and are highly reactive and very short lived. They can be generated by low-temperature electrochemical oxidation in the presence of

DMSO[252] or more commonly generated *in situ*[†] and trapped between Lewis-bases where the halonium ion forms a B···X⁺···B type structure (where B = Lewis-base, X = Br, I, see Figure 86iii).[253–255] This type of halogen bond structure was first observed using Raman and IR spectroscopy which suggests N···X⁺···N (N from pyridine, X = I or Br) bond linearity and symmetry.[256] This is also confirmed in the solid state structures of [bis(pyridine)iodine]⁺ and [bis(pyridine)bromine]⁺ complexes.[255] Experimental[257] and computational studies[258–260] demonstrate strong halonium interactions possess characteristics similar to that of a covalent bond.[254]

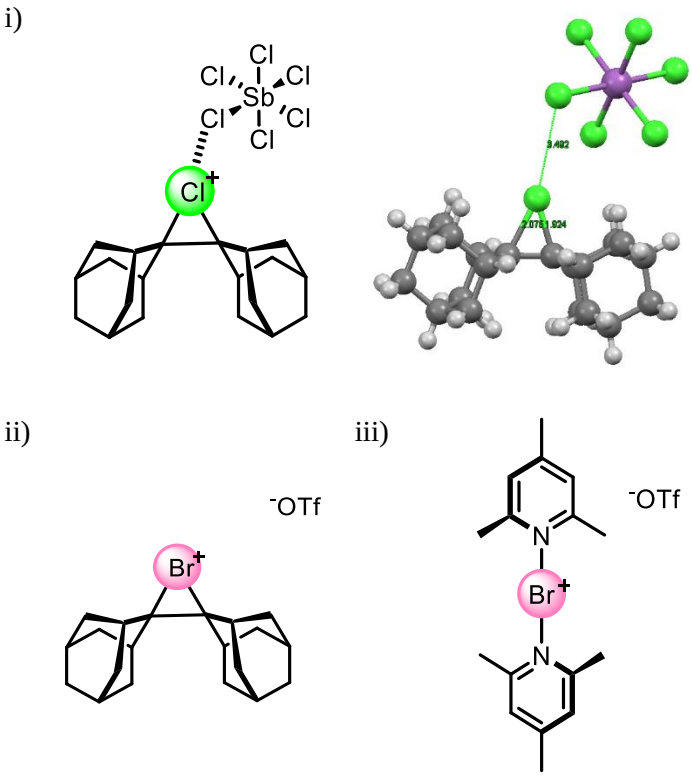

Figure 86. i) Molecular structure and X-ray crystal structure of unsymmetrically bridged 2,2'-bis(adamant-2-ylidene) chloronium hexachloroantimonate complex.[250] Crystal Structure ID: NOCHUI. ii) Bromonium transfer agents (bis-adamantylidene)bromonium triflate and iii) bis(sym-collidine)bromonium triflate

Halogen bonds arising from halogen cation interactions are significantly less well documented than hydrogen bonding analogues. When considering a short, strong hydrogen bond, donor distances are <2.5 Å with an effective bond order of 0.5.[261] Reported crystallographic and IR spectroscopic

[†] *In situ* generation means Lewis base and source of halogen are dissolved in solution and through intermolecular interactions, halonium species is stabilised through two Lewis base. See Figure 87i.

evidence of N···H^+···N interactions (N from 4-methylpyridine) revealed bond lengths to be N··· H = 1.305 Å and N···N = 2.610 Å where H^+ sits asymmetrically between the two N atoms.[262] While, computational studies of $[H_3N{\cdots}H^+{\cdots}NH_3]^+$ suggest that a symmetrical N···H^+···N bond requires N···N distances to be < 2.44 Å.[263]

Such entities are now widely considered to be three-centre-four-electron (3c-4e) bonds where interactions originating from halonium ions are strong halogen bond donors (100 – 150 kJ mol^{-1})[264] forming highly symmetric N···X^+···N bonds.[265] In the example of [pyridine···I^+···pyridine] the donation of lone pairs (lp) from each pyridine Lewis-base allows four electrons to be shared by three atomic centres: N···I^+···N (Figure 87i). The four electrons fill the bonding and non-bonding orbitals where I^+ has two positively charged regions corresponding to the empty *p*-orbital ($p_x^2p_y^2p_z^0$). This interaction has been reviewed by Sekar and co-authors where they state that depending on the hard/soft properties of halogens involved, interaction with N-donors can occur *via* two pathways[266]: i) a Lewis base can interact strongly with the halogen forming an ion-pair intermediate where the cationic species is a weak and polarised covalently bound halogen-N-donor, (Figure 87ii – fluorine centred example) and ii) a Lewis base forming a weak non-covalent halogen bond in a thermodynamically stable adduct (Figure 87ii– iodine centred example).

i)

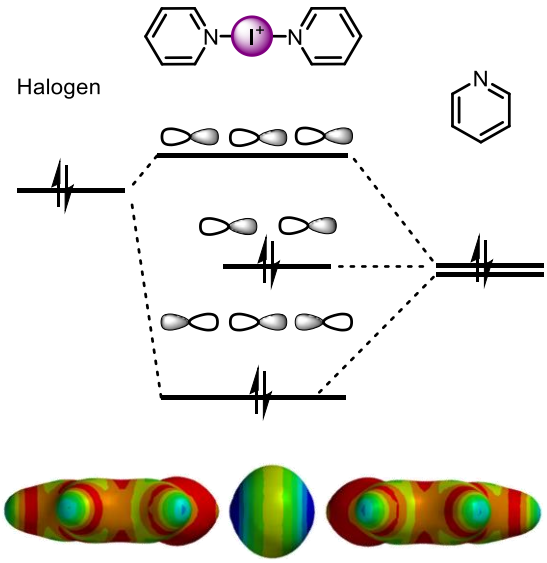

ii)

Figure 87. i) Molecular orbital diagram of N ⋯ I⁺ ⋯ N complex and MEP surface of [bis(pyridine)iodine]⁺ complex computed on a 0.008 au contour. Red < 350, blue >490 (kJ/mol). ii) DFT geometry optimised structure of symmetric N⋯X⁺⋯N halogen bonds for iodine (purple), bromine (red) and chlorine (yellow) and asymmetric halogen bond for fluorine-centered (green) structure. Adapted from literature Ref [267].

A commercially available halonium is Barluenga's Reagent [bis(pyridine)iodonium(I) tetrafluoroborate] commonly used in electrophilic halogenation cross-coupling and as an organic oxidant (Figure 88).[268]

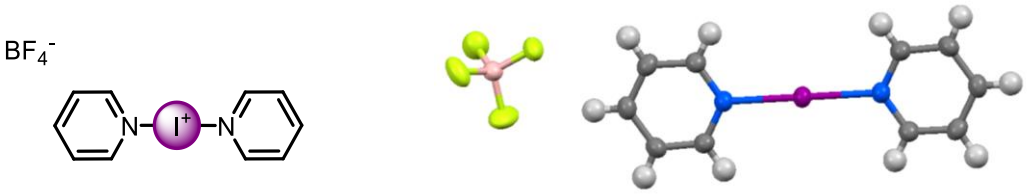

Figure 88. Crystal structure of Barluenga's reagent; iodo-bis(pyridine) tetrafluoroborate.[269] Crystal Structure ID: DOVYAQ

Prior to recent studies, the reactivity of N···X^+···N complexes increases with X = Cl > Br > I; the N···Cl^+···N complex has only been detected as a short lived species in the gas phase.[267] Recently, Erdelyi and co-workers studied the nature of N···Cl^+···N and N···F^+···N complexes *via* ^1H, ^{15}N and ^{13}C NMR spectroscopy in various organic solvents.[270] In CD_2Cl_2, the N···Cl^+···N interaction was found to be weaker than its bromine and iodine counterparts, but the complex maintained symmetry in solution. DFT studies found N···F^+···N interactions possess high formation energy barriers and NMR evidence reveals a covalent N-F bond and a weakly coordinated N-donor, suggesting the N···F^+···N interaction is asymmetrical (Figure 87ii).

4.1.2. Using Haloniums as Building Blocks for Supramolecular Chemistry

The poor stability and the synthetically challenging nature of halonium ions has been responsible for their lack of exploitation as building blocks for high-order structures in supramolecular chemistry. Many examples demonstrate how haloniums can be stabilised between two Lewis-bases. For example, Muniz and co-workers synthesised air and moisture-stable iodonium complexes stabilised by coordination of two carboxylate units as revealed by NMR spectroscopy as well as X-ray analysis. These substrates were then exploited in the chemo- and regioselective iodo-oxygenation of alkenes (Figure 89i).[271]

Another oxygen based donor serving as a stabilising complexing agent for iodoniums is DMSO forming O···I^+···O bonds (Figure 89*ii*). Computational calculations determined comparative stabilisation energies for DMSO···I^+···DMSO and CH_3CN···I^+···CH_3CN bonds[252] where the oxygen

atom of DMSO interacting with I^+ displayed a stabilisation energy of 118.9 kcal/mol. Notably, the coordination of a second DMSO enhanced the stabilisation by 36.1 kcal/mol. On the other hand, the CH_3CN interaction with I^+ has a smaller stabilisation energy of 101.5 kcal/mol. Sekar and co-workers took advantage of this stability and applied the DMSO complex in alkene functionalisation reactions.[100] Haukka and co-workers studied the unusually strong interaction between the iodonium cation between two thione XB acceptors where crystal structure shows almost linear (179°) S···I^+···S interactions with bond lengths between 2.6 – 2.7 Å (Figure 89*iii*).

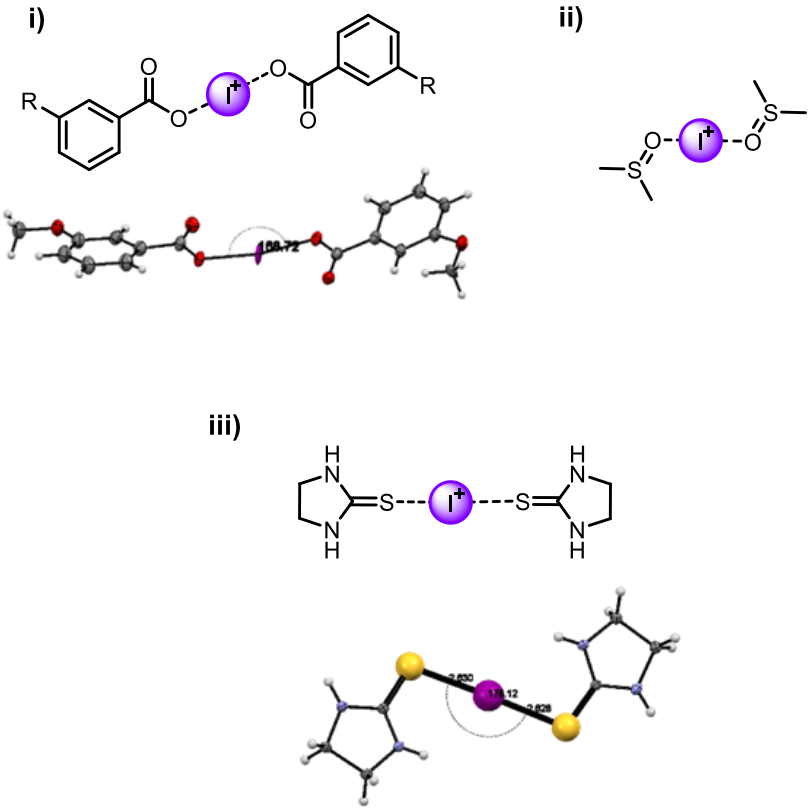

Figure 89. Iodonium 3c4e-interactions with XB donor ligands. i) Dicarboxylate iodonium complex. Crystal Structure ID: VAXBII, ii) DMSO stabilised iodonium complex. (no crystal structure available) and iii) thione iodonium complex. Crystal Structure ID: SOMLEN

Examples shown thus far involve small molecular stabilisation of haloniums. Some of these concepts were then translated to larger supramolecular structures. In multiple studies, Rissanen and co-

workers reported the synthesis and characterisation of self-assembled cavitands[†] through the *in situ* generation of iodonium ions coordinated through N···I^+···N bonds in acetonitrile (Figure 90i and ii).[272–274] By varying the N-donor ligand, the different conformations and flexibility of N···I^+···N interactions can lead to cavitands of different shapes and sizes. Dimeric capsules, can be obtained by using either a tripodal ligand with imidazole arms forming a final structure involving three XBs[273] (Figure 90i) or a tetrakis(3-pyridyl)ethylene precursor yielding a final structure with four well-defined XBs.[272] Tetrameric capsules have also been reported where the use of the bulky DABCO N-donor ligand in a tripodal system affords a cavitand as a result of a total of 6 XB interactions (Figure 90ii).[273]

Very recently, Erdelyi and co-workers synthesised a helicate-type structure using an oligo-aryl/pyridylene-ethylene backbone assembled in DCM via iodonium interactions (Figure 90iii).[265] Using DFT calculations, they determined the stabilisation of the structure is brought about by strong XBs and aryl-aryl interactions. The solid-state X-ray crystal structure showed unusually short distances (approximately 0.1 Å less than the sum of the van der Waals radii) between the two iodonium cations. The authors suggested that charge redistribution throughout the conjugated system allowed for this proximity, as the natural population analysis would otherwise indicate repulsive electrostatic interactions between the close lying iodonium units.

[†] Cavitands are capsule-like self-assembled supramolecular structures capable of binding guest/s within their internal 3-D cavity.

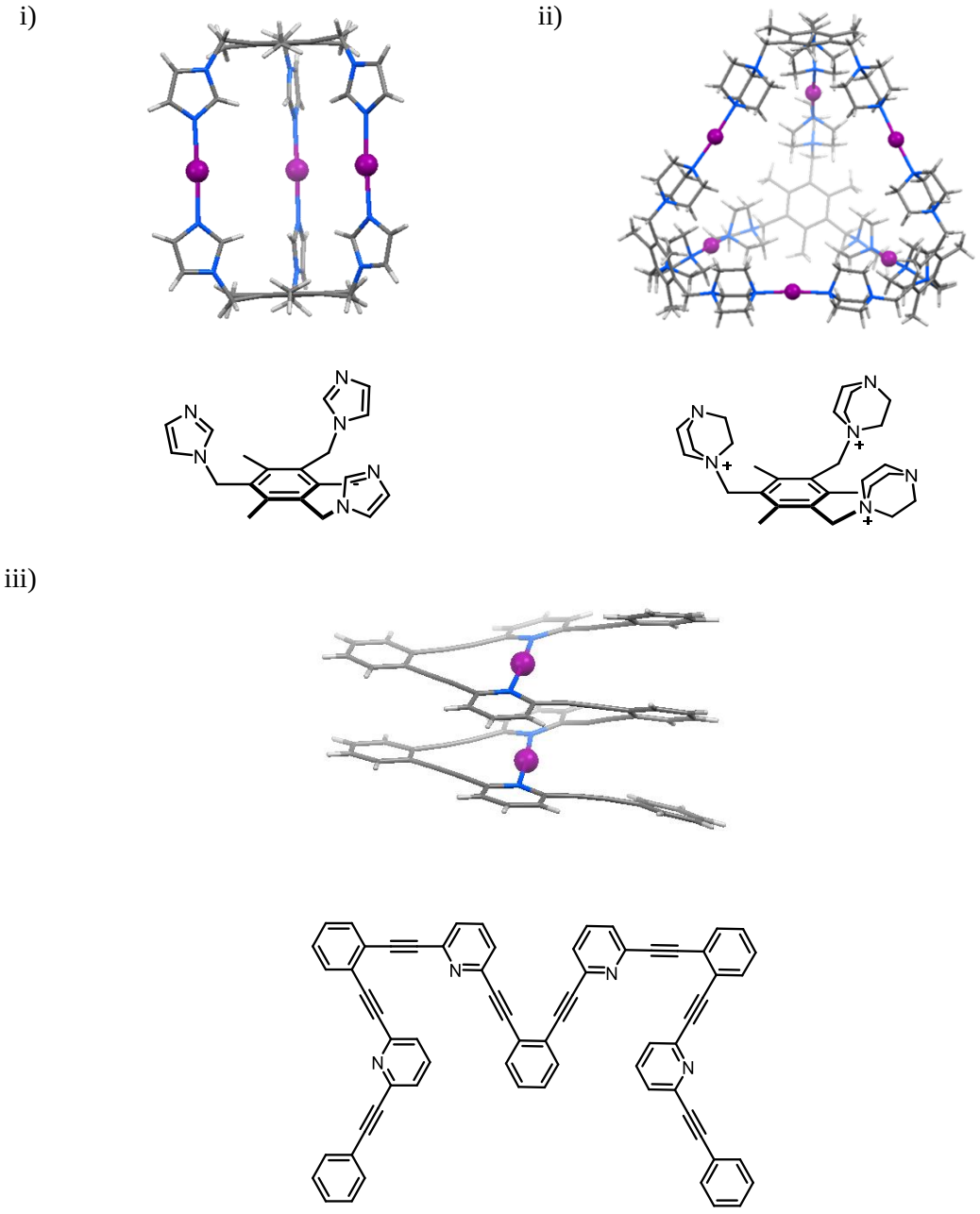

Figure 90. Molecular structure of building blocks to form iodonium complexes via N···I⁺···N interactions and their corresponding crystal structures. i) Dimeric cavitands with imidazolium tripod arms. Crystal Structure ID: WEHTEL ii) tetrametric cavitands with DABCO tripodal arms. Crystal Structure ID: WEHSUA iii) Fomation of helicate structure upon iodonium formation between pyridine-donor groups. All counterions are omitted for clarity. Crystal Structure ID: NOMCAW

4.1.3. Chapter Aims

The primary aim of this chapter is to explore the unprecedented formation of mechanically interlocked structures by iodonium halogen bonding interactions. As mentioned in earlier chapters,

the mechanical bond can provide a shielded 3D environment within an interlocked cavity, and thus has the potential to stabilise reactive species such as haloniums. This chapter investigates using the iodonium cation to template the assembly of pseudorotaxane and rotaxane assemblies.

4.2. Trapping Iodonium Between Homo-*N*-Donors

The stabilisation of iodonium between two pyridine motifs and pyridyl derivatives in general, is well established. Employing this N···I$^+$···N interaction as a means of templating a pseudorotaxane assembly between a pyridine containing macrocycle and 2,6-bis-pyridyl threading derivatives was investigated initially.

4.2.1. Synthesis of Pyridyl-based Components

In collaboration with Andrew Docker,[†] the synthesis of a series of different sized pyridyl macrocycles of varying polyether chain lengths and axle precursor 2,6-bis-azide functionalised pyridyl derivatives was undertaken (Figure 91).

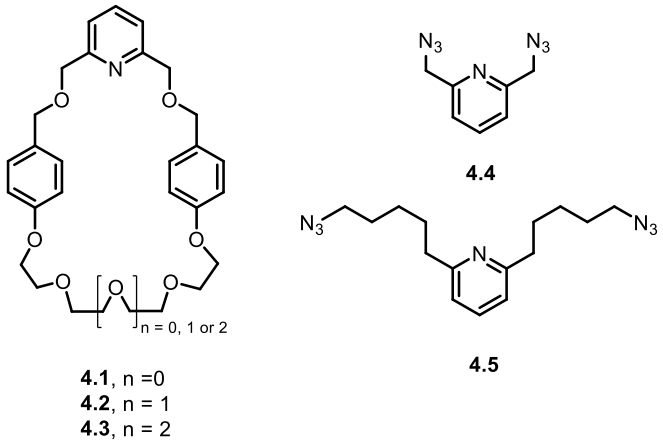

Figure 91. Target pyridine containing macrocycles and axle precursors.

Bis-azide pyridyl compound **4.4** was prepared in high yield by reaction of sodium azide with commercially available 2,6-dibromopyridine **4.6** (Scheme 24). The longer axle precursor **4.5**

[†] Synthesis was carried out by Andrew Docker in the Beer group.

required a multi-step synthetic route. A Sonogashira reaction between **4.6** and two equivalents of pentyn-1-ol at high temperatures in a sealed vial gave compound **4.7** in almost quantitative yields after purification by column chromatography (Scheme 24). Hydrogenation of the alkyne groups using 10% Pd/C and a hydrogen gas balloon in methanol afforded compound **4.8** in 70% yield. Reaction of **4.8** with MsCl, THF and base gave the bis-mesylate intermediate compound which was reacted immediately with sodium azide to afford the target long axle precursor **4.5** in 74% yield.

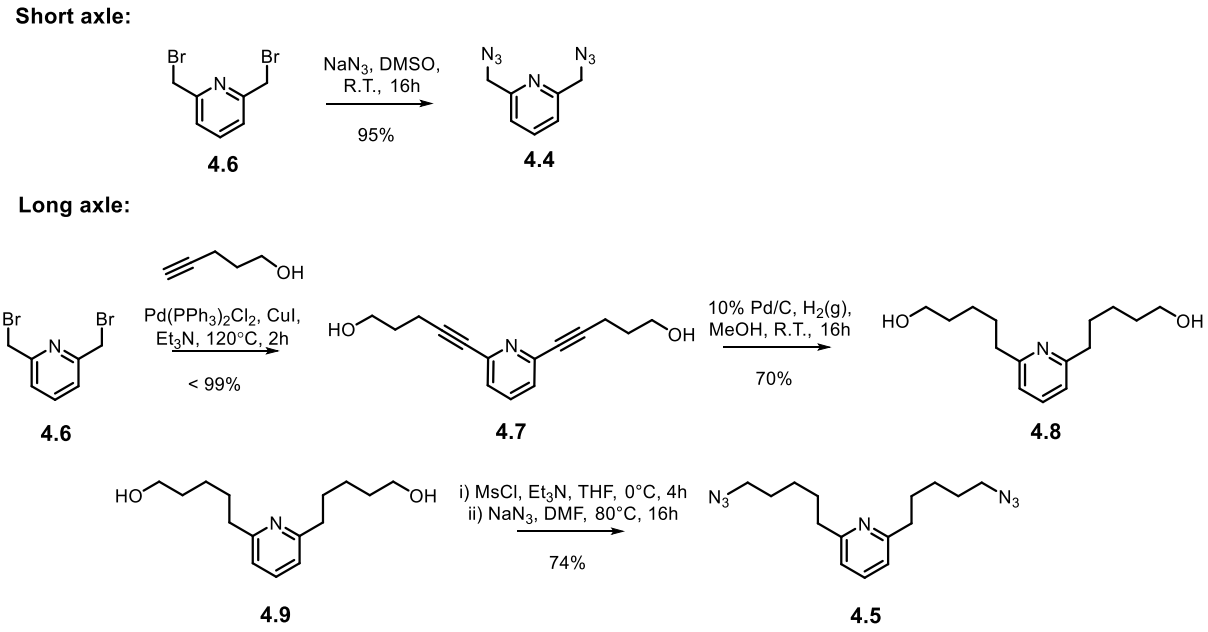

*Scheme 24. Synthesis of short axle **4.4** and long axle **4.5** precursors.*

Bis-alcohol **4.10** was prepared according to a literature procedure[275] (Scheme 25). In a solution of methanolic NaOH, 4-hydroxybenzyl alcohol was dissolved at room temperature. After removal of methanol, reaction of the sodium salt and corresponding bis-tosylate PEG in acetonitrile afforded bis-alcohol **4.10** in good yields. Williamson ether synthesis between corresponding macrocycle precursors bis-alcohol **4.10**, 2,6-dibromomethyl pyridine **4.6** and sodium hydride in THF afforded macrocycles **4.1**, **4.2** and **4.3** in 23-54% yields. In a similar reaction, macrocycle **4.11** was isolated in 45% yield from precursors **4.9** and 2,6-dibromomethyl pyridine **4.6**.

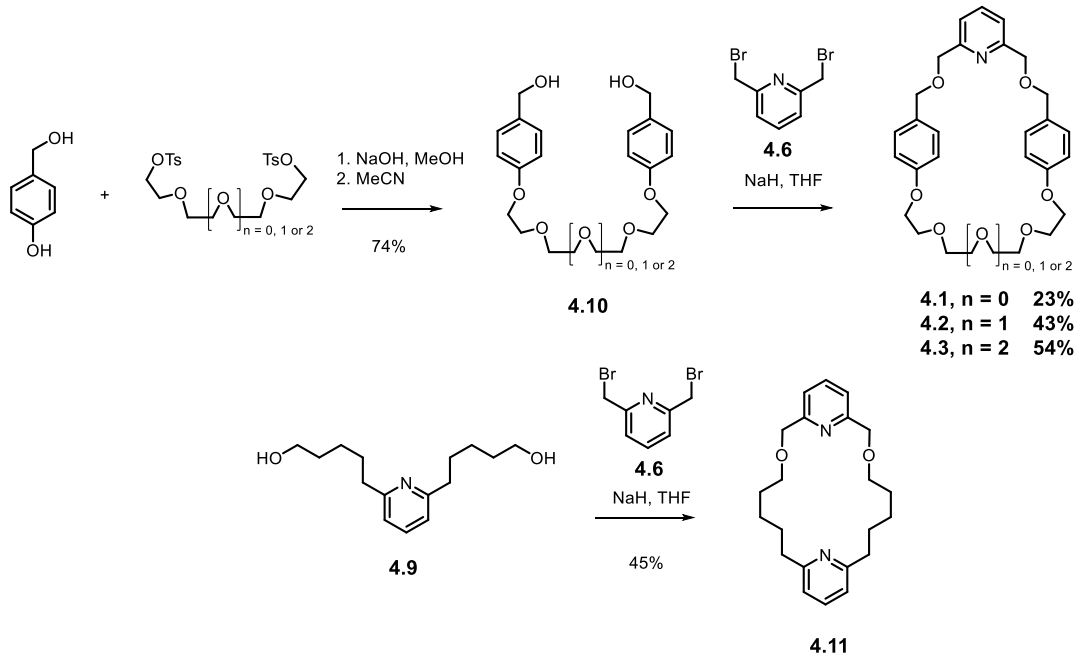

Scheme 25. Synthesis of macrocycle components.

4.2.2. Preliminary ^{1}H NMR Investigation of Iodonium Pseudorotaxane Assembly

The *in situ* generation of an iodonium complex between two pyridine units is typically achieved by initially forming a Ag(I)-bis(pyridine) complex in an organic solvent such as DCM. The subsequent addition of a DCM solution of iodine and removal of the AgI precipitate affords a solution of iodonium-bis-pyridine species.[276]

This synthetic methodology was used to investigate iodonium template pseudorotaxane assembly between pyridyl macrocycle **4.2** and pyridyl threads/axle precursors, analysed by ^{1}H NMR and ^{1}H-^{15}N HMBC‡ spectroscopy techniques. Initial ^{1}H NMR titration studies focused on employing commercial pyridine derivative 2,6-bis(methoxymethyl)pyridine and 2,6-lutidine.

‡ ^{1}H-^{15}N HMBC spectroscopy was carried out by Erdelyi group (Uppsala University).

Silver triflate was added in slight excess to a CD_2Cl_2 solution of macrocycle **4.2**. Complexation of Ag^+ was evidenced by the perturbation of the macrocycle's aromatic protons $H_{e/f}$ and methylene protons H_c and H_d (Figure 92b). Subsequently addition of an equimolar CD_2Cl_2 solution of 2,6-bis(methoxymethyl)pyridine led to further shifts in proton peaks corresponding to the two pyridyl donor groups of the macrocycle and interpenetrating 2,6-bis(methoxymethyl)pyridine molecule (Figure 92c). In particular, the macrocycle's aromatic protons shifted upfield, with H_f became more resolved while H_e remained broad. Two equivalents of iodine dissolved in CD_2Cl_2 were added, followed by filtration removal of AgI. This resulted in a ^1H NMR spectrum (Figure 92d) displaying very broad, significantly shifted proton signal features which are typical of an iodonium species stabilised between two pyridine donor groups.[277] These poorly resolved signals caused difficulty in their assignment, however, these observations provided preliminary evidence for successful iodonium species formation.

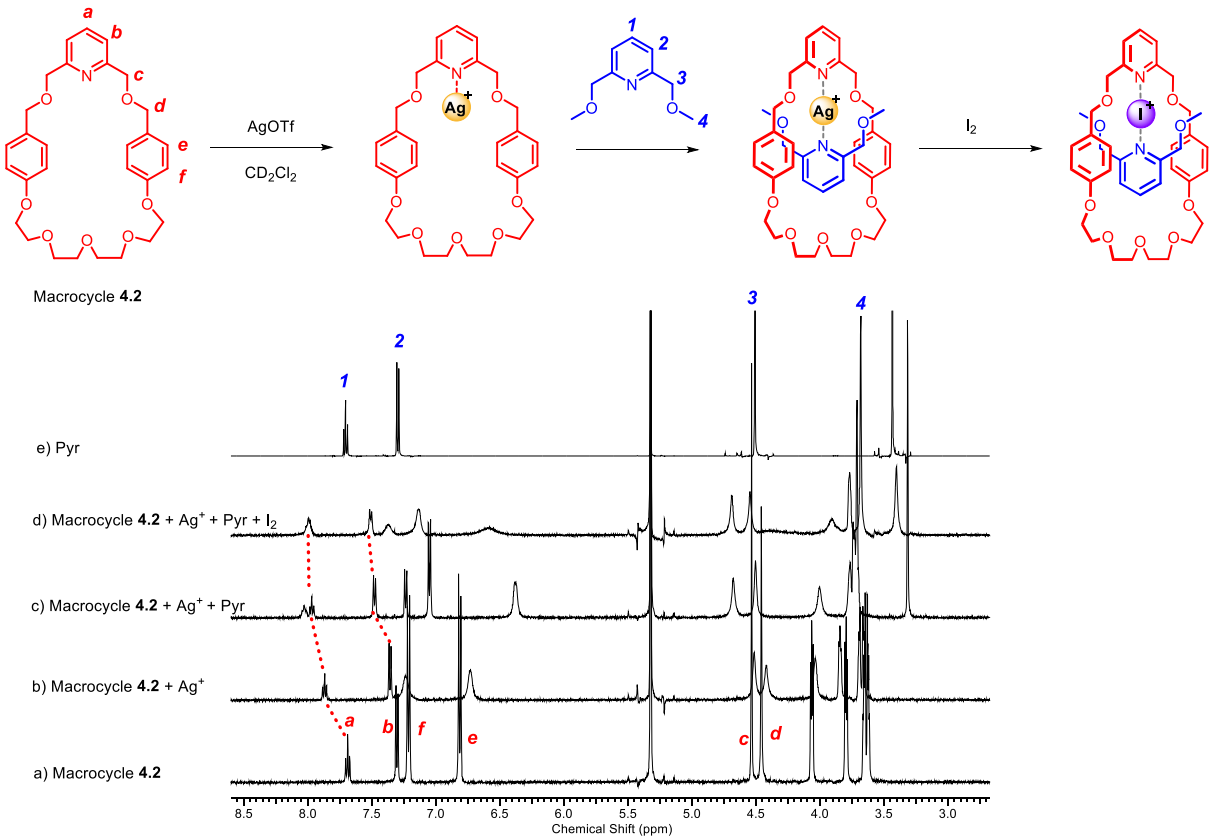

*Figure 92. Partial ^1H NMR spectra of host and guest components a) macrocycle **4.2**, b) macrocycle **4.2** + Ag^+ c) macrocycle **4.2** + Ag^+ + Pyr, d) macrocycle **4.2** + Ag^+ + Pyr + I_2, e) pyridine derivative only. Spectrums measured in CD_2Cl_2, T = 298 K. Ag = silver metal ion, Pyr = 2,6-bis(methoxymethyl)pyridine and I = iodine present in solution.*

Analogous ^1H NMR titration experiments were undertaken to assess iodonium formation between macrocycle **4.2** and 2,6-lutidine, which was chosen as it does not contain the potentially interfering oxygen atoms of the 2,6-methoxy group substituents. Upon addition of Ag^+, peak broadening of proton signals corresponding to pyridine and methylene groups H_a, H_b and H_c were observed (Figure 93b), consistent with complexation of Ag^+ within the macrocycle cavity through the pyridine *N*-donor group. Stepwise addition of 2,6-lutidine (Figure 93c) and iodine (Figure 93d) resulted in the broadening and subsequent merging of protons H_c and H_d closest to the binding site, while proton signals corresponding to 2,6-lutidine were difficult to assign due to peak broadening.

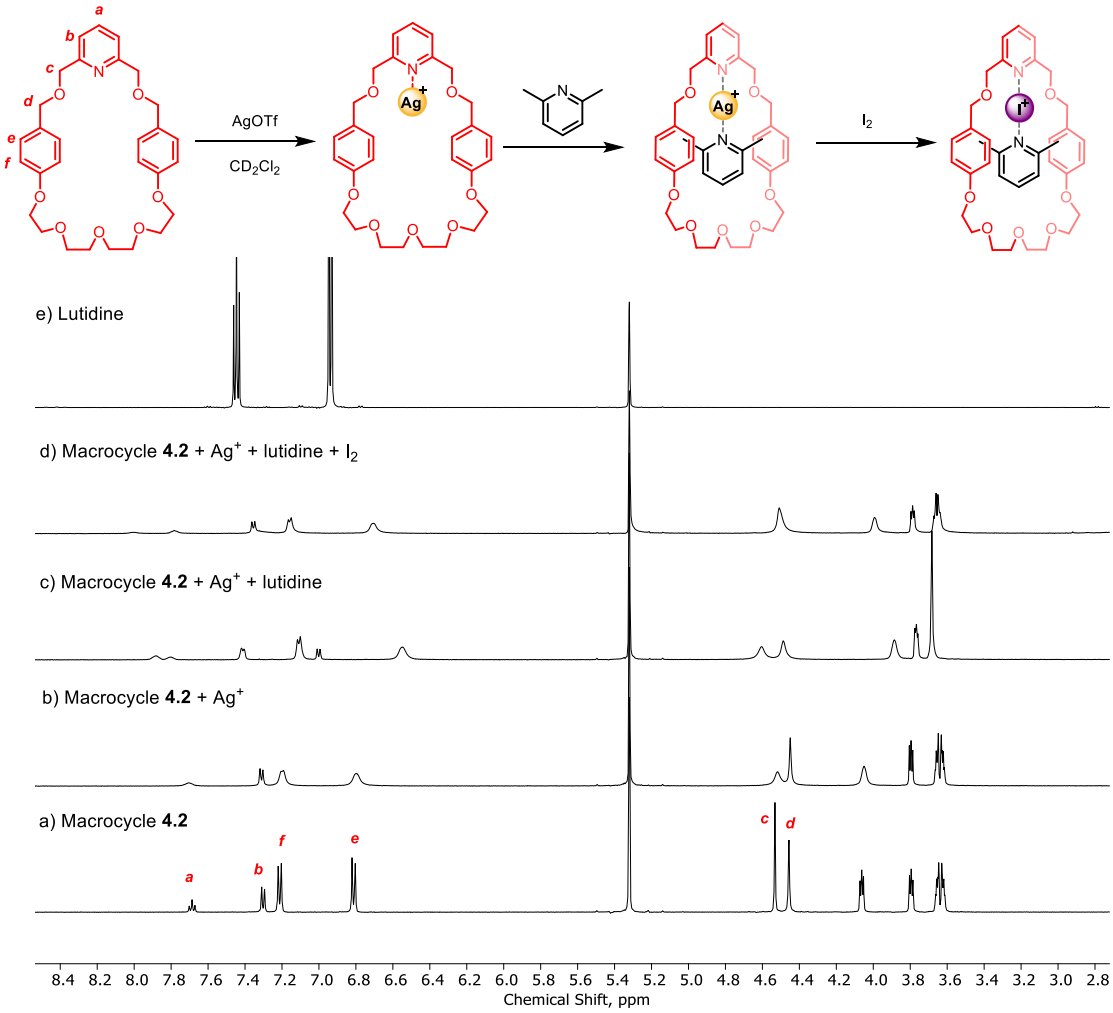

*Figure 93. Partial ^{1}H NMR spectra of host and guest components a) macrocycle **4.2**, b) macrocycle **4.2** + Ag^{+} c) macrocycle **4.2** + Ag^{+} + lutidine, d) macrocycle **4.2** + Ag^{+} + lutidine + I_2, e) pyridine derivative only. Spectrums measured in CD_2Cl_2, T = 298 K. Ag = silver metal ion, Pyr = 2,6-lutidine and I = iodine present in solution.*

To obtain more conclusive evidence for the formation of the iodonium species, ^{1}H-^{15}N HMBC spectroscopic analysis was undertaken by Prof. Mate Erdelyi and co-workers (Uppsala University). With the nitrogen atoms directly interacting with Ag^{+} or I^{+}, probing the $^{14\backslash15}N$ nuclei directly provides a useful tool to further investigate the chemical environment of the potential iodonium binding site.

The heteronuclear HMBC NMR analysis was initially carried out for macrocycle **4.2**, 2,6-lutidine and $AgBF_4$ in CD_2Cl_2. ^{1}H-^{15}N correlations are summarised in Table 9. A signal arising from ^{15}N was observed at *ca.* -120 ppm corresponding to a N···Ag^{+}···N complex in agreement with literature

reports (Figure 94i).[278] Nitrogen nuclei correlation with protons H_b and H_c corresponding to protons in close proximity to the pyridine unit in macrocycle **4.2** indicated successful coordination of Ag^+ within the macrocycle cavity where free macrocycle **4.2** has a ^{15}N NMR shift *ca*. -75 ppm.

Upon addition of iodine, ^{15}N NMR shifts observed at -175 ppm and -95 ppm correspond to the [bis(2,6-lutidine)iodine]$^+$ complex and an uncomplexed macrocycle pyridine derivative, respectively (Figure 94ii). The macrocyclic pyridine derivative has not been fully identified but could be a protonated *N*-derivative.

Table 9. ^{1}H-^{15}N correlation chemical shift

	^{1}H-^{15}N δ values	
Macrocycle **4.2**	-75 ppm	Not shown
[Macrocycle **4.2**-Ag-lutidine]$^+$ complex	-120 ppm	Figure 94i
[bis(2,6-lutidine)iodine]$^+$ complex	-175 ppm	Figure 94ii
Uncomplexed macrocycle **4.2** pyridine derivative	-95 ppm	Figure 94ii
2,6-lutidine	-72 ppm ($CDCl_3$)[279]	Not shown

Measurements carried out in CD_2Cl_2.

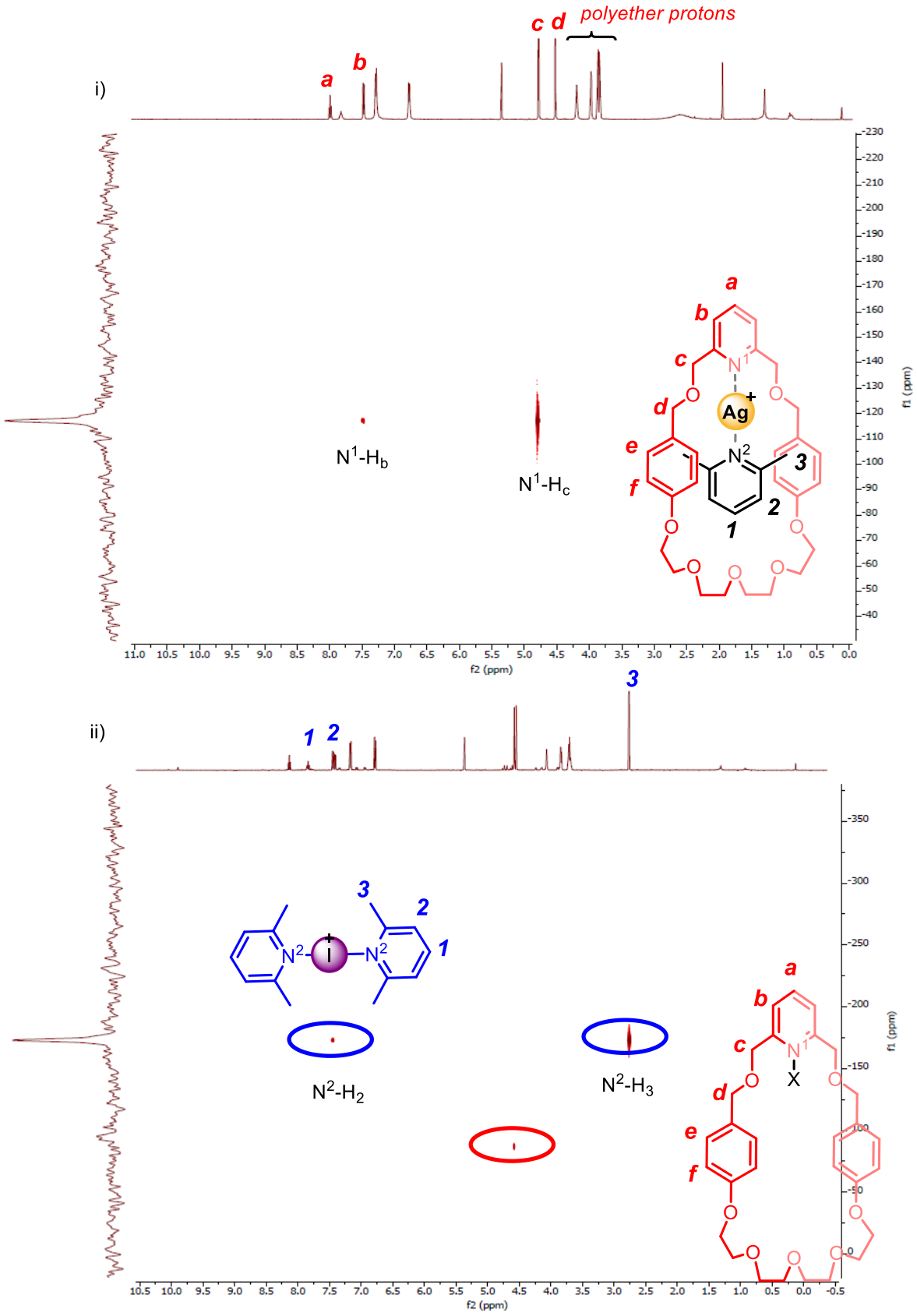

Figure 94. ^{1}H-^{15}N HMBC spectrum of i) macrocycle 4.2, Ag^{+} and 2,6-lutidine and ii) upon addition of iodine where X is likely protonated pyridine derivative. Solvent = CD_2Cl_2.

Although promising at first glance, a closer look at ^{1}H-^{15}N HMBC measurements (Figure 94) revealed the unsuccessful formation of iodonium between the macrocycle and 2,6-lutidine with no cross peaks corresponding to the desired macrocycle-I^{+}-lutidine structure, perhaps due to unfavourable steric and electronic coordination environments. Although formation of intermediate Ag^{+}-complex was successful (Figure 94i), the adjacent macrocycle oxygen donor atoms may also coordinate the metal cation to form a stabilised 2 N donor and 2 O donor tetrahedral coordination complex (Figure 95). While tetrahedral coordination is not unusual for Ag^{+}-complexes, iodonium species stabilisation might be detrimentally affected by this coordination environment, which results in the preferential formation of iodonium stabilised between two 2,6-lutidine units.

^{1}H-^{15}N HMBC NMR measurements were also carried out for macrocycle **4.2** with pyridine yielding very similar results. (see appendix E-1 and E-2 for ^{1}H-^{15}N HMBC spectra)

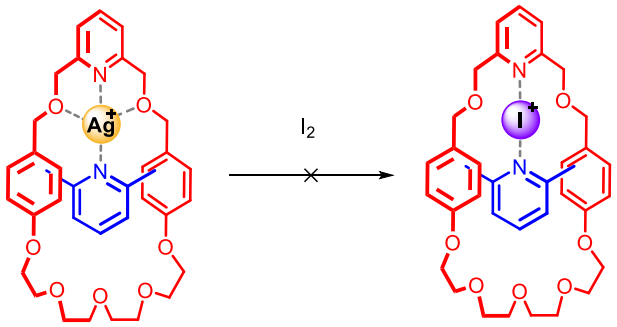

Figure 95. Ag^{+} preferential tetrahedral coordination to macrocycle involving interactions with N and O atoms. However, this initial coordination is unsuitable for iodonium coordination where the addition of iodine causes the extrusion of Ag^{+} and frees the macrocycle ultimately iodonium was observed to be stabilised between two lutidine units.

4.2.3. Synthesis and Isolation of Iodonium Complexes

The NMR titration studies for *in situ* formation of iodonium species between macrocycle **4.2** and simple pyridyl derivatives suggested competing preferential formation of the respective [bis(pyridyl)iodine]$^{+}$ complexes. In spite of this, attempts were undertaken to synthesise and isolate

an iodonium complexed pseudorotaxane assembly. It was hoped that the nature of the interpenetrated assembly may kinetically stabilise the iodonium species.

The method used for the preparation of iodonium complexed pseudorotaxane assemblies was adapted from the literature synthetic protocol employed for an iodonium complex between two pyridines (Scheme 26).[280] The corresponding macrocycle (**4.1**, **4.2** and **4.3**) was dissolved in a solution of DCM containing a slight excess of $AgBF_4$. Sequential addition of one equivalent of bis-azide pyridyl compound **4.5** and two equivalents of iodine in DCM resulted in a dark reddish-purple solution and yellow precipitate of AgI. The solution was then centrifuged and filtered and passed through a size exclusion column to afford the iodonium complexes as tan solids in 77-99% yields and characterised by ^1H and ^{13}C NMR. ESI mass spectrometry analysis failed to detect the cationic iodonium complexed species, where only respective macrocycle and bis-azide components were detected.

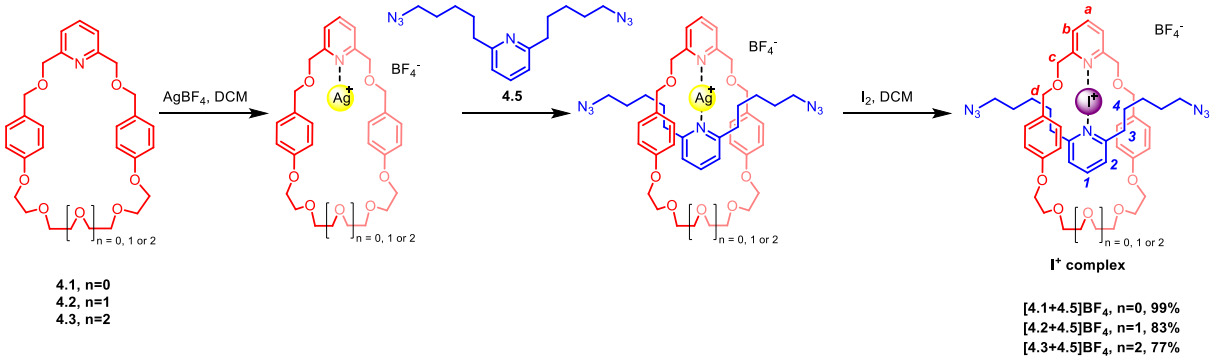

*Scheme 26. Synthesis of iodonium complex using macrocycles **4.1, 4.2, 4.3** and bis-azide **4.5** via Ag(I)-complex intermediates.*

All three isolated iodonium complexes displayed similar ^1H NMR spectra. For example, the ^1H NMR spectrum[‡] of [**4.1**+**4.5**]**BF$_4$** (Figure 96) reveals downfield shifts of pyridyl macrocycle (H_a and H_b) and pyridyl threading (H_1 and H_2) protons, concomitant with downfield proton perturbations of the methylene protons H_c, H_d, H_3 and H_4 of both components. These changes in the proton chemical

[‡] ^1H NMR spectrum of [**4.2**+**4.5**]**BF$_4$** and [**4.3**+**4.5**]**BF$_4$** can be found in appendix E-3 and E-4 respectively.

shifts suggest the formation of a pseudorotaxane-I^+ complex assembly. It is noteworthy that all three iodonium spectra exhibit sharp, resolved proton signals which contrasts the broader proton signals observed with the ^{1}H NMR iodonium titration studies between lutidine and macrocycle **4.2** (Figure 93d).

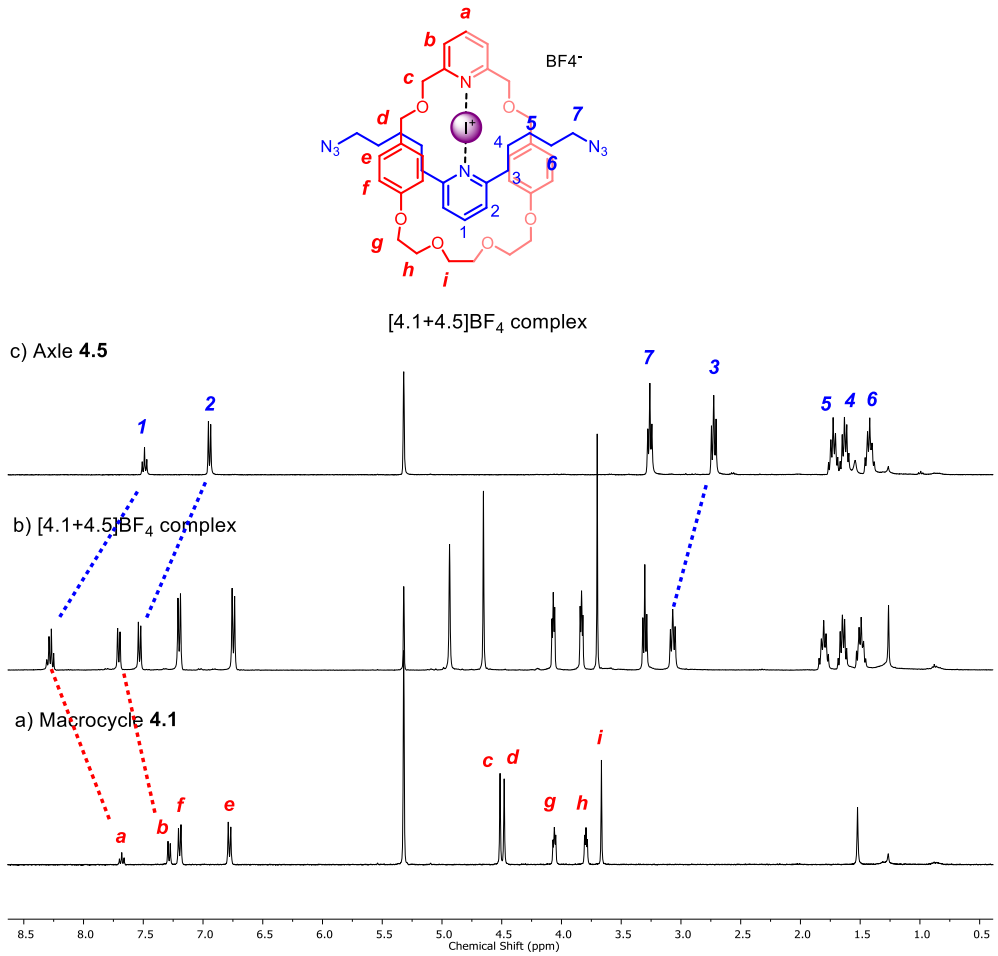

*Figure 96. ^{1}H NMR spectra of a) macrocycle **4.1**, b) isolated [**4.1**+**4.5**]BF_4 complex and c) axle **4.5** measured in CD_2Cl_2.*

Future work with Prof. Erdelyi's group will use ^{15}N NMR spectroscopy to provide additional evidence for the formation of the iodonium species. Following the successful isolation of these pseudorotaxane iodonium complexed species, an attempt to form [2]rotaxanes *via* a CuAAC stoppering method was undertaken (Scheme 27). A DCM solution of iodonium complex [**4.2**+**4.5**]BF_4 was added to an equimolar mixture of $Cu(CH_3CN)_4PF_6$ and TBTA, containing four equivalents of stopper terphenyl alkyne in dry DCM. The reaction was stirred at room temperature

overnight and monitored by ESI-MS, however, disappointingly no evidence of interlocked structure or axle was found.

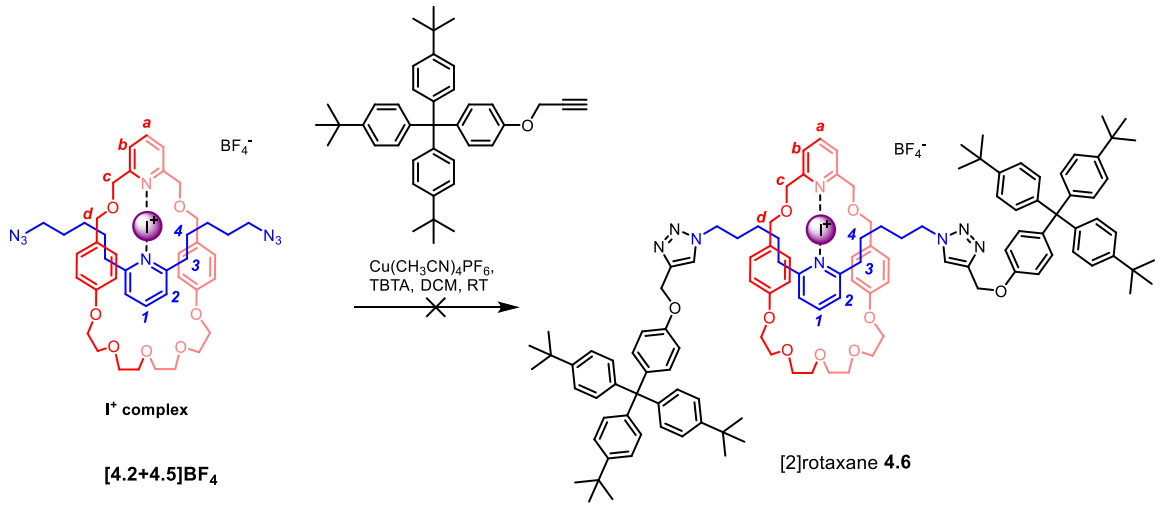

*Scheme 27. Attempted synthesis of [2]rotaxane **4.6** using a 'stoppering' method.*

Taking this into account, an alternative approach to investigating MIM halonium cation stabilisation was undertaken through the synthesis of a series of [2]rotaxanes containing interlocked N-donor pyridyl cavities suitable for subsequent iodonium complexation.

4.3. Mechanically Interlocked Molecules (MIMs) for Iodonium Stabilisation

MIMs provide unique cavities that can stabilise highly reactive species such as extended polyynes which are prone to exothermic polymerisation.[281] Anderson and co-workers reported a [3]rotaxane consisting of a phenanthroline macrocycle threaded through by two extended polyynes which was found to be thermally stable using measured using differential scanning calorimetry (Figure 97i).[282] MIMs have also been reported to stabilise the Cu(I)-intermediate of a CuAAC reaction within its cavity. Goldup and co-workers reported a Cu(I) triazolide within a [2]rotaxane cavity stable under aqueous conditions (Figure 97ii).[283]

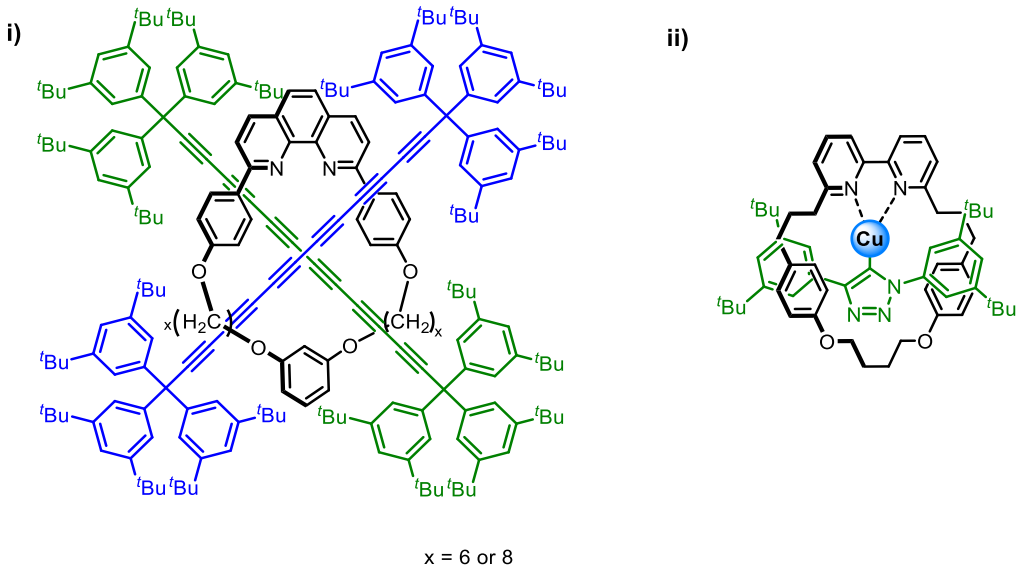

Figure 97. i) [3]rotaxane consisting of two threaded polyyne chains stabilised within the macrocyclic cavity.[282] ii) [2]rotaxane stabilisation of reactive organometallic species; Cu(I) triazolide intermediate.[283]

In an effort to exploit the potential mechanical bonding stabilisation of iodonium species, novel interlocked rotaxane structures containing N-donor pyridyl macrocycle and axle units were synthesised. In addition, rotaxanes with N-donor pyridyl macrocycles and triazole axle components were prepared for possible heteroleptic iodonium complexation. Thus far, only two examples of heteroleptic iodonium complex have been reported between pyridine and *N*,*N*-dimethylpyridin-4-amine (4-DMAP) and 4-ethylpyridine (4-Etpy).[284] The use of the triazole motif as a *N*-donor for iodonium stabilisation is unprecedented.

4.3.1. Synthesis of Homopyridyl [2]Rotaxanes

The six novel pyridyl [2]rotaxanes were synthesied *via* the AMT protocol using the *stoppering* method (Scheme 28). In a general procedure, an equimolar mixture of macrocycle (**4.1**, **4.2** or **4.3**) and $Cu(CH_3CN)_4PF_6$ dissolved in DCM, was combined with the corresponding azide (8 eqv; **4.5** or **4.4**) and stopper-alkyne (8 eqv) and the reaction stirred for 2 days.

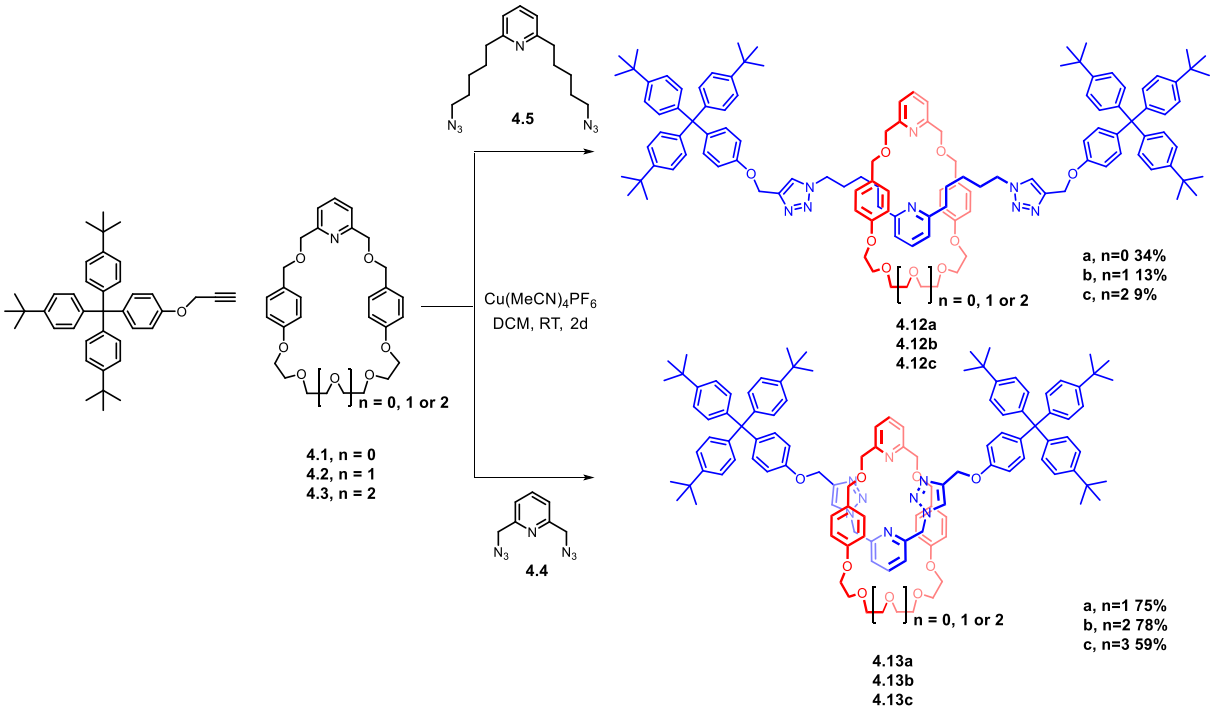

Scheme 28. Synthesis of [2]rotaxanes with varying macrocyclic sizes formed via Cu(I)-catalysed active metal template method.

Purification using preparatory TLC afforded [2]rotaxanes yields ranging from 9-78%. It is interesting to note that rotaxanes **4.13** were synthesised in a higher yield than rotaxanes **4.12** likely due to the shorter azide **4.4** used indicating efficient cycloaddition between azide and alkyne due to the close proximity of Cu(I) species when bound endotopically within the macrocycle. All rotaxanes were characterised by ^{1}H NMR, ^{13}C NMR and ESIMS, although 2D ROESY analyses did not reveal any noticeable cross peaks for rotaxanes **4.12**.

The ^{1}H NMR spectra of the isolated [2]rotaxanes all show indicative proton perturbations consistent with a mechanically interlocked structure. In Figure 98, the ^{1}H NMR spectrum shown for [2]rotaxane **4.12b** is compared with the corresponding free macrocycle **4.2** and long axle precursor **4.5**. In the alkyl region, upfield shifts were observed especially for protons H_3, H_4, H_d and H_c indicative of interlocked components in close proximity. Also the aromatic signals H_5 and H_6 corresponding to hydroquinone protons in the macrocycle component are shifted upfield likely as a result of aromatic interactions with the pyridine axle component. ESI analyses found peaks at m/z = 1853.1, 1897.2 and 1941.2 corresponding to [2]rotaxanes **4.12a**, **4.12b** and **4.12c.**

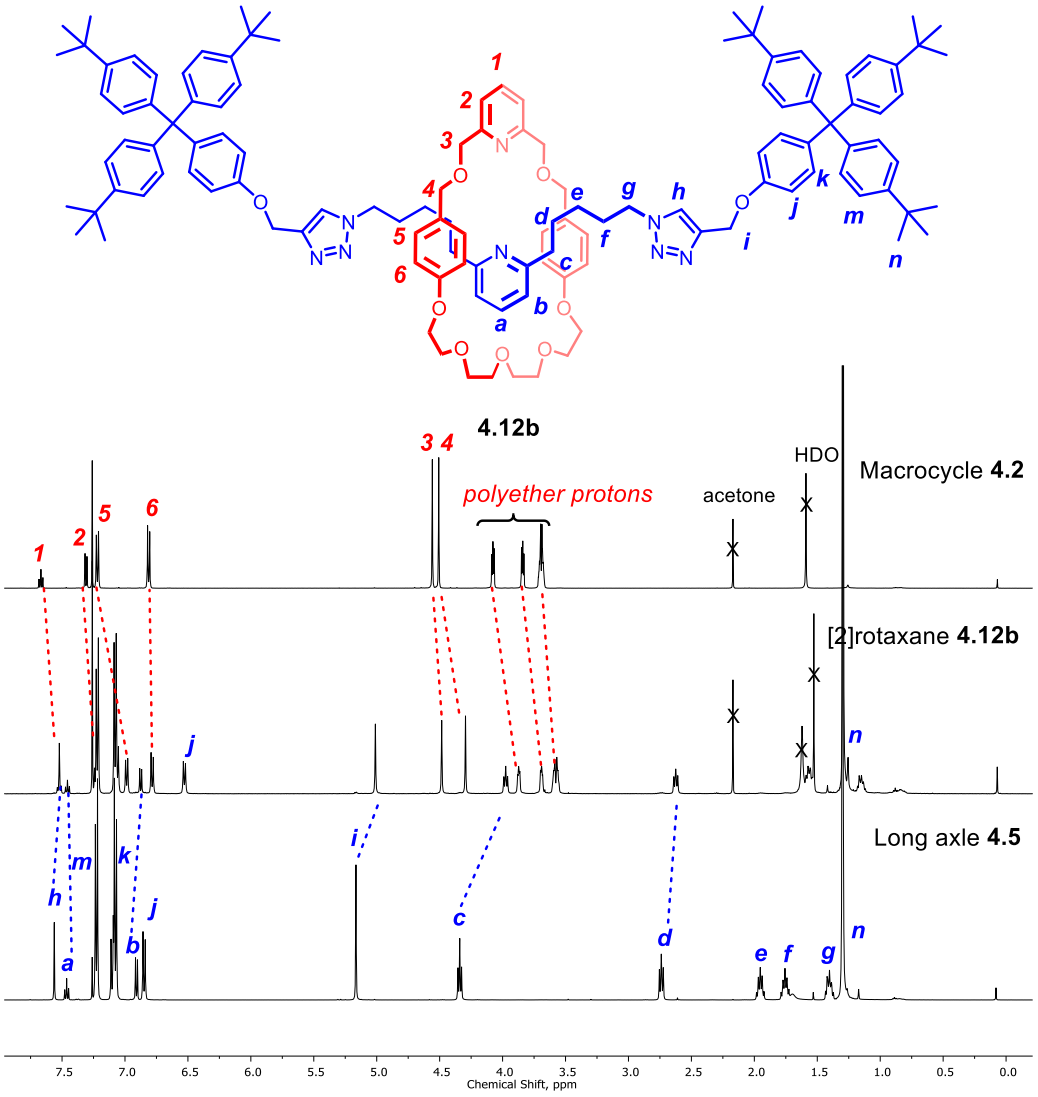

*Figure 98. Stacked ^{1}H NMR spectra of free macrocycle **4.2**, [2]rotaxane **4.12b** and long axle precursor **4.5** for comparison measured in $CDCl_3$.*

The ^{1}H NMR spectrum for [2]rotaxane **4.13b** shown in Figure 99 is also consistent with that of a mechanically interlocked structure with upfield chemical shifts observed in the alkyl region. In particular, the large upfield shifts of protons H_b and H_c ($\Delta\delta$ = 0.6 and 0.33 ppm respectively) potentially caused by shielding effects from the enclosing hydroquinone groups present on the macrocycle component. While the observed downfield shift of triazole proton H_d ($\Delta\delta$ = 0.10 ppm) suggesting formation of intramolecular hydrogen bonds with the macrocycle aromatic ring.

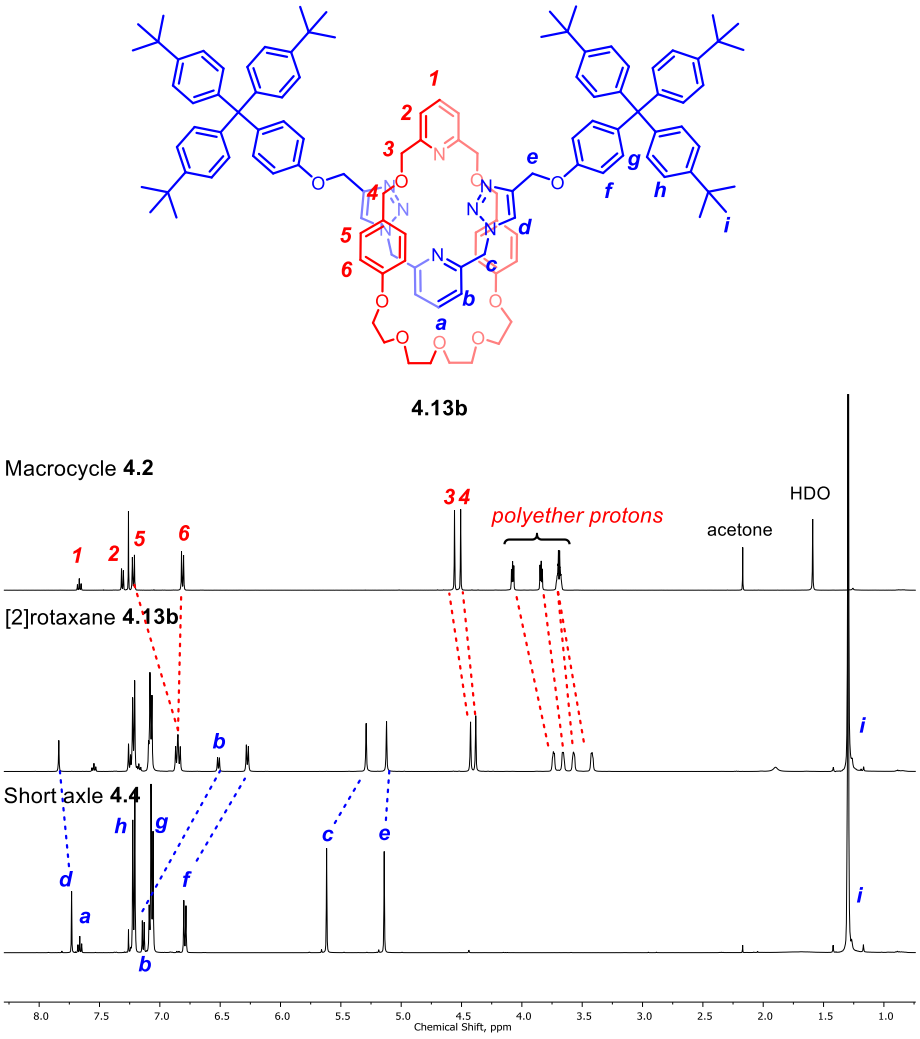

*Figure 99. Stacked ^{1}H NMR spectra of free macrocycle **4.2**, [2]rotaxane **4.13b** and short axle **4.4** for comparison measured in $CDCl_3$.*

This is supported by 2D ROESY NMR where cross-peak analyses found correlation between triazole proton H_d and protons H_5 and H_6 corresponding to aromatic signals arising from the macrocyclic component (Figure 100). Furthermore, ESI analyses found peaks at m/z = 1741.0, 1785.0 and 1829.0 corresponding to [2]rotaxanes **4.13a**, **4.13b** and **4.13c** respectively.

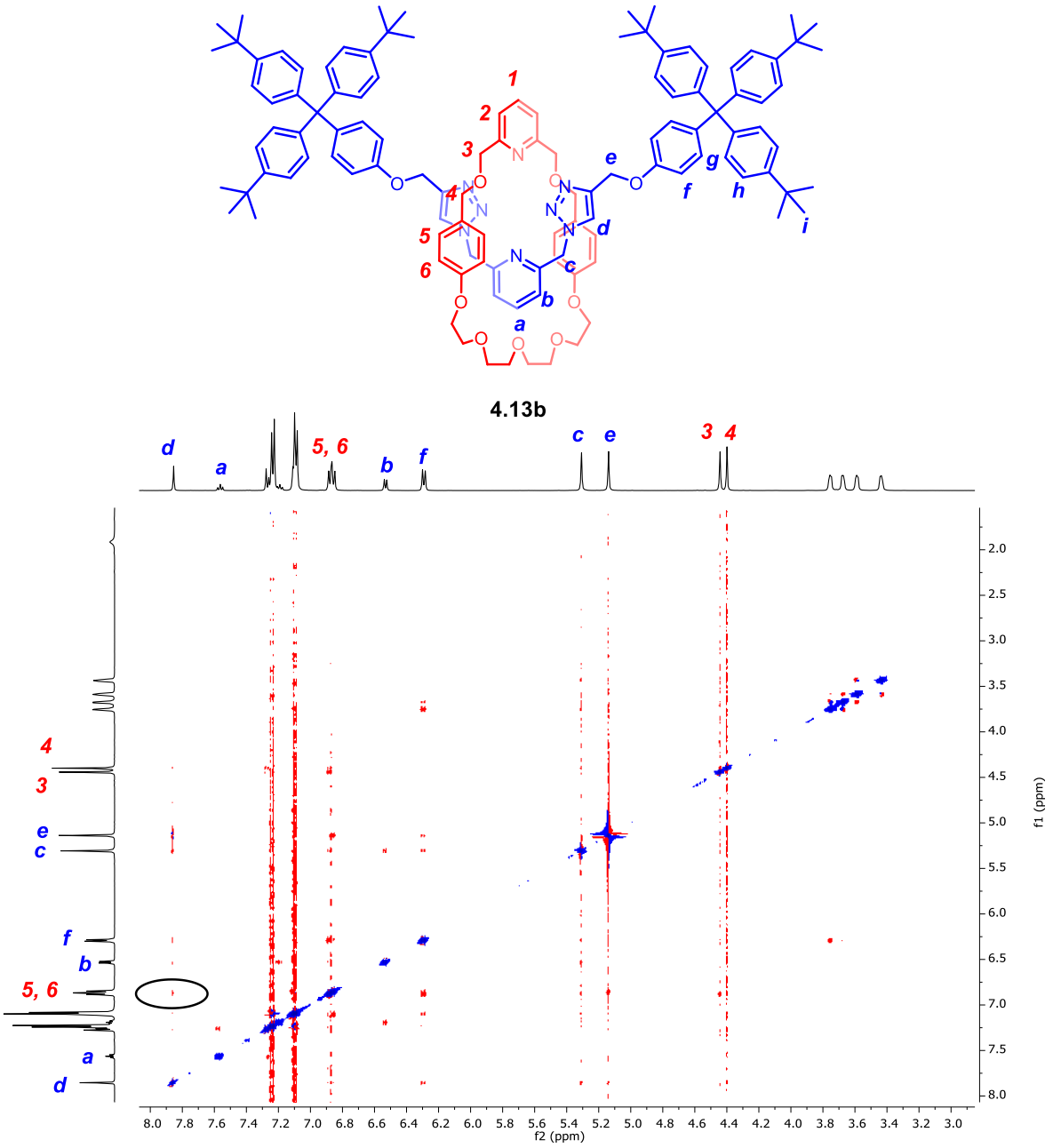

*Figure 100. 2D ROESY NMR of [2]rotaxane 4.13b showing crosspeak correlation between triazole proton Hd from the axle component and protons H5, H6 from the macrocyclic component. Solvent = $CDCl_3$. 2D ROESY NMR of rotaxane **4.13a** and **4.13c** can be found in Appendix E-5 and E-6 respectively.*

4.3.2. Synthesis of Heteropyridyl [2]Rotaxanes

Synthesis involving hetero-*N*-donor pyridyl macrocycle-triazole axle [2]rotaxanes were also carried out using the AMT method. Macrocycles (**4.1**, **4.2** or **4.3**) were dissolved in dichloromethane and an equimolar of Cu(I) was added (Scheme 29). Subsequently, stopper-azide (8.0 eqv) and stopper-alkyne (8.0 eqv) were added to the reaction and stirred overnight. The crude interlocked products were purified using preparatory thin layer chromatography to afford the rotaxanes in 56-76% yields. Rotaxanes were characterised by ^{1}H, ^{13}C NMR while ESIMS analyses found peaks at m/z = 1596.9, m/z = 1640.9 and m/z = 1685.0 corresponding to rotaxanes **4.14a**, **4.14b** and **4.14c** respectively.

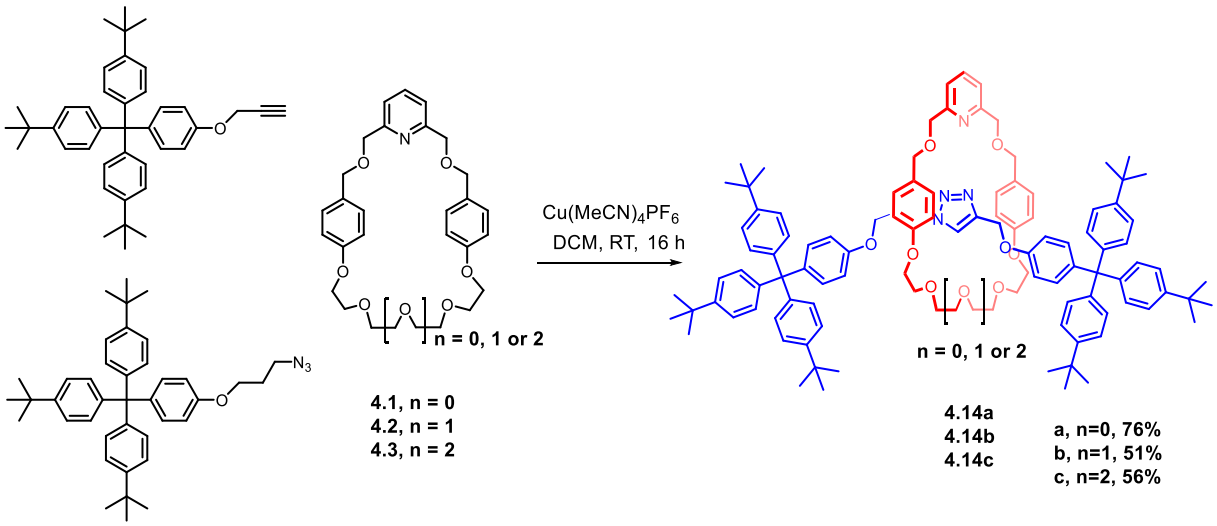

Scheme 29. Hetero-N-Donor (pyridine and triazole) [2]rotaxane with varying macrocyclic sizes formed via Cu(I)-catalysed active metal template method.

^{1}H NMR spectra of isolated [2]rotaxanes all show indicative proton perturbations consistent with a mechanically interlocked structure. In Figure 101, the ^{1}H NMR spectrum of [2]rotaxane **4.14a** is compared to the spectra of the free macrocycle **4.1** and triazole axle in CD_2Cl_2. In the alkyl region, upfield shifts were observed for all protons indicative of components in close proximity. In particular, the singlet signals for protons H_c and H_d in the free macrocycle became doublets at 4.42 ppm and 4.27 ppm corresponding to diastereomeric proton signals stemming from H_c/H_d protons experiencing a different environment to H_c'/H_d' where the [2]rotaxane is asymmetrical. This phenomenon was also observed for protons H_g and H_h where the triplet signals (4.06 and 3.79 ppm) in the free

macrocycle are multiplet signal in the rotaxane NMR spectrum while protons $H_{6\text{-}8}$ in the free axle component became broader in a rotaxane structure.

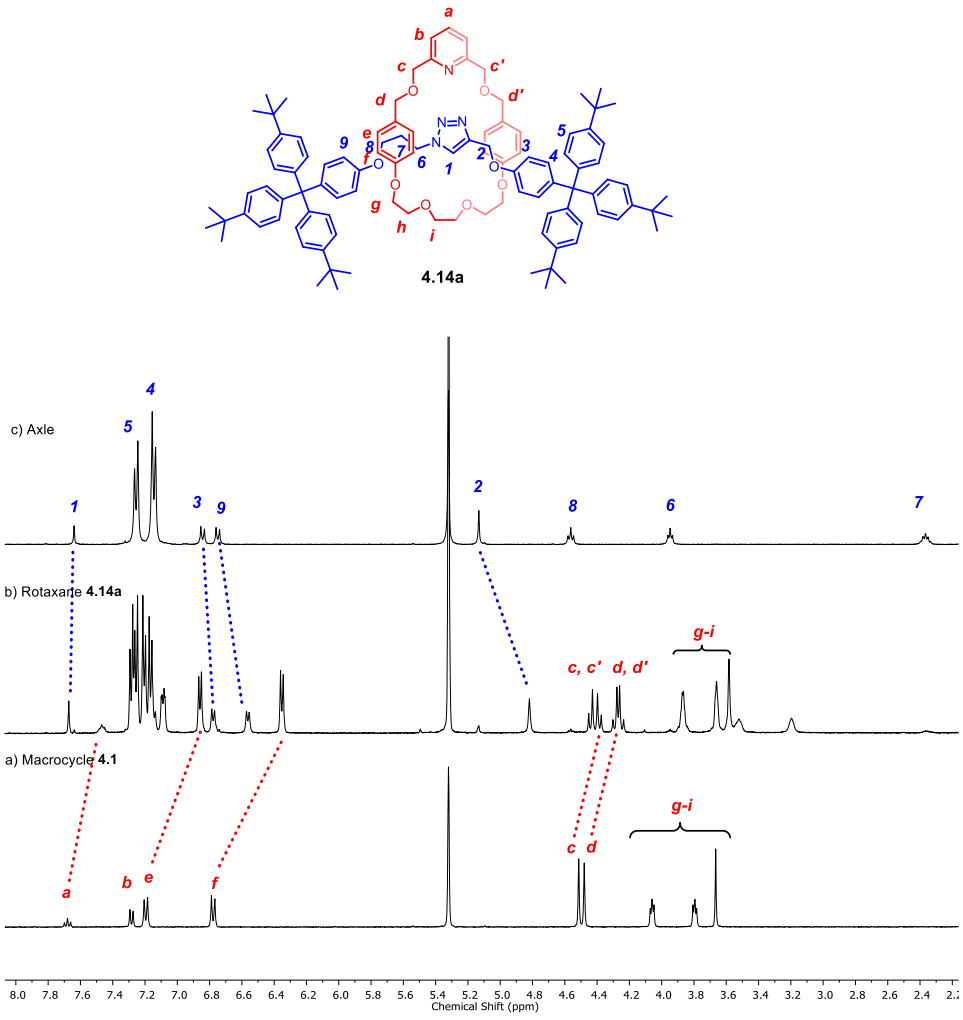

*Figure 101. ^{1}H NMR spectra of a) macrocycle **4.1**, b) [2]rotaxane **4.14a** and c) triazole-based axle measured in CD_2Cl_2.*

Due to the small ring size of macrocycle **4.1** in rotaxane **4.14a**, these trends are not present in rotaxanes **4.14b** and **4.14c**. Instead, ^{1}H NMR spectra of rotaxanes **4.14b** (Figure 102) and **4.14c** (Figure 103) reveal an overall upfield shift of signals with minimal changes to the overall integrity of proton signals. In both spectra, no changes in the splitting patterns of proton signals were observed other than some broadening of peaks for protons $H_{g\text{-}k}$ corresponding to CH_2 polyether chain in the macrocycle component. Upfield shifts were observed for triazole proton H1 and most of the aromatic proton signals corresponding to a more shielded environment as a result of a rotaxane structure.

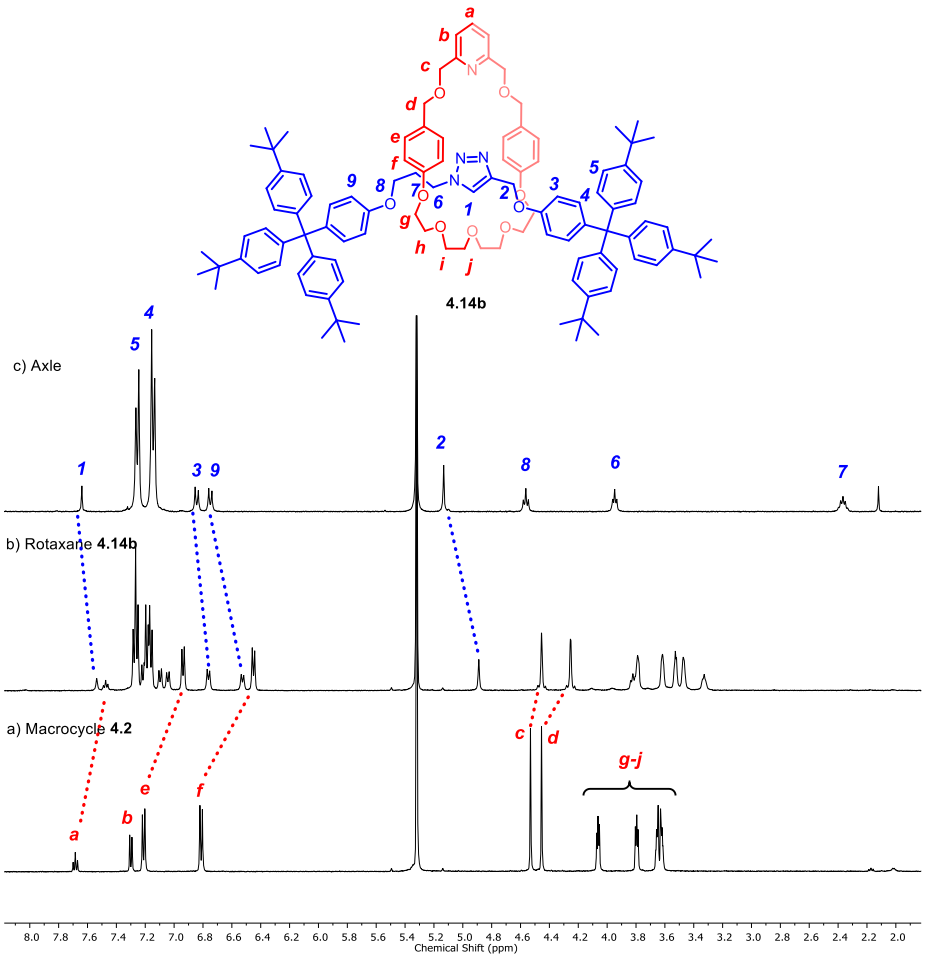

*Figure 102. ^{1}H NMR spectra of a) macrocycle **4.2**, b) [2]rotaxane **4.14b** and c) triazole-based axle measured in CD_2Cl_2.*

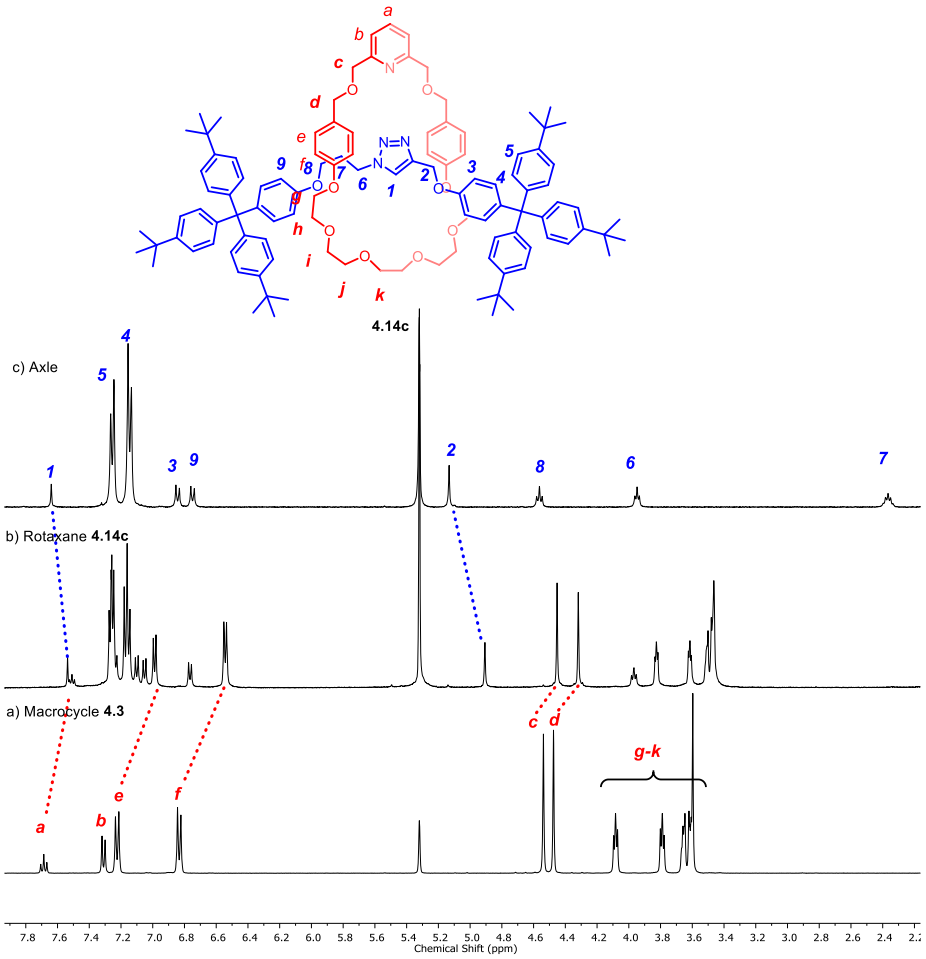

*Figure 103. ^{1}H NMR spectra of a) macrocycle **4.3**, b) [2]rotaxane **4.14c** and c) triazole-based axle measured in CD_2Cl_2.*

4.3.3. NMR Rotaxane-Iodonium Complexation Studies

Preliminary rotaxane-iodonium complexation studies were undertaken using ^{1}H NMR and ^{1}H-^{15}N HMBC NMR experiments, where the iodonium species was generated *in situ via* sequential $AgBF_4$/iodine addition.

Homo-[2]Rotaxane 4.13b

The stoichiometric addition of $AgBF_4$ to a solution of **4.13b** dissolved in CD_2Cl_2, caused proton peak perturbations suggesting successful coordination of Ag(I) metal ion within the cavity of [2]rotaxane **4.13b** (Figure 104b). Significant chemical shifts were observed for alkyl protons within close

proximity of the binding site *ie.* protons H_3, H_4, H_c and H_e. This is also evident in aromatic and pyridyl protons such as protons H_2 and H_b with peak broadening and shifts making it hard to assign.

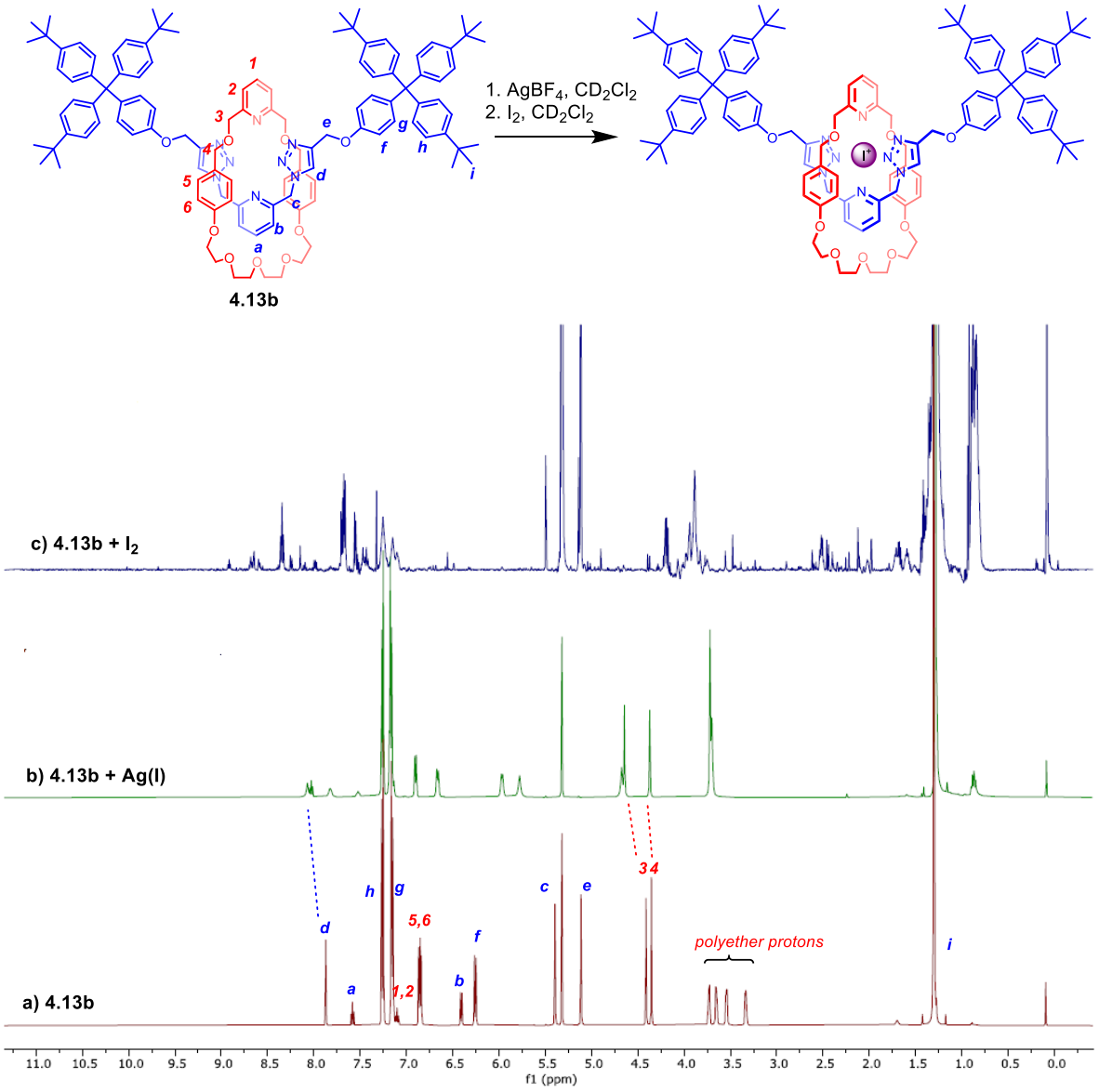

*Figure 104. ^{1}H NMR spectra of the a) [2]rotaxane **4.13b**, b) Ag^+-complexed [2]rotaxane and c) attempted generation of iodonium complex within the [2]rotaxne cavity showing rotaxane decomposition.*

This was further evidenced by ^{1}H-^{15}N HMBC measurements confirming the formation of an Ag(I)-complex. Heteronuclear correlation signals were obtained for free uncomplexed rotaxane **4.13b** (Figure 105) and Ag^+-complexed rotaxane **[4.13b-Ag]$^+$** (Figure 106). In the heteronuclear spectrum obtained for free rotaxane **4.13b** (Figure 105), four ^{15}N signals were identified at -134, -74, -28 and

-17 ppm corresponding to the different N units labelled in the structure; except for N5 which does not have any protons in close proximity for any correlation signals to be measured. Each of these ^{15}N nuclei are coupled to protons in close proximity; for example, N^4 corresponding to one of the nitrogens on the triazole unit, has correlation signals with its two closest protons H_d and H_c. In comparison, the ^{1}H-^{15}N HMBC spectra of rotaxane **[4.13b-Ag]**$^+$ (Figure 106) reveals three ^{15}N signals were observed at -134, -120 and -87 ppm. Correlation at -134 ppm appears to correspond to N4 previously identified in the free rotaxane measurement. Correlation at -120 ppm similar to [macrocycle **4.2**-Ag-lutidine]$^+$ complex (Table 9) is diagnostic of the successful binding of Ag^+ within the rotaxane cavity with *N*-pyridine from both macrocycle (N^1-H_3) and axle (N^1-H_a) components contributing directly to the metal chelation. While correlation corresponding to N^3-H_e has significantly shifted from -28 ppm in the free rotaxane to -87 ppm in the **[4.13b-Ag]**$^+$ complex is the result of a metal centre in close proximity.

Having demonstrated the successful formation of rotaxane **[4.13b-Ag]**$^+$, the subsequent addition of iodine dissolved in CD_2Cl_2 disappointingly resulted in decomposition of the rotaxane. This can be seen in the ^{1}H NMR spectrum with the increased amount of signals that could not be assigned (Figure 104c). Moreover, a ^{1}H-^{15}N HMBC spectrum could not be obtained. Mass spectroscopy measurements found fragments of free macrocycle **4.2**, decomposed stoppers and iodinated stoppers.

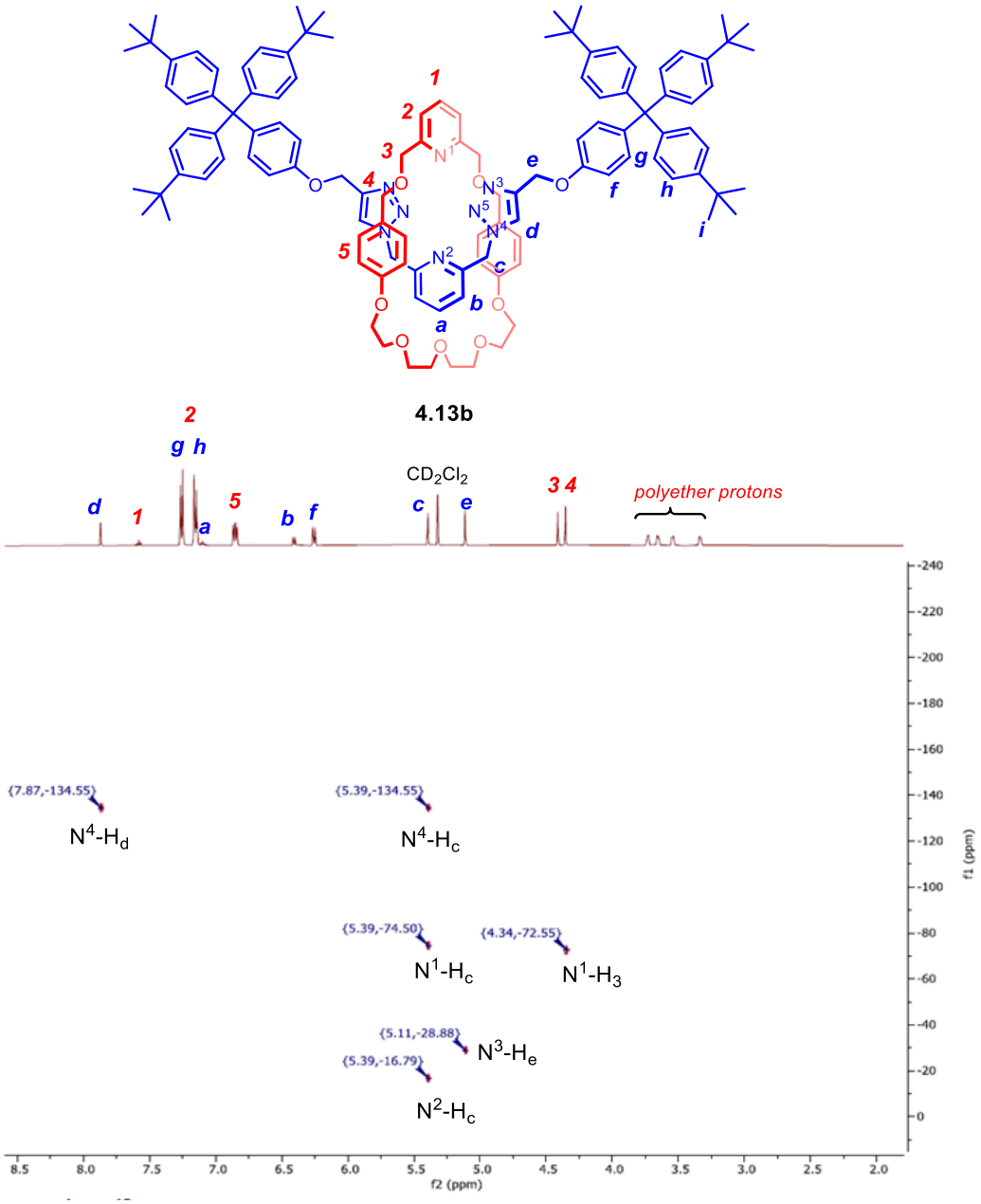

*Figure 105. ^{1}H-^{15}N HMBC NMR spectra of free [2]rotaxane **4.13b** in CD_2Cl_2*

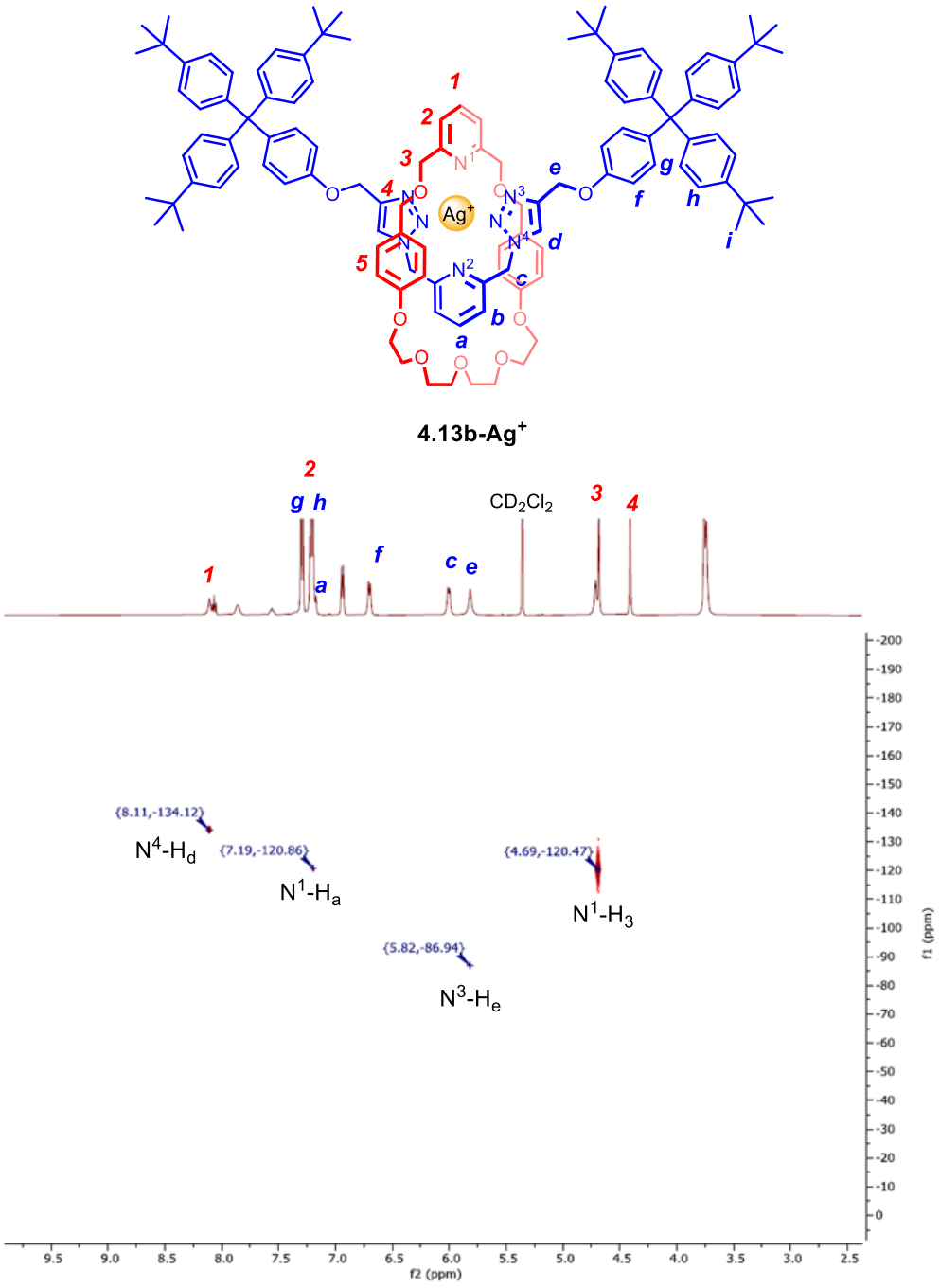

*Figure 106. ^{1}H-^{15}N HMBC NMR spectra of rotaxane complex [**4.13b** + Ag]BF_4 in CD_2Cl_2.*

Heteropyridyl Rotaxane 4.14b

An analogous attempt to complex iodonium between *N*-pyridine and *N*-triazole motifs of hetero-*N*-[2]rotaxane **4.14b** was investigated *via* ^{1}H NMR spectroscopy in CD_2Cl_2 (Figure 107). Similar to measurements carried out for homo-*N*-[2]rotaxane **4.13b**, complexation of Ag(I) by rotaxane **4.14b** was confirmed by ^{1}H NMR and ^{1}H-^{15}N HMBC measurements (Appendix E-7/8). Upon addition of Ag^{+} to rotaxane **4.14b**, proton perturbations were observed in both the alkyl and aromatic regions suggesting the complexation of the metal cation within the rotaxane structure. Notably, large shifts were observed for protons H_e, H_3 and H_4 (Figure 107b) which are in close proximity to the binding cavity while proton signals corresponding to polyether -CH_2 units in the macrocyclic component merged into a multiplet at 3.5 ppm suggesting the complexation introduced a more rigid rotaxane structure further limiting the macrocycle movement along the axle. This is also evidenced in the aromatic region with signals arising from stopper aromatic protons H_g and H_h appearing more symmetrical.

Once again, upon addition of iodine the ^{1}H NMR spectrum became complicated with the appearance of new signals indicating a high degree of rotaxane decomposition with desymmetrisation of aromatic and alkyl protons (Figure 107c).

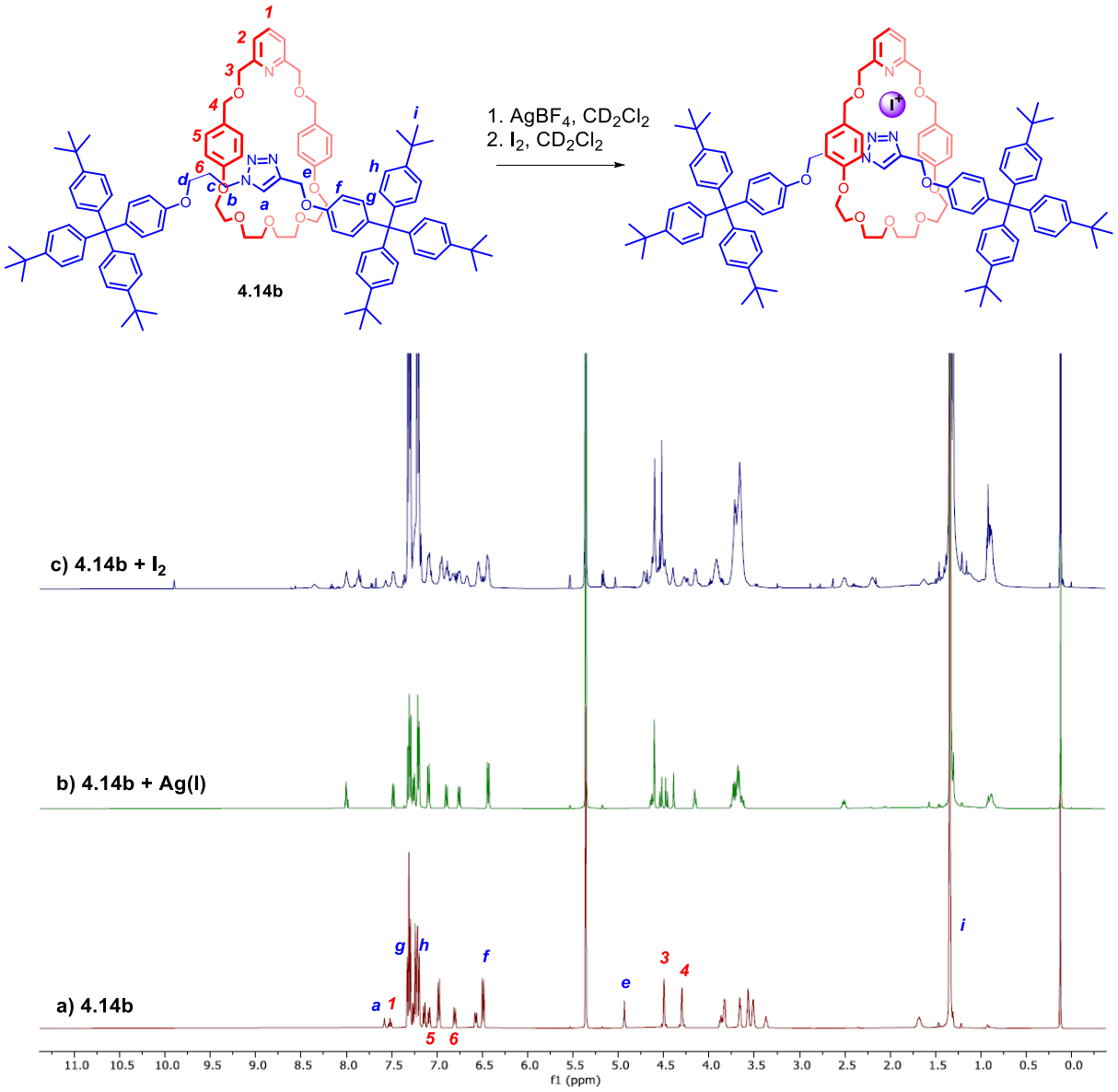

*Figure 107. ^{1}H NMR spectra of a) [2]rotaxane **4.14b**, b) Ag^{+}-complexed [2]rotaxane and c) attempted generation of iodonium complex within the [2]rotaxne cavity showing rotaxane decomposition.*

4.4. Conclusions and Future Work

In collaboration with fellow graduate student Andrew Docker, the synthesis of a range of pyridyl containing macrocycles and bis-azide axle precursors led to the successful preparation of [2]rotaxanes with varying axle lengths and *N*-donors. A combination of ^{1}H NMR and ^{1}H-^{15}N HMBC measurements were used to investigate the formation of iodonium species stabilised by heterocyclic *N*-donors. Preliminary ^{1}H NMR and ^{1}H-^{15}N HMBC measurements were used to monitor the *in situ* generation of iodonium species between macrocycle **4.2** and pyridyl *N*-donor 2,6-lutidine. The observations indicated successful formation of the intermediate Ag(I)-complex while subsequent reaction with I_2 revealed an iodonium species between two 2,6-lutidine instead of the expected macrocycle···I^+···2,6-lutidine complex. While the desired iodonium complex was not achieved, Ag^+ metal coordination interaction with adjacent macrocycle oxygen donor atoms could have contributed to the preferential formation of iodonium stabilised between two 2,6-lutidine units (Figure 95).

Nonetheless, this preliminary result confirmed the ease of making the intermediary Ag(I)-complex. Efforts were carried out to isolate the **[macrocycle 4.1-1.3 +4.5]BF_4** iodonium complex (Scheme 26). ^{1}H NMR studies of the [**4.1**+**4.5]BF_4** iodonium complex resulted in promising evidence for the formation of a new compound (Figure 96) with proton perturbations suggesting successful interpenetration of bis-azide axle precursor **4.5** through macrocycle **4.1** forming a pseudorotaxane assembly. Additional work will need to be carried out using ^{15}N NMR spectroscopy to further support this observation. As a proof-of-concept, attempts to synthesise rotaxane **4.6** *via* a CuAAC *stoppering* reaction failed to produce any evidence of axle or interlocked structure. *See future work on strained-alkyne for Cu(I)-free click chemistry.*

Synthesis of homopyridyl rotaxanes **4.13** and heteropyridyl rotaxanes **4.14** were carried out yielding a series of interlocked structures bearing different sized cavities and *N*-donor units for iodonium stabilisation. For both rotaxanes **4.13b** and **4.14b,** ^{1}H NMR and ^{1}H-^{15}N HMBC NMR confirmed the successful complexation of Ag^+ within the rotaxane's cavity, however, upon addition of iodine solution, the ^{1}H NMR spectra and mass spectrometry analysis suggested decomposition of rotaxanes.

4.4.1. Future work: Barluenga Reagent for Iodonium transfer

Future work could explore the generation of iodonium complexes through iodonium 'transfer' using commercially available Barluenga Reagent (BR, Figure 88) into a preorganised cavity such as a macrocycle or MIM.

In a proof-of-concept preliminary study, Barluenga 'transfer' experiment was carried out on macrocycle **4.2** and monitored *via* ^{1}H NMR spectroscopy in CD_2Cl_2 to which an equimolar solution of BR was added. A comparison of ^{1}H NMR spectra revealed modest changes to proton perturbations in the mixed solution (Figure 108). Pyridyl protons in the macrocycle H_a and H_b shifted slightly upfield by 0.12 and 0.08 ppm respectively while a new proton signal at *ca.* 8.5 ppm was observed. Methylene peaks H_c and H_d corresponding to the macrocycle combined to become a sharp singlet at *ca.* 4.6 ppm. Ideally, one of the pyridines of BR would dissociate and through macrocyclic effect, iodopyridine would bind within the cavity of the macrocycle forming a macrocyclic complex of iodonium-pyridine. However, if macrocyclic effect is weak and/or strong interaction of BR prevents dissociation to pyridine and [iodonium-pyridine]$^{+}$, BR could potentially thread through the macrocycle forming a pseudorotaxane complex (Figure 108).

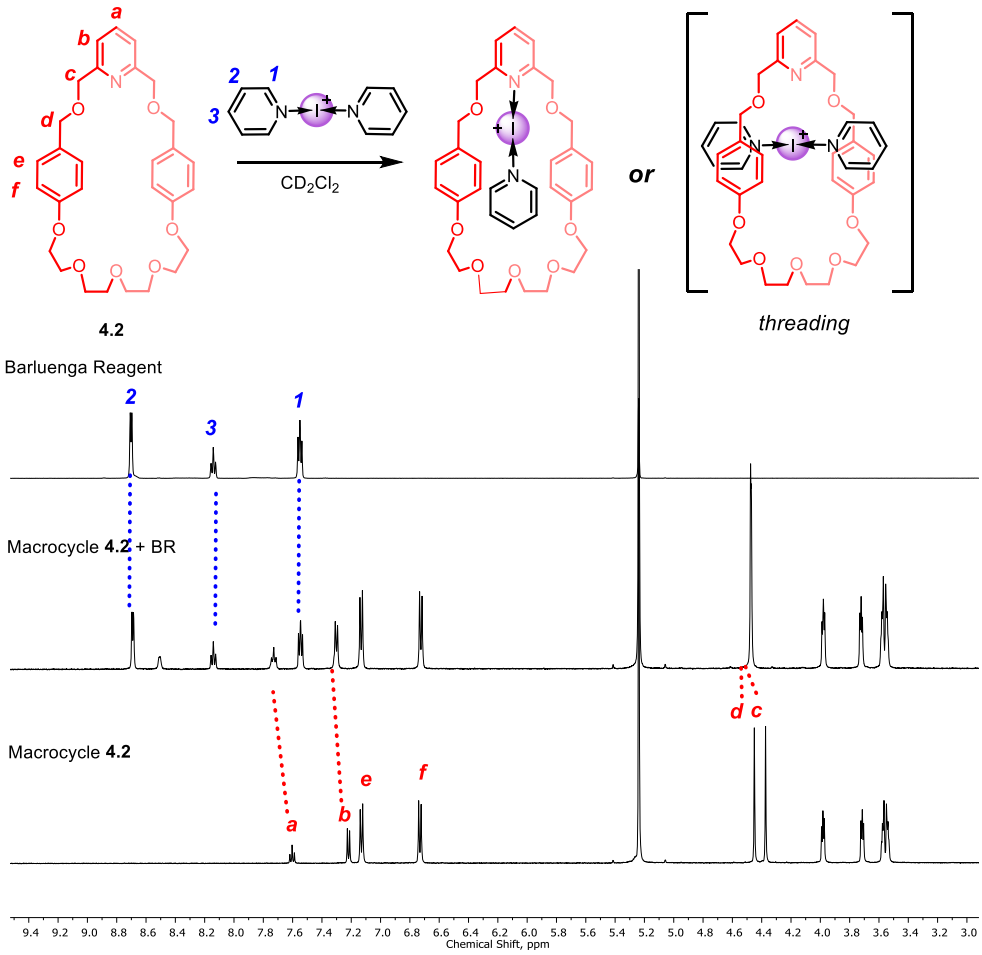

*Figure 108. ^{1}H NMR of Barluenga Reagent with macrocycle **4.2** in CD_2Cl_2.*

Preliminary measurements were also undertaken with [2]rotaxane **4.13c** (Figure 109). Upon addition of 1.0 eqv of BR, peaks corresponding to BR can be seen at 8.96, 8.13 and 7.54 ppm (red asterisk *) and proton perturbations from [2]rotaxane **4.13c** were observed. Amongst the many signals are the rise of three new signals at 8.52, 7.74 and 7.37ppm (green asterisk *) that could arise from free pyridine used where iodonium has been released from BR and transferred into the [2]rotaxane's cavity. These signals can be seen throughout the BR titration however, more measurements such as ^{1}H-^{15}N HMBC experiments need to be undertaken to confirm the formation of iodonium within the [2]rotaxane cavity.

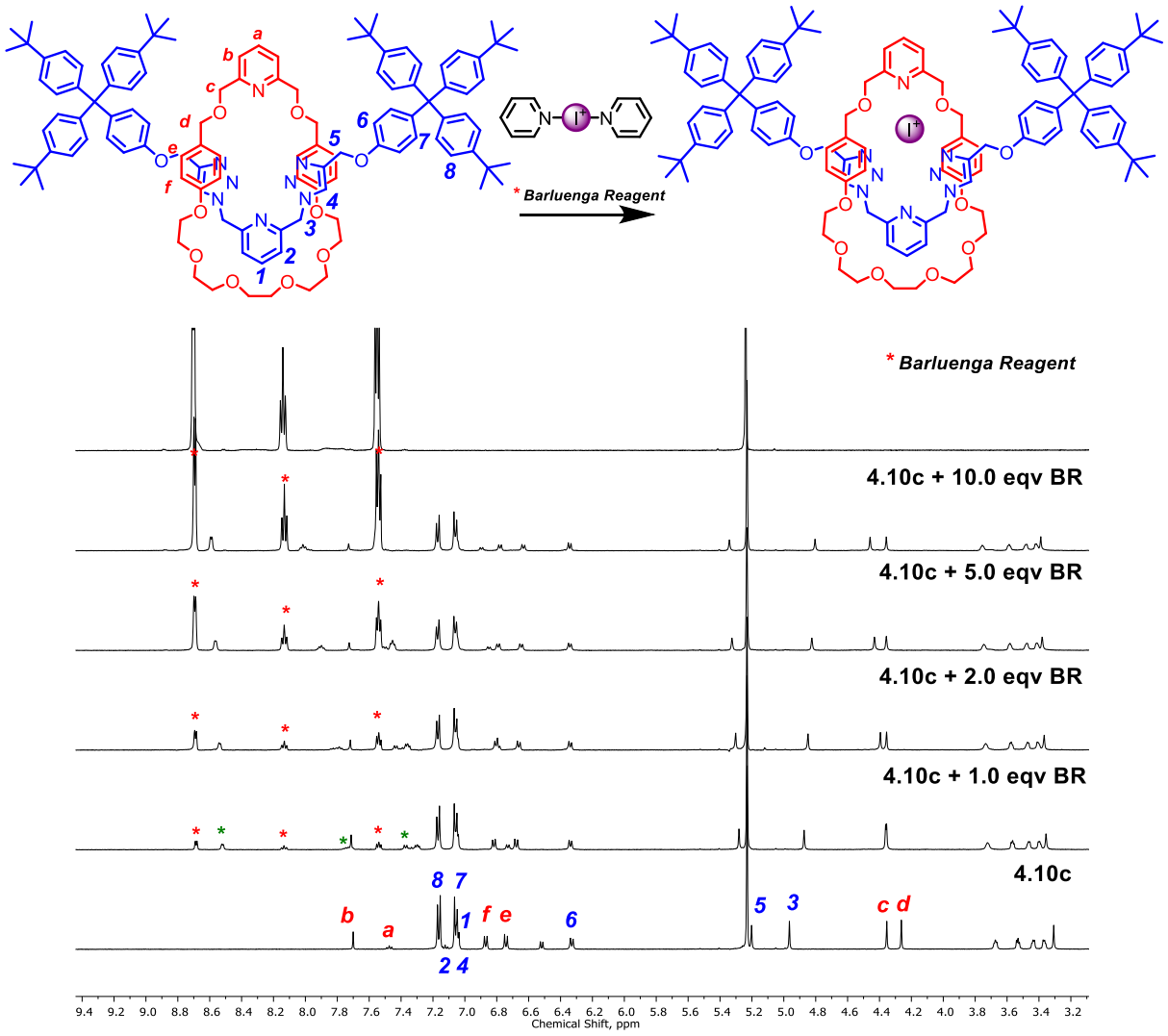

*Figure 109. ^{1}H NMR titration of BR into solution of [2]rotaxane **4.13c** in CD_2Cl_2. *BR signals, *new signals that does not correspond to BR or [2]rotaxane.*

4.4.2. Future work: Strained-Alkyne for Cu(I)-free click chemistry

Supramolecular mechanically bonded structural architectures often involve the use of the popular CuAAC 'click' reaction in their construction. In the presence of a highly reactive species such as iodonium, the presence of the metal catalyst can lead to competing reaction pathways leading to unwanted side products. To overcome this problem, strained-promoted azide-alkyne cycloaddition could be utilised instead[285] as illustrated in Scheme 30.

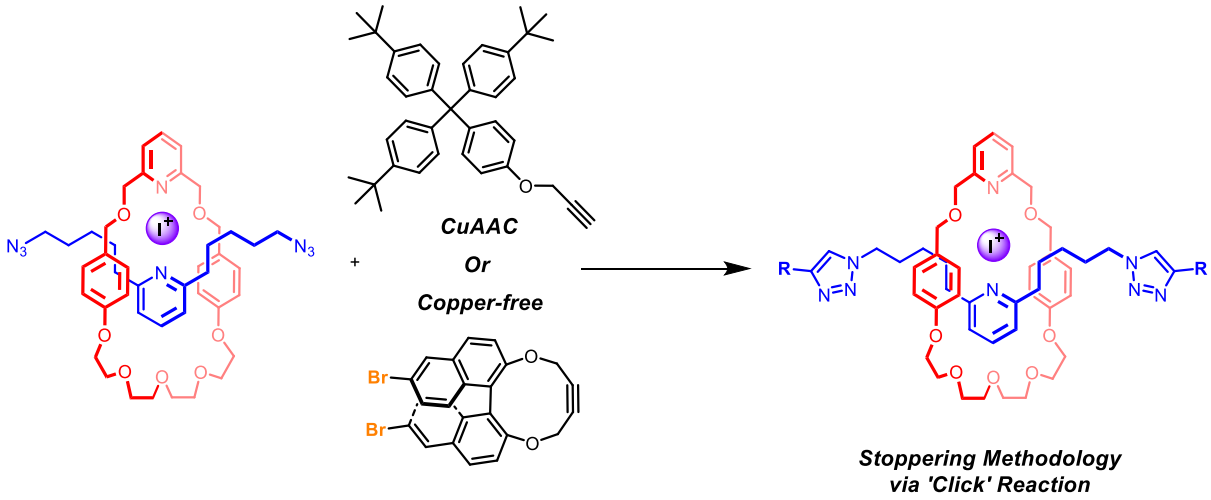

Scheme 30. Stoppering strategy to form [2]rotaxane structure with iodonium as a template. Terminal alkynes are often used in CuAAC reactions while strained alkynes are highly reactive and can proceed in an azide-akyne cycloaddition without the need of a Cu(I) catalyst.

5 | Conclusions Summary

The work in this thesis highlights the integration of σ-hole donor motifs into a variety of novel acyclic, macrocyclic and interlocked host structures for anion recognition applications. Chalcogen bonding and halogen bonding host-anion guest binding investigations were undertaken in aqueous/organic solvent mixtures using in particular NMR and fluorescence spectroscopy.

Chapter 2 investigated the thermodynamic properties of ChB-mediated anion binding, revealing insights into the nature of this poorly understood σ-hole interaction. By comparing a novel air and water stable cationic tellurium-based ChB donor motif $\mathbf{2.1_{Te}}$ (Figure 110), the observed augmented anion affinities displayed by the ChB host was shown to be driven by enthalpy.

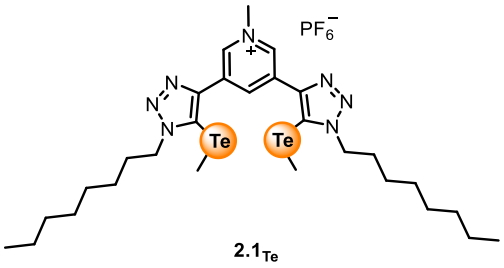

2.1Te

Figure 110. Cationic Te-based ChB donor ***2.1****Te*.

Chapter 3 described the synthesis of chiral XB receptors and application of σ-hole interactions for chiral anion binding. An anion template synthetic protocol was employed for the synthesis of a hybrid HB/XB chiral [2]rotaxane containing BINOL motifs and XB-donor groups incorporated into the axle component **3.32**S (Figure 111). Preparation of target rotaxanes were synthetically challenging potentially due to sterically bulky BINOL units, nonetheless, the hybrid HB/XB rotaxane was prepared in low yields.

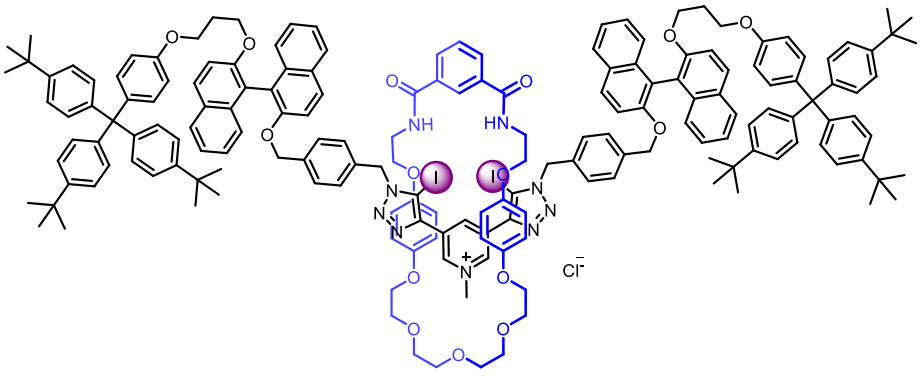

Rotaxane 3.32S

Figure 111. Hybrid HB/XB [2]rotaxane synthesised using a chloride template.

(*S*)/(*R*)-BINOL containing acyclic and macrocyclic hosts were also prepared and designed to bind chiral and geometric dicarboxylate guest species through four integrated iodotriazole donor groups (Figure 112). By monitoring fluorescence stemming from either BINOL or pyrene chromophore, photophysical experiments revealed affinity towards dicarboxylate guest species. Binding data obtained for acyclic receptors demonstrated enantioselectivity towards (*R*,*R*)-tartrate compared to its (*S*,*S*)-tartrate isomer, while host-guest size complementarity played a role in the affinity towards the

geometric phthalate isomers. Macrocyclic hosts fluorescence underwent significant fluorescent perturbations upon anion guest addition, however quantitative data could not be determined.

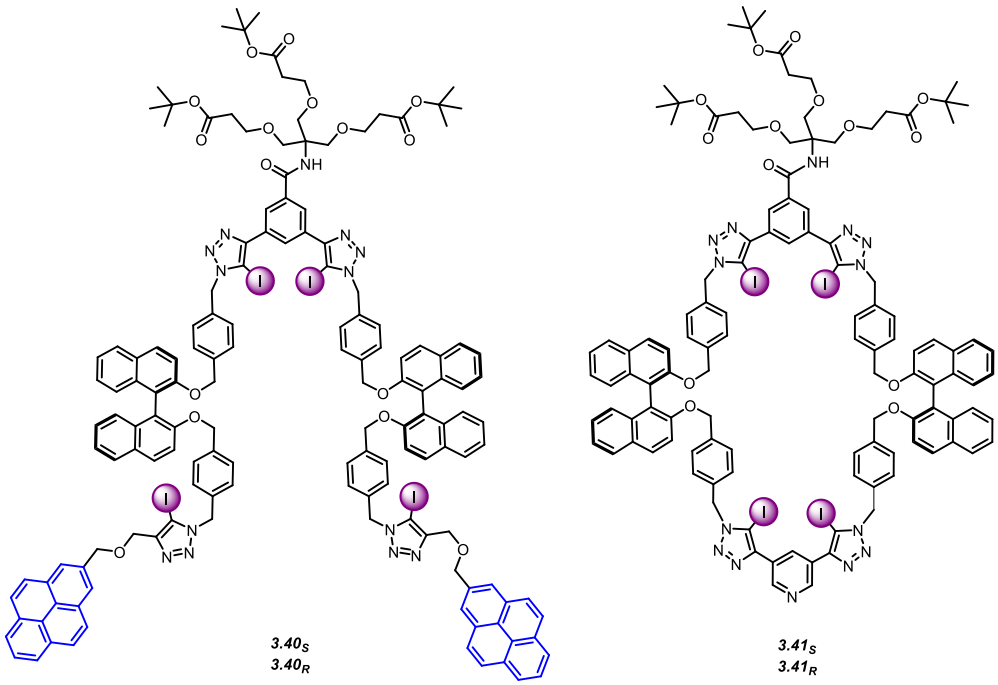

*Figure 112. Tetraiodotriazole receptors **3.40** and **3.41** bearing BINOL chiral discriminating units.*

Chapter 4 investigated the stabilisation of iodonium species by mechanically bonded interlocked structures. Initially, the stability of iodonium was first explored through the assembly of pseudorotaxanes consisting of pyridyl-derived macrocycle and axle precursor components. Following which, an active metal template synthetic method was employed to prepare [2]rotaxanes of varying macrocycle sizes and axle lengths were also prepared to study the stability of iodonium species in a preorganised and shielded cavity (Figure 113). Disappointingly, a combination of NMR spectroscopic techniques such as ^{1}H NMR and ^{1}H-^{15}N HMBC indicated the rotaxanes decomposed upon in situ generation of the iodonium species.

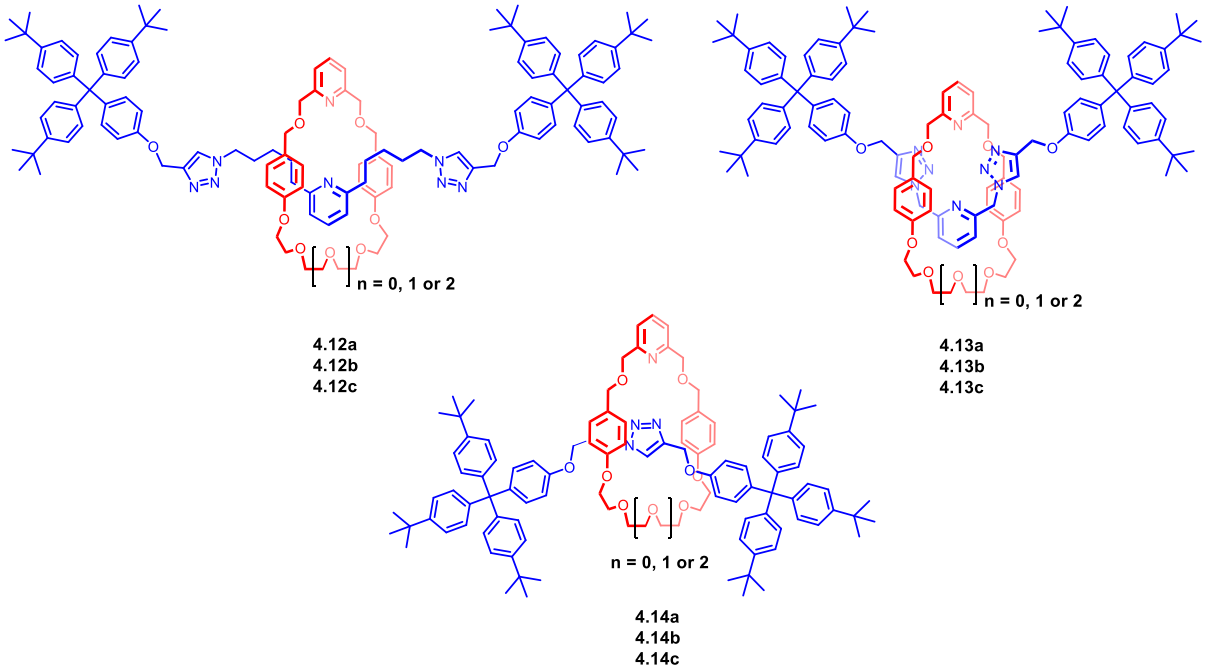

Figure 113. [2]rotaxanes containing different sized pyridyl macrocycle and various pyridyl and triazole axle components.

To conclude, the work described in this thesis explored host-guest relationships using new σ-hole donor motifs, in particular offering insights into the thermodynamic properties of rare ChB-anion interactions. This also included the fluorescence sensing of chiral and geometric carboxylate anions, as well as the introduction of a novel concept involving the potential stabilisation of the reactive halogen bond donor iodonium species by mechanically bonded rotaxane host structures.

6 | Synthetic Procedures of Novel Compounds & Appendices

6.1. General Information

6.1.1. Chemicals and solvents

All solvents and reagents were purchased from commercial suppliers and used as received unless otherwise stated. Dry organic solvents were degassed with nitrogen and then dehydrated by passing through an MBraun MPSP-800 column and used immediately. Deionised water was obtained through a micro filter using a Milli-Q_r Millipore machine. Triethylamine was distilled from potassium hydroxide and stored over the same base prior to usage. TBTA (tris(benzyltriazolemethyl)amine) was synthesised as described[286] and stored under ambient conditions. The various Grubbs catalysts (Grubbs II, Hoveyda-Grubbs, Stewart-Grubbs) and $[Cu(CH_3CN)_4]PF_6$ were stored in vacuum desiccators containing P_2O_5 powder in between usage. Ratios of solvent mixtures are reported by volume. Brine refers to a saturated aqueous solution of NaCl, aqueous ammonia (NH_4OH aq) refers to an approximately 10% solution of NH_3 in water, basic EDTA refers to a 0.02 M aqueous solution of EDTA in a 1% NH_3 solution, bleach refers to general purpose aqueous sodium hypochlorite solution typically containing *ca.* 10% NaClO (*wt/wt*), and petroleum ether refers to the fraction of petrol boiling between 40-60°C. Thin layer chromatography (TLC) analysis was performed using Merck silica Kieselgel 60 F254 0.25 mm, with spots visualised under UV light (254 nm) and/ or staining with $KMnO_4$ solution (only for silica TLC). Column chromatography was performed using silica gel (particle size 40-63 uM) under a positive N_2 head pressure, and preparatory TLC on 20 x 20 cm glass plates with 1 mm silica thickness. Amberlite® anion exchange columns were packed using IRA-400 resin beads containing styrene/divinylbenzene gel with quarternary ammonium matrix active groups (Cl^- salt), and prepared/preloaded by washing the beads sequentially with water and 1M NaOH (aq) till the eluent becomes colourless, water, 10% aqueous NH_4X (X = anion of interest), water and finally the organic solvent mixture (containing water) used for anion exchange.

Safety note: Organic azides, NaN_3, 1,2,3-triazole and the amide coupling agent HOBt used throughout this thesis are potentially explosive and should be handled with care and in small quantities. Direct heating under reduced pressure should be avoided, and especially for reactions with NaN_3. Chlorinated solvents (i.e. CH_2Cl_2, $CHCl_3$ and CCl_4) should be avoided even during reaction work-ups due to their potential for forming highly explosive poly-azidomethanes.[287,288] In addition, NaN_3 should not be used in the presence of acids due to formation of highly toxic HN_3 (g).[289] All reactions should be performed in the fume hood. Any transfer apparatus such as needles used for *n*-BuLi reactions should be quenched and soakled with an isopropanol/water mixture before disposal.

6.1.2. Instrumentations

NMR spectra were recorded on Bruker AVIII HD Nanobay 400 MHz, Bruker AVIIIHD 500 MHz and Bruker AVIIIHD 500 MHz (with ^{13}C cryoprobe) spectrometers. Chemical shifts are quoted in parts per million (ppm) relative to the residual solvent peak with signal splittings denoted as singlet (s), doublet (d), triplet (t), quartet (quart.), quintet (quint.), septet (sep.) and multiplet (m). Low resolution electrospray ionisation mass spectrometry (ESI-MS) was performed using the Waters Micromass LCT for characterisation of compounds previously reported in the literature, and high resolution ESI-MS was recorded using Bruker microTOF spectrometer for novel compounds. Microwave-assisted reactions were performed in a Biotage® Initiator 2.0 reactor using sealed standard Biotage pyrex-glass microwave vials with caps containing rubber septa. Fluorescence spectra were recorded on a Horiba Fluorolog®-3 spectrophotometer while absorption spectra were recorded on a Horiba Duetta™ spectrofluorometer using a quartz cuvette with path length of 1 cm. Optical rotation data were measured on a Perkin-Elmer 241 polarimeter with a path length of 1 dm (using the 589 nm sodium D), with concentrations (c) reported in g/100 mL and temperatures reported in °C.

6.2. Solution Titration Protocols

6.2.1. Tetrabutylammonium (TBA) Salts for Titration

Commercially available tetrabutylammonium (TBA) salts were used as purchased, where salts were dried on the high-vacuum and stored in vacuum desiccators at room temperature with P_2O_5 or silica bead desiccant. TBA salts of chiral[231] anions were adapted from reported procedures. TBA salts of amino acid derivatives, BINOL-PO_4 and dicarboxylates (Chapter 3) were prepared as described[230] from the commercially available acid(s) and 1.0 M solution of TBAOH in methanol and stored in vacuum desiccators with P_2O_5 at -20°C to minimise racemisation.

6.2.2. ^{1}H NMR Titrations

^{1}H NMR titration experiments were performed on a Bruker AVIIIHD 500 MHz spectrometer. In a typical experiment, a solution of the appropriate tetrabutylammonium (TBA) salt was added to 0.5 mL of a 1.0 or 1.5 mM solution of the receptor molecule at the pre-set temperature. Both TBA salt and receptor were dissolved in the same solvent. TBA was chosen as the counter-cation due to its non-coordinating nature. At least 17 data points are obtained for each titration to ensure a good fit to the appropriate host-guest binding models.

The values of the observed chemical shift and concentration of anion were entered into the WinEQNMR2[171] computer programme or BindFit[235,290] for every titration point. From initial estimates made of the binding constants and limiting chemical shifts, these parameters were refined using non-linear least-squares analyses to obtain the best fit between empirical and calculated chemical shifts based on a host-guest 1:1 or 1:2 binding stoichiometry (or otherwise stated). In all cases, convergence of the best fit values of the binding constants and their errors were obtained. For van't Hoff analyses, variable temperature (VT) ^{1}H NMR titration were performed using the same protocol with a range of temperatures. Prior to each titration and after each anion addition, the temperature of the solution in the NMR tube was allowed to equilibrate before ^{1}H NMR spectra was

recorded. In graphical binding isotherms, empirical data points are represented by the filled dots, while continuous lines represent the calculated binding curves.

6.2.3. Fluorescence Titrations

Fluorescence titration experiments were performed on a Horiba Fluorolog®-3 spectrophotometer. In a typical experiment, a solution of the appropriate tetrabutylammonium (TBA) salt was added to 1.0 mL of a known concentration solution of the receptor molecule. TBA salts were dissolved in the same receptor solution to keep host concentration constant throughout the titration. In a typical experiment, an aliquot of the anion solution was added to the receptor solution in the cuvette and same thoroughly mixed by upturning the cuvette several times before any spectra were recorded. Association constants were calculated from the optical titration data by non-linear global fitting analysis using Bindfit software.[235,290]

6.3. Syntheses from Chapter 2

The synthesis of compounds pyridine-3,5-bis(iodoalkyne)[198], 4-^{t}butylbenzyl azide[198], cationic receptor **2.2$_H$**[198], octyl-terminated pyridine-3,5-bis(iodotriazole) **(2.6$_I$)**[198], 4-^{t}butylbenzyl-terminated pyridine-3,5-bis(iodotriazole) (**2.8$_I$**)[172], triethylene glycol-bis-tosylate[291] and MOM-protected hydroquinone azide[174] have been described previously.

Compound 2.9$_{Te}$

***Note**: handle with care in fume cupboard due to malodourous nature of Te-containing volatiles formed in this reaction. All glassware in contact with the reaction products were deodorized by soaking in bleach for at least 6 hours.*

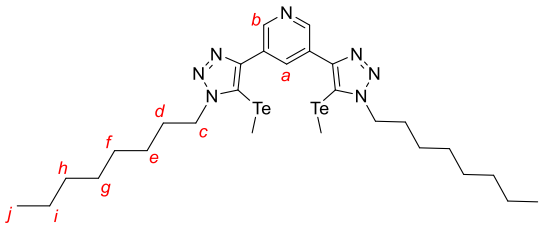

Powdered Te (130 mg, 1.02 mmol) was suspended in dry degassed THF (just sufficient to submerge the Te) and chilled in an ice bath to 0°C in a microwave vial. To the chilled vigorously-stirred suspension was added 1.6 M methyllithium solution in diethyl ether (0.64 mL, 1.02 mmol), and the reaction was sonicated and warmed up to ambient temperature before being left to stir at 1 hour in the dark to yield a brown suspension. Separately, bis-iodotriazole **2.6$_I$** (70.0 mg, 0.102 mmol) was suspended in dry THF (1.5 mL) and added portionwise to the brown suspension at ambient temperature, and the reaction vessel was sealed. The vigorously-stirred reaction was heated at 80 °C in the dark for 4 hours to afford a dark brown suspension. After cooling down to room temperature, iodomethane (0.051 mL, 0.82 mmol) was added to the suspension which was stirred for a further 30 minutes. Subsequently, the reaction was poured into water (20 mL) and the organics were extracted into chloroform (3 x 10 mL). The combined organics were dried with $MgSO_4$ and the solvent was removed *in vacuo* to afford the crude product as a brown malodourous solid. Purification by silica gel column chromatography (eluent: ethyl acetate/hexane 3:2 *v/v*) afforded the target compound as a yellow solid. **Yield:** 59 mg, 81%. **^{1}H-NMR** (500 MHz, $CDCl_3$) δ 9.27 (2H, d, ^4J = 2.2 Hz, H_b), 8.94 (1H, t, ^4J = 2.1 Hz, H_a), 4.61 (4H, t, ^3J = 7.5 Hz, H_c), 2.04 (6H, s, TeCH_3), 1.97 (4H, quint., ^3J = 7.0 Hz, H_d), 1.25 - 1.45 (20H, m, H_{e-i}), 0.89 (6H, t, ^3J = 6.8 Hz, H_j); **^{13}C-NMR** (125 MHz,

$CDCl_3$) δ 150.7, 148.3, 134.4, 127.4, 99.6, 51.5, 31.7, 31.0, 29.1, 26.6, 22.6, 14.1, -12.9; **^{125}Te-NMR** (158 MHz, $CDCl_3$) δ 88.0 Hz; **MS** (ESI +ve) *m/z* 724.17590 ($[M+H]^+$, $C_{28}H_{44}N_7{}^{130}Te_2$, calc. 724.17464).

Compound 2.1$_{Te}$

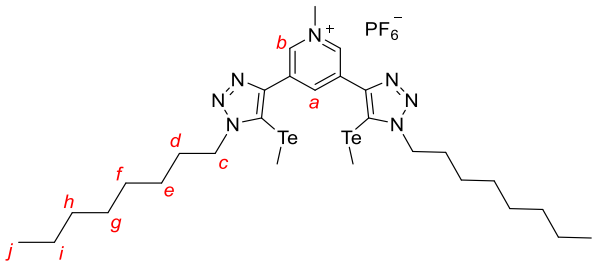

To a solution of compound **2.9$_{Te}$** (37 mg, 0.051 mmol) in dry dichloromethane (1.0 mL) was added iodomethane (0.032 mL, 0.51 mmol) portionwise and the reaction was stirred overnight at ambient temperature. Removal of solvent *in vacuo* afforded the iodide salt of the product as a yellow solid without further purification. Anion exchange was performed by dissolving the product in chloroform (30 mL), and washing successively with saturated aqueous sodium thiosulfate (5 mL), 0.1 M aqueous NH_4PF_6 (8 x 10 mL) and water (2 x 10 mL). Drying the organic layer with $MgSO_4$ and removal of the solvent afforded the desired product, as its PF_6^- salt, as a pale beige solid. **Yield:** 38 mg, 84 %. **^{1}H-NMR** (500 MHz, $CDCl_3$) δ 9.93 (1H, s, H_a), 9.36 (2H, s, H_b), 4.63 (4H, t, ^3J = 7.5 Hz, H_c), 4.59 (3H, s, pyN-CH_3), 2.14 (6H, s, TeCH_3), 1.98 (4H, quint., ^3J = 7.1 Hz, H_d), 1.26 - 1.40 (20H, m, H_{e-i}), 0.89 (6H, t, ^3J = 6.9 Hz, H_j); **^{13}C-NMR** (125 MHz, $CDCl_3$) δ 145.8, 141.2, 139.3, 133.1, 101.7, 51.7, 49.7, 31.7, 30.9, 29.1, 26.5, 22.6, 14.1, -11.6; **^{19}F-NMR** (376 MHz, $CDCl_3$) δ -73.1 (d, $^2J_{F-P}$ = 714 Hz); **^{31}P-NMR** (162 MHz, $CDCl_3$) δ -144.9 (sept., J_{P-F} = 714 Hz); **^{125}Te-NMR** (158 MHz, $CDCl_3$) δ 91.6 Hz; **MS** (ESI +ve) *m/z* 738.19153 ($[M]^+$, $C_{28}H_{46}N_7{}^{128}Te^{130}Te$, calc. 738.19160).

Compound 2.10$_{Se}$

Note: *handle with care in fume cupboard due to malodourous nature of Se-containing volatiles formed in this reaction. All glassware in contact with the reaction products were deodorized by soaking in bleach for at least 6 hours.*

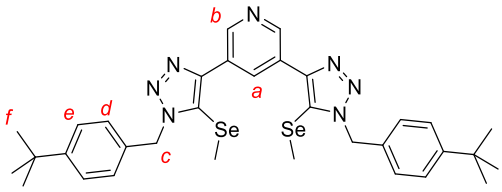

Elemental Se (261 mg, 3.30 mmol) was suspended in a minimum quantity of dry THF in a N_2-filled vial. To this suspension was added a 1.6 M solution methyllithium in diethyl ether (2.06 mL, 3.30 mmol) dropwise and the resulting light brown suspension vigorously stirred for 15 minutes. Separately, bis-iodotriazole[172] (250 mg, 0.330 mmol), was dissolved in dry THF (2.0 mL) and the solution was added to the stirred suspension dropwise and the vial sealed under N_2. The red solution was then stirred under reflux overnight. After cooling down to ambient temperature, iodomethane (0.16 mL, 2.6 mmol) was added and the reaction stirred for 30 minutes before being poured into brine (50 mL). The aqueous suspension was extracted with chloroform (4 x 20 mL) and the combined organics were dried with $MgSO_4$. The reddish-brown crude solid remaining after solvent removal *in vacuo* was purified by silica gel column chromatography (eluent: 30 % ethyl acetate in dichloromethane) to afford the target compound as a pale orange solid. **Yield:** 148 mg, 65 %. **^{1}H-NMR** (400 MHz, $CDCl_3$) δ 9.28 (2H, d, ^4J = 2.1 Hz, H_b), 9.05 (1H, t, ^4J = 2.1 Hz, H_a), 7.34 – 7.25 (4H, d, ^3J = 8.3 Hz, H_d), 7.22 (4H, d, ^3J = 8.3 Hz, H_e), 5.67 (4H, s, H_c), 1.81 (6H, s, SeCH_3), 1.22 (18H, s, H_f). **^{13}C-NMR** (101 MHz, $CDCl_3$) δ 151.7, 147.8, 147.6, 132.7, 132.3, 127.8, 127.0, 126.0, 120.2, 53.1, 34.7, 31.4, 10.1.**^{77}Se-NMR** (95 MHz, $CDCl_3$) δ 38.6. **MS** (ESI +ve) *m/z* 694.16697 ($[M]^+$, $C_{33}H_{40}N_7Se_2$, calc. 694.16701).

Compound 2.3Se

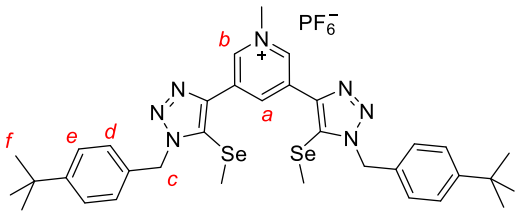

Bis-selenotriazole **2.10Se** (120 mg, 0.174 mmol) was dissolved in neat iodomethane (2 mL) and stirred overnight. Thereafter, excess iodomethane was removed in vacuo and purification by preparatory thin layer chromatography (eluent: 5% methanol in dichloromethane) afforded the product as a bright yellow solid. Anion exchange to the PF_6^- salt was performed by dissolving the compound in chloroform (50 mL) and washing this solution successively with saturated sodium thiosulfate (20 mL), 0.2 M aqueous NH_4PF_6 (8 x 25 mL) and water (2 x 25 mL). Drying the organic layer with $MgSO_4$ and solvent removal in vacuo afforded the target compound **2.3Se** as a beige solid. **Yield:** 119 mg, 80 %. **^{1}H-NMR** (500 MHz $CDCl_3$) δ 10.00 (1H, t, ^4J = 1.68 Hz, H_a), 9.35 (2H, d, ^4J = 1.66 Hz, H_b), 7.39 (4H, d, ^3J = 8.35 Hz, H_d), 7.28 (4H, d, J = 8.54 Hz, H_e), 5.74 (4H, s, H_c), 4.56 (3H, s, pyN-CH_3), 1.98 (6H, s, $SeCH_3$), 1.29 (18H, s, H_f). **^{13}C-NMR** (126 MHz, $CDCl_3$) δ 152.1, 143.1, 140.9, 137.9, 132.9, 131.6, 127.9, 126.2, 122.7, 53.3, 50.0, 34.8, 31.4, 11.0. **^{31}P-NMR** (202 MHz, CDCl3) δ -144.97 (JP-F = 713.0 Hz). **^{19}F-NMR** (470 MHz, CDCl3) δ -72.83, -74.35. **^{77}Se-NMR** (95 MHz, CDCl3) δ 35.75. **MS** (ESI +ve) m/z 709.18550 ($[M]^+$, $C_{34}H_{43}N_7Se_2$, calc. 709.19049).

Compound 2.11

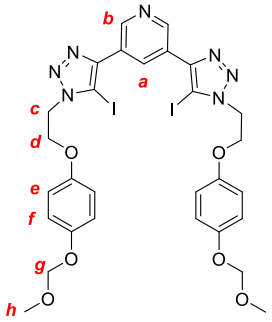

NaI (0.996 g, 6.64 mmol) was suspended in degassed anhydrous THF (16.5 mL), $Cu(ClO_4)_2{\cdot}6H_2O$ (1.218 g, 3.29 mmols) was added and the brown suspension was stirred for 5 minutes. MOM-protected hydroquinone azide (379.0 mg, 1.70 mol), TBTA (21.4 mg, 0.04 mmol), DBU (0.24 mL, 1.60 mmol) and 3,5-diethynylpyridine (102.0 mg, 0.802 mmol) were added in order. The reaction

was then diluted with degassed anhydrous acetonitrile (16.5 mL). The reaction was stirred in the dark for 2 days where solution turned into a lighter coloured suspension. The solvent was then evaporated and solids redissolved in chloroform (50 mL). The organic layer was washed successively with 0.01 M NH_4OH in EDTA solution (4 × 25 mL), brine (1 × 25 mL) and dried over $MgSO_4$. The solvent was evaporated in vacuo and solids purified by silica gel column chromatography (dry loaded, eluent: 2% methanol in dichloromethane, *v/v*) to give the product as a white solid. **Yield:** 0.568 g, 86 %. **^{1}H-NMR** (400 MHz, $CDCl_3$) δ 9.25 (2H, d, ^4J = 2.1 Hz, H_b), 8.85 (1H, t, ^4J = 2.1 Hz, H_a), 6.97 (4H, d, ^3J=9.2 Hz, H_e), 6.83 (4H, d, ^3J = 9.2 Hz, H_f), 5.10 (4H, s, H_g), 4.87 (4H, t, ^3J =5 .6 Hz, H_c), 4.47 (4H, t, ^3J=5.6 Hz, H_d), 3.46 (6H, s, H_h) **^{13}C-NMR** (126 MHz, $CDCl_3$) δ 153.1, 152.1, 148.3, 147.2, 133.3, 126.4, 117.8, 115.7, 95.3, 78.6, 66.9, 56.0, 50.2. **MS** (ESI +ve) *m/z* 826.0337 ($[M]^+$, $C_{29}H_{29}I_2N_7O_6$, calc. 826.0341).

Compound 2.12

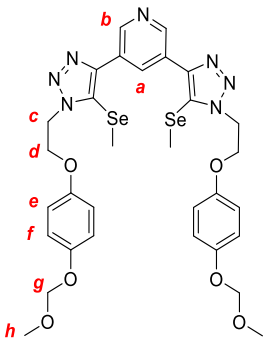

Powdered Se (167.4 mg, 2.12 mmol) was suspended in dry degassed THF (just sufficient to submerge the Se) and chilled in an ice bath to 0°C in a glass vial. To the chilled vigorously-stirred suspension was added 1.6 M methyllithium solution in diethyl ether (1.13 mL, 1.82 mmols), and the reaction was sonicated and warmed up to ambient temperature before being left to stir for 1 hour in the dark to yield a brown suspension. Separately, bis-iodotriazole **2.11** (249.8 mg, 0.303 mmol) was suspended in dry THF (minimum) and added portionwise to the brown resulting suspension at ambient temperature, and the reaction vessel was then sealed. The vigorously-stirred reaction was then heated at 80 °C in the dark for 16 hours to afford a dark brown suspension. After cooling back to room temperature, iodomethane (0.08 mL, 1.21 mmol) was added to the suspension which was stirred for a further 30 minutes. Subsequently, the solvent was removed in vacuo and redissolved in chloroform (10 mL). The reaction was poured into water (20 mL) and the organics were extracted into chloroform (3 x 10 mL). The combined organics were dried with $MgSO_4$

and the solvent was removed *in vacuo* to afford the crude product as a brown malodourous solid. Purification by silica gel column chromatography (eluent: ethyl acetate/hexane 3:2 *v/v*) afforded the target compound as an orange tan solid. **Yield:** 192 mg, 84% **^{1}H-NMR** (400 MHz, $CDCl_3$) δ 9.38 (2H, d, ^{4}J = 1.7 Hz, H_b), 9.16 (1H, t, ^{4}J = 2.0 Hz, H_a), 6.96 (4 H, d, ^{3}J = 9.0 Hz, H_e), 6.73 - 6.87 (4 H, d, ^{3}J = 9.0 Hz, H_f), 5.10 (4 H, s, H_g), 4.97 (4 H, t, ^{3}J = 5.4 Hz, H_c), 4.47 (4 H, t, ^{3}J = 5.4 Hz, H_d), 3.46 (6 H, s, H_h), 2.17 - 2.31 (6 H, m, *SeCH*$_3$). **^{13}C-NMR** ^{13}C NMR (101 MHz, $CDCl_3$) δ 153.1, 152.0, 147.9, 146.8, 132.7, 127.0, 121.8, 117.7, 115.6, 95.2, 67.3, 56.0, 48.7, 10.4. **MS** (ESI +ve) *m/z* 762.10515 ($[M]^+$, $C_{31}H_{36}N_7O_6Se_2$, calc. 762.10520).

Compound 2.13

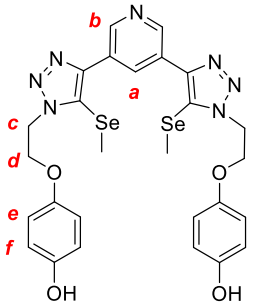

Acetyl chloride (0.15 mL, 2.1 mmol) was stirred with methanol (1.0 mL) at 0°C and stirred for a further 15 min at room temperature. This was then added to a solution of compound **2.13** dissolved in dichloromethane (minimal). Completion of reaction was checked by thin layer chromatography (eluent: 2% methanol v/w in dichloromethane, R_f = 0). Solvent was evaporated and product was used without further purification. **^{1}H-NMR** (500 MHz, Methanol-d_4) δ 10.03 (1H, s, H_a), 9.49 (2H, broad, H_b), 6.67 (2H, d, ^{3}J = 8.6 Hz, H_e), 6.62 (2H, d, ^{3}J = 8.6 Hz, H_f), 4.96 (2H, d, ^{3}J = 9.7 Hz, H_c), 4.43 (2H, t, ^{3}J = 4.8 Hz, H_c), 2.30 (6H, s, Se*CH*$_3$). **^{13}C-NMR** (126 MHz, *CD*$_3$*OD-d*$_4$) δ 152.9, 152.7, 125.6, 116.9, 116.8, 68.4, 54.8, 50.3, 11.2. **^{77}Se-NMR** (95 MHz, *CD*$_3$*OD-d*$_4$) δ 42.95. **MS** (ESI +ve) *m/z* 674.05272 ($[M]^+$, $C_{27}H_{28}N_7O_4Se_2$, calc. 674.05277).

Neutral macrocycle 2.14

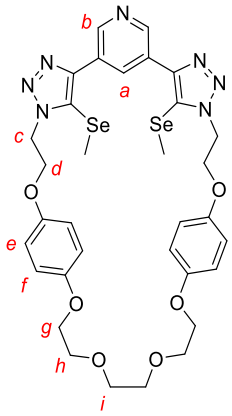

Bis-phenol **2.13** (170 mg, 0.253 mmol) and triethylene glycol-bis-tosylate[291] (83 mg, 0.253 mmol) were dissolved in degassed anhydrous DMF (10 mM) and stirred until the solids were dissolved. Cs_2CO_3 (1.158 g, 2.53 mmol) was added and the solution was heated to 70 °C for 16 hours. Solvent was then evaporated in vacuo and water (20 mL) was added. The aqueous layer was extracted with chloroform (3 × 10 mL) and the combined organic layer was washed with brine and dried over $MgSO_4$, filtered and the solvent removed *in vacuo*. Crude macrocycle was purified using preparatory thin layer chromatography (eluent: 2.5-4% methanol in dichloromethane) to obtain the product as a white solid. Yield: 51 mg, 26%. **^{1}H-NMR** (400 MHz, $CDCl_3$) δ 9.28 (2H, s, H_b), 8.99 (1H, s, H_a), 6.77 (4H, d, ^3J = 8.7 Hz, H_e), 6.68 (4H, d, ^3J = 8.7 Hz, H_d), 4.97 (4H, t, ^3J = 4.8 Hz, H_c), 4.41 (4H, t, ^3J = 4.8 Hz, H_d), 4.02 (4H, t, ^3J = 4.8 Hz, H_g), 3.78 (4H, t, ^3J = 4.7 Hz, H_h), 3.68 (4H, s, H_i), 2.15 (6H, s, SeCH_3). **^{13}C-NMR** (126 MHz, $CDCl_3$) δ 153.8, 152.3, 148.1, 146.7, 132.9, 127.0, 122.8, 115.9, 115.6, 70.9, 69.8, 68.3, 67.9, 48.8, 10.4. **^{77}Se-NMR** (95 MHz, $CDCl_3$) δ 45.7. **MS** (ESI +ve) *m/z* 788.12114 ($[M]^+$, $C_{33}H_{37}N_7O_6Se_2$, calc. 788.12085).

Cationic macrocycle 2.6$_{Se}$

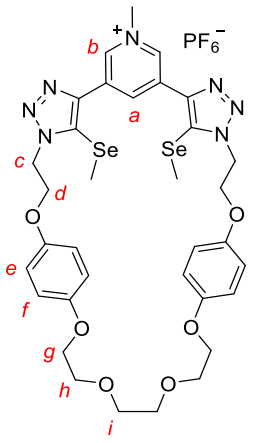

Macrocycle **2.14** (51 mg, 0.06 mmol) was dissolved in dry dichloromethane (1.0 mL) and iodomethane (0.1 mL) was added dropwise. The reaction was left to stir at room temperature for 16 hours. Solvent was removed *in vacuo* and solids re-dissolved in chloroform (20 mL). The organic layer was washed repeatedly with 0.1 M NH_4PF_6 (10 × 10 mL) and water (2 × 10 mL), dried over $MgSO_4$ and filtered. Solvent was removed in vacuo to afford the product as a pale-yellow solid. **Yield:** 29 mg, 56 %. **^{1}H-NMR** (500 MHz, d_6-acetone) δ 10.06 (1H, s, H_a), 9.59 (2H, d, ^4J = 1.4 Hz, H_b), 6.80 (8H, d, ^3J = 1.7 Hz, $H_{e,f}$), 5.14 – 5.08 (4H, m, H_c), 4.87 (3H, s, pyN-CH_3), 4.52 – 4.47 (5H, m, H_d), 4.04 – 3.98 (4H, m, H_g), 3.78 – 3.72 (4H, m, H_h), 3.62 (4H, s, H_i), 2.37 (6H, s, SeCH_3). **^{13}C-NMR** (126 MHz, d_6-acetone) δ 154.7, 153.1, 143.3, 142.7, 138.0, 133.3, 126.1, 116.5, 116.3, 71.5, 70.3, 69.0, 68.3, 49.9, 49.7,11.3. **^{77}Se-NMR** (95 MHz, d_6-acetone) δ 50.99. **MS** (ESI +ve) *m/z* 802.13644 ($[M]^+$, $C_{34}H_{40}N_7O_6Se_2$, calc. 802.13650).

Compound 2.8$_F$

The microwave-assisted halex protocol developed by Fokin and co-workers was used in this procedure.[170]

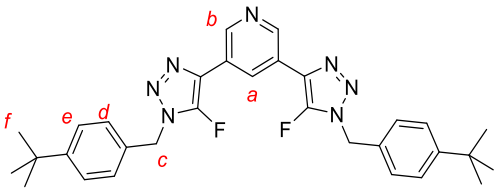

Bis-iodotriazole **2.8$_I$** (200 mg, 0.26 mmol) was dissolved in acetonitrile (25 mL) at 80°C. While hot, an aqueous solution (25 mL) of potassium fluoride (307 mg, 5.28 mmol) was added portionwise and stirred to give a white suspension. The reaction was heated in a microwave reactor at 175 °C for 10 minutes to give a yellow suspension (due to limitations in size of the microwave vials, with a maximum volume of 20 mL, this reaction was split and performed in three batches of 20, 20 and 10 mL respectively) to afford a yellow suspension. To the crude reaction mixture was added brine (20 mL), followed by chloroform (30 mL) and the mixture stirred till a clear biphasic mixture was obtained. The aqueous and organic layers were separated and the aqueous layer extracted with chloroform (2 x 10 mL). The combined organics were dried with $MgSO_4$ and the brown tar remaining after solvent removal *in vacuo* was purified by silica gel column chromatography (eluent: 30 % ethyl acetate in dichloromethane) to yield the product as a pale beige solid. **Yield:** 74 mg, 52%.**^{1}H-NMR** (400 MHz, $CDCl_3$) δ 9.01 (1H, s, H_b), 8.55 (1H, t, ^4J = 2.1 Hz, H_a), 7.41 (4H, d, ^3J = 8.4 Hz, H_e), 7.32 (4H, d, ^3J = 8.3 Hz, H_f), 5.46 (4H, s, H_c), 1.31 (18H, s, H_f). **^{13}C-NMR** (101 MHz, $CDCl_3$) δ 152.4, 151.6, 148.8, 145.9, 145.9, 130.3, 128.7, 128.1, 126.3, 125.2, 124.4, 124.3, 51.3, 34.8, 31.4. **^{19}F-NMR** (377 MHz, *$CDCl_3$*) δ -150.09 **MS** (ESI +ve) *m/z* 542.28349 ($[M]^+$, $C_{31}H_{34}N_7F_2$, calc. 542.28383).

Compound 2.4$_F$

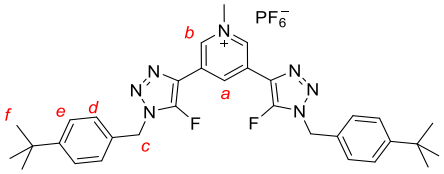

Fluorotriazole **2.8$_F$** (50 mg, 0.092 mmol) was dissolved in iodomethane (1.5 mL) and the reaction left to stir overnight. Following removal of excess iodomethane in vacuo, the yellow solid was re-dissolved in chloroform (50 mL) and washed successively with saturated sodium thiosulfate (20 mL),

0.2 M aqueous NH_4PF_6 (8 x 25 mL) and water (2 x 25 mL). Drying the organic layer with $MgSO_4$ and solvent removal *in vacuo* afforded the target compound **2.4$_F$** as a beige solid. **Yield:** 53 mg, 82 %. **^{1}H-NMR** (400 MHz, $CDCl_3$) δ 8.96 (1H, t, *J* = 1.7 Hz, H_a), 8.91 (2H, d, *J* = 1.6 Hz, H_b), 7.42 – 7.36 (4H, m, H_d), 7.28 (4H, d, *J* = 8.4 Hz, H_f), 5.43 (4H, s, H_c), 4.48 (3H, s, pyN-CH_3), 1.28 (18H, s, H_f). **^{13}C-NMR** (101 MHz, $CDCl_3$) δ 152.6, 149.7, 139.4, 134.2, 130.7, 130.7, 129.7, 128.2, 126.4, 120.9, 120.8, 51.6, 50.0, 34.8, 31.3, 29.8. **^{19}F-NMR** (377 MHz, $CDCl_3$) δ -78.34 - -68.83 (d, $^2J_{F-P}$ = 714 Hz), -144.76 (s, trz-F). **^{31}P-NMR** (162 MHz, $CDCl_3$) δ -123.4 – -165.4 (J_{P-F} = 714.0 Hz)**. MS** (ESI +ve) *m/z* 556.29861 ($[M]^+$, $C_{31}H_{36}N_7F_2$, calc. 556.29948).

Thioamide Macrocycle 2.22

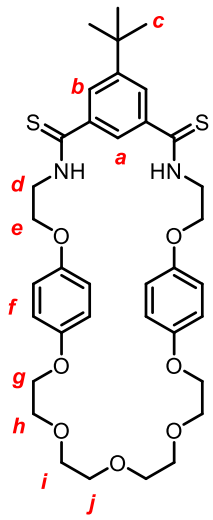

Isophthalamide macrocycle[136] (150 mg, 0.23 mmol) was dissolved in dry degassed dichloromethane (6 mL) and sealed in an air tight vial. Lawesson's Reagent (112 mg, 0.28 mmol) was dissolved in minimum dichloromethane and added to the reaction vessel. Reaction was stirred at 50°C overnight to afford thioamide macrocycle **2.22** after preparatory thin layer chromatography (3% methanol in dichloromethane) as a yellow solid. Yield: 77 mg, 51 %. **^{1}H-NMR** (400 MHz, acetone-d_6) δ 9.75 (2H, s, NH), 8.10 (2H, d, *J* = 1.6 Hz, H_b), 7.74 (H_a, t, *J* = 1.6 Hz, 1H), 6.90 – 6.78 (H_f, m, 8H), 4.30 (H_d, t, *J* = 5.0 Hz, 4H), 4.21 – 4.13 (H_e, m, 4H), 4.01 (4H, dd, *J* = 5.7, 3.7 Hz, H_g), 3.83 – 3.76 (4H, m, H_h), 3.63 (8H, m, *J* = 2.64, 2.16 Hz, H_i and H_j,), 2.81 – 2.76 (m, 2H), 1.35 (9H, s, H_c). δ **^{13}C-NMR** (101 MHz, acetone-d_6) δ 199.9, 154.3, 153.8, 151.8, 142.5, 142.4, 128.7, 121.7, 116.3, 116.3, 71.5, 71.4, 70.4, 69.0, 66.2, 47.2, 47.1, 35.6, 31.4. **MS** (ESI +ve) *m/z* 705.27 $[M + Na]^+$

[2]Catenane 2.25

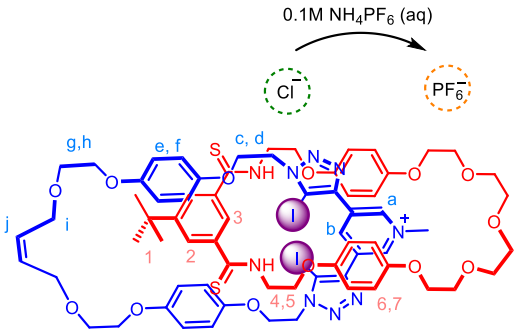

2.25•Cl

2.25•PF_6

Iodotriazole-(bis)alkene[172] **2.15·Cl** (100 mg, 0.105 mmol) and thioamide macrocycle **2.22** (71.4 mg, 0.105 mmol) were dissolved in dry degassed dichloromethane (10 mM) and stirred at room temperature for 15 mins before adding 10 % (*wt/wt*) Stewart-Grubbs catalyst. The reaction was stirred for 16 hours at room temperature and the resulting crude product subjected to purification via preparatory layer silica chromatography (2.5% methanol in dichloromethane). Pure [2]catenane **2.25·PF_6** was isolated after subsequent anion exchange to its PF_6^- salt by 3 x 10 mL aqueous washing with 0.1M NH_4PF_6 as a pale yellow solid (29.1 mg, 34 %). **^{1}H-NMR** (500 MHz, $CDCl_3$) δ 9.84 (1H, s, H_a), 9.36 (1H, s, H_a'), 8.79 (1H, s, H_2), 8.70 (1H, s, H_2'), 8.66 (1H, s, H_b), 7.72 (1H, s, H_3), 6.83 (4H, d, *J* = 8.58 Hz, $H_{e/f}$), 6.72 (10H, dd, *J* = 8.6 Hz, $H_{e/f}$ + NH), 6.44 (2H, d, *J* = 8.34Hz, $H_{6/7}$), 5.90 (d2H, , *J* = 8.3 Hz, $H_{6/7}$), 5.70 (2H, s, -CH_2), 5.54 (4H, d, *J* = 8.6 Hz, $H_{6/7}$), 5.21 (4H, d, *J* = 8.6 Hz, $H_{6/7}$), 4.93 (1H, br), 4.55(3H, br), 4.48 (2H, br,), 4.32 (3H, s, *N*-CH_3), 4.24 (2H ,br), 3.92 (8H,br), 3.78 (2H,br), 3.72 (2H, br), 3.66 (6H,), 3.47 (3H, br), 1.45 (9H, s, H_1). **^{13}C-NMR** (126 MHz, $CDCl_3$) δ 154.1, 153.2, 152.6, 143.2, 141.7, 131.0, 129.6, 116.3, 116.0, 115.3, 114.8, 78.5, 78.2, 78.0, 71.5, 71.4, 70.6, 69.4, 68.7, 68.4, 66.9, 65.5, 54.1, 50.9, 35.8, 31.6, 30.9. **^{19}F-NMR** (376 MHz, $CDCl_3$) δ -73.31, -75.21. **^{31}P-NMR** (162 MHz, $CDCl_3$) δ -135.78, -140.16, -144.54, -148.92, -153.30. **MS** (ESI +ve) *m/z* 1574.35200 ($[M]^+$, $C_{70}H_{82}O_{13}N_9I_2S_2$, calc. 1574.35574).

Compound 2.12$_{Te}$

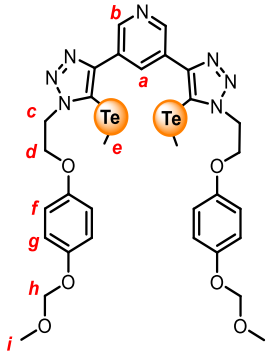

Powdered Te (338 mg, 0.36 mmol) was suspended in dry degassed THF (just sufficient to submerge the Te) and chilled in an ice bath to 0°C in a glass vial. To the chilled vigorously-stirred suspension was added 1.6 M methyllithium solution in diethyl ether (1.36 mL, 2.18 mmols), and the reaction was sonicated and warmed up to ambient temperature before being left to stir for 1 hour in the dark to yield a brown suspension. Separately, bis-iodotriazole **2.11** (325 mg, 2.55 mmol) was suspended in dry THF (minimum) and added portionwise to the brown resulting suspension at ambient temperature, and the reaction vessel was then sealed. The vigorously-stirred reaction was then heated at 70 °C in the dark for 2 hours to afford a dark brown suspension. After cooling back to room temperature, iodomethane (0.091 mL, 1.45 mmol) was added to the suspension which was stirred for a further 30 minutes. Subsequently, the solvent was removed in vacuo and redissolved in chloroform (10 mL). The reaction was poured into water (20 mL) and the organics were extracted into chloroform (3 x 10 mL). The combined organics were dried with $MgSO_4$ and the solvent was removed *in vacuo* to afford the crude product as a brown malodourous solid. Purification by silica gel column chromatography (eluent: ethyl acetate/hexane 3:2 *v/v*) afforded the target compound as an orange tan solid. **Yield:** 315 mg, 92%. **^{1}H-NMR** (400 MHz, $CDCl_3$) δ 9.29 (2H, d, *J* = 2.1 Hz, H_b), 8.98 (1H, t, *J* = 2.1 Hz, H_a), 6.95 (4H, d, $H_{f/g}$), 6.79 (4H, d, $H_{f/g}$), 5.09 (4H, s, H_h), 5.02 (4H, t, *J* = 5.28 Hz, H_c), 4.41 (4H, t, *J* = 5.31 Hz, H_d), 3.45 (6H, s, H_i), 1.99 (6H, s, H_e). No MS obtained.

Compound 2.13$_{Te}$

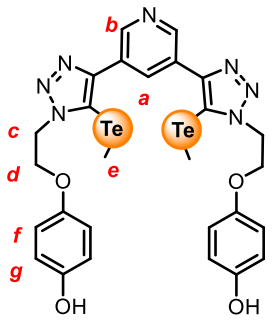

Acetyl chloride (0.15 mL, 2.1 mmol) was stirred with methanol (1.0 mL) at 0°C and stirred for a further 15 min at room temperature. This was then added to a solution of **2.12$_{Te}$** dissolved in dichloromethane (minimal). Completion of reaction was checked by thin layer chromatography (eluent: 2% methanol v/w in dichloromethane, R_f = 0). Solvent was evaporated and product was used without further purification. **^{1}H-NMR** (500 MHz, Methanol-d_4) δ 10.03 (1H, s, H_a), 9.49 (2H, broad, H_b), 6.67 (2H, d, ^{3}J = 8.6 Hz, H_e), 6.62 (2H, d, ^{3}J = 8.6 Hz, H_f), 4.96 (2H, d, ^{3}J = 9.7 Hz, H_c), 4.43 (2H, t, ^{3}J = 4.8 Hz, H_c), 2.30 (6H, s, SeCH_3). **^{13}C-NMR** (126 MHz, CD_3OD-d_4) δ 152.9, 152.7, 125.6, 116.9, 116.8, 68.4, 54.8, 50.3, 11.2. **^{77}Se-NMR** (95 MHz, CD_3OD-d_4) δ 42.95. **MS** (ESI +ve) *m/z* 770.1 ($[M+H]^+$ $C_{27}H_{27}N_7O_4Te_2$ calc. 769.02)

Compound 2.$_{14Te}$

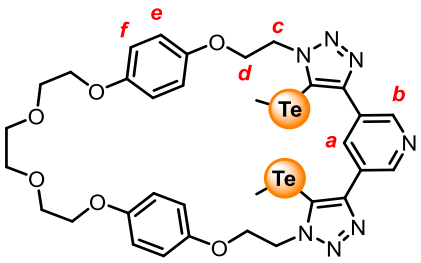

2.11$_{Te}$

Bis-phenol **2.13$_{Te}$** (170.5 mg, 0.22 mmol) and triethylene glycol-bis-tosylate[291] (72.2 mg, 0.22 mmol) were dissolved in degassed anhydrous DMF (10 mM) and stirred till solids were dissolved. Cs_2CO_3 (1.017 g, 2.22 mmol) was added and the solution was heated to 70 °C for 16 hours. Solvent was then evaporated in vacuo and water (20 mL) was added. The aqueous layer was extracted with chloroform (3 × 10 mL) and the combined organic layer was washed with brine and dried over $MgSO_4$, filtered and the solvent removed *in vacuo*. Crude macrocycle was purified using preparatory layer silica chromatography (eluent: 2.5-4% methanol in dichloromethane) to obtain the product as a white solid. **Yield:** 9.6 mg, **5**%. Compound **2.14$_{Te}$**: **^{1}H-NMR** (400 MHz, $CDCl_3$) δ 9.15 (2H, s, H_b), 8.91 (1H, s, H_a), 6.78 (4H, dd, H_e), 6.72 (4H, dd, H_f), 5.03 (4H, t, *J* = 4.8 Hz, H_c), 4.36 (4H, t, *J* = 4.7 Hz, H_d), 4.02 (4H, t, *J* = 4.6 Hz, polyether H), 3.80 (4H, dd, *J* = 5.6, 3.7 Hz, polyether H), 3.69 (4H, s, polyether H), 1.91 (6H, s, $TeCH_3$). **^{13}C-NMR** (126 MHz, $CDCl_3$) δ 153.8, 152.2, 150.3, 148.9, 134.2, 127.5, 115.9, 115.6, 103.3, 71.0, 69.8, 68.3, 68.0, 50.6, 31.7, 22.8, 14.3, -12.3.**^{125}Te-NMR** (158 MHz, $CDCl_3$) δ 116.6. **MS** (ESI +ve) *m/z* 884.09743 ($[M]^+$, $C_{33}H_{38}N_7O_6Te_2$, calc. 886.09849).

Compound 2.24$_{Te}$

***Note**: handle with care in fume cupboard due to malodourous nature of Te-containing volatiles formed in this reaction. All glassware in contact with the reaction products were deodorized by soaking in bleach for at least 6 hours.*

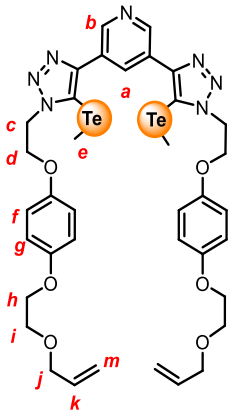

Powdered Te (200 mg, 0.22 mmol) was suspended in dry degassed THF (just sufficient to submerge the Te) and chilled in an ice bath to 0 °C in a microwave vial. To the chilled vigorously-stirred suspension was added 1.6 M methyllithium solution in diethyl ether (0.83 mL, 1.33 mmol), and the reaction was sonicated and warmed up to ambient temperature before being left to stir at 1 hour in the dark to yield a brown suspension. Separately, bis-iodotriazole **2.24$_{I}$** (197.0 mg, 11.55 mmol) was suspended in dry THF (minimal) and added portionwise to the brown suspension at ambient temperature, and the reaction vessel was sealed. The vigorously-stirred reaction was heated at 75 °C in the dark for 4 hours to afford a dark brown suspension. After cooling back to room temperature, iodomethane (0.055 mL, 0.88 mmol) was added to the suspension which was stirred for a further 30 minutes. Subsequently, the reaction was poured into water (20 mL) and the organics were extracted into chloroform (3 x 10 mL). The combined organics were dried with $MgSO_4$ and the solvent was removed *in vacuo* to afford the crude product as a brown malodourous solid. Purification by silica gel column chromatography (eluent: 5% methanol in dichloromethane/ethyl acetate 7:3 *v/v*) afforded the target compound as a yellow solid. **Yield:** 143 mg, 64 %. No materials were left for characterisation but successful synthesis of cationic compound 2.15Te shows that this material was indeed synthesised correctly.

Compound 2.15$_{Te}$

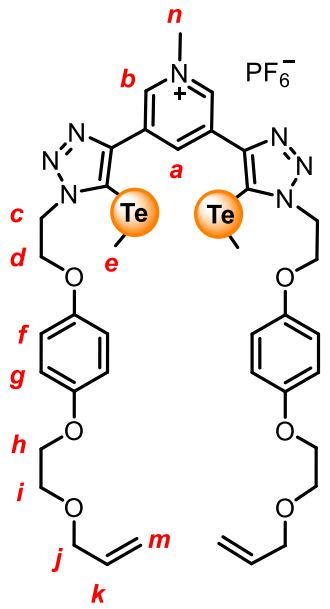

Tellurotriazole-(bis)alkene **2.24$_{Te}$** (143 mg, 0.153 mmol) was dissolved in dry dichloromethane (1.0 mL) and iodomethane (0.1 mL) was added dropwise. The reaction was left to stir at room temperature for 16 hours. Solvent was removed *in vacuo* and solids re-dissolved in chloroform (20 mL). The organic layer was washed repeatedly with 0.1 M NH_4PF_6 (10 × 10 mL) and water (2 × 10 mL), dried over $MgSO_4$ and filtered. Solvent was removed in vacuo to afford the product as a pale-yellow solid. **Yield:** 136 mg, 82 %. **^{1}H-NMR** (500 MHz, Chloroform-*d*) δ 9.86 (1H, d, *J* = 1.7 Hz, H_b), 9.31 (2H, d, *J* = 1.6 Hz, H_a), 6.83 – 6.77 (4H, m, $H_{f/g}$), 6.77 – 6.70 (4H, m, $H_{f/g}$), 5.91 (2H, ddt, *J* = 17.4, 10.4, 5.7 Hz, H_k), 5.28 (2H, dt, *J* = 17.3, 1.7 Hz, H_m), 5.18 (2H, dt, *J* = 10.4, 1.5 Hz, H_m), 4.99 (4H, t, *J* = 5.2 Hz, H_c), 4.54 (3H,s, H_n), 4.39 (4H,t, *J* = 5.2 Hz, H_d), 4.08 – 4.00 (9H,m, $H_{h/i}$), 3.77 – 3.69 (4H,m, H_j), 2.06 (6H, s, -$TeCH_3$). **^{13}C-NMR** (126 MHz, Chloroform-*d*) δ 153.78, 152.14, 145.64, 141.58, 138.91, 134.68, 133.08, 117.50, 115.82, 115.67, 104.55, 72.46, 68.69, 68.16, 67.42, 50.90, 49.82, -11.20. **^{125}Te-NMR** (95 MHz, Chloroform-*d*) δ 137.47. **^{31}P-NMR** (162 MHz, CDCl3) δ -131.56, -135.96, -140.36, -144.77, -149.17, -153.58, -153.60, -157.99. **^{19}F-NMR** (376 MHz, CDCl3) δ -71.74, -73.64.

6.4. Syntheses from Chapter 3

The synthesis of compounds **3.17-3.20**[231], **3.25-3.28**[227], **3.29-3.30**[292], **3.37**[232] have been previously described. Compound **3.38$_{S/R}$** was adapted from previously synthesised compound in which the manuscript is currently being prepared by Dr. Valentine Bunchuay.

Compound 3.6$_S$ and 3.6$_R$

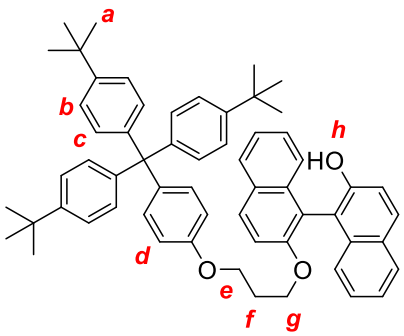

Stopper bromide 3.4[234] (1.13 g, 1.81 mmol), (*S*)-BINOL (0.5847 g, 2.04 mmol) KI (441 mg, 6.68 mmol) and K_2CO_3 (154 mg, 4.01 mmol) were dissolved in acetone (15 mL). Solution was heated at reflux and stirred overnight. Solvent was evaporated and solids redissolved in chloroform (50 mL). The organic layer was washed with water (3 × 20 mL), brine (1 × 20 mL) then dried over $MgSO_4$. The filtrate was filtered and solvent evaporated in vacuo. The crude mixture was purified by column chromatography (8:2 Hexane/Ethyl Acetate) to yield a white solid. Yield: 1.21 g, 81%. ^{1}H-NMR (500 MHz, Chloroform-*d*) δ 8.02 (1H, d, *J* = 9.0 Hz, H_{BINOL}), 7.88 (1H, d, *J* = 8.2 Hz, H_{BINOL}), 7.71 (1H,d, *J* = 8.9 Hz, H_{BINOL}), 7.68 – 7.63 (1H, d, *J* = 8.9 Hz, H_{BINOL}) , 7.46 (1H,d, *J* = 9.0 Hz, H_{BINOL}), 7.36 (1H,ddd, *J* = 8.1, 6.7, 1.2 Hz, H_{BINOL}), 7.30 – 7.16 (8H, m, Hc), 7.14 – 7.08 (6H, m, Hb), 7.06 – 6.96 (4H,m, H_{BINOL}), 6.38 – 6.31 (2H,m, H_d), 4.84 (1H, s, -OH), 4.20 (1H,dt, *J* = 9.4, 5.5 Hz, $H_{e/g}$), 3.50 (2H, ddt, *J* = 7.8, 9.6, 6.3 Hz, $H_{e/g}$), 1.95 – 1.86 (2H,m, H_f), 1.31 (27H, s, H_a). ^{13}C-NMR (126 MHz, $CDCl_3$) δ 156.49, 155.30, 151.30, 148.45, 144.39, 139.50, 134.11, 133.81, 132.22, 131.11, 130.90, 129.89, 129.72, 129.13, 128.31, 128.19, 127.44, 126.58, 125.09, 124.79, 124.43, 124.19, 123.36, 117.52, 116.38, 115.29, 115.13, 113.00, 66.07, 63.87, 63.19, 34.46, 31.56, 29.26. MS (ESI -ve) *m/z* 829.46281 ([M-H$^+$] $C_{60}H_{61}O_3$, calc. 829.46262)

Stopper 3.6$_R$ was prepared using the same synthetic steps with identical characterisation (2.30 g, 58 %).

Compound 3.13S and 3.13R

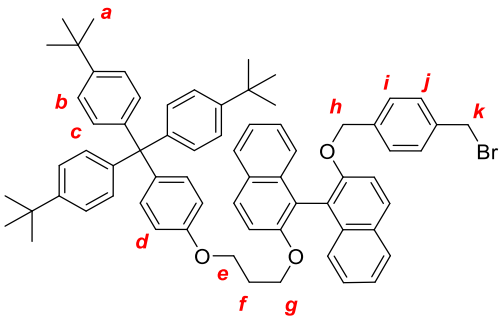

Stopper-(*S*)-BINOL **3.6S** (1.2 g, 0.001 mol), dibromoxylene (4.1123 g, 0.016 mols) and K_2CO_3 (0.4348 g, 0.003 mols) were suspended in acetone. The reaction mixture was refluxed overnight. Solvent was evaporated and solids redissolved in dichloromethane (20 mL). The organic layer was washed with water (3 × 10 mL), brine (1 × 10 mL) then dried over $MgSO_4$. The filtrate was filtered and the solvent evaporated in vacuo. The crude mixture was purified by column chromatography (6:4 Hexane/Dichloromethane) to yield a white solid. **Yield:** 1.3 g, 90 %. **^{1}H-NMR** (400 MHz, $CDCl_3$) δ 7.96 (1H, d, *J* = 9.0 Hz, H_{BINOL}), 7.88 (1H, d, *J* = 8.2 Hz, H_{BINOL}), 7.68 (2H, dd, *J* = 8.0, 8.4 Hz, H_{BINOL}), 7.44 (1H, d, *J* = 9.0 Hz, H_{BINOL}), 7.32 (1H, t, *J* = 7.4 Hz, H_{BINOL}), 7.26 – 7.17 (12H, m, H_b + H_{BINOL}), 7.17 – 7.12 (12H, m, H_c + H_{BINOL}), 6.97 (2H, d, *J* = 8.6 Hz, $H_{j/i}$), 6.80 (2H, d, *J* = 7.9 Hz, $H_{j/i}$), 6.28 (2H, d, *J* = 8.6 Hz, H_d), 4.89 (2H,s, H_h), 4.34 (2H, s, H_k), 4.17 – 4.06 (2H, m, $H_{e/g}$), 3.39 (2H, t, *J* = 6.4 Hz, $H_{e/g}$), 1.85 (2H,d, *J* = 6.4 Hz, H_f), 1.31 (27H, s, H_a). **^{13}C NMR** (101 MHz, $CDCl_3$) δ 156.52, 154.21, 153.91, 148.46, 144.43, 139.40, 138.04, 136.81, 134.24, 134.17, 132.16, 130.90, 129.53, 129.50, 129.41, 128.92, 128.05, 127.99, 127.19, 126.52, 126.46, 125.55, 125.41, 124.21, 123.95, 123.79, 120.98, 120.47, 116.03, 115.44, 113.00, 70.87, 65.96, 63.98, 63.21, 34.46, 33.41, 31.56, 29.36, 27.06. **MS** (ESI +ve) *m/z* 1037.43153 ($[M+Na]^+$, $C_{68}H_{69}BrO_3$ calc. 1037.43018)

Compound **3.13R** was synthesised following the same procedure with Stopper **3.22R** as the starting material. **Yield**: 2 g, 74%. **^{1}H-NMR** (400 MHz, $CDCl_3$) δ 7.96 (1H, d, *J* = 9.01 Hz, H_{BINOL}), 7.88 (1H, d, *J* = 8.27 Hz, H_{BINOL}), 7.68 (2H, dd, *J* = 18.29, 8.52 Hz, H_{BINOL}), 7.44 (1H, d, *J* = 9.41 Hz, H_{BINOL}), 7.36 – 7.20 (16H, m, H_b + H_{BINOL}), 7.11 (12H, q, *J* = 12.50, 10.75 Hz, H_c + H_{BINOL}), 6.97 (2H, d, *J* = 8.43 Hz, $H_{j/i}$), 6.80 (2H, d, *J* = 7.43 Hz, $H_{j/i}$), 6.28 (2H, d, *J* = 8.22 Hz, H_d), 4.89 (2H, s, H_h), 4.34 (2H, s, H_k), 4.21 – 4.04 (2H, m, $H_{e/g}$), 3.39 (2H, t, *J* = 6.52 Hz, $H_{e/g}$), 1.85 (2H, s, H_f), 1.31 (27H, d, *J* = 2.09 Hz, H_a). **^{13}C NMR** (101 MHz, $CDCl_3$) δ 156.51, 154.21, 153.90, 148.45, 144.42, 139.39, 138.03, 136.80, 134.23, 134.15, 132.15, 130.89, 129.53, 129.49, 129.40, 128.92, 128.04, 127.99, 127.18, 126.52, 126.46, 125.54, 125.40, 124.21, 123.94, 123.78, 120.96, 120.46, 116.02, 115.43, 112.99, 70.85, 65.95, 63.97, 63.20, 34.46, 33.42, 31.56, 29.35, 24.96. **MS** (ESI +ve) *m/z* 1053.4 ($[M+K]^+$ $C_{68}H_{69}BrO_3$ calc. 1053.40)

Compound 3.14$_S$ and 3.14$_R$

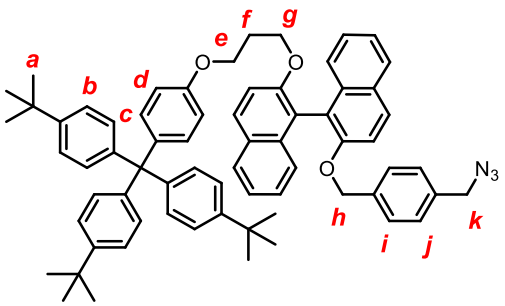

Compound **3.14$_s$** (1.3 g, 1.31 mmol) was dissolved in minimal DMSO (50 ml) and NaN_3 (0.26 g, 3.9 mmol) was added portionwise. Reaction was stirred at room temperature overnight. To the reaction mixture, water (100 ml) was added and the aqueous layer was extracted with ethyl acetate (3 × 50 mL) then dried over $MgSO_4$. The filtrate was filtered, and solvent evaporated in vacuo to give a clear oil. **Yield:** 209 mg, 88%. **^{1}H-NMR** (400 MHz, $CDCl_3$) δ 7.97 (1H, d, *J* = 8.99 Hz, H_{BINOL}), 7.88 (1H, d, *J* = 8.19 Hz, H_{BINOL}), 7.71 (1H, d, *J* = 9.01 Hz, H_{BINOL}), 7.68 – 7.63 (1H, m, H_{BINOL}), 7.45 (1H, d, *J* = 9.01 Hz, H_{BINOL}), 7.33 (1H, ddd, *J* = 8.03, 6.52, 1.34 Hz, H_{BINOL}), 7.29 – 7.17 (8H, m, H_b + H_{BINOL}), 7.14 (10H, dd, J = 11.5, 7.1 Hz, H_c + H_{BINOL}), 7.05 – 6.89 (4H, m, $H_{j/l}$ + H_{BINOL}), 6.86 (2H, d, *J* = 7.82 Hz, $H_{j/i}$), 6.34 – 6.26 (2H, m, H_d), 4.89 (2H, s, H_h), 4.19 (2H, s, H_k), 4.13– 4.06 (2H, m, $H_{e/g}$), 3.41 (2H, t, *J* = 6.45 Hz, $H_{e/g}$), 1.85 (2H, br, H_f), 1.32 (27H, s, H_a). **^{13}C NMR** (101 MHz, $CDCl_3$) δ 156.52, 154.22, 153.94, 148.46, 144.42, 139.41, 137.85, 134.44, 134.24, 134.16, 132.15, 130.89, 129.53, 129.50, 129.40, 128.07, 128.04, 127.99, 127.26, 126.51, 126.45, 125.56, 125.41, 124.20, 123.94, 123.77, 121.00, 120.47, 116.10, 115.44, 112.99, 77.48, 77.16, 76.84, 70.94, 65.97, 63.99, 63.20, 54.60, 41.14, 34.45, 31.55, 29.35. **MS** (ESI +ve) *m/z* 998.52345 ($[M+Na]^+$, $C_{68}H_{69}O_3N_3Na$ calc. 998.52311). **Optical rotation** *S*-isomer $[\alpha]_D^{25} = -21.6°$ (c 0.01, dichloromethane),

Stopper **3.29$_R$** was prepared using the same synthetic steps. **Yield**: 1.8 g, 94%. **^{1}H-NMR** (400 MHz, Chloroform-d) δ 7.93 (1H, d, *J* = 8.9 Hz, H_{BINOL}), 7.85 (1H, d, *J* = 8.2 Hz, H_{BINOL}), 7.68 (2H, dd, *J* = 7.1, 8.48 Hz, H_{BINOL}), 7.41 (1H, d, *J* = 9.1 Hz, H_{BINOL}), 7.34 – 7.19 (8H, m, H_c + H_{BINOL}), 7.14 (6H, s, H_b + H_{BINOL}), 7.12 – 7.05 (1H, m, H_{BINOL}), 7.00 (4H, t, *J* = 8.0 Hz, $H_{i/j}$ + H_{BINOL}), 6.84 (2H, d, *J* = 7.8 Hz, $H_{i/j}$), 6.34 – 6.27 (2H, m, H_d), 4.89 (2H, s, H_h), 4.16 – 4.03 (4H, m, H_h and $H_{e/g}$), 3.40 (2H,t, *J* = 6.4 Hz, $H_{e/g}$), 1.83 (2H, q, *J* = 5.6 Hz, H_f), 1.32 (27H, s, H_a). **^{13}C NMR** (101 MHz, $CDCl_3$) δ 156.5, 154.2, 153.9, 148.4, 144.4, 139.4, 137.8, 134.4, 134.2, 134.1, 132.1, 130.9, 129.8, 129.5, 129.4, 129.4, 129.2, 128.6, 128.5, 128.4, 128.2, 128.0, 128.0, 127.2, 126.5, 126.4, 125.5, 125.4, 124.2, 123.9, 123.7, 120.9, 120.4, 116.0, 115.3, 113.0, 77.5, 77.2, 76.8, 70.8, 65.9, 63.9, 63.2, 54.5, 41.0, 34.4, 31.5, 29.3, 24.9, 1.2.

MS (ESI +ve) *m/z* 998.52334 ($[M+Na]^+$, $C_{68}H_{69}O_3N_3Na$ calc. 998.52311). **Optical rotation** *R*-isomer $[\alpha]_D^{25} = 25.7°$ (c 0.01, dichloromethane)

Neutral axle 3.15S and 3.15R

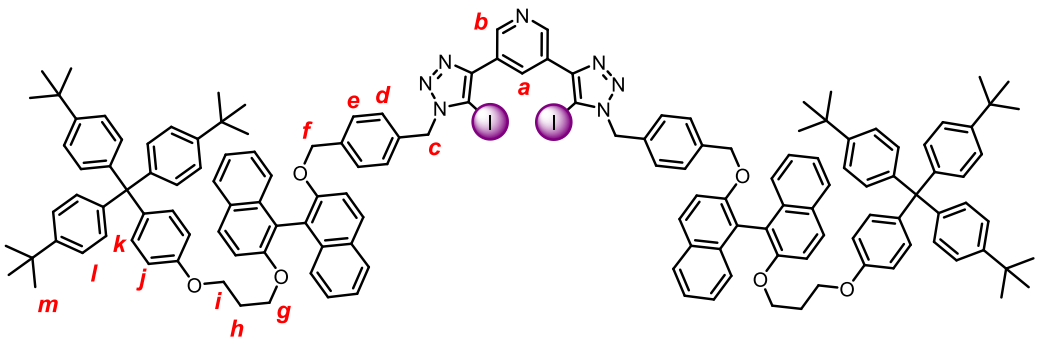

NaI (99 mg, 0.66 mmols) was suspended in dry degassed THF (1 mL), $Cu(ClO_4)\cdot 6H_2O$ (0.12 g, 0.33 mmols) was added and stirred for 5 mins. Then, stopper **3.14S** (0.17 g, 0.17 mmols), TBTA (2.2 mg, 4.12×10^{-3} mmols), DBU (24.7 uL, 0.165 mmols) then alkyne (11 mg, 8.24×10^{-5} mmols) were added sequentially. The reaction was then topped up with dry degassed acetonitrile (1 mL) and stirred in the dark for 5 days. The reaction was monitored via mass spectrometry for completion. Organic solvents were removed in vacuo and redissolved in chloroform. The organic layer was then washed with basic EDTA until all copper was removed. The organic layer was subsequently washed with bring and dried over $MgSO_4$ and solvent removed. The crude product was purified via column chromatography (SiO_2, DCM) to yield a dark yellow solid. **Yield:** 143 mg, 58%. **^{1}H-NMR** (500 MHz, $CDCl_3$) δ 9.22 (d, *J* = 2.1 Hz, 2H, Hb), 8.82 (t, *J* = 2.1 Hz, 1H, Ha), 7.95 (d, *J* = 8.9 Hz, 2H, H_{BINOL}), 7.86 (2H, d, *J* = 8.1 Hz, H_{BINOL}), 7.74 – 7.63 (m, 4H, H_{BINOL}), 7.43 (d, *J* = 8.98 Hz, 2H, H_{BINOL}), 7.34 – 7.08 (40H, m, H_{BINOL}+ $H_{stopper}$), 7.04 (4H,d, *J* = 7.9 Hz, H_{BINOL}), 7.01 – 6.95 (4H, m, H_c), 6.84 (4H,d, *J* = 7.9 Hz, H_d), 6.31 – 6.25 (4H, m, H_j), 5.54 (4H, s, H_f), 4.89 (4H, s, H_c), 4.11 (4H, dddd, *J* = 7.3, 9.1, 6.3, 4.8 Hz, H_g^1 + H_g^2), 3.39 (4H,t, *J* = 6.44 Hz, H_i), 1.89 – 1.81 (4H, m, H_h), 1.31 (54H,s, H_m).**^{13}C-NMR** (126 MHz, $CDCl_3$) δ 156.5, 154.2, 153.9, 148.5, 148.1, 147.4, 144.4, 139.4, 138.3, 134.2, 134.1, 133.0, 132.9, 132.2, 130.9, 129.6, 129.5, 129.5, 129.4, 128.1, 128.0, 127.8, 127.4, 126.5, 126.4, 126.3, 125.5, 125.4, 124.2, 124.0, 123.8, 121.1, 120.4, 116.1, 115.4, 113.0, 70.9, 65.9, 64.0, 63.2, 54.4, 53.6, 34.5, 31.6, 29.3. **MS** (ESI +ve) *not carried out but should be similar to* 3.15_R.

Axle 3.15_R was prepared using the same synthetic steps. **Yield:** 0.12 g, 63 %. **^{1}H-NMR** (500 MHz, $CDCl_3$) δ 9.23 (2H, d, *J* = 2.1 Hz), 8.82 (1H, t, *J* = 2.1 Hz), 7.95 (3H, d, *J* = 8.9 Hz), 7.86 (2H, d, *J* = 8.1 Hz), 7.71 (3H, d, *J* = 9.0 Hz), 7.68 – 7.63 (3H, m), 7.43 (3H, d, *J* = 9.0 Hz), 7.34 – 7.19 (24H, m), 7.19

– 7.06 (27H, m), 7.06 – 6.95 (10H, m), 6.84 (5H, d, *J* = 7.90 Hz), 6.31 – 6.25 (5H, m), 5.53 (4H, s), 4.89 (s, 4H), 4.11 (5H, dddd, *J* = 7.3, 9.1, 6.2, 4.7 Hz), 3.39 (4H, t, *J* = 6.43 Hz), 1.90 – 1.80 (5H, m), 1.31 (57H, s). **^{13}C-NMR** (126 MHz, $CDCl_3$) δ 156.5, 154.2, 153.9, 148.5, 148.1, 147.4, 144.4, 139.4, 138.3, 134.2, 134.1, 133.0, 132.9, 132.1, 130.9, 129.6, 129.5, 129.5, 129.4, 128.1, 128.0, 127.8, 127.4, 126.5, 126.4, 126.3, 125.5, 125.4, 124.2, 124.0, 123.8, 121.0, 120.4, 116.1, 115.4, 113.0, 76.9, 70.9, 65.9, 64.0, 63.2, 54.4, 53.6, 34.5, 31.6, 29.3. **MS** (ESI +ve) *m/z* 2331.92004 ($[M+H]^+$, $C_{145}H_{142}O_6N_7I_2$ calc. 2331.91390).

Cationic axle 3.16$_S$ and 3.16$_R$

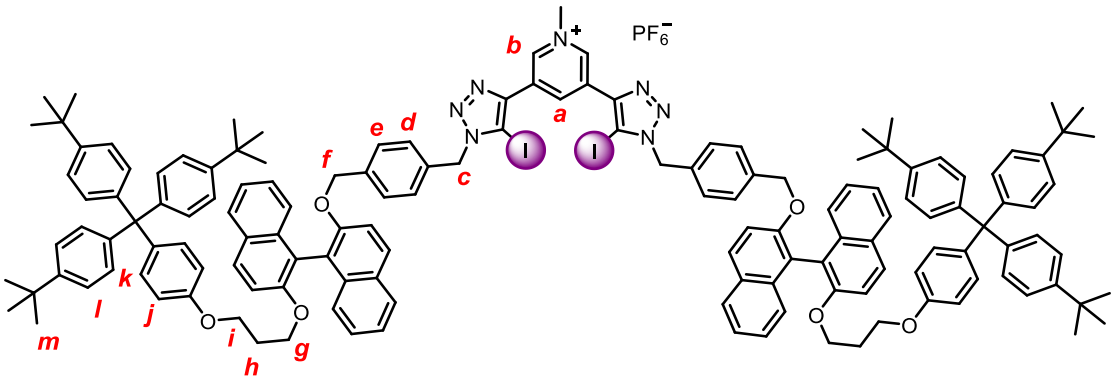

Neutral axle 3.16$_S$ (60 mg, 2.5×10^{-5} mols) was dissolved in dry dichloromethane (0.9 mL) and iodomethane (0.1 mL) was added dropwise. The reaction was monitored *via* TLC and MS. Upon completion, reaction was diluted by dichloromethane (10 mL) and the organic layer washed with 0.1 M NH_4PF_6 (3 × 10 mL), brine (3 × 10 mL) dried over $MgSO_4$ and evaporated in vacuo. **Yield:** 53 mg, 83%. **^{1}H-NMR** (400 MHz, Chloroform-*d*) δ 9.52 (1H,s, H_a), 8.92 (2H,s, H_b), 7.88 (2H, d, *J* = 8.7 Hz, H_{BINOL}), 7.78 (2H, d, *J* = 8.1 Hz, H_{BINOL}), 7.70 (2H, d, *J* = 8.9 Hz, H_{BINOL}), 7.63 (2H, d, *J* = 8.0 Hz, H_{BINOL}), 7.40 (2H, d, *J* = 9.0 Hz, H_{BINOL}), 7.32 – 7.17 (20H, m, H_{BINOL}+ $H_{stopper}$), 7.14 – 7.04 (22H, m, H_{BINOL}+ $H_{stopper}$), 6.98 (4H, dd, *J* = 8.0, 8.3 Hz, He + H_{BINOL}), 6.86 (4H, d, *J* = 7.8 Hz, Hd), 6.24 (2H, d, *J* = 8.7 Hz, H_j), 5.44 (4H, s, H_C), 4.88 (s, 4H, H_f), 4.13 (3H, s, N-CH_3), 4.07 (4H, ddd, J = 15.2, 11.7, 5.37 Hz, H_g), 3.35 (4H, t, *J* = 6.42 Hz, H_i), 1.85 – 1.77 (4H, m, H_h), 1.30 (54H, d, *J* = 2.13 Hz, H_m). **^{13}C-NMR** (126 MHz, $CDCl_3$) δ 156.5, 154.2, 153.9, 148.5, 144.4, 142.8, 140.9, 139.4, 138.5, 134.2, 134.1, 132.5, 132.2, 130.9, 129.6, 129.6, 129.5, 129.4, 128.4, 128.1, 128.0, 127.8, 126.6, 126.5, 125.5, 125.4, 124.2, 124.1, 123.8, 120.9, 120.3, 115.9, 115.4, 113.0, 70.9, 65.9, 64.0, 63.2, 54.6, 49.8, 34.5, 31.6, 29.3. **^{19}F-NMR** (376 MHz, $CDCl_3$) δ -71.3, -73.2. **^{31}P-NMR** (162 MHz, $CDCl_3$) δ -135.8, -140.2, -144.6, -149.0, -153.4 **MS** (ESI +ve) *m/z* 2345.9232 ($[M+H]^+$, $C_{146}H_{144}N_7O_6I_2$, calc. 2346.92955).

Compound 3.21

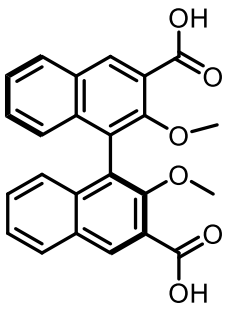

Compound **3.2** (500 mg, 1.59 mmol) and TMEDA (0.6 mL, 3.97 mmol) were suspended in dry diethyl ether (16 mL, 0.1M) and chilled to 0°C. 0.1M solution of *n*-BuLi in hexanes (2.5 mL, 3.97 mmol) were added dropwise to the reaction. The reaction was then allowed to warm to room temperature and stirred for 1 hour before heating to reflux for another 4 hours. After which, the reaction was allowed to cool to room temperature and dry ice (3 pellets) was added as solid and the reaction mixture was left to stir overnight at room temperature. The reaction was quenched with water (25 mL) and extracted with toluene (25 mL). The layers were separated and the aqueous layer acidified with 1M HCl solution and extracted with EtOAc (3 × 20 mL). The combined EtOAc layer was dried over $MgSO_4$ and solvent evaporated in vacuo to afford pure compound **3.6. Yield:** 409 mg, 61%. **^{1}H-NMR** (400 MHz, Chloroform-d) δ 8.92 (2H, d, *J* = 2.7 Hz, H_{BINOL}), 8.07 (2H, d, *J* = 8.2 Hz, H_{BINOL}), 7.58 – 7.49 (2H, m, H_{BINOL}), 7.48 – 7.39 (2H, m, H_{BINOL}), 7.17 (2H, d, *J* = 8.5 Hz, H_{BINOL}), 3.47 (6H, q, *J* = 1.5 Hz, O-CH_3). **^{13}C-NMR** (101 MHz, $CDCl_3$) δ 168.18, 154.29, 154.21, 136.35, 136.30, 136.20, 130.10, 130.06, 129.94, 129.88, 129.51, 129.29, 128.30, 128.03, 126.57, 126.52, 126.40, 125.51, 125.36, 125.11, 124.95, 123.61, 122.01, 114.38, 62.71, 62.68, 57.03. *Due to nature of aromaticity, many ^{13}C signals overlap. **MS** (ESI +ve) *m/z* 403.11773 ($[M+H]^+$ $C_{24}H_{19}O_6$, calc. 403.11761)

Cationic [2]rotaxane 3.32s

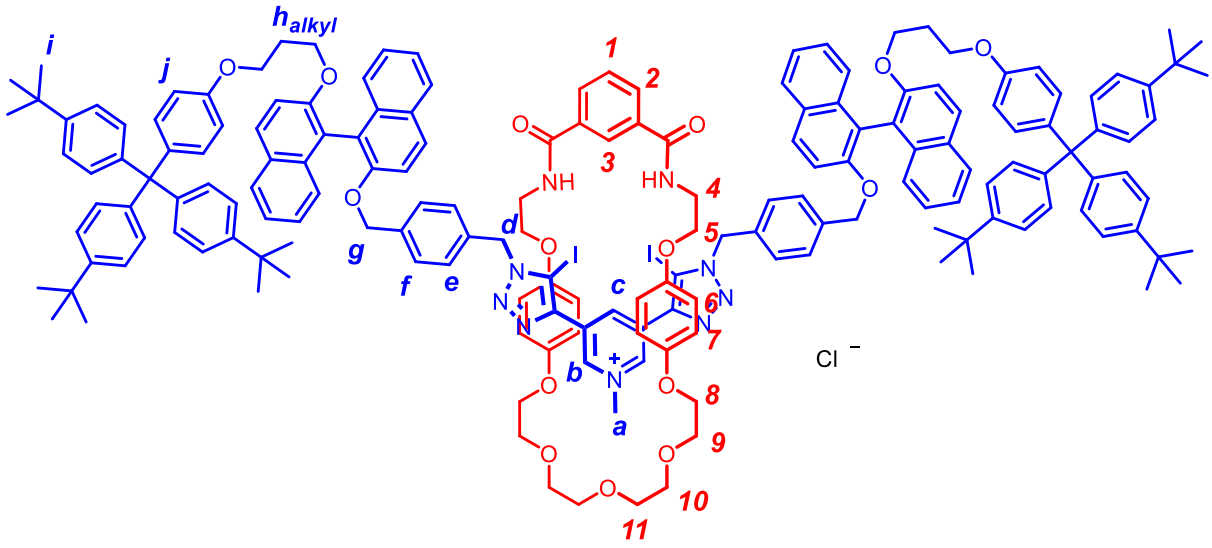

[2]rotaxane 3.32$_S$•Cl$^-$

Axle **3.16$_S$·Cl** (23 mg, 9.53 µmols) was dissolved in dichloromethane and macrocycle precursor **2.15** (4.4 mg, 9.53 µmols) was added to the reaction and stirred for 15 minutes. Subsequently, triethylamine (4.0 µL, 28.6 µmols) and acid chloride **2.13** (1.9 mg, 9.53 µmols) were added and the reaction mixture was stirred overnight under N_2 at room temperature. Purification of the crude reaction on preparatory thin layer chromatography (gradient eluent 3-4 % MeOH/DCM) afforded [2]rotaxane **3.32$_S$. Yield:** 1.1 mg, 4 %. **^{1}H-NMR** (500 MHz, Methanol-d$_4$) δ 9.43 (2H, s, H$_b$), 8.87 (1H, s, H$_c$), 8.02 (2H, dd, J = 7.8, 1.7 Hz, H$_2$), 7.97 (1H, s, H$_3$), 7.74 (2H, d, J = 9.0 Hz, H$_{BINOL}$), 7.69 (2H, d, *J* = 8.1 Hz, H$_{BINOL}$), 7.58 (2H, d, *J* = 9.0 Hz, H$_{BINOL}$), 7.52 (2H, d, J = 8.0 Hz, H$_{BINOL}$), 7.37 (1H, t, *J* = 7.8 Hz, H1), 7.30 – 7.16 (15H, m, H$_{stopper}$ + H$_{BINOL}$), 7.14 – 7.06 (12H,m, H$_{stopper}$ + H$_{BINOL}$), 7.06 – 6.95 (10H, m, H$_{stopper}$ + H$_{BINOL}$), 6.95 – 6.90 (4H, m, H$_f$), 6.87 (4H, d, *J* = 8.0Hz, H$_e$), 6.21 – 6.15 (4H, m, H$_j$), 5.86 – 5.80 (4H, m, H$_5$), 5.62 (4H, d, *J* = 8.9 Hz, H$_4$), 5.31 (4H, s, H$_d$), 4.89 (4H, s, H$_g$), 4.22 (2H, s, H$_{alkyl}$), 3.98 (4H, tt, *J* = 10.8, 5.6 Hz, H$_{alkyl}$), 3.89 – 3.84 (4H, m, H$_{8-11}$), 3.74 (4H, s, H$_{8-11}$), 3.66 (4H, s, H$_{8-11}$), 3.56 (4H, q, *J* = 5.6 Hz, H$_{8-11}$), 3.28 (d, *J* = 6.4 Hz, 6H, H$_{alkyl}$), 3.24 (2H, s), 1.27 (54H, s, H$_i$). **^{13}C-NMR** insufficient amounts were obtained to run a ^{13}C NMR. **MS** (ESI +ve) *m/z* 2941.18871 [M]$^+$, calc. 2940.18729

Receptor 3.40$_S$ and 3.40$_R$

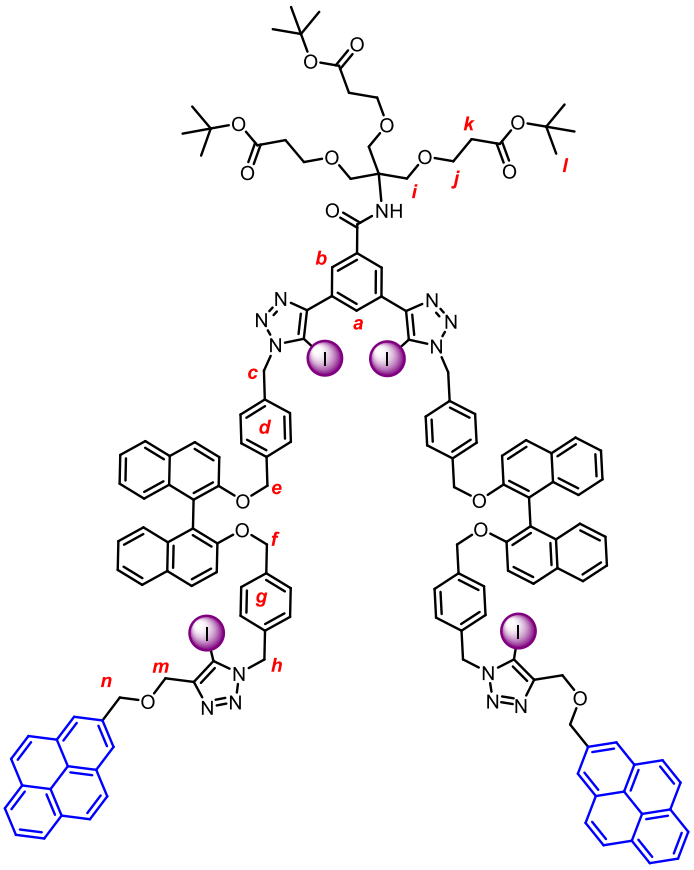

NaI (233 mg, mmol) was suspended in dry degassed THF (12 mL). $Cu(ClO_4)\cdot 6H_2O$ (28.8 mg, mmol) was added to the suspension and stirred for 5 mins. Then bis-azide **3.38** (40 mg, mmol), TBTA (0.5 mg, mmol), DBU (5.8 µL, mmol) and alkyne (11 mg, mmol) was added in that order. The reaction was topped up with dry degassed acetonitrile (12 mL) to make the total solvent volume to be 0.08 M based on the azide. Reaction was stirred over 2 days. Purification by preparatory TLC (2-3% Methanol in DCM gradient eluent) to give desired product. **Yield:** 21 mg, 34%. **^{1}H-NMR** (500 MHz, Chloroform-*d*) δ 8.62 (1H, t, *J* = 1.63 Hz, H_a), 8.38 (2H,d, *J* = 1.69 Hz, H_b), 8.29 (2H, d, *J* = 9.2 Hz, H_{pyrene}), 8.19 – 7.75 (25H, m, H_{pyrene} + H_{BINOL}), 7.37 – 7.24 (10H, m, H_{BINOL}), 7.23 – 7.11 (8H, m, H_{BINOL}), 6.95 (8H, dd, *J* = 8.2, 1.7 Hz, $H_{d/g}$), 6.83 (8H, d, *J* = 8.0 Hz, $H_{d/g}$), 6.68 (1H, s, -NH), 5.44 (8H, d, *J* = 8.2 Hz, H_e), 5.25 (4H, s, H_m), 4.93 (8H, d, *J* = 11.7 Hz, H_c^1 + H_c^2), 4.69 (4H, s, H_n), 3.85 (6H, s, H_i), 3.68 (6H, t, *J* = 6.3 Hz, H_j), 2.44 (6H, t, *J* = 6.3 Hz, H_k), 1.36 (27H, s, H_l). **^{13}C-NMR** (126 MHz, $CDCl_3$) δ 170.97, 167.02, 154.02, 149.15, 148.92, 138.09, 138.03, 136.45, 134.22, 133.32, 133.24, 131.51, 131.32, 131.16, 130.94, 130.91, 129.64, 129.60, 129.58, 129.54, 129.52, 128.78, 128.07, 128.05, 127.87, 127.75, 127.58, 127.55, 127.54, 127.20, 126.51, 126.49, 126.05, 126.02, 125.59, 125.57, 125.35, 125.33, 125.03, 124.79, 124.62, 123.96, 123.93, 123.76, 120.83, 120.80, 115.99, 115.96, 80.99,

80.59, 76.91, 70.98, 70.82, 70.79, 69.31, 67.29, 63.41, 60.47, 54.12, 54.05, 36.41, 28.18. **MS** (ESI +ve) *m/z* 2855.60579 ($[M]^+$, $C_{148}H_{132}N_{13}O_{16}I_4$, calc. 2855.61218).

Compound **3.45$_R$** was synthesised following the same procedure with the same characterisations. **Yield:** 47 mg, 34%

Receptor 3.41$_S$ and 3.41$_R$

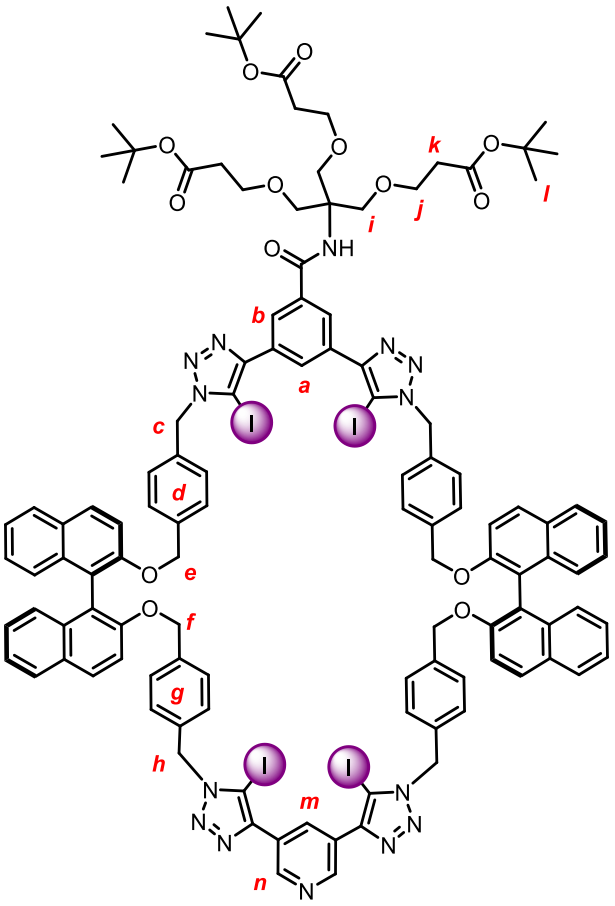

$Cu(MeCN)_4PF_6$ (5 mg, 1.4×10^{-5} mols) and TBTA (7.2 mg, 1.4×10^{-5} mols) were dissolved in dry degassed THF (5 mM) and stirred for 10 mins. Bis-azide (70 mg, 3.4×10^{-5} mols) was dissolved in THF (1 mL) and added to the copper-complex solution. Iodoalkyne was dissolved in THF (0.8 mL) was added by syringe pump over 12 hours and reaction was left to stir over 3 days. Solvent was evaporated and redissolved in $CHCl_3$ (10 mL) and the organic layer was washed with basic EDTA (3 × 20 mL) and brine (10 mL), dried over MgSO4 and solvent removed in vacuo. The resulting crude material was purified by prep TLC (5% MeOH in DCM) to afford a white power (15 mg, 16%). **^{1}H-NMR** (500 MHz, Chloroform-*d*) δ 9.24 (2H, d, *J* = 2.1 Hz, H_n), 8.84 (2H, dt, *J* = 6.2, 1.9 Hz, H_m + H_a), 8.46 (2H,d, *J* = 1.7 Hz, H_b), 7.90 (4H,dd, *J* = 9.0, 2.7 Hz, H_{BINOL}), 7.85 (4H, d, *J* = 8.1 Hz, H_{BINOL}), 7.32 (8H, ddd, *J* = 9.1, 6.8, 2.2 Hz, H_{BINOL}), 7.25 – 7.13 (8H,m, H_{BINOL}), 7.03 – 6.91 (12H,m, H_{BINOL} + $H_{g/d}$),

6.88 (d, *J* = 8.1 Hz, 4H, H_{BINOL}+ $H_{g/d}$), 6.74 (1H, s, NH), 5.64 (6H d, *J* = 15.2 Hz), 5.53 (d, *J* = 15.4 Hz, 2H), 5.09 (2H, d, *J* = 13.5 Hz), 5.06 – 4.96 (4H, m), 4.91 (2H, d, *J* = 13.2 Hz), 3.90 – 3.81 (6H, m, H_i), 3.68 (6H, t, *J* = 6.3 Hz, H_j), 2.43 (6H, t, *J* = 6.3 Hz, H_k), 1.36 (27H, s, H_l). **^{13}C-NMR** (126 MHz, $CDCl_3$) δ 171.04, 167.05, 153.94, 153.81, 148.94, 148.29, 147.33, 138.28, 138.05, 136.32, 134.28, 133.50, 133.11, 131.82, 131.12, 129.51, 129.48, 129.47, 129.15, 128.25, 128.09, 128.07, 127.73, 127.11, 127.07, 126.60, 126.55, 126.27, 125.84, 125.50, 125.46, 123.95, 123.90, 120.56, 120.53, 115.72, 115.61, 80.68, 79.99, 76.91, 70.47, 70.27, 69.31, 67.30, 60.46, 54.28, 54.25, 36.44, 28.18. **MS** (ESI +ve) *m/z* 2442.44643 ($[M+H]^+$, $C_{117}H_{109}N_{14}O_{14}I_4$, calc. 2442.44545).

Compound **3.44_R** was synthesised following the same procedure with similar characterisations. **Yield:** 13 mg, 16%.

6.5. Syntheses from Chapter 4

Compound **4.13**$_{Br}$[293] and Compound **4.14**$_{Br}$[294] were adapted from literature procedures. Stoppers alkyne **2.29** and azide **2.28** have previously been described by Aucagne and co-workers.[126]

General procedure for rotaxanation:

Macrocycle (1.0 eqv) was dissolved in dry degassed DCM (10 mM). Subsequently, $Cu(CH_3CN)_4PF_6$ (1.0 eqv) was added to the reaction and stirred for 15 mins. Bis-azide (1.0 eqv) was then added and stirred for another 5 mins before stopper alkyne (5.0 eqv) was added and the reaction left to stir overnight at room temperature. Crude material was purified by preparatory TLC (Ethyl Acetate/DCM 7:3) to obtain white solid.

Compound 4.12

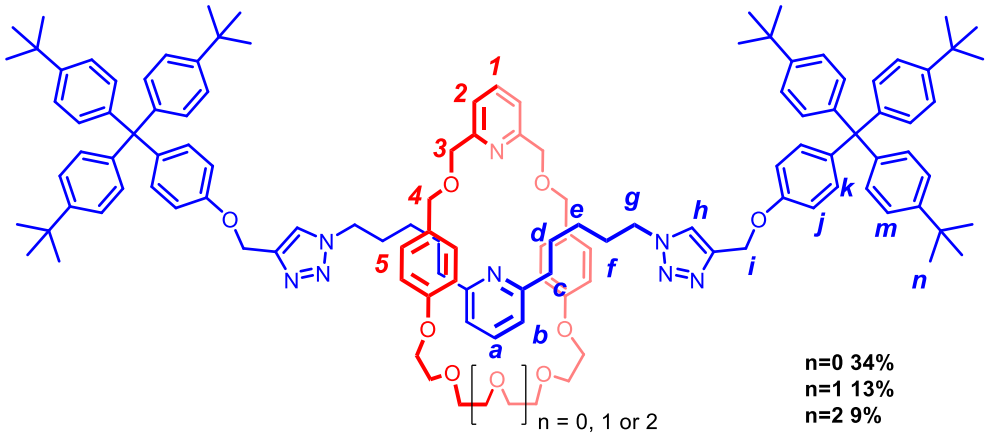

Compound 4.12a: **Yield:** 14 mg, 34%. **^{1}H-NMR** (500 MHz, Chloroform-d) δ 7.55 (6H, dd, br, H_1 + H_2 + H_a + H_b), 7.22 (21H dd, *J* = 8.6, 1.8 Hz), 7.13 – 7.04 (25H, m), 6.91 (6H, d, *J* = 8.2 Hz), 6.88 – 6.83 (m, 2H, H_h), 6.81 (d, J = 8.45 Hz, 4H), 6.43 (4H, d, *J* = 8.0 Hz), 5.16 (2H, s), 4.98 (3H, s), 4.44 (4H, s), 4.32 (6H, d, *J* = 19.1 Hz), 4.00 – 3.79 (9H, m), 3.74 (4H, d, J = 4.27 Hz), 3.66 (4H, s), 1.95 (3H, *J* = 7.3 Hz), 1.76 (3H, J = 7.8 Hz), 1.54 (5H, dd, J = 10.9, 5.07Hz), 1.30 (82H, s), 1.26 (3H, s), 1.09 (3H, s). **^{13}C-NMR** (126 MHz, $CDCl_3$) δ 158.3, 157.5, 156.2, 156.2, 148.4, 148.3, 144.4, 144.2, 144.1, 143.9, 140.2, 139.9, 137.1, 132.3, 132.2, 130.7, 130.4, 129.3, 124.1, 123.1, 122.4, 119.9, 114.2, 113.3, 113.2, 72.5, 70.8, 70.5, 69.7, 67.0, 63.1, 62.1, 61.9, 50.3, 49.8, 38.2, 34.3, 31.4, 30.1, 29.7, 29.4, 29.3, 14.1. **MS** (ESI +ve) *m/z* 1853.12963 ($[M+H]^+$, $C_{122}H_{147}N_8O_8$, calc. 1853.13700).

Compound 4.12b: **Yield:** 6 mg, 13%. **^{1}H-NMR** (500 MHz, Chloroform-d) δ 7.51 (d, J = 7.55 Hz, 3H, Hb + H1), 7.46 (t, J = 7.65 Hz, 1H, Ha), 7.26 – 7.19 (m, 12H, $H_{stoppers}$), 7.07 (dd, J = 9.65, 7.72 Hz, 16H, $H_{stoppers}$), 6.99 (d, J = 8.39 Hz, 4H, H5), 6.88 (d, J = 7.68 Hz, 2H, Hh), 6.81 – 6.76 (m, 4H, H5), 6.53 (d, J = 8.45 Hz, 4H, Hj), 5.01 (s, 4H, Hi), 4.48 (s, 4H, H3), 4.29 (s, 4H, H4), 3.98 (t, J = 7.58 Hz, 4H, Hg), 3.87 (t, J = 4.53 Hz, 4H, CH_2-polyether), 3.69 (dd, J = 5.62, 3.23 Hz, 4H, CH_2-polyether), 3.62 – 3.53 (m, 8H CH_2-polyether), 2.62 (t, J = 7.87 Hz, 4H, Hc), 1.29 (s, 54H, Hn). **^{13}C-NMR** (126 MHz, $CDCl_3$) δ 207.1, 161.4, 158.4, 157.7, 156.4, 148.4, 144.3, 144.0, 140.1, 137.2, 136.6, 132.4, 130.9, 130.1, 129.5, 124.2, 123.1, 120.1, 120.0, 114.3, 113.4, 85.3, 72.4, 71.3, 70.9, 70.8, 69.6, 67.3, 63.2, 62.0, 50.1, 38.3, 34.4, 31.5, 31.1, 29.9, 29.8, 29.4, 27.6, 26.4, 1.2. **MS** (ESI +ve) *m/z* 1897.15533 ($[M+H]^+$, $C_{124}H_{151}N_8O_9$, calc. 1897.16321).

Compound 4.12c: **Yield:** 4 mg, 9%. **^{1}H-NMR** (500 MHz, Chloroform-d) δ 7.53 (3H, d, *J* = 13.0 Hz, H_b + H1), 7.45 (1H, t, *J* = 7.6 Hz, H_a), 7.27 (2H, s, H_2), 7.25 – 7.19 (12H, m, H_m), 7.07 (16H, dd, J = 8.6, 6.4 Hz, H_k), 7.04 – 7.00 (4H, m, H_5), 6.87 (2H, d, *J* = 7.6 Hz, H_h), 6.81 – 6.74 (4H,m, H_5), 6.62 – 6.57 (4H, m, H_j), 5.02 (4H, s, H_i), 4.48 (4H, s, H_3), 4.35 (4H, s, H_4), 4.05 (4H, t, *J* = 7.5 Hz, CH_2-polyether), 3.92 – 3.86 (4H, m, CH_2-polyether), 3.69 (4H, dd, J = 5.7, 3.8 Hz, CH_2-polyether), 3.61 – 3.53 (12H, m, CH_2-polyether), 2.66 – 2.60 (4H, m), 1.29 (54H, s, H_n). **^{13}C-NMR** (126 MHz, $CDCl_h$) δ 161.4, 158.5, 157.8, 156.4, 148.5, 144.3, 144.0, 140.1, 137.2, 136.7, 132.4, 130.9, 129.9, 129.7, 124.2, 123.1, 120.3, 120.0, 114.5, 113.4, 72.4, 71.7, 70.9, 70.9, 70.8, 69.7, 67.3, 63.2, 62.0, 50.1, 38.3, 34.4, 31.5, 30.0, 29.4, 26.4. **MS** (ESI +ve) *m/z* 1941.18139 ($[M+H]^+$, $C_{126}H_{155}N_8O_{10}$, calc. 1941.18943).

Compound 4.13

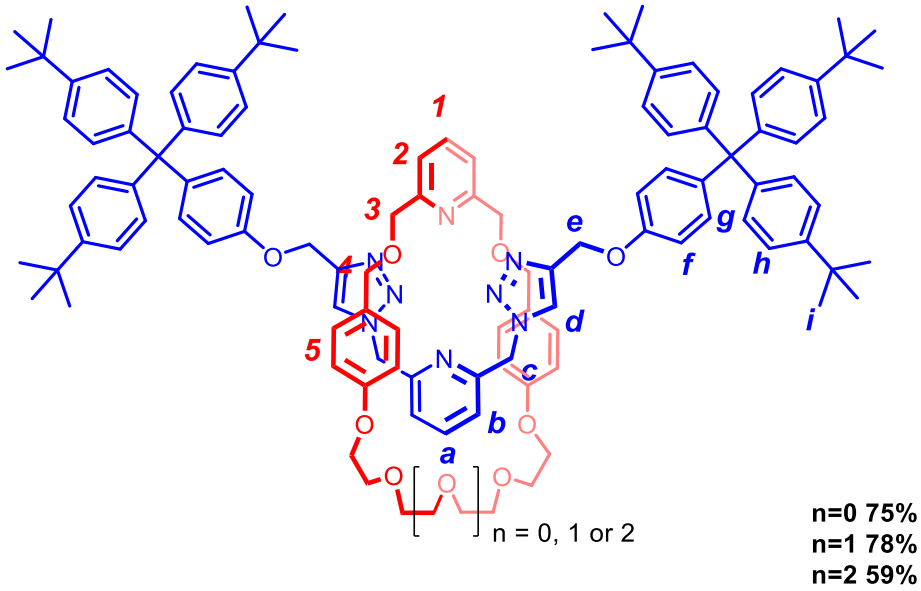

Compound 4.13a: **Yield:** 28 mg, 75%. **^{1}H-NMR** (500 MHz, Chloroform-d) δ 7.87 (2H, s, H_b), 7.52 (1H, t, *J* = 7.7 Hz, H_a), 7.44 (1H, t, *J* = 7.74 Hz, H_1), 7.23 (12H, d, *J* = 8.6= Hz, H_h), 7.19 (2H, d, *J* = 7.7 Hz, H_2), 7.12 – 7.07 (12H, m, H_g), 7.07 – 7.02 (4H, m, H_g), 6.89 (2H, d, *J* = 7.7 Hz, H_d), 6.77 (8H, d, *J* = 8.6 Hz, H_5), 6.17 (4H, d, J = 8.3 Hz, H_f), 5.18 (4H, s, H_e), 4.91 (4H, s, H_3), 4.40 (4H, s, H_c), 4.36 (4H, s, H_4), 3.85 (4H, dd, *J* = 5.7, 2.8 Hz, $H_{polyether}$), 3.73 – 3.67 (8H, m, $H_{polyether}$), 1.30 (54H, s, H_i). **^{13}C-NMR** (126 MHz, $CDCl_3$) δ 158.03, 157.65, 156.34, 154.29, 148.41, 144.36, 144.30, 139.95, 138.41, 137.12, 132.26, 130.84, 130.11, 129.18, 124.72, 124.18, 121.68, 120.40, 113.93, 113.40, 77.41, 77.16, 76.91, 72.69, 71.37, 70.64, 69.88, 66.84, 63.20, 61.92, 54.68, 34.42, 31.53. **MS** (ESI +ve) *m/z* 1741.00423 ($[M+H]^+$, $C_{114}H_{131}N_8O_8$, calc. 1741.01180).

Compound 4.13b: **Yield:** 30 mg, 78%. **^{1}H-NMR** (500 MHz, Chloroform-d) δ 7.84 (2H, s, H_b), 7.55 (1H,t, *J* = 7.72 Hz, H_a), 7.26 – 7.14 (16H, m, H_1 + H_2 + $H_{stoppers}$), 7.11 – 7.05 (16H, m, $H_{stoppers}$), 6.85 (8H, m, *J* = 10.7, 8.6 Hz, H_5), 6.51 (2H, d, *J* = 7.7 Hz, H_d), 6.27 (4H, d, *J* = 8.2 Hz, H_f), 5.29 (4H, s, H_e), 5.12 (4H, s, H_c), 4.43 (4H, s, H_3), 4.38 (4H, s, H_4), 3.74 (4H, dd, *J* = 5.8, 2.9 Hz, $H_{polyether}$), 3.66 (4H, dd, *J* = 5.8, 3.0 Hz, $H_{polyether}$), 3.57 (4H, dd, *J* = 5.9, 2.9 Hz, $H_{polyether}$), 3.42 (4H, dd, *J* = 5.8, 3.0 Hz, $H_{polyether}$), 1.30 (54H, s, H*i*). **^{13}C-NMR** (126 MHz, $CDCl_3$) δ 158.03, 157.65, 156.41, 154.12, 148.46, 144.23, 144.21, 140.14, 138.61, 137.32, 132.40, 130.84, 129.88, 129.39, 124.63, 124.18, 121.03, 120.59, 113.76, 113.35, 77.41, 77.16, 76.91, 72.59, 71.82, 70.70, 69.71, 66.98, 63.20, 62.06, 54.89, 34.42, 31.52. (**MS** (ESI +ve) *m/z* 1785.03083 ($[M+H]^+$, $C_{116}H_{135}N_8O_9$, calc. 1785.03801).

Compound 4.13c: **Yield:** 23 mg, 59%. **^{1}H-NMR** (500 MHz, Chloroform-d) δ 7.81 (2H, s, H_b), 7.55 (1H, t, *J* = 7.7 Hz, H_a), 7.26 (2H, d, J = 7.76 Hz, H_2), 7.24 – 7.20 (12H, m, H_h), 7.18 (1H, t, *J* = 7.77 Hz, H_1), 7.08 (16H, dd, *J* = 8.5, 5.6 Hz, H_g), 6.99 – 6.94 (4H, m, H_5), 6.86 – 6.80 (4H, m, H_5), 6.58 (2H, d, *J* = 7.7 Hz, H_d), 6.45 – 6.40 (4H, m, H_f), 5.27 (4H, s, H_e), 5.10 (4H, s, H_c), 4.46 (4H, s, H_3), 4.38 (4H, s, H_4), 3.77 (4H, dd, *J* = 5.8, 3.5 Hz, $H_{polyether}$), 3.65 (4H, dd, *J* = 5.7, 3.5 Hz, $H_{polyether}$), 3.56 (4H, dd, *J* = 5.8, 2.9 Hz, $H_{polyether}$), 3.49 (4H, dd, *J* = 5.7, 3.0 Hz, $H_{polyether}$), 3.44 (4H, s, $H_{polyether}$), 1.30 (54H, s, H_i). **^{13}C-NMR** (126 MHz, $CDCl_3$) δ 158.24, 157.71, 156.42, 154.44, 148.47, 144.24, 144.19, 140.16, 138.53, 137.33, 132.41, 130.85, 129.90, 129.67, 124.67, 124.19, 121.25, 120.62, 114.17, 113.36, 77.41, 77.16, 76.91, 72.42, 71.86, 70.82, 70.74, 70.66, 69.63, 67.12, 63.20, 61.97, 54.96, 34.42, 31.52. **MS** (ESI +ve) *m/z* 1829.05741 ([M+H]$^+$, $C_{118}H_{139}N_8O_{10}$, calc. 1829.06422).

Compound 4.11

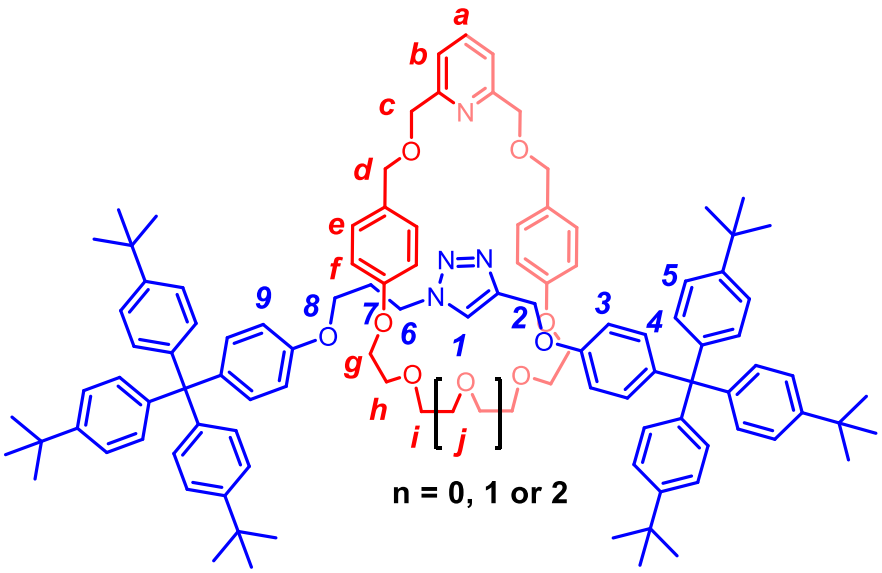

4.14a
4.14b
4.14c

a, n=0, 76%
b, n=1, 51%
c, n=2, 56%

Compound 4.14a: Yield, 90 mg, 76%. **^{1}H-NMR** (500 MHz, CD_2Cl_2) δ 7.68 (1H, s, H_1), 7.47 (1H, t, H_a), 7.32 – 7.12 (28H, m, H_5 + H_4 + H_b), 7.09 (4H dd, *J* = 8.8, 2.0 Hz,), 6.86 (4H, dd, H_e), 6.77 (2H, d, *J* = 8.5 Hz, H_3), 6.56 (2H, d, *J* = 8.4 Hz, H_9), 6.35 (4H, dd, H_f), 4.81 (2H, s, H_2), 4.51 – 4.35 (4H, m, H_c + H_c'), 4.31 – 4.21 (4H, m, H_d + H_d'), 3.91 – 3.82 (4H, m, $H_{g\text{-}i}$), 3.70 – 3.62 (4H, m, $H_{g\text{-}i}$), 3.62 – 3.55 (4H, m, $H_{g\text{-}i}$), 3.56 – 3.44 (2H, m, $H_{g\text{-}i}$), 3.26 – 3.11 (2H, m, $H_{g\text{-}i}$), 1.30 (54H, d, J = 4.5 Hz, ^{t}bu). **^{13}C-NMR** (126 MHz, CD_2Cl_2) δ 158.82, 157.05, 156.84, 148.93, 145.24, 145.14, 140.28, 140.03, 132.54, 132.29, 132.16, 130.98, 130.83, 130.04, 125.42, 124.88, 124.83, 124.68, 120.52, 114.62, 114.10, 114.00,

113.73, 78.15, 77.90, 77.65, 72.91, 71.47, 71.15, 70.18, 67.64, 65.07, 63.72, 63.68, 62.17, 47.08, 34.75, 31.65, 29.15, 1.32. **MS** (ESI +ve) *m/z* 1596.95966 ($[M+H]^+$, $C_{107}H_{127}N_4O_8$, calc. 1596.96820).

Compound 4.14b: Yield, 126 mg, 51%. **^{1}H-NMR** (500 MHz, CD_2Cl_2) δ 7.54 (1H, s, H_1), 7.47 (1H, t, *J* = 7.7 Hz, H_a), 7.30 – 7.13 (26H, m, H_5), 7.10 (2H, d, *J* = 8.5 Hz, H_5), 7.04 (2H, d, *J* = 8.4 Hz, H_b), 6.94 (4H, d, J = 8.26 Hz, H_e), 6.76 (2H, d, J = 8.30 Hz, H_3), 6.53 (2H, d, *J* = 8.45 Hz, H_9), 6.45 (4H, d, *J* = 8.1 Hz, H_f), 4.89 (2H, s, H_2), 4.45 (4H, d, *J* = 2.3 Hz, H_c), 4.25 (4H, d, *J* = 2.6 Hz, H_d), 3.85 – 3.76 (6H, m, H_8 + H_g), 3.62 (4H, d, *J* = 4.60 Hz, H_h), 3.53 (4H, t, *J* = 4.4 Hz, H_i), 3.47 (4H, q, *J* = 3.3 Hz, H_j), 3.33 (2H,s, H_6), 1.64 (2H, s, H_7), 1.30 (54H, d, J = 2.4 Hz, H-^{t}Bu). **^{13}C-NMR** (126 MHz, CD_2Cl_2) δ 158.74, 158.25, 156.93, 156.90, 148.92, 148.90, 145.24, 145.12, 143.70, 140.32, 140.03, 137.49, 132.34, 132.15, 130.99, 130.39, 130.14, 124.86, 124.83, 120.45, 114.57, 114.04, 114.01, 78.15, 77.90, 77.65, 72.65, 71.73, 71.19, 71.13, 70.00, 67.72, 64.72, 63.69, 62.11, 47.31, 34.76, 31.66, 29.88, 1.32. **MS** (ESI +ve) *m/z* 1640.89493 ($[M+H]^+$, $C_{109}H_{131}N_5O_9$, calc. 1640.98184).

Compound 4.14c: Yield, 109 mg, 56%. **^{1}H-NMR** (500 MHz, CD_2Cl_2) δ 7.55 – 7.48 (2H, m, H_1 + H_a), 7.25 (14H, td, *J* = 9.9, 9.2, 6.7 Hz, H_5), 7.16 (12H, dd, J = 10.2, 7.8 Hz, H_4), 7.10 (2H, d, H_5), 7.05 (2H, d, H_b), 6.99 (4H, d, H_e), 6.76 (2H, d, H_3), 6.54 (4H, d, *J* = 8.8, 2.1 Hz), 4.91 (2H, s), 4.45 (2H, s), 4.32 (2H, s), 3.97 (2H, t, *J* = 7.4 Hz), 3.83 (t, *J* = 4.7 Hz, 4H), 3.62 (4H td, *J* = 5.8, 3.6 Hz), 3.54 – 3.49 (4H, m), 3.49 – 3.43 (6H, m), 1.80 (2H, t, *J* = 7.1 Hz), 1.30 (54H, d, *J* = 1.3 Hz). **^{13}C-NMR** (126 MHz, CD_2Cl_2) δ 158.83, 158.31, 156.95, 156.91, 148.93, 148.90, 145.19, 145.09, 143.72, 140.36, 140.11, 137.52, 132.38, 132.25, 130.99, 130.37, 130.25, 125.42, 124.85, 124.83, 120.69, 114.75, 114.01, 113.92, 78.16, 77.90, 77.65, 72.61, 72.13, 71.28, 71.17, 71.09, 69.99, 67.77, 64.73, 63.67, 62.13, 47.40, 34.75, 31.65, 30.12, 1.32. **MS** (ESI +ve) *m/z* 1685.01380 ($[M+H]^+$, $C_{111}H_{135}N_4O_{10}$, calc. 1685.02063).

Appendix A Chapter 2

A1 ^{1}H NMR Anion Binding Studies

General procedure

^{1}H NMR titration experiments were performed on a Bruker AVIII 500 MHz spectrometer. In a typical experiment, a solution of the appropriate tetrabutylammonium (TBA) salt was added to 0.5 mL of a 1.0 mM solution of the receptor molecule at the pre-set temperature in pure d_6-acetone, CD_3CN, d_6-DMSO or CD_3CN/ D_2O 99:1 *v/v*. Both TBA salt and receptor were dissolved in the same solvent. TBA was chosen as the counter-cation due to its non-coordinating nature. At least 17 data points are obtained for each titration to ensure a good fit to the appropriate host-guest binding models. The binding of anions with all receptors were found to be fast on the NMR timescale. The values of the observed chemical shift and concentration of anion were entered into the WinEQNMR2[171] computer programme for every titration point. From initial estimates made of the binding constants and limiting chemical shifts, these parameters were refined using non-linear least-squares analyses to obtain the best fit between empirical and calculated chemical shifts based on a host-guest 1:1 binding stoichiometry (unless otherwise stated). In all cases, convergence of the best fit values of the binding constants and their errors were obtained.

A2. Variable-Temperature (VT) 1H NMR Titration Studies

An identical protocol as that described in Appendix A1 was used, except that the titrations were performed at different temperatures. At each temperature, the NMR tube containing the host and guest solution was first allowed to reach thermal equilibrium before the spectrum was recorded after the addition of each aliquot of anion. Data fitting to the appropriate host-guest binding isotherm was performed using the WinEQNMR2[171] software as aforementioned to obtain the K_a values.

A2-1 VT ^{1}H NMR with 2.1$_{Te}$ in dry CD_3CN

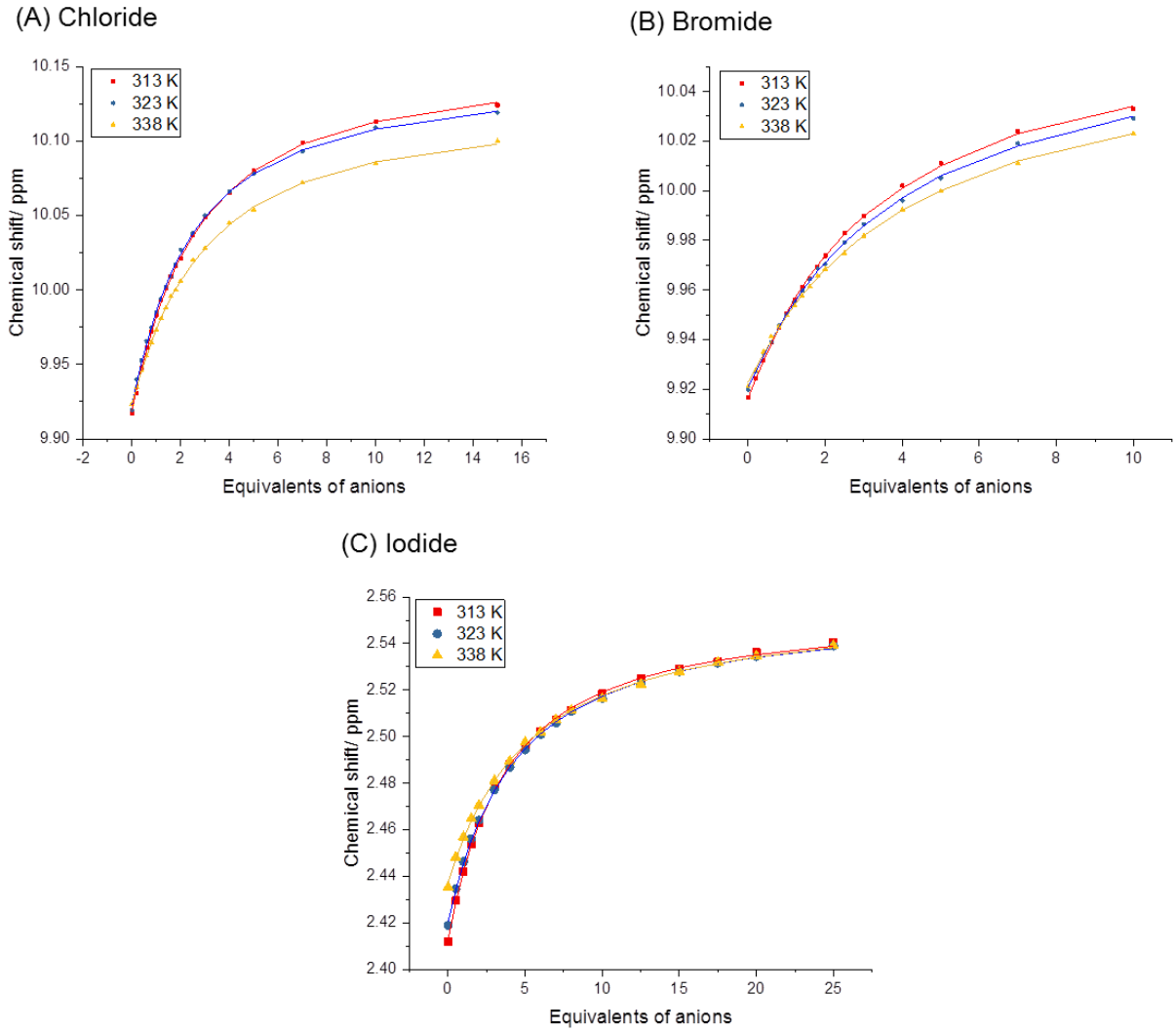

*Fig. A2-1. Changes in the chemical shifts of internal pyridinium aromatic proton H_a of receptor **2.1$_{Te}$** with increasing quantities of (A) Cl^-, (B) Br^- and (C) $TeCH_3$ protons of **2.1$_{Te}$** with I^- in CD_3CN at 313, 323 and 338 K ([**2.1$_{Te}$**] = 1.0 mM). H_a was not monitored for the I^- titrations due to the small shifts observed compared with those of $TeCH_3$.*

A2-2 VT ^{1}H NMR with 2.2H in dry CD_3CN

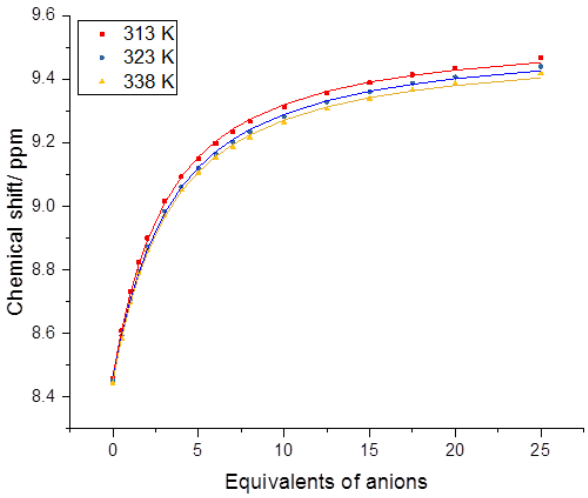

Fig. A2-2. Changes in the chemical shifts of the triazole protons of receptor ***2.2$_H$*** *with increasing quantities of Cl^- in dry CD_3CN at 313, 323 and 338 K ([**2.2$_H$**] = 1.0 mM).*

A2-3 VT 1H NMR with 2.1$_{Te}$ in CD_3CN/D_2O 99:1

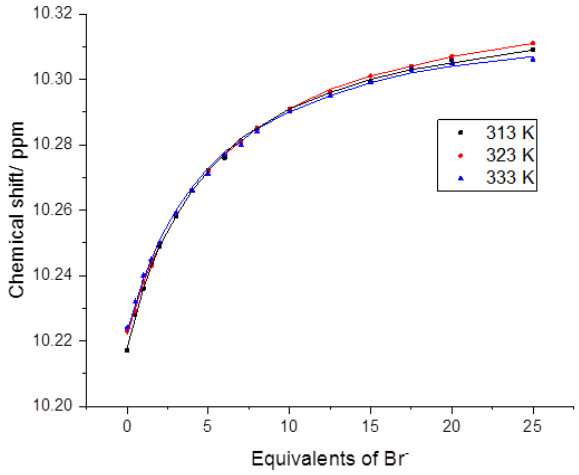

Fig. A2-3. Changes in the chemical shifts of internal pyridinium aromatic proton H_a of receptor ***2.1$_{Te}$*** *with increasing quantities of Br^- in CD_3CN/ D_2O 99:1 v/v at 313, 323 and 338 K ([**2.1$_{Te}$**] = 1.0 mM).*

A2-4 VT 1H NMR with 2.3$_{Se}$ in d$_6$-acetone

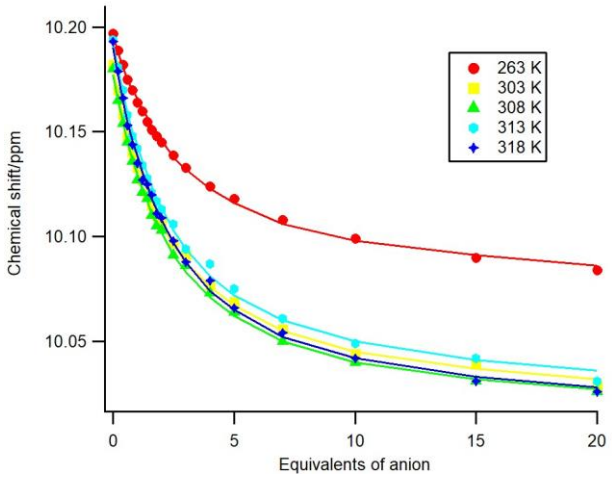

*Fig. A2-4. Changes in the chemical shifts of internal pyridinium aromatic proton H$_a$ of receptor **2.3$_{Se}$** with increasing quantities of Cl$^-$ in d$_6$-acetone at 263, 298, 313, 308 and 318 K ([**2.3$_{Se}$**] = 1.0 mM).*

A2-5 VT 1H NMR with 2.1$_{Te}$ in d$_6$-acetone

*Fig. A2-5. Changes in the chemical shifts of internal pyridinium aromatic proton H$_a$ of receptor **2.1$_{Te}$** with increasing quantities of I$^-$ in d$_6$-acetone at 263, 298, 308 and 318 K ([**2.1$_{Te}$**] = 1.0 mM).*

A2-6 VT 1H NMR with macrocycle 2.5$_{Se}$ in d$_6$-acetone

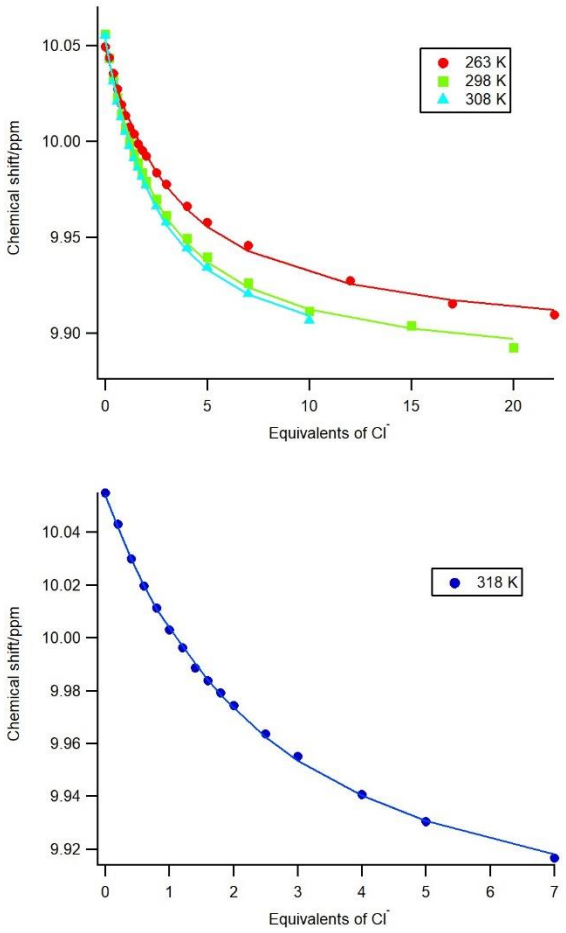

*Fig. A2-6. Changes in the chemical shifts of internal pyridinium aromatic proton H$_a$ of receptor **2.5$_{Se}$** with increasing quantities of Cl$^-$ in d$_6$-acetone at 263, 298, 308 and 318 K ([**2.5$_{Se}$**] = 1.0 mM). Titration at 318 K could only be performed up to 7.0 equivalents of Cl$^-$ due to precipitation of the host-guest complex at higher quantities.*

*Table A2-7. 1:1 stoichiometric association constants (K_a/ M^{-1}) of receptors **2.1$_{Te}$** and **2.2$_H$** at various temperatures in dry and wet CD_3CN.[a]*

T/ K	Receptor **2.1$_{Te}$**				Receptor **2.2$_H$**
	Dry CD_3CN			CD_3CN/ D_2O 99:1	Dry CD_3CN
	Cl^-	Br	I^-	Br^-	Cl^-
298	652 (13)	501 (16)	305 (11)	183 (4)	263 (8)
313	484 (3)	348 (9)	216 (5)	141 (3)	252 (7)
323	410 (18)	295 (8)	175 (3)	117 (3)	242 (7)
338	356 (3)	242 (2)	139 (2)	102 (3)	229 (8)

[a] Values of K_a determined using WinEQNMR2 software[171] by monitoring internal proton H_a in all cases, a host-guest 1:1 stoichiometric binding model was used; errors (±) in parentheses.

*Table A2-8. 1:1 stoichiometric association constants (K_a/ M^{-1}) of receptors **2.Se, 2.1$_{Te}$ and 3.Se** at various temperatures in d_6-acetone.[a]*

	Receptor 2.3$_{Se}$	**Receptor 2.1$_{Te}$**	**Receptor 2.5$_{Se}$**
T/ K	Cl^-	I^-	Cl^-
263	419 (22)	5877 (215)	328 (21)
298	528 (25)	3528 (54)	450 (23)
313	541 (26)	-	-
308	536 (38)	3027 (55)	492 (22)
318	554 (35)	2678 (60)	538 (25)

*[a] Values of K_a determined using WinEQNMR2 software[171] by monitoring the upfield shifts of the internal pyridinium proton H_a in selenium-containing receptors **2.3$_{Se}$** and **2.5$_{Se}$** and downfield shifts of $TeCH_3$ for **2.1$_{Te}$**; errors (±) in parentheses.*

Appendix B Crystallographic Data

Data collection

All crystals suitable for X-ray diffraction described herein were grown by the author. Data was collected using synchrotron radiation at 100(2) K at Diamond Light Source (DLS), Beamline I19[295] using a Cryostream N_2 open-flow cooling device on the diffractometer.[296] The data were collected by Andrew Docker and Dr Jason Lim with help from Dr Amber Thompson and Dr Kirsten Christen, whilst structure solution and refinement were carried out by Dr Jason Lim. Cell parameters and intensity data (including inter-frame scaling) were processed using CrysAlis Pro (CrysAlis Pro, Agilent Technologies, 2010). Subsequently, the structure was solved using charge-flipping methods using SUPERFLIP,[297] and refined using full-matrix least-squares on F^2 within the CRYSTALS suite[298,299] All non-hydrogen atoms were refined with anisotropic displacement parameters. Where appropriate, disordered portions were modelled using refined partial occupancies, and geometric restraints were applied to ensure physically reasonable models. Thermal and vibrational restraints were applied as well to maintain sensible ADPs. The majority of the hydrogen atoms were located from the difference map, while those which were not visible were repositioned geometrically. The H atoms were initially refined with soft restraints on the bond lengths and angles to regularise their geometry and U_{iso}(H), after which the positions were refined with riding constraints.[300] When the hydrogen atoms were attached to atoms with large thermal ellipsoids or when the data was of poor quality, the hydrogen atoms were placed at geometric positions and refined using riding constraints. The same approach was used for inserting H atoms at geometric positions on the thioamide motifs.

Following the construction of a stable and physically-plausible model, the weights were optimised using the Chebyshev F^2 weighting scheme,[301] anomalous reflections were omitted and for poorly-diffracting samples, the absent high-angle data were pruned using the Wilson plot. This approach generally led to refinement convergence to give the final structure.

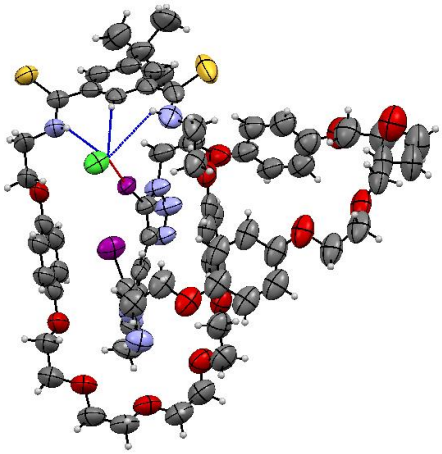

Table B1. Crystal structure data and refinement details for catenane ***2.25·Cl*** *as its chloride salt.*

Experimental details	
Chemical formula	$C_{70}H_{82}ICIN_9O_{13}S_2$
M_r	1610.87
Crystal system, space group	Monoclinic, *C*2/*c*
Temperature/ K	100(2)
a, *b*, *c*/ Å	26.7929 (4), 23.9624 (3), 25.8082 (4)
β / °	100.1939 (17)
Unit cell volume/ Å^3	16307.9 (4)
Z	8
μ/ mm^{-1}	0.92
Crystal size/ mm	0.02 x 0.02 x 0.01
No. of measured, independent and observed [$I > 2.0\sigma(I)$] reflections	88763, 13931, 10892
R_{int}	0.111
$(\sin \theta/\lambda)_{max}$ / Å^{-1}	0.590
Refinement	
$R[F^2 > 2\sigma(F^2)]$, $wR(F^2)$, S	0.124, 0.284, 0.91
No. of reflections	13864
No. of parameters	1147
$\Delta\rho_{max}$, $\Delta\rho_{min}$ (e Å^{-3})	4.47, -1.65

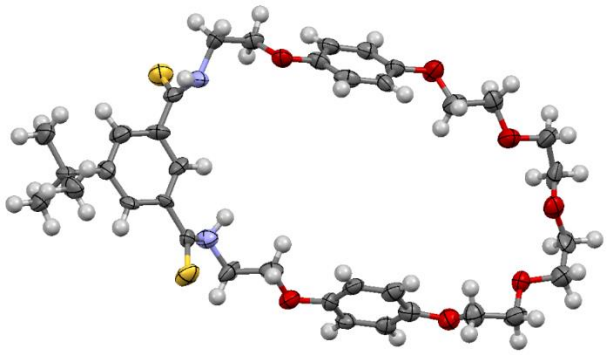

Table B2. *Crystal structure data and refinement details for macrocycle* ***2.17****.*

Experimental details	
Chemical formula	$C_{36}H_{46}N_2O_7S_2$
M_r	682.90
Crystal system, space group	Triclinic, P-1
Temperature/ K	100(2)
a, *b*, *c*/ Å	11.6273 (7), 20.3845 (13), 23.3080 (14)
α, β, γ / °	84.133 (5), 76.955 (5), 81.759 (5)
Unit cell volume/ Å^3	5312.2 (6)
Z	6
μ/ mm^{-1}	0.20
Crystal size/ mm	0.04 x 0.03 x 0.02
No. of measured, independent and observed [$I > 2.0\sigma(I)$] reflections	85370, 31654, 8888
R_{int}	0.160
$(\sin \theta/\lambda)_{max}$ / Å^{-1}	0.715
Refinement	
$R[F^2 > 2\sigma(F^2)]$, $wR(F^2)$, S	0.142, 0.311, 1.07
No. of reflections	11045
No. of parameters	1270
$\Delta\rho_{max}$, $\Delta\rho_{min}$ (e Å^{-3})	0.75, −0.83

Appendix C Computational

Starting structure was optimised for geometry at the B3LYP level, with the H, C and N atoms being described with the 6-21G++ basis set, while the Se atom was described with the aug-cc-pVDZ-PP basis set, obtained from the EMSL database.[302,303] In this work, the $V(\mathbf{r})$ was evaluated on the 0.001 electrons Bohr^{-3} contour of $\rho(\mathbf{r})$. The electrostatic potential surface ranges, between the most negative and most positive values, were calculated using the WFA-SAS[304] or *multiwfn*[305,306] program.

Appendix D Chapter 3

*Table D1. Fluorescence intensity of receptor **3.41$_S$** in acetonitrile and calculated percentage change in fluorescence.*

Receptor **3.41S**	Fluorescence Intensity (a.u.)–[a]			% change		
	0 eqv	20 eqv	1000 eqv	0 - 20 eqv	20-1000 eqv	0-1000 eqv
Cl	22319900	31280800	20512800	40	-34	-8
Br	18399600	25609300	19238700	39	-25	5
I	18792700	21009700	8704230	12	-59	-54
D-Tar/(S)-Tar	18347800	27244926.7	20275019.1	48	-26	11
L-Tar/(R)-Tar	18982300	27345112.4	21302834.3	44	-22	12
D-Glu/(S)-Glu	22275900	35761959.5	26641106.3	61	-26	20
L-Glu	19168400	35515999.3	30588903.2	85	-14	60
Phthalate	18787700	27375630.5	12869409.7	46	-53	-32
Isophthalate	18290900	28090406.6	7033309.1	54	-75	-62
Terephthalate	18831400	27097597.2	7508730.56	44	-72	-60

[a] *Fluorescence intensity taken at peak maxima with consistency at 357nm.*

Appendix E Chapter 4

In situ NMR Studies Protocol

In a general procedure for *in situ* NMR solution studies, a stock solution of host was prepared where the effective concentration of host in 0.5 mL of CD_2Cl_2 in the NMR tube is 1.5 mM. Due to insolubility of $AgBF_4$ in CD_2Cl_2, a known amount was weighed out and added the host solution to solid $AgBF_4$. An iodine stock solution was made and 2.0 eqv (based on $AgBF_4$) was then added to the complex solution which generated a precipitate of AgI. This suspension was then passed through a syringe filter (PTFE, 0.2 µm pore size, 25 mm disc diameter) to obtain a solution of the iodonium complex with excess iodine. Initial studies using ^1H NMR showed broadening of peaks and large signal perturbations upon Ag(I) complexation and the formation of the presumed iodonium species. Each ^1H NMR spectrum of the [2]rotaxane, [2]rotaxane+Ag and [2]rotaxane+I_2 are that of the same sample.

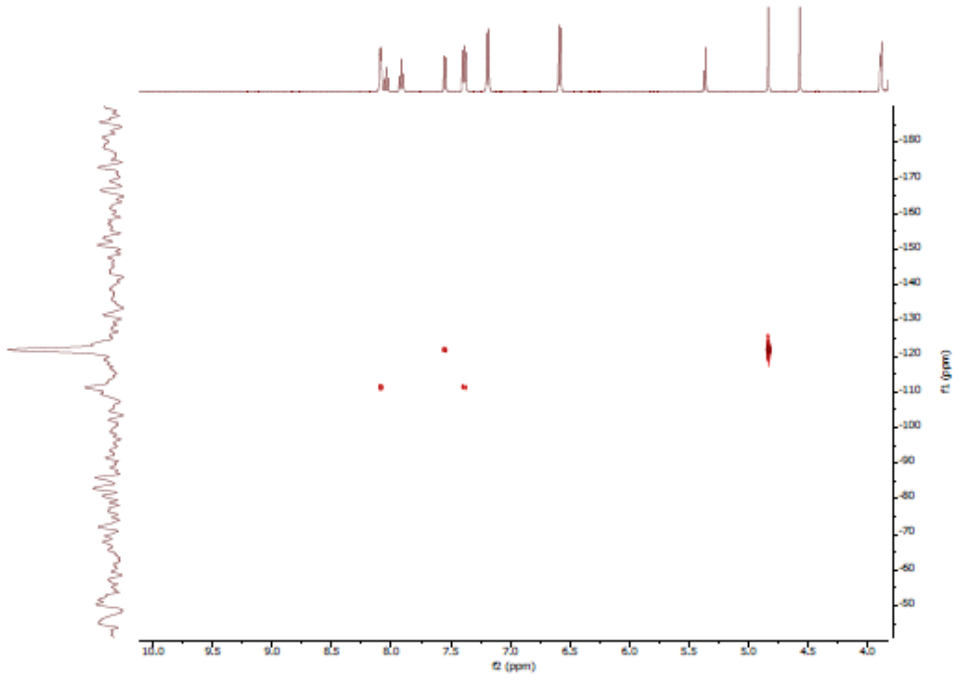

*Fig E-1. ^1H-^{15}N HMBC spectrum of Ag^+-complex of macrocycle **4.2** and pyridine. The ^{15}N NMR shifts of both pyridine and of macrocycle **4.2** correspond to shifts expected for an Ag^+ complex (ca. -120 ppm).*

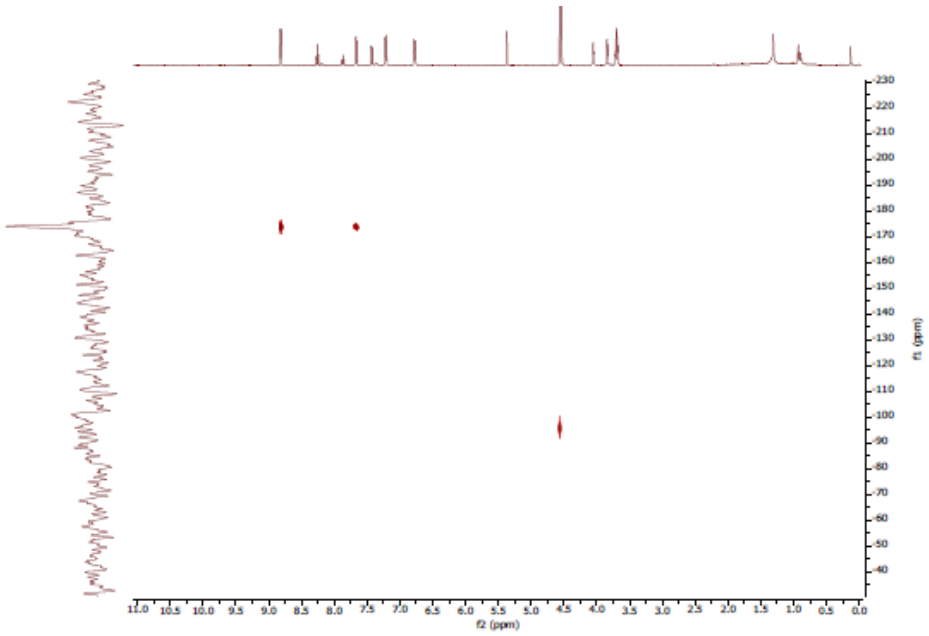

*Fig E-2. $^{1}H - ^{15}N$ HMBC spectrum of [macrocycle **4.2** + I^{+} + pyridine]. The ^{15}N NMR shift observed for pyridine (ca. -175 ppm) corresponds to that of a [bis(pyridine)iodine]$^{+}$ complex whereas the -95 ppm ^{15}N NMR shift of macrocycle **4.2** corresponds to an non-complexed, possibly slightly protonated pyridine derivative, or a pyridine that coordinates with low probability in a dynamic system. (The non-complexed macrocycle **4.2** has ^{15}N NMR shift ca. -75 ppm).*

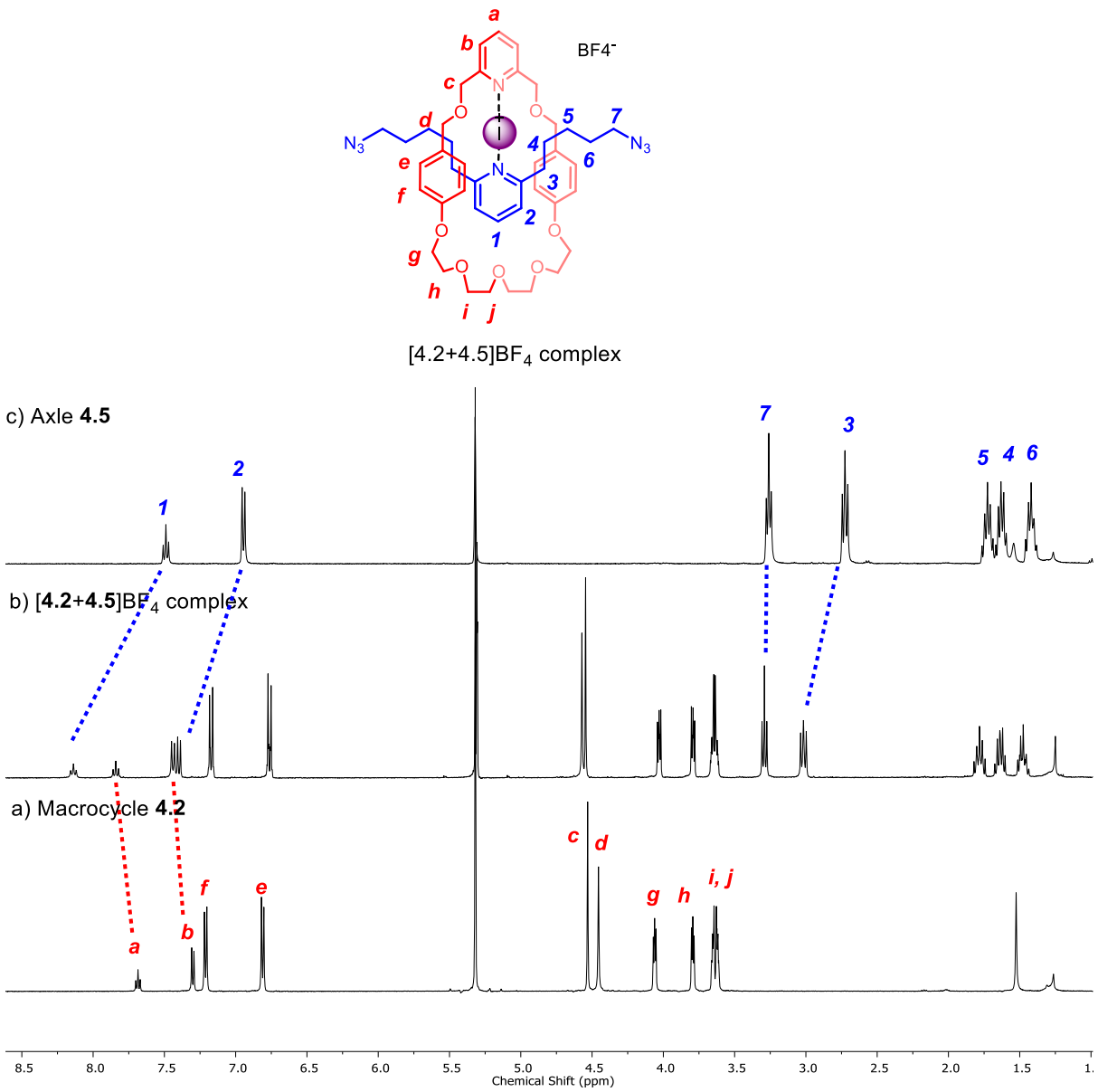

*Fig E-3. ^{1}H NMR spectra of a) macrocycle **4.2**, b) isolated [**4.2**+**4.5**]BF_4 complex and c) axle **4.5** measured in CD_2Cl_2.*

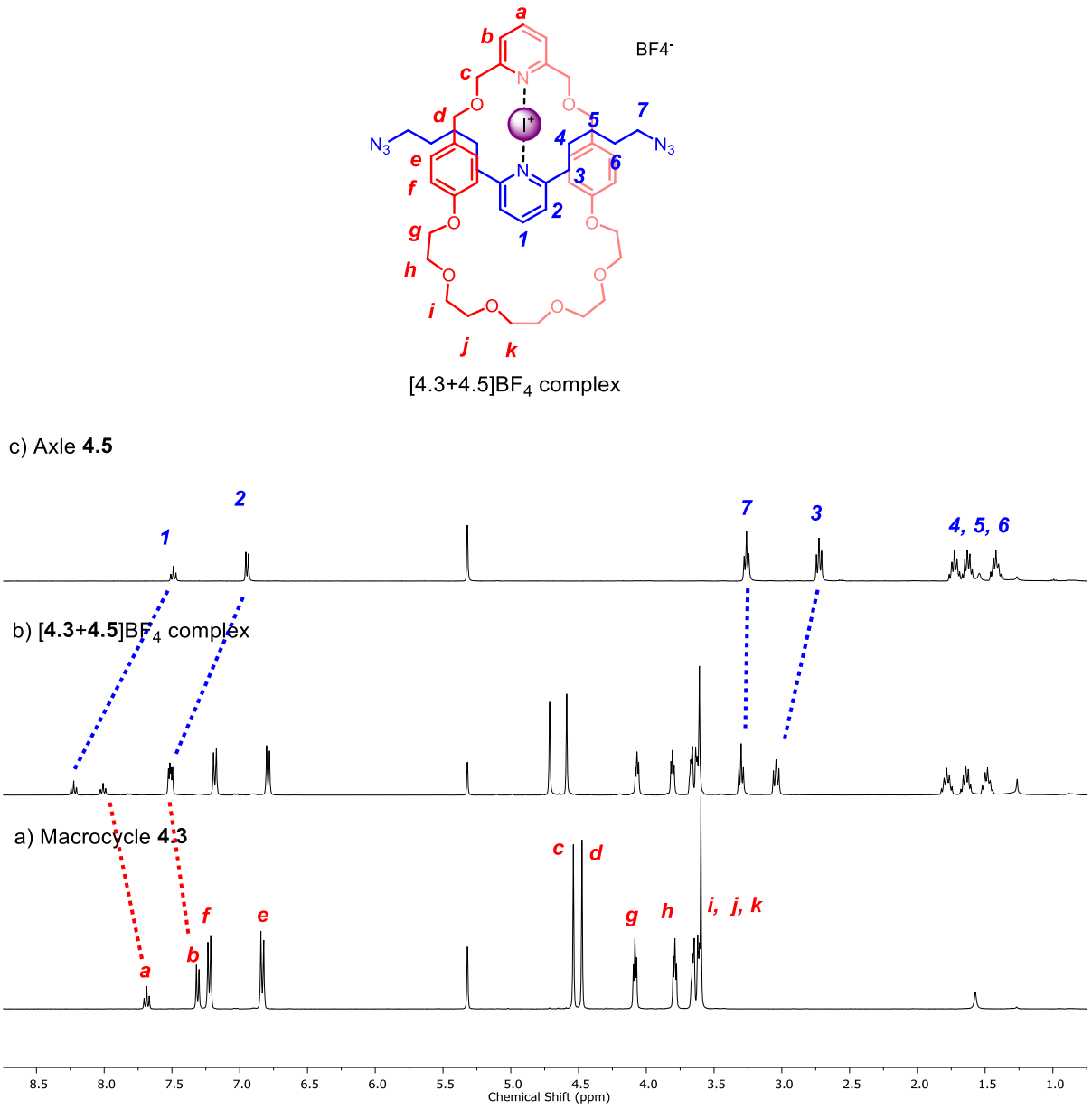

*Figure E-4. ^{1}H NMR spectra of a) macrocycle **4.3**, b) isolated [**4.3**+**4.5**]BF_4 complex and c) axle **4.5** measured in CD_2Cl_2.*

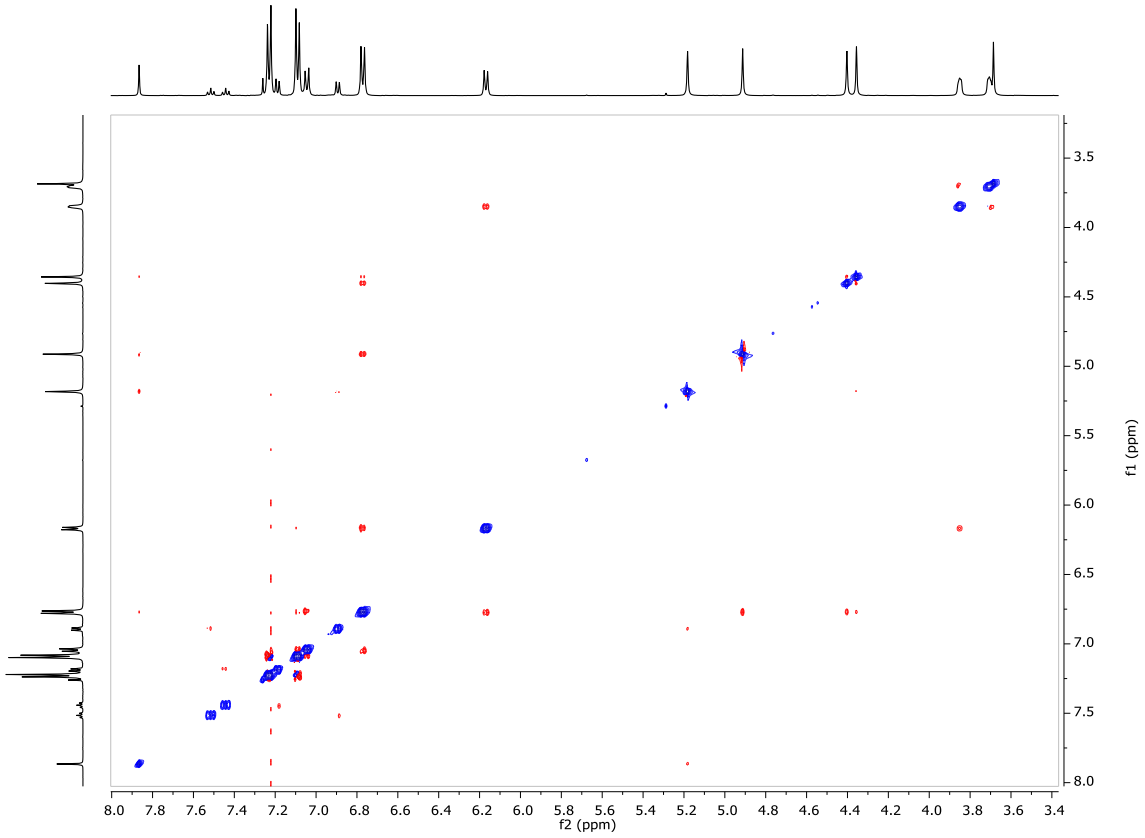

*Fig E-5. 2D ROESY NMR spectra of rotaxane **4.13a** measured in $CDCl_3$.*

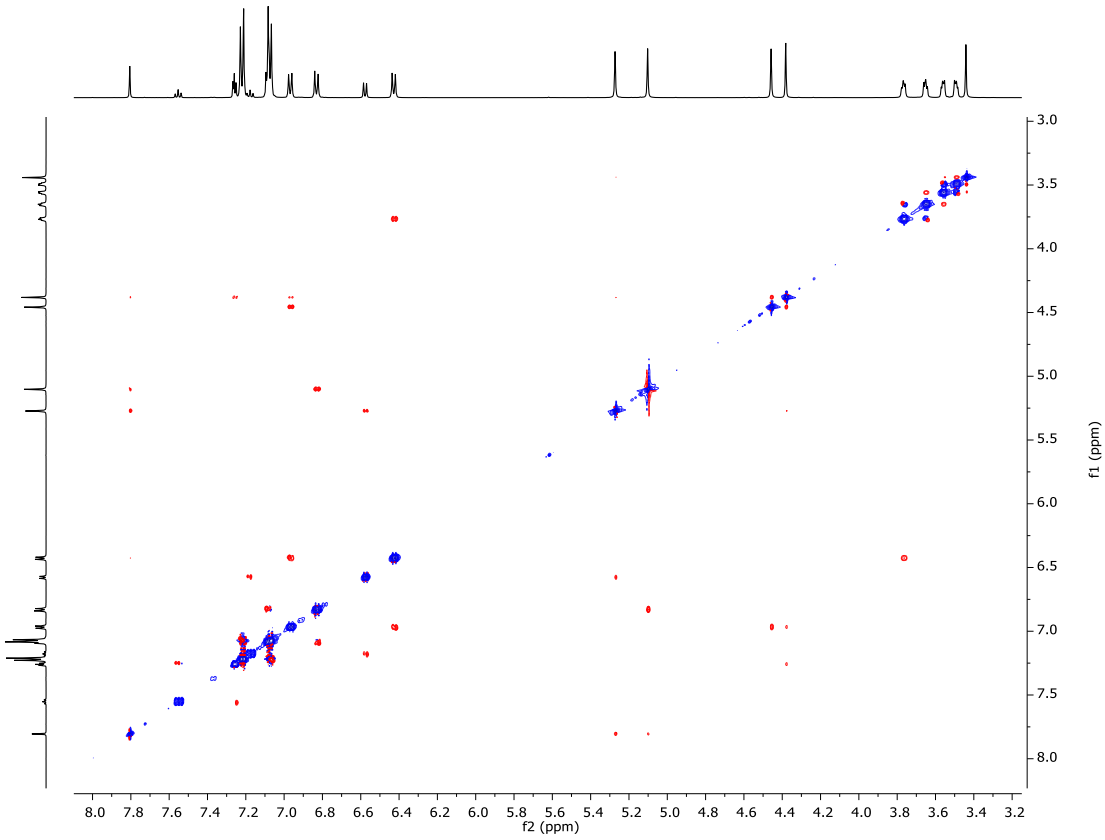

*Fig E-6. 2D ROESY NMR spectra of rotaxane **4.13c** measured in $CDCl_3$.*

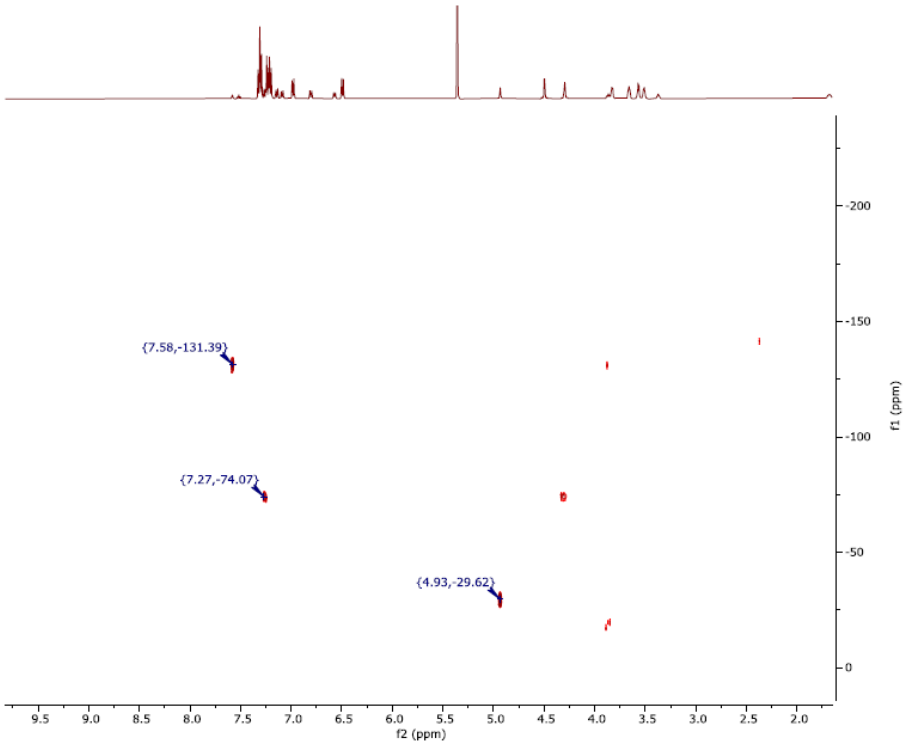

*Fig E-7. ^{1}H-^{15}N HMBC spectra of rotaxane **4.14b** in CD_2Cl_2.*

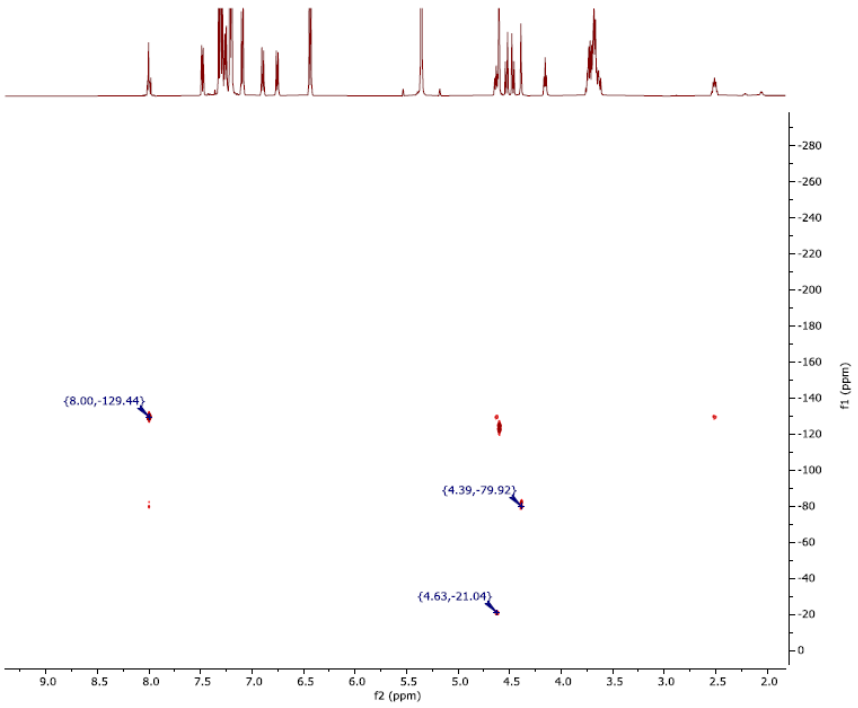

*Fig E-8. ^{1}H-^{15}N HMBC spectra of rotaxane complex [**4.14b** + Ag]BF_4 in CD_2Cl_2.*

REFERENCES

(1) Pedersen, C. J. **1988** *Angew. Chemie Int. Ed. English 27* (8), 1021–1027.

(2) Lehn, J. . **1988** *Angew. Chemie Int. Ed. English 27*, 89–112.

(3) Kyba, E. P.; Helgeson, R. C.; Madan, K.; Gokel, G. W.; Tarnowski, T. L.; Moore, S. S.; Cram, D. J. **1977** *J. Am. Chem. Soc. 99* (8), 2564–2571.

(4) Dietrich-Buchecker, C. O.; Sauvage, J. P.; Kern, J. M. **1984** *J. Am. Chem. Soc. 106* (10), 3043–3045.

(5) Anelli, P. L.; Spencer, N.; Fraser Stoddart, J. **1991** *J. Am. Chem. Soc. 113* (13), 5131–5133.

(6) Feringa, B. L. **2017** *Angew. Chemie - Int. Ed. 56* (37), 11060–11078.

(7) Broichhagen, J.; Frank, J. A.; Trauner, D. **2015** *Acc. Chem. Res. 48* (7), 1947–1960.

(8) Velema, W. A.; Szymanski, W.; Feringa, B. L. **2014** *J. Am. Chem. Soc. 136* (6), 2178–2191.

(9) Joachim, C.; Rapenne, G. **2013** *ACS Nano 7* (1), 11–14.

(10) Badjić, J. D.; Balzani, V.; Credi, A.; Silvi, S.; Stoddart, J. F. **2004** *Science (80-.). 303*, 1845–1849.

(11) Hua, Y.; Flood, A. H. **2010** *J. Am. Chem. Soc. 132* (37), 12838–12840.

(12) Kalny, D.; Elhabiri, M.; Moav, T.; Vaskevich, A.; Rubinstein, I.; Shanzer, A.; Albrecht-Gary, A. M. **2002** *Chem. Commun. 2* (13), 1426–1427.

(13) Barrell, M. J.; Leigh, D. A.; Lusby, P. J.; Slawin, A. M. Z. **2008** *Angew. Chemie - Int. Ed. 47* (42), 8036–8039.

(14) Tantama, M.; Yellen, G. 1st ed.; Elsevier Inc., 2014; Vol. 547.

(15) Kubik, S. **2009** *Chem. Soc. Rev. 38* (2), 585–605.

(16) Yang, Y.; Ballent, W.; Mayer, B. K. **2016** *FEMS Microbiol. Lett. 363* (20), 1–6.

(17) Luecke, H.; Quiocho, F. A. **1990** *Nature 347* (6291), 402–406.

(18) Dabrowa, K.; Ulatowski, F.; Lichosyt, D.; Jurczak, J. **2017** *Org. Biomol. Chem. 15* (28), 5927–5943.

(19) Dutzler, R.; Campbell, E. B.; Cadene, M.; Chait, B. T.; MacKinnon, R. **2002** *Nature 415* (6869), 287–294.

(20) Custelcean, R.; Moyer, B. A. **2007** *Eur. J. Inorg. Chem.* No. 10, 1321–1340.

(21) Brown, A.; Beer, P. D. **2016** *Chem. Commun. 52* (56), 8645–8658.

(22) Gale, P. A.; Howe, E. N. W.; Wu, X. **2016** *Chem 1* (3), 351–422.

(23) Vickers, M. S.; Beer, P. D. **2007** *Chem. Soc. Rev. 36* (2), 211–225.

(24) Marcus, Y. **1993** *J. Chem. Soc., Faraday Trans. 89* (4), 713–718.

(25) S.R. Izatt, R.L. Bruening, K.E. Krakowiak, R. M. I. 2003; pp 147–173.

(26) Yu, G.; Chen, X. **2019** *Theranostics 9* (11), 3041–3074.

(27) Koshland, D. E. **1994** *Angew. Chemie 106* (23–24), 2468–2472.

(28) Cram, D. J. **1988** *Angew. Chemie Int. Ed. English 27* (8), 1009–1112.

(29) Bhalla, V. **2018** *Resonance 23* (3), 277–290.

(30) Arunan, E.; Desiraju, G. R.; Klein, R. A.; Sadlej, J.; Scheiner, S.; Alkorta, I.; Clary, D. C.; Crabtree, R. H.; Dannenber, J. J.; Hobza, P.; et al. **2011** *Pure Appl. Chem. 83* (8), 1637–1641.

(31) Desiraju, G. R.; Shing Ho, P.; Kloo, L.; Legon, A. C.; Marquardt, R.; Metrangolo, P.; Politzer, P.; Resnati, G.; Rissanen, K. **2013** *Pure Appl. Chem. 85* (8), 1711–1713.

(32) Bader, R. F. W.; Carroll, M. T.; Cheeseman, J. R.; Chang, C. **1987** *J. Am. Chem. Soc. 109* (26), 7968–7979.

(33) Kolář, M. H.; Hobza, P. **2016** *Chem. Rev. 116* (9), 5155–5187.

(34) Clark, T.; Hennemann, M.; Murray, J. S.; Politzer, P. **2007** *J. Mol. Model. 13* (2), 291–296.

(35) Cavallo, G.; Metrangolo, P.; Milani, R.; Pilati, T.; Priimagi, A.; Resnati, G.; Terraneo, G. **2016** *Chem. Rev. 116* (4), 2478–2601.

(36) Wang, H.; Wang, W.; Jin, W. J. **2016** *Chem. Rev. 116* (9), 5072–5104.

(37) Legon, A. C. **2017** *Phys. Chem. Chem. Phys. 19* (23), 14884–14896.

(38) Bauzá, A.; Frontera, A. **2015** *Angew. Chemie - Int. Ed. 54* (25), 7340–7343.

(39) Garrett, G. E.; Gibson, G. L.; Straus, R. N.; Seferos, D. S.; Taylor, M. S. **2015** *J. Am. Chem. Soc. 137* (12), 4126–4133.

(40) Garau, C.; Frontera, A.; Quiñonero, D.; Ballester, P.; Costa, A.; Deyà, P. M. **2003** *ChemPhysChem 4* (12), 1344–1348.

(41) Quiñonero, D.; Garau, C.; Frontera, A.; Ballester, P.; Costa, A.; Deyà, P. M. **2002** *Chem. Phys. Lett. 359* (5–6), 486–492.

(42) Giese, M.; Albrecht, M.; Rissanen, K. **2016** *Chem. Commun. 52* (9), 1778–1795.

(43) Frontera, A.; Gamez, P.; Mascal, M.; Mooibroek, T. J.; Reedijk, J. **2011** *Angew. Chemie - Int. Ed. 50* (41), 9564–9583.

(44) Taylor, R.; Kennard, O. **1982** *J. Am. Chem. Soc. 104* (19), 5063–5070.

(45) Desiraju, G. R.; Steiner, T. Oxford University Press, 1999.

(46) Lim, J. Y. C.; Beer, P. D. **2018** *Chem 4* (4), 731–783.

(47) Lehn, J. M.; Sonveaux, E.; Willard, A. K. **1978** *J. Am. Chem. Soc. 100* (15), 4914–4916.

(48) Blondeau, P.; Segura, M.; Pérez-Fernández, R.; De Mendoza, J. **2007** *Chem. Soc. Rev. 36* (2), 198–210.

(49) Echavarren, A.; Galán, A.; Lehn, J. M.; Mendoza, J. De. **1989** *J. Am. Chem. Soc. 111* (13), 4994–4995.

(50) Park, C. H.; Simmons, H. E. **1968** *J. Am. Chem. Soc. 90* (9), 2431–2432.

(51) Pascal, R. A.; Spergel, J.; Van Engen, D. **1986** *Tetrahedron Lett. 27* (35), 4099–4102.

(52) Kubik, S.; Kirchner, R.; Nolting, D.; Seidel, J. **2002** *J. Am. Chem. Soc. 124* (43), 12752–12760.

(53) Qin, L.; Hartley, A.; Turner, P.; Elmes, R. B. P.; Jolliffe, K. A. **2016** *Chem. Sci. 7* (7), 4563–4572.

(54) Qin, L.; Wright, J. R.; Lane, J. D. E.; Berry, S. N.; Elmes, R. B. P.; Jolliffe, K. A. **2019** *Chem. Commun.* 12312–12315.

(55) Li, Y.; Yang, G. H.; Shen, Y. Y.; Xue, X. S.; Li, X.; Cheng, J. P. **2017** *J. Org. Chem. 82* (16), 8662–8667.

(56) Ema, T.; Okuda, K.; Watanabe, S.; Yamasaki, T.; Minami, T.; Esipenko, N. A.; Anzenbacher, P. **2014** *Org. Lett. 16* (5), 1302–1305.

(57) Gunnlaugsson, T.; Davis, A. P.; O'Brien, J. E.; Glynn, M. **2002** *Org. Lett. 4* (15), 2449–2452.

(58) Snellink-Ruël, B. H. M.; Antonisse, M. M. G.; Engbersen, J. F. J.; Timmerman, P.; Reinhoudt, D. N. **2000** *European J. Org. Chem. 2000* (1), 165–170.

(59) Yun, K. K.; Han, N. L.; Singh, N. J.; Hee, J. C.; Jin, Y. X.; Kim, K. S.; Yoon, J.; Myung, H. H. **2008** *J. Org. Chem. 73* (1), 301–304.

(60) Busschaert, N.; Gale, P. A.; Haynes, C. J. E.; Light, M. E.; Moore, S. J.; Tong, C. C.; Davis, J. T.; Harrell, W. A. **2010** *Chem. Commun. 46* (34), 6252–6254.

(61) Spooner, M. J.; Gale, P. A. **2018** *Supramol. Chem. 30* (5–6), 514–519.

(62) Tong, C. C.; Quesada, R.; Sessler, J. L.; Gale, P. A. **2008** *Chem. Commun.* No. 47, 6321–6323.

(63) Camiolo, S.; Coles, S. J.; Gale, P. A.; Hursthouse, M. B.; Sessler, J. L. **2001** *Acta Crystallogr. Sect. E Struct. Reports Online 57* (9), o816–o818.

(64) Kim, J. Il; Juwarker, H.; Liu, X.; Lah, M. S.; Jeong, K. S. **2010** *Chem. Commun. 46* (5), 764–766.

(65) McDonald, K. P.; Hua, Y.; Flood, A. H. In *Anion Recognition in Supramolecular Chemistry*; 2010; pp 341–366.

(66) Farnham, W. B.; Roe, D. C.; Dixon, D. A.; Calabrese, J. C.; Harlow, R. L. **1990** *J. Am. Chem. Soc. 112* (21), 7707–7718.

(67) Yoon, D. W.; Gross, D. E.; Lynch, V. M.; Sessler, J. L.; Hay, B. P.; Lee, C. H. **2008** *Angew. Chemie - Int. Ed. 47* (27), 5038–5042.

(68) Ramabhadran, R. O.; Liu, Y.; Hua, Y.; Ciardi, M.; Flood, A. H.; Raghavachari, K. **2014** *J. Am. Chem. Soc. 136* (13), 5078–5089.

(69) Liu, Y.; Zhao, W.; Chen, C.-H.; Flood, A. H. **2019** *Science (80-.). 365*, 159–161.

(70) Yawer, M. A.; Havel, V.; Sindelar, V. **2015** *Angew. Chemie - Int. Ed. 54* (1), 276–279.

(71) Amendola, V.; Bergamaschi, G.; Boiocchi, M.; Legnani, L.; Presti, E. Lo; Miljkovic, A.; Monzani, E.; Pancotti, F. **2016** *Chem. Commun. 52* (72), 10910–10913.

(72) Kumar, A.; Pandey, P. S. **2008** *Org. Lett. 10* (2), 165–168.

(73) Cho, J.; Verwilst, P.; Kang, M.; Pan, J. L.; Sharma, A.; Hong, C. S.; Kim, J. S.; Kim, S. **2020** *Chem. Commun. 56* (7), 1038–1041.

(74) Gilday, L. C.; White, N. G.; Beer, P. D. **2013** *Dalt. Trans. 42* (44), 15766–15773.

(75) Mercurio, J. M.; Knighton, R. C.; Cookson, J.; Beer, P. D. **2014** *Chem. - A Eur. J. 20* (37), 11740–11749.

(76) Ruiz-Botella, S.; Vidossich, P.; Ujaque, G.; Peris, E.; Beer, P. D. **2017** *RSC Adv. 7* (19), 11253–

11258.

(77) Mole, T. K.; Arter, W. E.; Marques, I.; Félix, V.; Beer, P. D. **2015** *J. Organomet. Chem. 792*, 206–210.

(78) Geer, M. F.; Mazzuca, J.; Smith, M. D.; Shimizu, L. S. **2013** *CrystEngComm 15* (46), 9923–9929.

(79) Wasilewska, A.; Gdaniec, M.; Połoński, T. **2007** *CrystEngComm 9* (3), 203–206.

(80) Guardigli, C.; Liantonio, R.; Mele, M. L.; Metrangolo, P.; Resnati, G.; Pilati, T. **2003** *Supramol. Chem. 15* (3), 177–188.

(81) Sarwar, M. G.; Dragisic, B.; Sagoo, S.; Taylor, M. S. **2010** *Angew. Chemie Int. Ed. 49* (9), 1674–1677.

(82) Mele, A.; Metrangolo, P.; Neukirch, H.; Pilati, T.; Resnati, G. **2005** *J. Am. Chem. Soc. 127* (43), 14972–14973.

(83) Tepper, R.; Schulze, B.; Görls, H.; Bellstedt, P.; Jäger, M.; Schubert, U. S. **2015** *Org. Lett. 17* (23), 5740–5743.

(84) Mungalpara, D.; Stegmüller, S.; Kubik, S. **2017** *Chem. Commun. 53* (37), 5095–5098.

(85) Borissov, A.; Lim, J. Y. C.; Brown, A.; Christensen, K. E.; Thompson, A. L.; Smith, M. D.; Beer, P. D. **2017** *Chem. Commun. 53* (16), 2483–2486.

(86) Borissov, A.; Marques, I.; Lim, J. Y. C.; Félix, V.; Smith, M. D.; Beer, P. D. **2019** *J. Am. Chem. Soc. 141* (9), 4119–4129.

(87) Caballero, A.; Zapata, F.; White, N. G.; Costa, P. J.; Félix, V.; Beer, P. D. **2012** *Angew. Chemie Int. Ed. 51* (8), 1876–1880.

(88) Serpell, C. J.; Kilah, N. L.; Costa, P. J.; Félix, V.; Beer, P. D. **2010** *Angew. Chemie Int. Ed. 49* (31), 5322–5326.

(89) Chakraborty, S.; Maji, S.; Ghosh, R.; Jana, R.; Datta, A.; Ghosh, P. **2019** *Chem. Commun. 55* (10), 1506–1509.

(90) Lim, J. Y. C.; Beer, P. D. **2018** *New J. Chem. 42* (13), 10472–10475.

(91) Riel, A. M. S.; Decato, D. A.; Sun, J.; Massena, C. J.; Jessop, M. J.; Berryman, O. B. **2018** *Chem. Sci. 9* (26), 5828–5836.

(92) Chowdhury, B.; Sinha, S.; Ghosh, P. **2016** *Chem. - A Eur. J. 22* (50), 18051–18059.

(93) Lo, W. K. C.; Huff, G. S.; Cubanski, J. R.; Kennedy, A. D. W.; McAdam, C. J.; McMorran, D. A.; Gordon, K. C.; Crowley, J. D. **2015** *Inorg. Chem. 54* (4), 1572–1587.

(94) Khatua, S.; Samanta, D.; Bats, J. W.; Schmittel, M. **2012** *Inorg. Chem. 51* (13), 7075–7086.

(95) Chowdhury, B.; Dutta, R.; Khatua, S.; Ghosh, P. **2016** *Inorg. Chem. 55* (1), 259–271.

(96) Zhao, H.; Gabbaï, F. P. **2010** *Nat Chem 2* (11), 984–990.

(97) Semenov, N. A.; Lonchakov, A. V; Pushkarevsky, N. A.; Suturina, E. A.; Korolev, V. V; Lork, E.; Vasiliev, V. G.; Konchenko, S. N.; Beckmann, J.; Gritsan, N. P.; et al. **2014** *Organometallics 33* (16), 4302–4314.

(98) Garrett, G. E.; Carrera, E. I.; Seferos, D. S.; Taylor, M. S. **2016** *Chem. Commun. 52* (64), 9881–

9884.

(99) Benz, S.; Macchione, M.; Verolet, Q.; Mareda, J.; Sakai, N.; Matile, S. **2016** *J. Am. Chem. Soc. 138* (29), 9093–9096.

(100) Lim, J. Y. C.; Marques, I.; Thompson, A. L.; Christensen, K. E.; Félix, V.; Beer, P. D. **2017** *J. Am. Chem. Soc. 139* (8), 3122–3133.

(101) Chen, L.; Xiang, J.; Zhao, Y.; Yan, Q. **2018** *J. Am. Chem. Soc. Commun. 140* (23), 7079–7082.

(102) Wang, W.; Zhu, H.; Liu, S.; Zhao, Z.; Zhang, L.; Hao, J.; Wang, Y. **2019** *J. Am. Chem. Soc. 141* (23), 9175–9179.

(103) Benz, S.; Mareda, J.; Besnard, C.; Sakai, N.; Matile, S. **2017** *Chem. Sci. 8* (12), 8164–8169.

(104) Gale, P. A.; Caltagirone, C. **2015** *Chem. Soc. Rev. 44* (13), 4212–4227.

(105) Chatphueak, N.; Suksai, C. **2019** *Polyhedron 170*, 742–748.

(106) Kaur, K.; Saini, R.; Kumar, A.; Luxami, V.; Kaur, N.; Singh, P.; Kumar, S. **2012** *Coord. Chem. Rev. 256* (17–18), 1992–2028.

(107) Otón, F.; Tárraga, A.; Velasco, M. D.; Espinosa, A.; Molina, P. **2004** *Chem. Commun. 4* (14), 1658–1659.

(108) Nishizawa, S.; Kato, Y.; Teramae, N. **1999** *J. Am. Chem. Soc. 121* (40), 9463–9464.

(109) Kaur, M.; Cho, M. J.; Choi, D. H. **2014** *Dye. Pigment. 103*, 154–160.

(110) Xu, S.; Chen, K.; Tian, H. **2005** *J. Mater. Chem. 15* (27–28), 2676–2680.

(111) Sessler, J. L.; Cho, D. G. **2008** *Org. Lett. 10* (1), 73–75.

(112) Liu, D.; Wu, W. H.; Liu, Y. J.; Wu, X. L.; Cao, Y.; Song, B.; Li, X.; Zhang, W. Bin. **2017** *ACS Cent. Sci. 3* (5), 473–481.

(113) Hudson, B.; Vinograd, J. **1967** *Nature 216* (5116), 647–652.

(114) Weigandt, J.; Chung, C. L.; Jester, S. S.; Famulok, M. **2016** *Angew. Chemie - Int. Ed. 55* (18), 5512–5516.

(115) List, J.; Falgenhauer, E.; Kopperger, E.; Pardatscher, G.; Simmel, F. C. **2016** *Nat. Commun. 7*, 1–7.

(116) Wasserman, E. **1960** *J. Am. Chem. Soc. 82* (16), 4433–4434.

(117) Schill, G.; Lüttringhaus, A. **1964** *Angew. Chemie 76* (13), 567–568.

(118) Harrison, I. T.; Harrison, S. **1967** *J. Am. Chem. Soc. 89* (22), 5723–5724.

(119) Mohr, B.; Weck, M.; Sauvage, J. P.; Grubbs, R. H. **1997** *Angew. Chemie (International Ed. English) 36* (12), 1308–1310.

(120) Fuller, A. M.; Leigh, D. A.; Lusby, P. J.; Oswald, I. D. H.; Parsons, S.; Walker, D. B. **2004** *Angew. Chemie - Int. Ed. 43* (30), 3914–3918.

(121) Sauvage, J. P.; Ward, M. **1991** *Inorg. Chem. 30* (20), 3869–3874.

(122) Hamann, C.; Kern, J. M.; Sauvage, J. P. **2003** *Inorg. Chem. 42* (6), 1877–1883.

(123) Goldup, S. M.; Leigh, D. A.; Lusby, P. J.; McBurney, R. T.; Slawin, A. M. Z. **2008** *Angew. Chemie - Int. Ed. 47* (37), 6999–7003.

(124) Zapata, F.; Blackburn, O. A.; Langton, M. J.; Faulkner, S.; Beer, P. D. **2013** *Chem. Commun. 49* (74), 8157–8159.

(125) Ayme, J. F.; Gil-Ramírez, G.; Leigh, D. A.; Lemonnier, J. F.; Markevicius, A.; Muryn, C. A.; Zhang, G. **2014** *J. Am. Chem. Soc. 136* (38), 13142–13145.

(126) Aucagne, V.; Hänni, K. D.; Leigh, D. A.; Lusby, P. J.; Walker, D. B. **2006** *J. Am. Chem. Soc. 128* (7), 2186–2187.

(127) Lu, C. H.; Qi, X. J.; Cecconello, A.; Jester, S. S.; Famulok, M.; Willner, I. **2014** *Angew. Chemie - Int. Ed. 53* (29), 7499–7503.

(128) Ashton, P. R.; Glink, P. T.; Stoddart, J. F.; Tasker, P. A.; White, A. J. P.; Williams, D. J. **1996** *Chem. Eur. J. 2* (6), 729–736.

(129) Luo, Q. F.; Zhu, L.; Rao, S. J.; Li, H.; Miao, Q.; Qu, D. H. **2015** *J. Org. Chem. 80* (9), 4704–4709.

(130) Amabilino, D. B.; Ashton, P. R.; Reder, A. S.; Spencer, N.; Stoddart, J. F. **1994** *Angew. Chemie Int. Ed. English 33* (12), 1286–1290.

(131) Loeb, S. J.; Wisner, J. A. **2000** *Chem. Commun. 4* (10), 845–846.

(132) Tiburcio, J.; Davidson, G. J. E.; Loeb, S. J. **2002** *Chem. Commun. 2* (12), 1282–1283.

(133) Zhu, K.; Vukotic, V. N.; Noujeim, N.; Loeb, S. J. **2012** *Chem. Sci. 3* (11), 3265–3271.

(134) Loeb, S. J.; Wisner, J. A. **1998** *Chem. Commun.* No. 24, 2757–2758.

(135) Hübner, G. M.; Gläser, J.; Seel, C.; Vögtle, F. **1999** *Angew. Chemie - Int. Ed. 38* (3), 383–386.

(136) Wisner, J. A.; Beer, P. D.; Drew, M. G. B. **2001** *Angew. Chemie - Int. Ed. 40* (19), 3606–3609.

(137) Wisner, J. A.; Beer, P. D.; Drew, M. G. B.; Sambrook, M. R. **2002** *J. Am. Chem. Soc. 124* (42), 12469–12476.

(138) Sambrook, M. R.; Beer, P. D.; Wisner, J. A.; Paul, R. L.; Cowley, A. R.; Szemes, F.; Drew, M. G. B. **2005** *J. Am. Chem. Soc. 127* (7), 2292–2302.

(139) Hamilton, D. G.; Prodi, L.; Feeder, N.; Sanders, J. K. M. **1999** *J. Chem. Soc. - Perkin Trans. 1* No. 8, 1057–1065.

(140) Fujimoto, T.; Sakata, Y.; Kaneda, T. **2000** *Chem. Commun. 1* (21), 2143–2144.

(141) Okada, M.; Harada, A. **2003** *Macromolecules 36* (26), 9701–9703.

(142) Bąk, K. M.; Porfyrakis, K.; Davis, J. J.; Beer, P. D. **2020** *Mater. Chem. Front. 4* (4), 1052–1073.

(143) Cirulli, M.; Kaur, A.; Lewis, J. E. M.; Zhang, Z.; Kitchen, J. A.; Goldup, S. M.; Roessler, M. M. **2019** *J. Am. Chem. Soc. 141* (2), 879–889.

(144) Collins, C. G.; Peck, E. M.; Kramer, P. J.; Smith, B. D. **2013** *Chem. Sci. 4* (6), 2557–2563.

(145) Barat, R.; Legigan, T.; Tranoy-Opalinski, I.; Renoux, B.; Péraudeau, E.; Clarhaut, J.; Poinot, P.; Fernandes, A. E.; Aucagne, V.; Leigh, D. A.; et al. **2015** *Chem. Sci. 6* (4), 2608–2613.

(146) De Bo, G.; Gall, M. A. Y.; Kitching, M. O.; Kuschel, S.; Leigh, D. A.; Tetlow, D. J.; Ward, J. W. **2017** *J. Am. Chem. Soc. 139* (31), 10875–10879.

(147) Tachibana, Y.; Kihara, N.; Takata, T. **2004** *J. Am. Chem. Soc. 126* (11), 3438–3439.

(148) Lim, J. Y. C.; Yuntawattana, N.; Beer, P. D.; Williams, C. K. **2019** *Angew. Chemie - Int. Ed. 58*

(18), 6007–6011.

(149) Pérez, E. M. **2017** *Chem. - A Eur. J. 23* (52), 12681–12689.

(150) López-Moreno, A.; Nieto-Ortega, B.; Moffa, M.; De Juan, A.; Bernal, M. M.; Fernández-Blázquez, J. P.; Vilatela, J. J.; Pisignano, D.; Pérez, E. M. **2016** *ACS Nano 10* (8), 8012–8018.

(151) Bleiholder, C.; Werz, D. B.; Köppel, H.; Gleiter, R. **2006** *J. Am. Chem. Soc. 128* (8), 2666–2674.

(152) Gilday, L. C.; Robinson, S. W.; Barendt, T. A.; Langton, M. J.; Mullaney, B. R.; Beer, P. D. **2015** *Chem. Rev. 115* (15), 7118–7195.

(153) Fanfrlík, J.; Přáda, A.; Padělková, Z.; Pecina, A.; Macháček, J.; Lepšík, M.; Holub, J.; Růžička, A.; Hnyk, D.; Hobza, P. **2014** *Angew. Chemie - Int. Ed. 53* (38), 10139–10142.

(154) Nagao, Y.; Hirata, T.; Goto, S.; Sano, S.; Kakehi, A.; Iizuka, K.; Shiro, M. **1998** *J. Am. Chem. Soc. 120* (13), 3104–3110.

(155) Wonner, P.; Vogel, L.; Düser, M.; Gomes, L.; Kniep, F.; Mallick, B.; Werz, D. B.; Huber, S. M. **2017** *Angew. Chemie - Int. Ed. 56* (39), 12009–12012.

(156) Benz, S.; Lopez-Andarias, J.; Mareda, J.; Sakai, N.; Matile, S. **2017** *Angew. Chem. Int. Ed. 56*, 812–815.

(157) Ho, P. C.; Rafique, J.; Lee, J.; Lee, L. M.; Jenkins, H. A.; Britten, J. F.; Braga, A. L.; Vargas-Baca, I. **2017** *Dalt. Trans. 46* (20), 6570–6579.

(158) Chen, L.; Xiang, J.; Zhao, Y.; Yan, Q. **2018** *J. Am. Chem. Soc. 140*, 7079–7082.

(159) Mahmudov, K. T.; Kopylovich, M. N.; Guedes Da Silva, M. F. C.; Pombeiro, A. J. L. **2017** *Dalt. Trans. 46* (31), 10121–10138.

(160) Pascoe, D. J.; Ling, K. B.; Cockroft, S. L. **2017** *J. Am. Chem. Soc. 139* (42), 15160–15167.

(161) Chivers, T.; Laitinen, R. S. **2015** *Chem. Soc. Rev. 44* (7), 1725–1739.

(162) Park, H.; Edgar, L. J.; Lumba, M. A.; Willis, L. M.; Nitz, M. **2015** *Org. Biomol. Chem. 13* (25), 7027–7033.

(163) Stefani, H. A.; Pena, J. M.; Manarin, F.; Ando, R. A.; Leal, D. M.; Petragnani, N. **2011** *Tetrahedron Lett. 52* (34), 4398–4401.

(164) Stefani, H. A.; Silva, N. C. S.; Vasconcelos, S. N. S.; Manarin, F.; Souza, F. B. **2013** *Tetrahedron Lett. 54* (22), 2809–2812.

(165) Stefani, H. A.; Vasconcelos, S. N. S.; Manarin, F.; Leal, D. M.; Souza, F. B.; Madureira, L. S.; Zukerman-Schpector, J.; Eberlin, M. N.; Godoi, M. N.; De Souza Galaverna, R. **2013** *European J. Org. Chem.* No. 18, 3780–3785.

(166) Wonner, P.; Steinke, T.; Vogel, L.; Huber, S. M. **2020** *Chem. - A Eur. J. 26* (6), 1258–1262.

(167) Wonner, P.; Dreger, A.; Vogel, L.; Engelage, E.; Huber, S. M. **2019** *Angew. Chemie - Int. Ed. 58* (47), 16923–16927.

(168) Brotherton, W. S.; Clark, R. J.; Zhu, L. **2012** *J. Org. Chem. 77* (15), 6443–6455.

(169) Hein, J. E.; Tripp, J. C.; Krasnova, L. B.; Sharpless, K. B.; Fokin, V. V. **2009** *Angew. Chem. Int. Ed. 48*, 8018–8021.

(170) Worrell, B. T.; Hein, J. E.; Fokin, V. V. **2012** *Angew. Chem. Int. Ed. 51*, 11791–11794.

(171) Hynes, M. J. **1993** *J. Chem. Soc. Dalt. Trans.* No. 2, 311–312.

(172) Robinson, S. W.; Mustoe, C. L.; White, N. G.; Brown, A.; Thompson, A. L.; Kennepohl, P.; Beer, P. D. **2015** *J. Am. Chem. Soc. 137* (1), 499–507.

(173) Bianchi, A.; Garcia-Espana, E.; Bowman-James, K. WILEY-VCH, Weinheim, 2012.

(174) Lim, J. Y. C.; Bunchuay, T.; Beer, P. D. **2017** *Chem. - A Eur. J. 23* (19), 4700–4707.

(175) Langton, M. J.; Robinson, S. W.; Marques, I.; Félix, V.; Beer, P. D. **2014** *Nat Chem 6* (12), 1039–1043.

(176) Schulz, N.; Sokkar, P.; Engelage, E.; Schindler, S.; Erdelyi, M.; Sanchez-Garcia, E.; Huber, S. M. **2018** *Chem. - A Eur. J. 24* (14), 3464–3473.

(177) Walter, S. M.; Kniep, F.; Rout, L.; Schmidtchen, F. P.; Herdtweck, E.; Huber, S. M. **2012** *J. Am. Chem. Soc. 134* (20), 8507–8512.

(178) Gutmann, V. **1976** *Electrochim. Acta 21* (9), 661–670.

(179) Richardi, J.; Fries, P. H.; Krienke, H. **1998** *J. Chem. Phys. 108* (10), 4079–4089.

(180) Richardi, J.; Fries, P. H.; Fischer, R.; Rast, S.; Krienke, H. **1998** *Mol. Phys. 93* (6), 925–938.

(181) Richardi, J.; Fries, P. H.; Fischer, R.; Rast, S.; Krienke, H. **1997** *J. Mol. Liq. 73–74*, 465–485.

(182) Assaf, K. I.; Ural, M. S.; Pan, F.; Georgiev, T.; Simova, S.; Rissanen, K.; Gabel, D.; Nau, W. M. **2015** *Angew. Chemie 127* (23), 6956–6960.

(183) Fiala, T.; Sleziakova, K.; Marsalek, K.; Salvadori, K.; Sindelar, V. **2018** *J. Org. Chem. 83* (4), 1903–1912.

(184) Abraham, M. H. *Chem. Soc. Rev.* 1993, pp 73–83.

(185) Sessler, J. L.; Eller, L. R.; Cho, W. S.; Nicolaou, S.; Aguilar, A.; Lee, J. T.; Lynch, V. M.; Magda, D. J. **2005** *Angew. Chemie - Int. Ed. 44* (37), 5989–5992.

(186) Jadhav, V. D.; Herdtweck, E.; Schmidtchen, F. P. **2008** *Chem. - A Eur. J. 14* (20), 6098–6107.

(187) Berger, M.; Schmidtchen, F. P. **1999** *J. Am. Chem. Soc. 121* (43), 9986–9993.

(188) Zieliński, T.; Jurczak, J. **2005** *Tetrahedron 61* (16), 4081–4089.

(189) Lee, H.-J.; Choi, Y.-S.; Lee, K.-B.; Park, J.; Yoon, C.-J. **2002** *J. Phys. Chem. A 106* (30), 7010–7017.

(190) Choudhary, A.; Gandla, D.; Krow, G. R.; Raines, R. T. **2009** *J. Am. Chem. Soc. 131* (21), 7244–7246.

(191) Hossain, M. A.; Kang, S. O.; Llinares, J. M.; Powell, D.; Bowman-James, K. **2003** *Inorg. Chem. 42* (17), 5043–5045.

(192) White, N. G.; Beer, P. D. **2012** *Chem. Commun. 48* (68), 8499–8501.

(193) Jicsinszky, L.; Iványi, R. **2001** *Carbohydr. Polym. 45* (2), 139–145.

(194) Banala, S.; Süssmuth, R. D. **2010** *ChemBioChem 11* (10), 1335–1337.

(195) Inoue, Y.; Kanbara, T.; Yamamoto, T. **2003** *Tetrahedron Lett. 44* (28), 5167–5169.

(196) Chmielewski, M. J.; Jurczak, J. **2005** *Chem. - A Eur. J. 11* (20), 6080–6094.

(197) Spence, G. T.; Beer, P. D. **2013** *Acc. Chem. Res. 46* (2), 571–586.

(198) Robinson, S. W.; Beer, P. D. **2017** *Org. Biomol. Chem. 15* (1), 153–159.

(199) Langton, M. J.; Marques, I.; Robinson, S. W.; Félix, V.; Beer, P. D. **2016** *Chem. - A Eur. J. 22* (1), 185–192.

(200) Lim, J. Y. C.; Beer, P. D. **2015** *Chem. Commun. 51* (17), 3686–3688.

(201) Kluska, K.; Adamczyk, J.; Krężel, A. **2018** *Coord. Chem. Rev. 367*, 18–64.

(202) Akrivos, P. D. **2001** *Coord. Chem. Rev. 213* (1), 181–210.

(203) Raper, E. S. **1994** *Coord. Chem. Rev. 129* (1), 91–156.

(204) Bauza, A.; Quinonero, D.; Deya, P. M.; Frontera, A. **2013** *CrystEngComm 15* (16), 3137–3144.

(205) Blackmond, D. G. **2011** *Philos. Trans. R. Soc. B Biol. Sci. 366* (1580), 2878–2884.

(206) Nguyen, L. A.; He, H.; Pham-Huy, C. **2018** *Int. J. Biomed. Sci. 49* (6), 1116–1155.

(207) Wu, G. **2013** *Amino Acids 45* (3), 407–411.

(208) Phipps, R. J.; Hamilton, G. L.; Toste, F. D. **2012** *Nat Chem 4* (8), 603–614.

(209) Yabushita, K.; Yuasa, A.; Nagao, K.; Ohmiya, H. **2019** *J. Am. Chem. Soc. 141* (1), 113–117.

(210) Lämmerhofer, M. **2010** *J. Chromatogr. A 1217* (6), 814–856.

(211) Casabianca, H.; Graff, J. -B; Jame, P.; Perrucchietti, C.; Chastrette, M. **1995** *J. High Resolut. Chromatogr. 18* (5), 279–285.

(212) Gal, J. **2011** *Chirality 23*, 1–16.

(213) Rickhaus, M.; Mayor, M.; Juríček, M. **2016** *Chem. Soc. Rev. 45* (6), 1542–1556.

(214) Easson, L. H.; Stedman, E. **1933** *Biochem J. 27* (4), 1257–1266.

(215) D. Mesecar, Daniel E. Koshland, A. **2000** *IUBMB Life (International Union Biochem. Mol. Biol. Life) 49* (5), 457–466.

(216) Mesecar, A. D.; Koshland Jr., D. E. **2000** *Nature 403* (February), 614–615.

(217) Abrol, R.; Sundaresan, V. **2002** *Protein Sci. 11* (6), 1330–1339.

(218) Sundaresan, V.; Abrol, R. **2005** *Chirality 17* (SUPPL.), 30–39.

(219) Wainer, I. W. *Encyclopedia of Separation Science*; 2000.

(220) Koshland, D. E. **1958** *Proc. Natl. Acad. Sci. 44* (2), 98–104.

(221) Cherbavaz, D. B.; Lee, M. E.; Stroud, R. M.; Koshland, D. E. **2000** *J. Mol. Biol. 295* (3), 377–385.

(222) Granda, J. M.; Jurczak, J. **2013** *Org. Lett. 15* (18), 4730–4733.

(223) Guo, L. E.; Hong, Y.; Zhang, S. Y.; Zhang, M.; Yan, X. S.; Cao, J. L.; Li, Z.; James, T. D.; Jiang, Y. B. **2018** *J. Org. Chem. 83* (24), 15128–15135.

(224) Turiel, M. G.; Garrido-González, J. J.; Simón, L.; Sanz, F.; Lithgow, A. M.; Morán, J. R.; Arriba, F. D. Á. L.; Alcázar, V. **2020** *Org. Lett. 22*, 867–872.

(225) Jamieson, E. M. G.; Modicom, F.; Goldup, S. M. **2018** *Chem. Soc. Rev. 47* (14), 5266–5311.

(226) Schmidt, T.; Schmieder, R.; Müller, W. M.; Kiupel, B.; Vögtle, F. **1998** *European J. Org. Chem.* No. 9, 2003–2007.

(227) Lim, J. Y. C.; Marques, I.; Beer, P. D. **2017** *J. Am. Chem. Soc. 139*, 12228–12239.

(228) Corra, S.; De Vet, C.; Groppi, J.; La Rosa, M.; Silvi, S.; Baroncini, M.; Credi, A. **2019** *J. Am. Chem. Soc. 141* (23), 9129–9133.

(229) Mitra, R.; Thiele, M.; Octa-Smolin, F.; Letzel, M. C.; Niemeyer, J. **2016** *Chem. Commun. 52* (35), 5977–5980.

(230) Lim, J. Y. C.; Marques, I.; Félix, V.; Beer, P. D. **2018** *Chem. Commun. 54* (77), 10851–10854.

(231) Lim, J. Y. C.; Marques, I.; Ferreira, L.; Félix, V.; Beer, P. D. **2016** *Chem. Commun. 52* (32), 5527–5530.

(232) Lim, J. Y. C.; Marques, I.; Felix, V.; Beer, P. D. **2018** *Angew. Chemie (International Ed. 57*, 584–588.

(233) Pu, L. **2012** *Acc. Chem. Res. 45* (2), 150–163.

(234) Zheng, H.; Zhou, W.; Lv, J.; Yin, X.; Li, Y.; Liu, H.; Li, Y. **2009** *Chem. - A Eur. J. 15* (47), 13253–13262.

(235) Thordarson, P. **2011** *Chem. Soc. Rev. 40* (3), 1305–1323.

(236) Klein, H. A.; Beer, P. D. **2019** *Chem. - A Eur. J. 25* (12), 3125–3130.

(237) Aotake, T.; Tanimoto, H.; Hotta, H.; Kuzuhara, D.; Okujima, T.; Uno, H.; Yamada, H. **2013** *Chem. Commun. 49* (35), 3661–3663.

(238) Vishe, M.; Lathion, T.; Pascal, S.; Yushchenko, O.; Homberg, A.; Brun, E.; Vauthey, E.; Piguet, C.; Lacour, J. **2018** *Helv. Chim. Acta 101* (1).

(239) Bains, G. K.; Kim, S. H.; Sorin, E. J.; Narayanaswami, V. **2012** *Biochemistry 51* (31), 6207–62197.

(240) Kalyanasundaram, K.; Thomas, J. K. **1977** *J. Am. Chem. Soc. 99* (7), 2039–2044.

(241) Nakajima, A. **1982** *Spectrochim. Acta Part A Mol. Spectrosc. 38* (6), 693–695.

(242) Avakyan, V. G.; Nazarov, V. B.; Koshkin, A. V.; Alfimov, M. V. **2015** *High Energy Chem. 49* (3), 177–182.

(243) Watkins, A. R. **1974** *J. Phys. Chem. 78* (19), 1885–1890.

(244) Kasha, M. **1952** *J. Chem. Phys. 20* (1), 71–74.

(245) Maier, J. M.; Li, P.; Ritchey, J. S.; Yehl, C. J.; Shimizu, K. D. **2018** *Chem. Commun. 54* (61), 8502–8505.

(246) Ma, L.; White, P. S.; Lin, W. **2002** *J. Org. Chem. 67* (22), 7577–7586.

(247) Jiménez, M. B.; Fuentes De Arriba, Á. L.; Calle, E.; Caballero, M. C. **2012** *Supramol. Chem. 24* (5), 361–368.

(248) Saha, I.; Wang, E. B.; Parish, C. A.; Ghosh, K. **2017** *ChemistrySelect 2* (17), 4794–4799.

(249) Roberts, I.; Kimball, G. E. **1937** *J. Am. Chem. Soc. 59* (5), 947–948.

(250) Mori, T.; Rathore, R.; Lindeman, S. V.; Kochi, J. K. **1998** *Chem. Commun.* No. 8, 927–928.

(251) Cui, X. L.; Brown, R. S. **2000** *J. Org. Chem. 65* (18), 5653–5658.

(252) Ashikari, Y.; Shimizu, A.; Nokami, T.; Yoshida, J. I. **2013** *J. Am. Chem. Soc. 135* (43), 16070–16073.

(253) Guha, S.; Kazi, I.; Mukherjee, P.; Sekar, G. **2017** *Chem. Commun. 53* (79), 10942–10945.

(254) Koskinen, L.; Hirva, P.; Kalenius, E.; Jääskeläinen, S.; Rissanen, K.; Haukka, M. **2015** *CrystEngComm 17* (6), 1231–1236.

(255) Hakkert, S. B.; Erdélyi, M. **2014** *J. Phys. Org. Chem. 28*, 226–233.

(256) Haque, I.; Wood, J. L. **1968** *J. Mol. Struct. 2* (3), 217–238.

(257) Georgiou, D. C.; Butler, P.; Browne, E. C.; Wilson, D. J. D.; Dutton, J. L. **2013** *Aust. J. Chem. 66* (10), 1179–1188.

(258) Mitoraj, M. P.; Michalak, A. **2013** *J. Mol. Model. 19* (11), 4681–4688.

(259) Syzgantseva, O. A.; Tognetti, V.; Joubert, L. **2013** *J. Phys. Chem. A 117* (36), 8969–8980.

(260) Politzer, P.; Murray, J. S.; Clark, T. **2013** *Phys. Chem. Chem. Phys. 15* (27), 11178–11189.

(261) Gilli, P.; Bertolasi, V.; Ferretti, V.; Gilli, G. **1994** *J. Am. Chem. Soc. 116* (3), 909–915.

(262) Glidewell, C.; Holden, H. D. **1982** *Acta Crystallogr. Sect. B Struct. Crystallogr. Cryst. Chem. 38* (2), 667–669.

(263) Merlet, P.; Peyerimhoff, S. D.; Buenker, R. J. **1972** *J. Am. Chem. Soc. 94* (24), 8301–8308.

(264) Lindblad, S.; Mehmeti, K.; Veiga, A. X.; Nekoueishahraki, B.; Gräfenstein, J.; Erdélyi, M. **2018** *J. Am. Chem. Soc. 140*, 13503–13513.

(265) Vanderkooy, A.; Gupta, A. K.; Földes, T.; Lindblad, S.; Orthaber, A.; Pápai, I.; Erdélyi, M. **2019** *Angew. Chemie - Int. Ed. 58* (27), 9012–9016.

(266) Guha, S.; Kazi, I.; Nandy, A.; Sekar, G. **2017** *European J. Org. Chem. 2017* (37), 5497–5518.

(267) Eberlin, M. N.; Kotiaho, T.; Shay, B. J.; Yang, S. S.; Cooks, R. G. **1994** *J. Am. Chem. Soc. 116* (6), 2457–2465.

(268) Barluenga, J. **1999** *Pure Appl. Chem. 71* (3), 431–436.

(269) Kim, Y.; McKinley, E. J.; Christensen, K. E.; Rees, N. H.; Thompson, A. L. **2014** *Cryst. Growth Des. 14* (12), 6294–6301.

(270) Karim, A.; Reitti, M.; Carlsson, A. C. C.; Gräfenstein, J.; Erdélyi, M. **2014** *Chem. Sci. 5* (8), 3226–3233.

(271) Muñiz, K.; García, B.; Martínez, C.; Piccinelli, A. **2017** *Chem. - A Eur. J. 23* (7), 1455.

(272) Turunen, L.; Warzok, U.; Puttreddy, R.; Beyeh, N. K.; Schalley, C. A.; Rissanen, K. **2016** 14239–14242.

(273) Turunen, L.; Peuronen, A.; Forsblom, S.; Kalenius, E.; Lahtinen, M.; Rissanen, K. **2017** *Chem. - A Eur. J. 23* (48), 11714–11718.

(274) Warzok, U.; Marianski, M.; Hoffmann, W.; Turunen, L.; Rissanen, K.; Pagel, K.; Schalley, C. A. **2018** *Chem. Sci. 9* (44), 8343–8351.

(275) Perez-Inestrosa, E.; Desvergne, J. P.; Bouas-Laurent, H.; Rayez, J. C.; Rayez, M. T.; Cotrait, M.;

Marsau, P. **2002** *European J. Org. Chem. 1* (2), 331–344.

(276) Lindblad, Mehmeti, K.; Veiga, A. X.; Nekoueishahraki, B. **2018** *J. Am. Chem. Soc. 140*, 13503–13513.

(277) Lindblad, S.; Mehmeti, K.; Veiga, A. X.; Nekoueishahraki, B.; Gräfenstein, J.; Erdélyi, M. **2018** *J. Am. Chem. Soc. 140*, 13503–13513.

(278) Kleinmaier, R.; Arenz, S.; Karim, A.; Carlsson, A. C. C.; Erdélyi, M. **2013** *Magn. Reson. Chem. 51* (1), 46–53.

(279) Pazderski, L.; Pawlak, T.; Sitkowski, J.; Kozerski, L.; Szłyk, E. **2010** *Magn. Reson. Chem. 48* (6), 417–426.

(280) Carlsson, A. C.; Mehmeti, K.; Uhrbom, M.; Karim, A.; Bedin, M.; Puttreddy, R.; Kleinmaier, R.; Neverov, A. A.; Nekoueishahraki, B. **2016**.

(281) Cantrill, S. **2012** *Nat. Chem. 4* (8), 592–592.

(282) Movsisyan, L. D.; Franz, M.; Hampel, F.; Thompson, A. L.; Tykwinski, R. R.; Anderson, H. L. **2016** *J. Am. Chem. Soc. 138* (4), 1366–1376.

(283) Winn, J.; Pinczewska, A.; Goldup, S. M. **2013** *J. Am. Chem. Soc. 135* (36), 13318–13321.

(284) Ward, J. S.; Fiorini, G.; Frontera, A.; Rissanen, K. **2020** *Chem Comm*.

(285) Agard, N. J.; Baskin, J. M.; Prescher, J. A.; Lo, A.; Bertozzi, C. R. **2006** *ACS Chem. Biol. 1* (10), 644–648.

(286) Lee, B. Y.; Park, S. R.; Jeon, H. B.; Kim, K. S. **2006** *Tetrahedron Lett. 47* (29), 5105–5109.

(287) Hassner, A.; Stern, M.; Gottlieb, H.; Frolow, F. **1990** *J. Org. Chem. 55* (8), 2304–2306.

(288) Hassner, A.; Stern, M. **1986** *Angew. Chem. Int. Ed. 25* (5), 478–479.

(289) Dalmia, A.; Savinell, R. F.; Liu, C. C. **1996** *J. Electrochem. Soc. 143* (6), 1827–1833.

(290) Brynn Hibbert, D.; Thordarson, P. **2016** *Chem. Commun. 52* (87), 12792–12805.

(291) Ai, T.; Qiu, L.; Xie, J.; Geraghty, R. J.; Chen, L. **2016** *Bioorganic Med. Chem. 24* (4), 686–692.

(292) Lim, J. Y. C. University of Oxford, 2017.

(293) Liu, G. H.; Tang, W. J.; Fan, Q. H. **2003** *Tetrahedron*.

(294) Harris, T.; dos Passos Gomes, G.; Ayad, S.; Clark, R. J.; Lobodin, V. V.; Tuscan, M.; Hanson, K.; Alabugin, I. V. **2017** *Chem 3* (4), 629–640.

(295) Nowell, H.; Barnett, S. A.; Christensen, K. E.; Teat, S. J.; Allan, D. R. **2012** *J. Synchrotron Radiat. 19* (3), 435–441.

(296) Cosier, B. J.; Glazer, A. M. **1986** *J. Appl. Crystallogr. 19* (2), 105–107.

(297) Palatinus, L.; Chapuis, G. **2007** *J. Appl. Crystallogr. 40* (4), 786–790.

(298) Betteridge, P. W.; Carruthers, J. R.; Cooper, R. I.; Prout, K.; Watkin, D. J. **2003** *J. Appl. Crystallogr. 36* (6), 1487–1487.

(299) Parois, P.; Cooper, R. I.; Thompson, A. L. **2015** *Chem. Cent. J. 9* (1), 1–14.

(300) Cooper, R. I.; Thompson, A. L.; Watkin, D. J. **2010** *J. Appl. Crystallogr. 43* (5 PART 1), 1100–1107.

(301) Carruthers, J. R.; Watkin, D. J. **1979** *Acta Crystallogr. Sect. A 35* (4), 698–699.

(302) Pritchard, B. P.; Altarawy, D.; Didier, B.; Gibson, T. D.; Windus, T. L. **2019** *J. Chem. Inf. Model. 59* (11), 4814–4820.

(303) Schuchardt, K. L.; Didier, B. T.; Elsethagen, T.; Sun, L.; Gurumoorthi, V.; Chase, J.; Li, J.; Windus, T. L. **2007** *J. Chem. Inf. Model. 47* (3), 1045–1052.

(304) Bulat, F. A.; Toro-Labbé, A.; Brinck, T.; Murray, J. S.; Politzer, P. **2010** *J. Mol. Model. 16* (11), 1679–1691.

(305) Lu, T.; Chen, F. **2012** *J. Mol. Graph. Model. 38*, 314–323.

(306) Lu, T.; Chen, F. **2012** *J. Comput. Chem. 33* (5), 580–592.